IJERT
ISSN : 2278 - 0181

THESIS

Thesis ID : IJERTTH0006

Study of Multimode Fiber Optic Sensor

Dr. S. Venkateswara Rao

JNTUH College of Engineering, Hyderabad
India.

Published By

International Journal of
Engineering Research and Technology
(www.ijert.org)

International Journal of Engineering Research & Technology (IJERT)
ISSN: 2278-0181

Study of Multimode Fiber Optic Sensor

S.VENKATESWARA RAO

H. T. No. 31714P/PH

Thesis submitted to
Research and Development Cell
Jawaharlal Nehru Technological University Hyderabad
for the award of
Doctor of Philosophy
in **Physics**
2010

International Journal of Engineering Research & Technology (IJERT)
ISSN: 2278-0181

DECLARATION

I here by declare that the thesis "STUDY OF MULTIMODE FIBER OPTIC SENSOR" submitted to Jawaharlal Nehru Technological University Hyderabad, Hyderabad is my own and has not been submitted to any other University / Institute previously for the award of any degree or diploma.

Hyderabad

Date: S. VENKATESWARA RAO

RESEARCH AND DEVELOPMENT CELL

JAWAHARLAL NEHRU TECHNOLOGICAL UNIVERSITY HYDERABAD

HYDERABAD – 500 085, A.P., INDIA

2010

CERTIFICATE

This is to certify that the thesis / dissertation entitled "STUDY OF MULTIMODE FIBER OPTIC SENSOR" by Sri S. Venkateswara Rao for the award of Ph. D. Degree in Physics by the Jawaharlal Nehru Technological University Hyderabad; Hyderabad is a record of bonafide work carried out by him under my guidance and supervision.

The results embodied in this thesis have not been submitted to any other university / institute previously for the award of any other degree or diploma.

Hyderabad Signature of Supervisor

Date:

ACKNOWLEDGEMENT

At the outset, I thank **Almighty** for being with me in every walk of my life. I am happy about my successful completion of this task of giving a shape and presenting my work in the form of a thesis **"Study of multimode fiber optic sensor"**, under the guidance of **Dr. B. S. Bellubbi, Professor of Physics** (Retired.), Jawaharlal Nehru Technological University Hyderabad, Hyderabad. I would like to express my sense of gratitude to him for his timely suggestions, cooperative approach in guiding and taking keen interest during the progress of the work and finalization of the thesis.

It is my privilege to thank **Dr. Adeel Ahmad, Professor of Physics,** Nizam College, Osmania University, Hyderabad, for providing valuable information on bio fluids and permitting me to use the Biophysics Laboratory, without whose cooperation, cordial and friendly approach throughout the work, I would not have completed this task.

I extend my sincere thanks to **Dr. T. Radhakrishna, Professor of Physics** (Retired), Jawaharlal Nehru Technological University Hyderabad, Hyderabad for his kind encouragement and acceptance to approach him for any help at any time unconditionally during my research.

I thank **Dr. S. Chandralingam, Professor&** Head, Dept. of Physics, J N T U Hyderabad College of Engineering, JNTU Hyderabad, Hyderabad, for his cooperation and providing the Research facilities available in the department. My heartfelt thanks are due to **Dr. P. Rama Rao, Professor of Physics (Retired)** and **Dr. T. Achyuta Rao, Professor of Physics (Retired)**, JNTUH, Hyderabad for

their moral support throughout my association with them in the Physics Department. I express my thanks to researchers of Department of Physics, Nizam College, Hyderabad. Thanks are due to my colleagues of Department of Physics, JNTUH College of Engineering for their heartful co - operation.

Special thanks are due to **Prof. D. N. Reddy, Vice Chancellor** of Jawaharlal Nehru Technological University Hyderabad, Hyderabad under whose leadership, and with whose blessings my Research work was speeded up for the completion. I extend my special thanks to **Prof. E. Saibaba Reddy, Registrar**, 'JNTU Hyderabad; Hyderabad, who has encouraged me to complete my work with war foot at the stage of completion of my Research. I thank **Prof. N.V. Raman Rao, Principal**, JNTUH College of Engineering, Hyderabad for his co operation and encouragement.

I am thankful to **Ms. Gouri, daughter of Dr. B.S. Bellubbi, Professor of Physics,** for her co-operation and help in preparing the computer format of my thesis. I would like to extend my sincere thanks to **Mrs. Mangala madam wife of Dr. B.S. Bellubbi, Professor of Physics** for her motherly treatment whenever I go to their home for any help, during my research work.

I am grateful to my mother **Kannamma** and my father **Guravaiah** (late) whose blessings shown me the path to complete this work. I am very much thankful to my daughter **Haindavi Shivani**, and my son **Sai Jaihind** for bearing me silently, missing their timely love and affection from me and out of whose sacrifices this work is completed. Thanks are also due to my wife **Sathyavedamani** for her patience and perseverance in shouldering the domestic responsibilities, and supporting me to complete the thesis.

ABSTRACT

In the present work, an attempt has been made to develop a fiber optic glass refractive index sensor to measure the refractive index of various liquids in the index range of 1.30 to 1.50 within the temperature range of about 25°C to 80°C. A U-shaped glass probe acts as a core is used as a sensing element which is provided by a liquid cladding whose refractive index is less than that of the core. Both the ends of the U-shaped probe is connected by plastic clad silica (PCS) fibers, which inturn connected to one to the laser light source, and the other to the light detector. The refractive index of the liquid acting as a cladding is varied by mixing different proportions of the Benzene and alcohols like (Methanol, Propanol, Butanol, and Cyclohexane). This method gives an idea about the variation of the optic power output depending upon the density and refractive index of the liquid surrounding the core. This method helps in the study of power loss versus density and refractive index of the liquid.

Chapter 1 outlines the various kinds of sensors in general and optical fibers in particular. Types of sensors, their working mechanism, and merits and demerits have been analyzed in detail with reference to their sensitivity, compatibility, portability, cost effectiveness, reliability, immunity to other parameters, display parameters etc. Sufficient number of references more relevant to the work has been given for ready reference on several kinds of sensors. A detailed description on the genesis of work was provided at the end of the chapter in which the important role played by temperature and light used to determine the refractive index has been stressed clearly.

Chapter 2 introduces the optical fiber technology starting with the principle of light transportation through optical fibers and their detailed classification in terms of material and geometry of construction. The description of optical fiber structure and how the light is guided through the fiber obeying total internal reflection is dealt in detail. The electromagnetic theory of light for the wave propagation along the fiber wave guide is presented. The other two basic components of any fiber optic system i.e. optical sources and

detectors have been very extensively discussed as they form part as terminal equipment of the construction. To transmit data / information through a fiber wave-guide, an optical source at the input end and a detector at the output end of the fiber are required. The source at the input end and the detector at the output end should match with the coupling of light emitted from these sources into the optical fibers are discussed. When the optical power emerges at the second end of the fiber, it must be converted into an electrical signal. A photo detector performs this function. The performance parameters of PIN and avalanche photo-detector are discussed. The optical power loss mechanism has been discussed well in depth, which has lead to the development of the enormous number of fiber optic sensors and systems. The various optical power losses as light passes through the fiber are also presented. The classification of sensors based on the modification of light characters i.e. intensity, phase, frequency, wavelength and their mechanism has been described in this chapter. A discussion on theory of refractive index has been initiated at the end of the chapter which can be a backbone for the experimentation.

Chapter 3 deals with the experimental methods, and the techniques, that are implemented in the present research work. Designing of sensor is the one of the crucial aspects in constructing any sensing device used to measure an environmental parameter. The geometry, the assembly of components, the external feature of the structure and the construction of sensor varies from sensor to sensor. The design depends mainly on the two interacting factors in the sensor system, i.e. one the measurand to be measured and the second the measuring standard that measures the measurand. Detailed work is carried out using different designs of U-shaped glass rods and the results are compared with reference to their efficiency in measuring the maesurand. The dependence of geometrical parameters on the working mechanism has been presented with a strong theoretical back ground.

Further, this chapter explains the arrangement of the entire experimental setup and the components involved in the system. In the experimental procedure an attempt is made to test the sensor using the binary mixtures, viz. Methanol mixed in Benzene, Propyle

alcohol mixed in Benzene, Butanol mixed in Benzene and Cyclohexane mixed in Benzene. A volume of 10ml mixture is prepared from individual solutions of Methanol, Propyle Alcohol, Butanol and Cyclohexane in Benzene. The experimental arrangement consists of a solid thin glass rod bent in the form of U-shape attached with a Plastic clad silica (PCS) fiber. Light is injected from a laser source (λ = 633nm.) at one end of the U-shaped rod through a Plastic Clad Silica (PCS) fiber coupled to a laser diode. The output end of the rod is connected to an optical power meter through another similar PCS optical fiber. The whole arrangement of the U-shaped rod is immersed in a beaker containing methanol, propyle alcohol, butanol and benzene mixture of various volumes and the variation of the optical output power are noted. The output power is calibrated in terms of the refractive index of the liquid. The R.I. of the liquid is estimated with the help of output power which is in close agreement with the values given in literature. Sensor is standardized by drawing a calibration curve between refractive index recorded from the Abbe's refractometer and the power recorded in the output detector. Thus, the measurement of refractive index of any liquid is explained using the so developed standard graph between the power output and the refractive index.

The experimental work is further extended to study the possibility of working of the sensor at various temperatures especially within the range of about 25°C and 80°C. This chapter discusses in detail the calibration and hence the determination of the refractive index of any unknown liquid whose refractive index lies between 1.30 and 1.50 and in the temperature range as stated above.

Chapter 4 begins with a brief introductory review on different types of oils viz. plant oils, aromatic oils, vegetable oils, essential oils, fragrance oils, animal oils, aromatic and petrochemical oils. The basic chemical structures of plant and the presence of various acids and fats were discussed in this chapter in a greater extent. The available sources and the parts from which they can be extracted especially in the case of plant oils are discussed clearly. About forty oils of edible / essential / aromatic / plant / medicinal in nature were collected from the local market for the study of the refractive index using optical fiber glass

refractometer. It further dedicates to explain the sample preparation and sample maintenance and also gives the detailed account of the related literature on the edible and medicinal oils. It also describes that how care is taken in the preservation of the samples during the course of the experimentation. Additional data also has been collected as to their scientific nomenclature their botanical family to which they belong, their common names and also the specific gravity of each every oil. A brief description about their availability, cultivation, type of land in which they can be grown, structural features, applications of usage and odor etc have was given in support of the other properties. And finally this chapter dedicates to describe the experimental technique in the determination of the refractive index of both edible and medicinal oils. These values are shown and proved to be in good agreement with the values reported in the literature.

Chapter 5 is devoted for the study of refractive index of human urine at standard pressure and temperature. The discussion initiates to give the detailed description on the human urine. The introductory part of the chapter aims at defining the human urine and its origin in the human body. The chemical composition and constituents of the human urine was presented in the subsequent articles of the chapter in a greater depth. As the main source of the urine in the human body, the structure, the various part of the kidney, and functioning in the process of filtration of the blood and the extraction of urine from the human body has also been described. The functional responsibilities assigned to different parts of the kidney are also been added at this contest. Emphasis is give especially on one of the main components of the urine i.e. on urea and its chemical composition, empirical formula and on its molecular structure. A good number of references, corresponding to the work on the determination of refractive index of human urine have been provided at the end of the chapter. A brief account on how the samples are collected, and as well as maintained during the course of experimentation is also explained in one of the sub topics in the chapter.

The experimental work was started by collecting samples from twenty five persons within the age group of 22 years and 60 years with the random health conditions.

The experimental procedure is discussed on how the refractive index of the human urine can be found using the fiber optic glass refractometer using the standard graph explained in the third chapter. The results are analyzed by plotting the graphs between refractive index, and optical power output collected from the light detector at the terminal equipment. At the end of the chapter the measurement of human urine is thoroughly discussed and the possible advantages have been assessed by comparing with other refractive measuring devices.

. The importance of the present work is explained with possible applications for fiber optic sensors. Fiber optic sensors are being developed and used in two major ways. The first is as a direct replacement for existing sensors where the fiber sensor offers significantly improved performance, reliability, safety and cost advantages to the end user. The second area is the development and deployment of fiber optic sensors in new market areas. For the case of direct replacement, the inherent value of the fiber sensor, to the customer, has to be sufficiently high to displace older technology. Because this often involves replacing technology and the customer is familiar with the improvements must be substantial.

One other area where fiber optic sensors are being mass produced is the field of medicine where they are being used to measure blood gas parameters and dosage levels. Because these sensors are completely passive they pose no electrical shock threat to the patient and their inherent safety has lead to a relatively rapid introduction. The automotive industry, construction industry and other traditional users of sensors remain relatively untouched by fiber sensors, mainly because of cost considerations. This can be expected to change as the improvements in optoelectronics and fiber optic communications continue to expand along with the continuing emergence of new fiber optic sensors.

STUDY OF MULTIMODE FIBER OPTIC SENSOR

CONTENTS

TABLES

FIGURES AND GRAPH

PHOTOGRAPHS

CHAPTER 1

Introduction

1.1 What is a sensor?

Sensor is a device which has the role of converting a change in the magnitude of one physical parameter into a change in the magnitude of a second, different parameter, which can be measured more conveniently, more accurately and more comfortably.

Sensor is nothing but a measuring device which measures any environmentally available parameter. A sensor's sensitivity indicates how much the sensor's output changes when the measured quantity changes. Technological progress allows more and more sensors to be manufactured on a microscopic scale as micro sensors for the improvement of the sensitivity. In most cases, a microsensor reaches a significantly higher speed and sensitivity compared with macroscopic approaches.

One of the important criteria for the measurement of a parameter of any phenomena is the range of measure of the parameter to be measured, the ‘dynamic range’ of a sensor. In most of the cases it is difficult to measure the same parameter of different substances simply with single sensor for which the dynamic range is fixed. Therefore, it is important to define the measuring range of a parameter to be measured with a particular sensor. Thus, the different sensors have different measuring ranges of a particular parameter. Some sensors are developed in such a way that even they can be used to measure the other parameters, called multi-meters.

Design parameters of the sensor are also influenced by the state of the substance whose parameter is being measured, environment around, nature of the parameter i.e. whether the parameter is physical, biological, chemical, optical, magnetic, electrical, mechanical, or acoustical etc. Assessing all the factors aforementioned will provide a clear picture of, how to design a particular sensor. Another advanced character of sensor is that the determination of measurement of different parameters simultaneously by

multiplexing the information within the sensor. This property helps in gathering the information of measurement of several measurands at a time using a single sensor device. At the same time, online measurement of parameters of different measurands will provide the time to time monitoring of the measurands. This character further can be qualified, if the measurements are expressed with display units such as by interfacing the sensor with a suitable and compatible computer unit.

Measurement of parameters when the measurand is in remote with respect to the sensor unit will help knowing the knowledge of the physical quantities from far off, enabling the convenience and comfort in the measurement of distant objects. Sometimes it is necessary to measure the parameter of the measurand in the radiation fields such as war fields, atomic power plants, nuclear power plants, fields near the transmission lines etc. This quality of the sensor to access the information, from otherwise inaccessible regions, enhances the versatility of the sensor functioning in the measurement at hazardous locations of the measurand.

The general characters of a sensor such as cost, weight, portability, reliability, ruggedness, immunity to other field like electromagnetic interference (EMI), radio frequency interference (RFI), immunity to other parameters also play an important role in the final design of any particular sensor. Thus, the sensor designed with adding sophisticated, characters can be a multidimensional, in measuring many parameters with efficiently, conveniently, accurately, comfortably with long lasting character.

1.2 Types of sensors

Sensors can be classified according to the type of energy transfer that they detect as an output. The design of sensors began with mechanical sensors, which were later replaced by electronic ones. Mechanical sensors measure a change in length, size or weight caused by moisture deposition. Disadvantages of mechanical sensors are that they are not readily compatible with modern, electronic digital sensor technology. They also are reported to give inconsistent results. Mechanical sensors are used in the measurement of mechanical parameters such as acceleration, position, pressure, knock, rotation, etc.

Piezoelectric sensing is the ability of certain crystals to produce a voltage when subjected to mechanical stress. The word is derived from the Greek piezein, which means to squeeze or press. The effect is reversible; piezoelectric crystals, subject to an externally applied voltage, can change shape by a small amount. The effect is of the order of nanometers, but nevertheless finds useful applications such as the production and detection of sound, generation of high voltages, electronic frequency generation, and ultra-fine focusing of optical assemblies etc.

Sensors are of many other kinds. Sensors are used to detect or / and measure a huge variety of conditions which include: speed, temperature, level, pressure, motion, rotation, distance, presence or the light/absence of an object and also many more other types. The sensors may be many versions each may be designed to operate with different ranges or they may be used with different sensing principle.

Sensors react to the environment in which they are placed in some cases and this reaction can be used to measure the property intended to sense. A common temperature detector which contains a platinum wire, is known as an RTD (resistance temperature detector), for example. The changes in the resistance can be used for the measurement of the temperature, as the electrical resistance of the wire changes with the temperature. Whenever the variation of an electrical property of a sensing element is a measure of a property being detected, this type of principle will be used by many sensors.

The other sensor types emit a signal and either measure the reflection of the signal bouncing off an object in front of it or measure that how the area reacts to the emission. One of the commonest sensors used today are the inductive proximity sensors. They use to sense the properties of the area in front of it by emitting a small electromagnetic field. The sensors can be used to sense if a door is closed or check if a machine is in the required part of a cycle, or can be used to detect a metal object in front of them. This type of principle is used by many other sensors like magnetic and capacitive. Some sensors measure the light reflected back by sending a light signal. These are mainly the photoelectric type, which come in a multitude of varieties. Some of the reflective mode sensors check if a beam from a reflector being whether interrupted, some direct detection

mode sensors directly detect a reflected signal and the opposed mode sensor detect an interruption of the beam by sending a beam to another sensor. The ultrasonic and radar sensors measure the reflected signal from the object being detected in their operation. Every one is familiar with the way a bat can see and working of the radar guns of police with the reflecting signals and the wonder of unborn babies, which are produced from the reflected ultrasonic signals.

The common mercury thermometer is a very simple sensor. It continuously measures the temperature of the surrounding environment, such as the air or a liquid. The mercury in the bulb is the sensing surface that reacts to the kinetic energy associated with the temperature of the surrounding environment. This physical signal is transformed into a change in the volume of mercury, which then expands up in the glass tube. Temperature gradation markings have been placed along the glass tube to calibrate the expansion. While this device is a non-electrical, analog sensor, most sensors today have a transduction component that creates an electrical signal. Such signals are also analog, but are most often converted into digital signals during the conditioning phase.

Over the years, many other types of sensors have been developed to measure physical properties: motion, light frequency and intensity, pressure, acoustic waves, distance, mass flow, motion, etc. Most of these devices were designed to take individual measurements in time and space. In other cases, though, we desire a broader “picture” such as a two-dimensional image of an object.

Imaging technologies have been developed to take a series of individual measurements that can then be displayed in a rectangular grid, much like a photograph. Medical imaging (ultrasound, X-ray computed tomography, magnet resonance imaging, and positron emission tomography) is one of the more obvious application areas for two- and three-dimensional imaging, although some of these are also used for agriculture and food applications. In most cases, these techniques measure internal mass-density distributions that elucidate material structure.

While sensors are typically placed near the object being measured, there can also be important benefits to sensing objects from some distance. The whole field of remote sensing has developed out of an interest in making measurements of the Earth's surface from airborne, or space-based, observing platforms. Remote sensing allows us to gather measurements over wide geographic areas quickly and easily. These measurements are typically limited to passive reflectance data, although recently airborne laser ranging systems (Lidar) have been developed to accurately measure topography and forest vegetation.

Aside from the physical properties mentioned above, there is also great interest in identifying and quantifying the presence of materials, either biological i.e. bacteria, for example, or chemical i.e. ammonia, for example may be present in the air, in water, or on surfaces. Because we are looking for very small objects like cells or molecules, sensors need to be very sensitive to small quantities, and need to distinguish those elements among a large number of other cells or molecules with high specificity.

Because sensor surfaces must have a high affinity to specific elements, methods and materials developed in the area of nano-scale science and technology are often used to construct sensing surfaces. An interesting aspect of biosensors is that their sensor surfaces often contain some biological entity examples include protein, antibody, enzyme, etc. that is used to “recognize” attach to the target cells.

Unlike remote sensing, biochemical sensors need to be in close proximity to the elements being detected, so that many target cells or molecules can be readily captured. Two of the major research and development efforts for biochemical sensors are: Delivery of a sufficient quantity of the target species to the sensors and assuring high affinity between the sensor surface and the target species.

Electrical and mechanical sensors are widely used to characterize the performance and properties of components and systems, but are also found in household objects. Sensors are electrical or mechanical components that are used to measure a property or behavior of an object or system. Some sensors measure properties directly, other sensors

measure properties indirectly, using conversions or calculations to determine results. Sensors are used by scientists and engineers during research and testing activities, but they can also be found in many household objects, such as temperature sensors in an oven to accelerometers, in an automobile airbag system. Sensors are generally categorized by the type of phenomenon that they measure, rather than the functionality of the sensor itself.

Mechanical sensors measure a property through mechanical means, although the measurement itself may be collected electronically. An example of a mechanical sensor is a strain gauge. The strain gauge measures the physical deformation of a component by experiencing the same strain as the component, yet the change in resistance of the strain gauge is measured electrically. Other types of mechanical sensors include: Pressure sensors, Accelerometers, Potentiometers, Gas and fluid flow meters, Humidity sensors.

Electrical sensors measure electric and magnetic properties. An example of an electrical sensor is an ohmmeter, which is used to measure electrical resistance between two points in a circuit. An ohmmeter sends a fixed voltage through one probe, and measures the returning voltage through a second probe. The drop in voltage is proportional to the resistance, as dictated by Ohm's Law. Other electrical sensors include: Voltmeter/Ammeter, Metal detector, RADAR, Magnetometer, Thermal sensors. Although all thermal sensors measure changes in temperature, there are a variety of types of thermal sensors, each with specific uses, temperature ranges, and accuracies. Some types of thermal sensors include: Thermometers, Thermocouples, Thermistors, Bi-metal thermometers.

Chemical sensors generally detect the concentration of a substance in the air or in a liquid. Some chemical sensors, such as pH glass electrodes are designed to be sensitive to a certain ion. Some other types of chemical sensors include: Oxygen sensors, Carbon monoxide detectors, Redox electrodes. Optical sensors detect the presence of light waves. This could include light in the visible spectrum, or outside the visible spectrum, in the case of infrared sensors. Some types of optical sensors include: Photo-detectors, Infrared sensors, Fiber optic sensors, Interferometers.

There are many other types of sensors that fall into one of the broad categories described here. Some of these sensors include: Radiation sensors, including Geiger counters and dosimeters, Motion sensors, including radar guns and speedometers, Acoustic, including sonar and seismometers, Gyroscopes etc. Sensors can be found in many everyday objects, including touch-sensitive buttons and screens, infrared remote controls, motion-sensitive lighting, and home thermostats.

1.3 Optical sensors

Optical sensors detect in the presence of light waves. This could include light in the visible spectrum, or outside the visible spectrum in the case of infrared sensors. Some types of optical sensors include: Photo-detectors, Infrared sensors, Fiber optic sensors, Interferometers etc. Fiber optic sensors are efficient and highly sensitive measuring devices in which visible light is used as a measuring quantity to measure many parameters of environmentally available objects (measurands) by making use of optical fiber as a guiding medium for its transportation.

Comparing to other sensing devices, sensors using light wave as a sensing standard unit plays an important role in measuring many measurands, fields, and phenomena characters etc. more accurately with very high sensitivity. The reason for this is the measuring standard used in the light wave technique is the light wave itself. The length of the light wave is very small comparing to the other waves like electrical, radio, and micro, waves etc. As the light wave size is very small, it is possible with it to measure the characters of the objects or phenomena whose values are comparable (nearby) with the size of the light wave. And also as the light wave size is almost in Angstrom level i.e. almost one billionth (or one croreth) part of a millimeter, it is possible to measure the parameters of the objects or phenomena whose values (changes) are almost in the same range.

That is how the sensing capacity with the light wave is very high and accurate. To handle this much small object (light) is again a difficult task, but fortunately we have a choice of handling it by using a fiber optic wire, making the light wave to confine within the fiber wire.

The light wave and the fiber wire together along with terminal equipment form a system, the fiber optic sensor (communication) system. The design of such device changes not only with respect to the measurand it measures, but also to the changes in the characters like, wavelength, intensity, polarization, and phase of the wave when it interacts with the measurand. On the basis of the change (modulation) in the character of the carrier wave, the sensors can be classified into four types, they include: Intensity modulated fiber optic sensors, Phase modulated fiber optic sensor, Polarization modulated fiber optic sensor, Wavelength modulated fiber optic sensor. In the case of intensity modulated sensors the intensity of the light that is transmitting through the fiber will be varied according to the changes in the measurand parameter.

In the case of phase modulated sensors, the phase of the light wave changes with respect to a corresponding change in the measurand parameter. Similarly polarization and wavelength of the light wave varies according to the variations in the measurand parameter in the case polarization modulated and wavelength modulated sensors respectively. However, out of these four, the intensity and phase modulated ones offer the wide spectrum of optical fiber sensors. The Table 1 indicates the summarized optical modulation schemes by the measurand.

Table 1.1: Summarized optical modulation schemes by the measurand

Sensing technique	*Type of information*	*Physical mechanism*	*Detection circuitry*	*Typical examples*
Intensity modulation	By detecting the changes in the intensity	emission, absorption or R.I. change of transmitted light	Analog / digital	Pressure, displacement, R.I., temperature, liquid level etc.
Phase modulation	By detecting phase changes	Interference between signal and reference signal in an interferometer	Fringe counting	Pressure, rotation, magnetic field etc.
Polarization modulation	By detecting the changes in angle of polarization	Changes in gyratory optical tensor	Polarization analyzer and amplitude comparison	Magnetic field and current measurement of high voltage transmission lines
Wavelength modulation	By detecting the change in the wavelength	Spectral dependence variation of absorption and emission	Amplitude comparison at two fixed λ's	Temperature measurement

During early seventies, when technology of fibers for telecommunication was evolving, it was observed that the transmission characteristics of optical fibers are highly sensitive to certain external perturbations like bends, micro- bends, pressure, strain etc. A great deal of effort was made at that time to reduce the sensitivity of signal carrying optical fibers to such external effects through suitable fiber designs.

On this observation of sensitivity of optical fibers to external perturbations, an alternate thought began to exploit this sensitivity of optical fibers to construct a large variety of sensors and instruments. Some of the key features of this new technology which offer substantial benefits as compared to conventional electrical sensors are:

- Sensed signal is immune to electromagnetic interference (EMI) and radio frequency interference (RFI).
- Sensing system is safe in explosive environments.
- Highly reliable and secure with no risk of fire or spark.
- They occupy low volume and are light in weight.
- As a point sensor they can be used to sense measurands otherwise inaccessible.
- Potentially resistant to nuclear or ionizing radiations.
- High voltage insulation.
- Affords remote sensing by locating the sources and detectors, far away from the sensor head.
- Large band width offers multiplexing of a large number of individual sensors in fiber network for continuous sensing along the fiber length called distributed sensing.
- Chemically inert and mechanically flexible.

These advantages were sufficient to attract intensive R & D effort around the world to develop a new class of sensors based of fiber optics. This has eventually led to emergence of a variety of fiber optic sensors for accurate sensing and measurement of physical parameters and fields include: refractive index, pressure, temperature, liquid level, liquid PH, antibodies, electric current, rotation, displacement, acceleration, acoustic field, electric field, magnetic field, strain and so on. Initial developmental work

had concentrated predominantly on military applications like fiber optic hydrophones for submarine and under sea applications and gyroscopes for applications in ships, missiles and aircrafts. Gradually, a large number of civilian applications have also picked up. At present they are playing a major role in industrial, medical, aerospace, and consumer applications.

Fiber optic sensors can be broadly categorized into two classes on the basis of the interaction of the light with the measurand. They are Intrinsic type and Extrinsic type sensors. In the case of intrinsic sensors, modulation of the carrier signal takes place within the fiber thereby the transmission characters of the fiber changes, resulting a change in the output signal. One or more of the physical properties of the guided light, e.g. intensity, phase, polarization and wavelength is modulated by the measurand. In the case of extrinsic sensors, modulation of the carrier signal takes place out side the fiber, and where in, the fibers simply act as conductors of light to transport light signal to and from the sensor head.

Fiber optic sensors can also be classified on the basis of their application: physical sensors (e.g. measurement of temperature, stress, etc.); chemical sensors (e.g. measurement of pH content, gas analysis, spectroscopic studies, etc.); bio-medical sensors (inserted via catheters or endoscopes which measure blood flow, glucose content and so on). Both, the intensity types and the interferometric types of sensors can be considered in any of the above applications.

Intensity modulated fiber optic sensors can again be classified into many. Some of them include: Intensity modulation through misalignment, intensity modulation through shutter, **i**ntensity modulation through reflection, **i**ntensity modulation through evanescent coupling (Refractive Index) Sensor, intensity modulation through bending, intensity modulation through micro bending, intensity modulation through change in R. I., intensity modulation through temperature, intensity modulated fiber optic distributed sensor.

1.4 Survey of literature

Measurement of chemical concentration has been reported in literature since 1946 using optical fibers. Since then optical fibers found applications in biomedical and environmental [1-4], chemical [5-8], biochemical [9-12] sensing.

The bending radius of the optical probe and the influence of the core diameter of the fiber and the refractive index of the fluid on the sensors sensitivity are experimentally evaluated in the description of a fiber optic evanescent field absorption sensor which is based on a U – shaped sensing probe [13].

In an another investigation, the effect of probe clearance on the rising velocity and chord length of bubbles in a bubble column was examined in measurement with the two-channel U – shaped optical fiber probe method [14].

Khijwania and Gupta [15] presented a comparative experimental study of the fiber optic evanescent field absorption sensor based on straight and U – shaped probes.

Biagi et al [16] explained the employment of fiber optics as waveguides in laser generation of ultrasonic waves for Non Destructive Evaluation (NDE) has the advantages of very high miniaturization and geometrical versatility, electromagnetic compatibility, ionizing radiation safety, the possibility of keeping the optoelectronic unit away from the test object.

Singh et al. [17] described a sol – gel derived coating U – shaped optical fiber sensor for measurement of critical micelle concentration of surfactants.

Sing and Ogita [18] described the detection of critical micelle concentration (CMC) in surfactant solutions using uniform and U – shaped optical fiber in sensing region.

Milan Sak – Bosnar et al [19] stressed out an overview on non – electrochemical surfactant sensors is given with special attention to work published since 1993 and the importance of surfactants in modern biotechnology.

Khijwania et al. [20] proposed polymer coated U – shaped fiber optic evanescent field absorption sensor having high sensitivity and linear dynamic range.

Gupta and Ratnanjali [21] reported a U – shaped fiber optic humidity sensor based on the moisture dependence absorption of light by the phenol red doped poly-methyle metha-crylate (PMMA) film over a small portion of the U – bent of the plastic clad silica (PCS) fiber.

Khijwania et al. [22] experimentally investigated the influence of the bending radius of the probe on the sensitivity of the fiber optic evanescent field absorption sensor based on the U – shape probe.

Argha Benarjee et al. [23] described an optical fiber which shown to sense refractive index of a liquid in which the fiber is partially striped of its cladding, in which the uncladded sensing region is immersed in a liquid over a wide range of refractive index and to a high degree of precision.

Gupta et al. [24] studied fabricated and characterized U – shaped fiber optic pH probes utilizing evanescent field absorption spectroscopy and dye doped sol – gel immobilization technology presented and the influence of bending radius of the probe and the numerical aperture of the fiber on the sensitivity of the sensor.

Ogita et al. [25] described a simple U – shaped optical fiber probe, for critical micelle concentration measurement, using evanescent adsorption and characterization.

Singh et al. [26] a sol – gel derived coating U – shaped active cladding optical fiber sensor for measurement of critical micelle concentration of surfactants has been studied.

A patent [27] explained an apparatus for measuring the refractive index of fluids comprises a substantially U- shaped sensor rod made of a transparent material and submersible in the fluid.

Singh et al. [28] studied the optical fiber chemical sensor mainly based on adsorption or absorption technique for the measurement of critical micelle concentration (CMC).

Cesar Elosua, et al. [29] described a classification of the fiber optic sensors has been made according to the sensing mechanism taking into account the sensing material and the implementation of them for the detection of volatile organic compound (VOC).

Wolfbeis et al. [30] described a Fiber optic sensors (FOS) for defined chemical, environmental, and biochemical significance and to new schemes and materials are by.

Jagdish et al. [31] classified various types of fiber optic sensors with relevant constructional geometries and graphical representations by.

The specification report [32]on optical sensors details the associated requirements of optical sensors for such applications where focus is given on wearability of the whole monitoring system, through integration of the sensors into wearable textiles, making it compatible for ambulatory monitoring and prevention of SIDS.

Jayanth Kumar et al. [33] presented an intensity modulated intrinsic fiber optic sugar sensor for on – line determination of the concentration of sugar content in sugarcane juice in sugar industry.

Thomas Lee et al. [34] discussed the details of fabricating an off – line fiber optic sensor (FOS) based on evanescent wave absorption for detecting trace amounts of Fe^{3+} in water.

Suresh Kumar et al. [35] described a fiber optic technique for detecting trace amounts of nitrite compounds in water, based on evanescent field absorption in a test solution formed by the reaction of nitrite compounds in water with suitable chemical reagents.

Thomas Lee et al. [36] demonstrated the possibility of using a permanently micro-bent bare optical fiber for detecting chemical species.

Turan et al. [37] described a multimedia document about the basic theory of applied photonics and the measurement supporting web – based interactive fiber optic sensor.

A new approach [38] for the measurement of a refractive index is presented, following the introduction of a novel feature based on the selection of a large number of angles of incidence along a direction of symmetry at the prism ambient interface, without moving the incident beam.

Turan et al. [39] discussed the development of work of a flexible fiber optic refractometer for measuring the refractive index of aqueous solutions as the concentration or density of a solute increases, the refractive index increases proportionately.

Venkateswara raju et al [40] reported the possibility of devising a simple but reliable temperature sensor for liquids using a plastic fiber with a portion of the cladding is removed along its length.

Shiquan et al [41] reported the porous sol gel silica (PSGS) membrane coated on the surface of an optical fiber used as a transducer for sensing humidity level in air and a PSGS membrane doped with an ammonia indicator dye has been coated on an optical fiber to sense ammonia in air.

Choudhary et al [42] reported the investigation of fiber optic evanescent field absorption sensor in respect of the concentration of dye as well as its ph value.

Ramponi et al [43] illustrated a new method for the determination of the refractive index of liquid samples, based on Cerenkov second harmonic generation from suitable planar waveguides.

Shukla et al [44] reported the various physicochemical principles of MgO film obtained by using a precursor prepared by sol-gel technique. The aim of this work is to produce films with nano size particles so as to employ them for sensor applications, as adsorption in such films increases many folds due to increase in surface area.

Jayanth Kumar et al [45] described a method to detect the sugar concentration in a sugar solution using a cladding removed plastic fiber made of polymethyle-methacrylate (PMMA) of 1 meter length.

Gupta et al [46] presented the fabrication and characterization of U – shaped fiber optic pH probes utilizing evanescent field absorption spectroscopy and dye doped sol – gel immobilization technology.

Geetha et al [47] reported a side polished polymer optical fiber based on refractive index sensor with wide sensing range and a method for tuning the sensitivity and sensing range by selective excitation at higher launching angles.

Gupta et al [48] presented a long – range fiber optic PH sensor prepared by immobilizing a mixture of three PH – sensitive dyes on the surface of the fiber core using sol – gel technology.

Sharma et al [49] presented the fabrication and characterization of side – polished single mode optical fiber PH sensor utilizing evanescent field absorption spectroscopy and dye doped sol – gel immobilization technology.

Gupta et al [50] presented a fiber optic pH sensor based on evanescent wave absorption prepared by removing the cladding over a small length in the middle portion of the fiber.

Sing et al [51] explained the detection of critical micelle concentration (CMC) in surfactant solutions using an optical fiber based on adsorption effect in sample solution.

Schoch et al [52] reported a fiber optic probe for in situ sensing of liquid level, concentration and / or phase change contains the optical and electrical components as well as a reference fluid so that the components are at the temperature of the fluid to be monitored.

Cramp et al [53] described an apparatus for detecting changes in chemical or physical parameters, comprises a sensing optical fiber having a core surrounded by a relatively sensitive cladding the absorption spectrum of which varies with changes in chemical or physical parameters when these are applied to the cladding, and a transmissive optical fiber having a core surrounded by a relatively insensitive cladding for connecting at least one of the ends of the sensing fiber arm to a remote light source and a remote detector.

Fields et al [54] reported a micro-bend sensor in which the micro-bend of optical fiber is exploited to measure many physical parameters / physical variables.

Nelson et al [55] demonstrated the vibration induced intensity modulation of light in bend fibers.

Lagakos et al [56] reported a micro-bend generic sensor to determine several environmental changes like temperature, acceleration, electric and magnetic fields.

Spenner et al [57] reported a fiber optic refractometer to detect the refractive index of liquids. The same mechanism is used to measure the acid levels in batteries.

Kumar et al [58] explained the use of a bare tapered multimode fiber as a fiber optic refractometer, in which a small portion of the plastic jacketing is removed from the PCS fiber. This bare portion of the fiber is then converted into a taper by heating and immersing the taper zone in liquid of refractive index n_2 less than that of refractive index of core n_1.

Kee et al [59] demonstrated a low – loss, long range single – ended distributed optical fiber sensor to measure both temperature and strain simultaneously and unambiguously by using the Landau placzek ratio and cascaded Mach – zehnder interferometric filters.

Schullz et al [60] demonstrated a fiber optic Bragg grating configuration for the measurement and monitoring / recording with a high level of completeness the actual seismic response of structures and non – destructive seismic damage assessment techniques based on dynamic signal analysis.

Tsutomu et al [61] demonstrated a thermally insensitive pressure measurement upto 300 degree c utilizing fiber Bragg gratings written onto a side – hole single mode fiber. The resulting temperature sensitivity is about 300 times lower than normal FBG's.

Kee et al [62] explained a high apatial resolution single – ended spontaneous Brillouin – based distributed temperature sensor for a 500m length of single – mode silica fiber. Using a short pulse – width laser source at 1.5µm, measurements down to a spatial resolution of 20cm and temperature resolution of 4.4°c were achieved.

Wood et al [63] demonstrated the techniques for using optical fibers to monitor the cure of composite materials in real time during manufacture and to monitor the in service structural health of composite structures.

Lees et al [64] demonstrated a distributed optical fiber temperature sensing (DTS) for monitoring the temperature at many points without necessitating the accurate positioning of individual desscrete sensors based on spontaneous brillouin scattering.

Wait et al [65] reported a distributed temperature sensing based on brillouin scattering which offers considerably increased range beyond the theoretical limit of the spontaneous Raman based sensor.

Kee et al [66] described both theoretical and experimental results obtained in an investigation of a new technique for increasing the dynamic range of 1.65 µm optical time domain – reflectometer (OTDR) systems.

Lees et al [67] reported latest results on a compact, diode pumped optical fiber distributed temperature sensor based on brillouin scattering.

Fernando et al [68] presented an overview of the deployment of optical fiber sensors in a selected range of applications including a general introduction to optical fibers and a review of the sensing mechanisms that are available to monitor strain, temperature, pressure, chemical species, damage, acoustic emission and the use of optical fiber sensors in medical applications.

Heredero et al [69] described a micromechanical optical fiber current sensor. A measurement range of 0 – 70A and a minimum detectable intensity of 20mA were obtained with this sensor.

Lee et al [70] demonstrated an interferometric fiber optic sensor using a light emitting diode (LED) as the optical source. The predicted behavior is confirmed by experiments in which the temperature of the sensor FPI is changed while that of the reference is held constant.

Kee et al [71] demonstrated a fiber optic filtering system for simultaneous distributed strain and temperature sensing for a range of 15Kms based on brillouin intensity and frequency shift variations in optical fibers.

Eric udd et al [72] explained the embedding of single and multi – axis optical fiber strain sensor within the liquid molded load cells for the measurement of shear – strain and load within bridge bearings to monitor the health and longevity of the structure.

Schulz et al [73] demonstrated a fiber bragg grating sensor system in smart structure applications for measuring multi-axis strain, transverse strain, temperature, bridge scouring, ice, and traffic flow.

Marcin et al [74] calculated the sensitivity of phase and group modal birefringence to hydrostatic pressure versus wavelength in two birefringence holey fibers of different construction.

Udd et al [75] outlined improvements that have been made in a multi-axis fiber grating strain sensor that can also be used in certain cases to measure temperature. The current status and future prospects for these sensors are outlined.

Waclaw et al [76] presented the method for measurement of modal birefringence and its sensitivity to temperature and hydrostatic pressure in the spectral range from 633 to 843nm by using interferometric techniques.

Udd et al [77] demonstrated a mechanism for measuring transverse strain and birefringence using fiber optic gratings, writing fiber gratings onto polarization maintaining optical fiber. For bridges and other civil structures, this opens up a series of new opportunities where multiaxis strain sensing may be effectively used for monitoring the health of the system.

Gareth et al [78] reported a high power Q – switched erbium doped fiber laser, using a novel, large mode area, single transverse mode fiber. Peek powers in excess of 4kw, and pulse widths of 10ns have been reported at a repetition rate of 500Hz.

Huai et al [79] demonstrated a novel Raman - based distributed temperature sensor (DTS) system using a laser source at a wavelength of 1.65μm, utilizing conventional telecommunication single mode silica fibers over a range exceeding 10Km.

Kee et al [80] proposed a novel method of increasing the dynamic range of a 1.65μMotdr system through the use of delayed Raman amplification within the sensing fiber. By delaying the pump pulse with respect to the OTDR pulse, amplification of the latter may be delayed by tens of kilometers.

Kee et al [81] described a compact design based on Raman shifting of the output of an Erbium – doped Q – switched fiber laser operating at 1.5µm for obtaining a pulsed source at 1.6µm. The temperature measurement extracted from the antistokes Raman signal at 1.5µm was made over a sensing range of 10.1Km, with a spatial resolution of 10m and temperature resolution of 4°c.

Kee et al [82] presented an efficient technique to measure both the intensity and frequency shift at every point along the sensing fiber with a low loss filtering device utilizing two measurements, it is possible to compute accurately the strain and temperature profile.

Krska et al [83] described the development and validation of a new MIR fiber optic physicochemical sensor system for the continuous in situ analysis of chlorinated hydrocarbons (CHCs) in water. This setup enables the simultaneous in situ detection of the most common chlorinated hydrocarbons in concentrations between 1 to 50 mg / L in water by employing a fiber sensing part only 10cm in length.

Conzen et al [84] described a fiber optic evanescent field absorbance sensor (EFAS), consists of a commercially available silicone – clad quartz glass fiber sensing element coiled on a Teflon support. In this study aqueous solutions of typical drainage – water contaminants like dichloromethane, chloroform, and trichloroethylene were measured in the 900 – 2100nm spectral range.

Klunder et al [85] reported a coiled fiber optic chemical sensor for the remote detection of volatile organic compounds, such as trichloroethylene (TCE), 1, 1-dychloroethylene (DCE), and gasoline, in aqueous solutions. The temperature dependent absorption is found to be linear and is proportional to the coefficient of the absorption of the cladding material.

Blair et al [86] examined the diffusion rates of various polar and non polar analytes in dimethylsiloxane with the use of a commercially available 200µm silica – core / 300

μm silicon – cladding fiber as the optical element for evanescent wave spectroscopy in the near – infrared spectral region.

Egami et al [87] demonstrated a new type of fiber optic pH sensor, which is the application of evanescent wave spectroscopic technique. The result of experiment was of 1.0 in pH.

Merschman et al [88] described a method for the determination of aromatic contaminants in water samples that combines solid – phase microextraction and ultraviolet evanescent wave absorption (UV – EWA) spectroscopy. This method shows promise in determining the total aromatic concentrations of water samples contaminated with gasoline.

Sukhdev roy et al [89] presented a simple, intrinsic intensity modulated fiber optic sensor for determining adultration of petrol and diesel by kerosene based on modulation of intensity of light guided in the fiber due to change in the refractive index of the cladding formed by adultrated fuel and the phenomenon of evanescent wave absorption.

Dunkers et al [90] explained the construction and implementation of a high – index silica-based fiber optic mini-bundle sensor with a Fourier transform near infrared spectrometer in the spectral region from 10,000 to 4500 cm.

Gupta et al [91] studied the response of the fiber optic evanescent field absorption sensor and analyzed experimentally. The dependence of evanescent absorbance on sample (dye) concentration has been found to be nonlinear, in contradiction to theoretical predictions.

Zaatar et al [92] reported a fiber optic evanescent wave sensor for the monitoring of air pollution and species concentrations in various environments. This sensor offers the possibility to be linked to fiber optics for remote measurements and dangerous locations.

Sekimoto et al [93] developed a new optical fiber hydrogen sensor which uses the absorption change of the evanescent field in the clad region. The sensor developed has potential to measure the spatial distribution along the fiber line, unlike the traditional hydrogen sensors that measure the concentration of a certain spatial point.

Kishen et al [94] developed a fiber optic biosensor (FOB) to monitor mutans streptococci activity in human saliva. The investigation highlights the potential benefits of this sensor to monitor mutans streptococci activity in saliva.

Wong et al [95] reported a sol – gel derived film doped with beta – cyclodextrin fiber optic evanescent wave fluorosensor for detection of riboflavin. The sensor is easy to operate, simple to construct, and requires a minimal number of optical components.

Kalowatz et al [96] introduced an innovative etching technique for tapering silver halide fibers. The evanescent field sensitivity is raised by more than one order of magnitude, demonstrated by calibration curves of tetrachloroethylene in hexane recorded with a tapered sensor fiber coupled to a Fourier transform infrared (FT – IR) spectrometer.

Woerdeman et al [97] designed a fiber optic cure sensor based on evanescent wave fluorescence spectroscopy to probe the inter-phase region of glass reinforced composites. In this study, a model based on mode coupling theory is developed to determine whether the fiber provides information about the bulk resin or the inter-phase between the fiber and the matrix.

Thomas lee et al [98] described the design and fabrication of a micro-bent fiber optic sensor that can be used for pH sensing. This paper demonstrates how a bare plastic fiber can be modified for pH sensing in a simple and cost effective manner.

Yeh et al [99] explained the construction of a fiber optic evanescent wave absorption sensor based on an organo functionalized silica cladding. The sensor was used to

quantify the cu (II) content in samples and has the dynamic range of 0.5 – 100ppm and a detection limit of 56ppb.

Suresh Kumar et al [100] presented the design and development of a cost – effective, simple, sensitive and portable LED based fiber optic evanescent wave sensor for simultaneously detecting trace amounts of chromium and nitrite in water. The performance and characteristics of this system establish the usefulness of the technique for detecting very low concentrations of the dissolved contaminants.

Preejitha et al [101] described a novel method and instrumental system to determine the total protein concentration in a liquid sample. The response time and reusability of the FOPS are evaluated. This unique sensing method presents a sensitive and accurate platform for the quantification of protein.

Okazaki et al [102] characterized a fiber optic hydrogen gas sensor using catalyst – supported tungsten trioxide (WO_3). The high sensitivity in the low temperature range together with the line –sensing feature is very promising for the continuous monitoring of hydrogen leak for fuel –cell cars and other equipments utilizing hydrogen.

Mitsuhiro iga et al [103] described a noble sensing technique using a hetero-core structured fiber optic sensor based on evanescent wave interaction for the purpose of acidity measurements. The sensor response exhibited remarkable increases of absorption with increasing acidity at the wavelength of around 520nm. The sensitivities of 11.5 and 14.2 dB / m have been obtained for HNO_3 and H_2SO_4 solutions respectively.

Kharat et al [104] proposed theoretically the designing of single mode and multimode optical fiber sensing probes, which can be prepared by removing a few centimeters of cladding near the distal end of the step index optical fiber. It was found that step etching and tapering enhances the strength and penetration depth of the evanescent wave significantly.

Petr Tobis et al [105] investigated several approaches for fiber optic evanescent wave detection of small amounts of liquid hydrocarbons. A novel approach employing straight fibers coated with a thin siloxane coating and an output mode filter is described as a promising technique for increasing the detection sensitivity of fiber optic evanescent wave sensors to petrol fuels.

Marasu et al [106] discussed the structure of the sensing element of a gold deposited optical fiber sensor and quantitative analysis of various alcohols. The response curves of the sensors were calculated from SPR theoretical equations while considering of the distribution in the thickness of the deposited gold films.

Lyons et al [107] reported an optical fiber sensor system capable of detecting contaminants (e.g. particles, inorganic or organic species) in water and other fluids. In this article experimental results are presented for a single optical fiber sensor located at a distance of 150m from the transmitted / receiver of the system.

King et al [108] reported a three – sensor element multipoint optical fiber sensor system capable of detecting varying ethanol concentrations in water for use in industrial process water system. The sensor system is interrogated using a technique known as optical time domain reflectometry, as this method is capable of detecting attenuation over a distance.

Reilly et al [109] demonstrated two novel external cavity lasers experimentally. The first utilizes a Bragg grating fabricated in highly birefringent optical fiber and offers the ability to switch between modes that are separated in polarization and wavelength. The second utilizes two spatially separate Bragg grating fabricated in mono-mode fiber.

King et al [110] reported a dial element multipoint optical fiber sensor system capable of detecting ethanol in water supplies is reported. The sensor system utilizes a U-bend configuration for each sensor element in order to maximize the sensitivity of the system and is interrogated using a technique known as optical time domain reflectometery.

Raichlin et al [111] reported a novel fiber optic evanescent wave spectroscopy (FEWS) method for measuring the absorption spectra of samples in contact with a segment of an optical fiber that serves as a sensing element. The theoretical results were verified experimentally by measurements of methanol and water.

Chen-chun et al [112] reported a the development of a fiber Bragg grating (FBG) interrogation system that is capable of detecting independently and simultaneously the two orthogonally polarized signals reflected from a polarization maintaining (PM) FBG. The interrogation system is capable of decoding the complex spectral responses of a PM FBG subjected to a transverse load.

Jan Turan et al [113] described the development of a flexible fiber optic refractometer for measuring the concentration of aqueous solutions, which bases on that as the concentration or density of a solute increase, the refractive index increases proportionately.

Ilev et al [114] reported a new simple auto collimation scheme of a fiber – optic refractometer, which allows determining the refractive index and dispersion of solid – state and liquid optical materials with accuracy exceeding 5.10^{-5}.

Zhang et al [115] reported a novel fiber optic sensor, which is capable of accurately measuring yeast concentrations in suspension over a range of 0 to 16 g/l. The sensor reported relies upon light being radiated through the cladding of one fiber and detected at the end of an adjacent receiving fiber.

Arrue et al [116] analyzed the redistribution of light power and the radiated power along a bent section of a plastic optical fiber (POF). A theoretical approach for understanding and hence optimizing, the major factors that affect the behavior of sensors utilizing losses in fiber bends is reported.

Anna et al [117] given an overview of fiber optic sensors for in vivo biomedical monitoring with particular attention to the advantages that these sensors are able to offer compared to the performance of traditional devices.

Maisenholder et al [118] demonstrated a monolithically integrated optical sensor chip for measurement of analyte refractive index changes. The monolithic optical sensor consists of a Mach-Zehnder interferometer with an interferometer with an integrated DBR laser source, transparent semiconductor waveguides a modulator and an integrated waveguide detector.

Joel et al [119] reported a simple, compact, and low cost optical fiber refractive index (RI) sensor. It consists of a multimode fiber in which a short section of standard single mode fiber (SMF) is inserted. The device can operate at different wavelengths, which makes it attractive for diverse applications.

Ainhoa et al [120] developed some sensitive and versatile evanescent wave sensing systems featuring polished optical fiber based sensor designs with low cost light sources for the measurement of temperature, relative humidity and pH. The work describes the fabrication of three types of sensors based on standard silica, single mode fibers.

Anderson et al [121] developed an immunoassay system which was not only rapid and sensitive but also highly versatile. Use of long optical fibers allows a variable distance between the assay location and the optoelectronic components.

Mac craith et al [122] reported an intrinsic evanescent wave fiber optic sensor for oxygen. The sensor exhibits excellent performance using blue LED excitation and silicon photodiode detection, and establishes the viability of low cost portable sensor devices based on the sol gel process.

Preejitha et al [123] described a novel method to measure the total serum protein concentration. The sensor offers a rapid, single step method for quantifying protein concentrations without destroying the sample. This unique sensing method presents a sensitive and accurate platform for the quantification of protein.

Alekseenk et al [124] developed a technique for measuring the frequency responses of the thickness of a film of liquid at difficulty accessed locations and on intricately

shaped objects on the basis of reflection type fiber optic sensors. The static, dynamic, and angular characteristics of these sensors are presented.

Katov et al [125] reported a new method of detecting phase modulation, based on using an "external" optical waveguide interferometer. This detection is weakly dependent on the length, position, and external conditions of the propagation channel for the phase modulated light and, in many cases may prove more efficient than conventional method of constructing phase modulated fiber optic systems.

David et al [126] demonstrated a fiber optic heterodyne vibrometer configuration based on the use of birefringent optical fiber components. The heterodyne processing is moved to the receiving section of the interferometer, reducing the optomechanical stability requirements of the system and enabling optimization of the reference to signal beam ratio intensity.

George et al [127] demonstrated the use of an optical fiber as a position sensitive detector in the photothermal deflection technique for thermal characterization of solids. To validate the sensitivity and accuracy of the setup, the thermal diffusivity of an n-type indium phosphide wafer is measured and compared with the literature values.

Stephen et al [128] reported an interferometric fiber grating interrogation system utilizing a depolarized erbium ring laser used to interrogate transversely strained gratings written through the polyimide coating with 1mm spatial resolution, and the interferometric results were compared to waveforms tsken using a broad band source and OSA.

Saeed et al [129] reported a sensor in which an optical fiber is tapered, preferably adibatically, and has a material coated on it for chemical bonding with fluorophores. When the fluorophores couple with the material, evanescent radiation generated fibers causes the fluorophores to fluoresce, and the fluoroscence is coupled back into the fiber.

Hirsch feld [130] reported an optical waveguide particularly useful in assay apparatus employing total internal reflection of excitation radiation at the interface between the waveguide and a surrounding liquid phase of lower index of refraction.

Mc Intyre et al [131] demonstrated a low cost, durable, and accurate fiber optic temperature sensor in operating fuel cells. The sensor platform, capable of high spatial resolution thermal mapping of the membrane electrode assembly and provide precise thermal data to fuel cell developers for modal verification.

Khaliq et al [132] reported a sensor, which surrounding a long period grating (LPG), fabricated in a standard optical fiber, with a material with a high thermo-optic coefficient enhances the temperature sensitivity of the LPG. Temperature sensitivities as high as 19 nm $°C^{-1}$ has been reported.

Dwyer et al [133] investigated the temperature dependence of the strain sensitivity of fiber Bragg gratings written into a number of different fiber types. It was found that the strain response changed on average by 0.21 ± 0.03 fm $\mu\varepsilon^{-1}°C^{-1}$ over a range of temperatures between 100 - 400°C.

James et al [134] reported a sensor in which the thermal response of the attenuation bonds of an optical fiber long period grating was monitored over a temperature range of 4.2 – 280K. a linear dependence of the central wavelength of the bond, of gradient 0.2nm k^{-1}, was observed over the range 77-280K.

Olszak et al [135] presented a technique, which allows simple and potentially automated determination of the optical path length imbalance in ESPI systems that utilize source wavelength modulation to obtain phase shifting. The method is based on modulating the emission wavelength of the laser synchronously with the framing rate of the CCD / image processing board and recording the average speckle intensity of the image.

Duncan et al [136] reported a method for calculating distance from fiber optic tip of sensor to reflective surface by high pass filtering fringe signal gathered by a spectrometer, calculating power spectral density of the filtered signal, and using a calibrated distance vs. peak spectral density wavelength curve to determine the measured distance.

Duncan et al [137] reported a fiber optic pressure sensor which includes a light source, a reflective sensor diaphragm movable in accordance with pressure in the medium and an optical fiber coupled to the light source for delivering a first wave-front of light to the reflective sensor diaphragm.

Potter et al [138] reported a simple signal processing technique for interrogating miniature low finesse Fabry-perot interferometric sensor. The technique enables broadband signals to be recovered at their fundamental frequency for signal amplitudes up to Π. The technique is demonstrated using a dual wavelength source derived from a multimode laser diode, to obtain quadrature outputs from a 20µm cavity, which are processed using a analogue electronics.

Duncan et al [139] described improved transmissive magneto optical sensors that may be used to determine the magnitude and phase of a magnetic field surrounding a conductor, and when in contact with the conductor, the surface temperature of the conductor. They preferably include cylindrically symmetrical components, thereby making the sensor readily mass producible.

Duncan et al [140] reported a system for gathering transmitting, and storing data captured from remote monitoring sites positioned in the field. The system has specific applicability to distributed chemical sensing and reporting, and distributed power monitoring and reporting.

1.5 Genesis of the investigation

The Abbe's refractometer is used in many areas of interest worldwide, but there are some problems. The measuring prism in many refractometers is constructed out of soft

glass that is easily scratched. If the glass prism is touched by any hard and / or sharp object, such as a pipette tip or metal spatula, it will immediately be damaged. The sealer around the prism may be degraded by certain solvents. The refractometer should not be cleaned or used with the following solvents such as Dimethyleformamide, Dimethylacetamide, Phenols, Acetic acid solutions. Other solvents may degrade the sealer at slower rates and should not be used as the normal cleaning solvents such as tetrahydrofuran, simple esters, and acetone. Strong acids and bases will etch the prism glass. There are other problems associated in taking readings with Abbe's refractometer. There is no obvious distinction between light and dark regions. Volatile samples may evaporate before taking a reading. The illuminating light should be adjusted properly. The borderline between light and dark regions never becomes sharp, even after adjusting the compensator dial. Thus the refractive index measured is not correct or at least not consistent with what is expected.

A thorough literature survey and on the basis of the very extensive study of the available old and the latest refractometers, it is decided and proposed to carry out the research work on designing a new refractometer to measure the refractive index of any given liquid in the dynamic range of 1.33 to 1.50 at normal pressure and temperatures from 30°C to 80°C. The refractometer developed can be a versatile, and can be a sophisticated and can be unique for many good reasons. The refractometer is developed making use of the latest fiber optic technology and its role in designing of the fiber optic sensor principles. The principle mechanism and the component assembly are entirely different from that of the existing methods and it is expected to offer very high sensitivities along with many other advantages. The measuring standard in this method is naturally and artificially available sodium light consisting of very fine dimensions it certainly yields high degree of sensitivity. The main idea behind sensor design is to aim at avoiding the drawbacks and set backs faced by the old and the present day generations of the refractometers.

It gives readings instantaneous without any ambiguities on a digital display meter. Most of the advantages offered by the optical fiber technology in the field of communications, can all be extended in the present investigation. It is expected to add up

a number of sophisticated features both internally and externally within a short span of time, in future. On the basis of these lines, it is concluded to take up this challenging task of designing a fiber optic glass refractometer.

References

[1] Holst G, Mizaikoff B, Fiber optic sensors for environmental sensing. Handbook of optical fiber sensing technology, Edited by J.M. Lopez – Hgnera, John Wily and sons Ltd. 2001:729-749.

[2] Doetrocj AM., Measurement of pollutants, chemical species, water environmental research 1996:68: 391-406.

[3] Schowtzer G., Optical sensing of hydrocarbons in air or in water using UV absorption in the evanescent field of fibers, Sensors and actuators B 1997: 38: 150-153.

[4] Mizaikoff B et al. Infrared fiber optic gas sensor for chlorofluorohydrocarbons", Vibrational spectroscopy 1995: 8: 103-108.

[5] Wolfbeis, Fiber optic chemical sensors and biosensors, CRC press, Boca Raton, Florida, 1991, 1992: vol. 1 & 2.

[6] Stewart G, Jin W, Culshaw B. Prospects for fiber optic evanescent field gas sensors using absorption in the near infrared, sensors & actuators B 1997: 38: 42-47.

[7] Chan K., Ito H., An optical fiber based gas sensor for remote adsorption measurement of low level methane gas in near infrared region, J light wave Technology 1984: 2: 234.

[8] Wolfbeis OS, Posch HE., Ffiber optic fluorescing sensor for ammonia, Anal. Chim. Acta. 1986:185:321.

[9] Rowe – Taitt CA, Liglaer FS., Ffiber optic biosensors - Hand book of optical fiber sensing technology, Edited by J. M. Lopez Hignera, John Wiley & Sons Ltd., 2001:687-700.

[10] Ferguson JA, Boyles TC, Adams CP, Walt DR, Fiber optic DNA biosensors micro-array for the analysis of expression, Nature Biotechnology 1996: 14: 1681.

[11] Healy BG, Li L and watt DR, Multi-analyte biosensors on optical imaging bundles. Biosensors & Bioelectronecs, 1997: 12: 521.

[12] Baker SLR, Kopelman R, Meyer TE, Cusanovich MA, Fiber optic nitric oxide selective biosensors and nano-sensors, Analytical chemistry 1998: 70: 971 – 976.

[13] B. D. Gupta, H. Dodeja, A. K. Tomar, Fiber optic evanescent field absorption sensor based on a U-shaped probe, Optical and quantum electronics 28 (1996) 1629 – 1639.

[14] Ken – Ichi Kikuchi, Hiroshi Takahashi, Takatoshi Koike and Shigeki chiba, Effect of clearance between two sensor probes on measured values of bubble properties in a bubble column, Journal of chemical engineering of Japan, vol. 32, No. 1, pp. 162-165, 1999.

[15] S. K. Khijwania and B. D. Gupta, Fiber optic evanescent field absorption sensor: Effect of fiber parameters and geometry of the probe, optical quantum electronics 31: 625 – 636, 1999.

[16] E. Biagi, L. Masotti, and M. Pieraccine, All optical fiber ultrasonic sources for non destructive testing and clinical diagnosis, optical sources & Microsystems: new concepts, materials, technologies, Edited by Martelucci et al, Kluwer Academic / Plenum publishers, New York, 2000.

[17] C. D. Singh, H. Isobe, H. Katsumara and M. Ogita, Measurements of critical micelle concentration (CMC) using U-shaped optical fiber doped porous sol – gel cladding, Sensors & transducers Magazine, Vol. 38, issue 12, December 2003, pp. 67-73.

[18] C. D. Singh and M. Ogita, Detection of critical micelle concentration (CMC) using uniform and U-shaped optical fiber in sensing region, Appl. Phys. B79, 103-105 (2004).

[19] Milan sak – bosnar, Zorana Grabaric and Bozidar S. Grabaric, Surfactant sensors in Biotechnology part 2 – Non – Electrochemical sensors, Food Technol, Biotechnol. 42(3), 207–212 (2004).

[20] S. K. Khijwania, and B. D. Gupta, Fiber optic evanescent field absorption sensor with high sensitivity and linear dynamic range, Department of physics, Indian institute of Technology, New Delhi, 1998.

[21] B. D. Gupta and Ratnanjali, A novel probes for a fiber optic humidity sensor, Physics Department, Indian Institute of Technology, Delhi, India, 2001.

[22] S. K. Khijwania, B. D. Gupta, Maximum achievable sensitivity of the fiber optic evanescent field absorption sensor based on the U – shaped probe, Department of physics, Indian Institute of Technology, New Delhi, 1999.

[23] Argha Banarjee, Sayak mukherjee, biman jana, rishi kumar verma, rahul das, mrinmoy chakroborty, tapan kumar khan, radish mohan hallen, vandana singh, ashutosh saxena, sandip biswas, ram swarup rajput, paramhans tewari, anjan kumar ghosh, vishal saxena, satyendra kumar, pinaki gupta bhaya, roseph john, fiber optic sensing of liquid refractive index, sensors and actuators B 123 (20070) 594-605.

[24] B. D. Gupta, Navneet K. Sharma, Fabrication and characterization of U – shaped fiber optic pH probe, Dept. of Physics, Indian institute of Technology, New Delhi, 2001.

[25] M. Ogita, C. D. Singh, Y. Shibatha and T. Fujinami, A simple U- shaped fiber optic probes for measurement of critical micelle concentration (CMC) in surfactant solutions, IEEE, 2003.

[26] C. D. Singh, M. Ogita, Particle size effect on porous sol-gel doped cladding U-shaped optical fiber critical micelle concentration (CMC) sensor; Appl. Phys. B 79, 389 – 391 (2004).

[27] Patent No. 4806013, Refractometer for fluids, website http://www. Freepatentsonline. Com / 4806013.html.

[28] Singh Chandra deep, Study on chemical sensor using an optival fiber based on chemical adsorption and optical absorption effect, 2005, website http:// www.lib.shizuoka.ac.jp/gakui/416/gde

[29] Cesar Elosua, Ignacio R. Matias, Candido Bariain and Francisco J. Arregui, Volatile organic compound optical fiber sensors: A review, sensors 2006, 6, 1440 – 1465, ISSN 1424 – 8220, website –http://www.mdpi.org/sensors.

[30] Otto S. Wolfbies, Fiber optic chemical sensors and biosensors, Analytical chemistry, vol. 76, No.12, June 15, 2004, 3269.

[31] Jagdish P. Sing, Optical fiber sensors, NSF/RISE workshop / short course, July 9, 2007.

[32] Information society technologies, Optical fiber sensors embedded into technical textile for healthcare – proposal / contract no: FP6 – 027869, D1.2 – specification report on optical sensors, Annex1, optical fiber sensors: principles and state of the art.

[33] A Jayanth Kumar, N M Gowri, R. Venkateswara raju, G Nirmala, B S Bellubbi and T Radha Krishna, Study of fiber optic sugar sensor, pramana, volume 67, Number 2/Agust, 2006, pp 383 – 387.

[34] S Thomas Lee, P Suresh Kumar, K P Unnikrishnan, VPN Nampoori, CPG Vallabhan, S Sugunan and P Radha Krishnan, Evanescent wave fiber optic sensors for trace analysis of Fe^{3+} in water, Meas. Sci. Technol. 14858-861, May 2003.

[35] P Suresh Kumar, CPG Vallabhan, VPN Nampoori, VN Siva sankara pillai and P Radhakrishnan, A fiber optic evanescent wave sensor used for the detection of trace nitrites in water, Journal of optics A: pure and applied optics, 4 – 247 – 250, 2002.

[36] Thomas Lee S, Nibu A, George, P Suresh kumar, P Radha Krishnan, CPG Vallabhan, and VPN Nampoori, Chemical sensing with micro-bent optical fiber, optics letters, vol. 26, issue 20, pp. 1541 – 1543.

[37] Turan J, Ovsenik L, Fiber optic refractometer instrument used for measurement practicing in applied photonics, International conference on telecommunications in modern satellite, cable and broadcasting service, vol.2, issue, 1-3, pp. 488-491.

[38] L M Bali, R K Shukla, Priyanka Srivastava, Anchal Srivastava, Atul Srivastava, and A Kulshreshtha, New approach to the measurement of refractive index, optical engineering, May 2005, vol. 44, issue 5, 058002.

[39] Turan J, Carome EF, Ovsenik L, Fiber optic refractometer for liquid index of refraction measurement, International conference on Telecommunications in modern satellite cable and broadcasting service 2001, vol.2, issue, 2001, pp. 489 – 492.

[40] R Venkateswara Raju, T Radhakrishna, BS Bellubbi, NM Gouri, G Nirmala, A Jayanth kumar, TR Annapurna, Fiber optic temperature sensor using a plastic fiber, J. pure & appl. Phy., vol. 17, No.3, 2005, pp.135-138.

[41] Shiquan Tao, Joseph C. Fanguy, Lina Xu, Sol-gel derived porous silica as a constituent material for designing optical fiber chemical sensor, 3rd International conference on smart materials structures systems, june 8-13,2008, Acireale, Sicily, Italy.

[42] P K Choudhury, T Yoshino, On the pH response of fiber optic evanescent field absorption sensor having a U – shped probe: An experimental analysis, Optika-International Journal for light and Electron optics, volume 114, Number 1, 1April 2003, pp. 13-18 (6).

[43] R Ramponi, M Marangoni and R. Osellame, Optical waveguide refractometer, optical sensors and Microsystems, Springer US, 2002, pp. 41-51.

[44] S K Shukla, GK Parashar, AP Mishra, Puneet Misra, BC Yadav, RK Shukla, LM Bali and GC Dubey, Nano-like magnesium oxide films and its significance in optical fiber humidity sensor, sensors and actuators B: Chemical, volume 98, issue 1, 1march 2004, pages 5-11.

[45] A Jayanth kumar, T Radha Krishna, BS Bellubbi, NM Gowri, R Venkateswara Raju, G Nirmala and T R Annapurna, Intensity modulated fiber optic sugar sensor – study of wavelength dependence, J. pure and Appl. Phy. Vol.17, No.3, May – June, 2005, pp. 119 – 122.

[46] B D Gupta, Navneet K Sharma, Fabrication and characterization of U – shaped fiber –optic pH probes, Dept. of Phy., Indian Institute of technology, New Delhi, 2001.

[47] K Geetha, M Rajesh, C P G Vallabhan, V P N Nampoori and P Radhakrishnan, design of a refractometer with wide dynamic range using side polished polymer optical fiber, International school of photonics, Cochin University of Science and Technology, Cochin, Kerala, 2003, e – mail: geetha @ cusat.ac. in.

[48] B. D. Gupta, Sonu Sharma, A long range fiber optic pH sensor prepared by dye doped sol gel immobilization technique, Elsevier science B.V., volume 154, issue 5-6, 15th September 1998, pages 282-284.

[49] Navneeth K Sharma, BD Gupta, Fabrication and characterization of pH sensor based on side polished single mode optical fiber, Physics Dept., Indian Institute of Technology, New Delhi, 2002.

[50] B D Gupta, DK. Sharma, Evanescent wave absorption based fiber optic pH sensor prepared by dye doped sol gel immobilization technique, Elsevier science B.V., Volume 140, issue 1-3, 15 July 1997, pages 32-35.

[51] C D Singh, M Ogita, Detection of critical micelle concentration (CMC) using uniform and U – shaped optical fiber in sensing region, Appl. Phys. B79, 103-105 (2004).

[52] Stephen A, Schoch, and Howard W Sibley, Fiber optic probe and method of making and using, U. S. patents Documents, patent Number: 4,639,594, Jan. 27, 1987.

[53] John H. W. Cramp, St. Helenl, Robert F. Reid, Optical fiber sensor, U. S. patent Documents, patent number: 4,600,310, July 15, 1986.

[54] J N Fields, Asawa, C K Smith C P, and Morrison RJ, Fiber optic hydrophone, Advances in ceramics 2, Ed. B. Bendow and S S Mitra, Am. Ceram. Soc., 529 – 539 (1981).

[55] D F Nelsor et al, Vibration induced modulation of fiber guide transmission, in Proc. Topical Meet, on Optical Fiber Transmission TUF 7-1 to TU-E7-4, 1977.

[56] N Lagakos, Cole J H, and Bucaro J A, Microbend fiber optic sensor, App. Opt. 26, 2171 – 2176 (1987).

[57] K Spenner, M D Singh, H Schulte, and H J Boehnel, Experimental investigation on fiber optic liquid level sensors and refractometers, Proc. 1st int. conf. on opt. fib. Sensors, London, 96-99 (1983).

[58] A Kumar, Subrahmoniam T V B, Sharma A D, Thyagarajan K, Pal BP and Goyal I C, A novel refractometer using Tapered Optical Fibers, Electron, Letts. 20,534 – 535 (1984).

[59] Huai H Kee, Gareth P Lees, and Trevor P Newson, All fiber system for simultaneous interrogation of distributed strain and temperature sensing by spontaneous Brillouin scattering, 2000, optical society of America.

[60] Written L. Schultz, Joel P. Conte, Eric Udd, John M Seim, Static and dynamic testing of bridges and highways using long gage fiber bragg grating based strain sensors, Whitten @ teleport.com;www:http://bluer.com.

[61] Tsutomu yamate, Rogerio T Ramos and Robert J Schroeder, Thermally insensitive pressure measurements upto 300 degree C using fiber bragg gratings written onto side hole single mode fiber, Erric Udd, Blue Road Research, 255 NE 205th Avenue, Fairview, Oregon 97024 USA.

[62] H H Kee and T P Newson, 1.5 μm Brillouin based fiber optic distributed temperature sensor with high spatial resolution of 20 cm, Southampton SO17 1BJ, Uited Kingdom.

[63] K H Wood, T L Brown, M C Wu, C B Gause, Fiber optic sensors for cure / Health monitoring of composite materials, NASA Langley research center, M/S 231, Hampton, VA 23681 – 2199.

[64] Gareth P Lees, Peter C wait Arther H Hartog and Trevor P Newson, Recent advances in distributed optical fiber temperature sensing using the Landau – placzek, optoelectronics research center, University of Southampton, UK.

[65] P C Wait, K De Souza, T P Newson, A theoretical comparison of spontaneous Raman and brillouin based fiber optic distributed temperature sensor, Elsevier science BV, optics communications 144 (1997) 17 – 23.

[66] Huai H Kee, Gareth P Lees, and Trevor, P Newson, Extended range optical time domain reflectometry system at 1.65 µm based on delayed Raman amplification, optical society of America, 1998.

[67] Gareth P Lees, Peter wait and Trevor P Newson, Novel optical fiber distributed temperature sensor based on the Landau – placzek ratio, optoelectronics research center, University of Southampton, Hampshire, England, SO17 1BJ.

[68] G F Fernando, D J Webb, and Pierre Fendinand, Optical fiber sensors, MRS Bulletin /May 2002, website:www.mrs.org/publications/bulletin.

[69] R L Heredero, Ramon Fernandez de Caleya, Hector Guerrero, Pere Los Santos, Mari cruz Acero, and JAUME Esteve, Micromachined optical fiber current sensor, optical society of America, Applied optics/vol. 38, No. 25/1 september 1999.

[70] Chung E Lee and Henry F Taylor, Fiber optic fabry perot temperature using a low coherence light source, IEEE, 1991.

[71] H H Kee, G.P. Lees and T P Newson, Low loss, low cost spontaneous Brillouin – based system for simultaneous distributed strain and temperature sensing, optical society of America, 1999.

[72] Eric Udd, Whitten L Schultz, John Seim, Kelli corona Bittick, Jim Dorr, Kerry slattery, H Martin layor, Galen Mc Gill Fiber optic smart bearing load structure, E mail: erricudd@aol. Com; web:www.Blue R. R.com.

[73] Whitten L Schultz, Eric Udd, John M. seim, and Galen E. Mc Gill, Advanced fiber grating strain sensor systems for bridges, structures, and highways, Email:whitten@teleport.com, web: www.BlueRR.com.

[74] Marcin szpulak, Tadeusz Martynkien, and walcaw Urbanczyk, Effect of hydrostatic pressure on phase and group modal birefringence in microstructured holey fibers, optical society of America, 2004.

[75] Erric Udd, Whitten L Schulz, and john M Seim, Advanced fiber optic sensor cable of multiparameter sensing, Email:EricUdd@aol.com; web: www. Blue RR.com.

[76] Waclaw Urbanczyk, Tadeusz Martynkien, and Wojtek J. Bock, Dispersion effects in elliptical core highly birefringent fibers, Optical society of America, 2001.

[77] Erric Udd, Whitten Schulz and John Seim, Distributed multiaxis fiber grating strain sensor: Applications for bridges, Email: Eric Udd @ aol. Com., web: www.blue RR. Com.

[78] Gareth P. Lees, D. Taverner, D. J. Richardson, L. Dong and Trevor P. Newson, A Q-switched Erbium doped fiber laser utilizing a novel large mode area fiber, Paper reference no: 1396, Optoelectronics research centre, University of Southampton, S017 IBJ. United Kingdom.

[79] Huai Hoo Kee, Gareth P. Lees and Trever P. Newson, A novel 1.6 μm Raman based distributed temperature sensor, Optoelectronics Research center, University of Southampton, Southampton, S017 IBJ. United Kingdom. Email HHK @ ORC. SOTON. AC. UK.

[80] H H Kee, G. P. Lees and T P Newson, A method of increasing the range of 1.65μm long range OTDR system based on Raman amplification, Electronics and computer science, University of Southampton, Southampton, SO 17 1BJ. United kingdom, Email: hhk @ orc. Soton. Ac. Uk.

[81] H H Kee, G. P. Lees and T P Newson, Aistributed optical fiber sensing at 1.65μm using a Q-switched fiber laser, optoelectronics research center, University of Southampton, Highfield, Southampton SO17 1BJ, UK.

[82] H H Kee, GP.Lees and T P Newson, Simultaneous independent distributed strain and temperature measurements over 15 Km using spontaneous Brillouin scattering, Optoelectronics research center, University of Southampton, Highfield, Southampton SO17 1BJ, UK.

[83] Krska R, Taga K, Kuelluer, New IR fiber optic chemical sensor for in situ measurements of chlorinated hydrocarbons in water, Society for applied spectroscopy, volume 47, issue 9, pages 1297 – 1539 (September 1993), pp. 1484 – 1487 (4).

[84] Conzen J P, Burck J, Ache H J., Characterization of a fiber otic evanescent wave absorbance sensor for non polar organic compounds, society for Applied spectroscopy, volume 47, issue 6, pages 677-859 (June 1993) pp. 753 – 763 (11).

[85] Klunder G L., Burck J, Ache H J, Silva R J, Russo R. E., Temperature effects on a fiber optic evanescent wave absorption sensor, society for applied spectroscopy, volume 48, issue 3, pages 289- 416 (march 1994), pp. 387 – 393 (7).

[86] Blair, Dianna S, Burgess, Lioyd W, Brodsky, Anatol M, Study of analyte diffusion into a silicone clad fiber optic chemical sensor by evanescent wave spectroscopy, society for applied spectroscopy, vol. 49, issue 11, pages 1545 – 1719 (November 1995), pp. 1636 – 1645 (10).

[87] C. Egami K, Takeda, M.Isai and M Ogita, Evanescent wave spectroscopic fiber optic pH sensor, Elsevier science B.V., Volume 122, issue 4-6, January 1996, pages 122-126, 1995.

[88] Merchman, Sheila A, Tilotta, David C, Fiber optic sensor for aromatic compounds in water based on solid phase microextraction and ultraviolet evanescent wave absorption sensor, Society for applied spectroscopy, volume 52, issue 1, pages 10A – 53A and 1-169 (January 1998), pp. 106-111 (6).

[89] Sukhdev Roy, Fiber optic sensor for determining adultration of petrol and diesel by kerosene, Elsevier science S.A., volume 55, issues 2-3, 11 may 1999, pages 212-216.

[90] Dunkers, Joy P, Flynn, Kathleen M, Huang, Mitchell T, Mc Donough, Walter G, Fourier transform near infrared monitoring of reacting resins using an evanescent wave High Index fiber optic sensor, society for applied spectroscopy, volume 52, issue 4, pages 150A-164A and 477-628 (April 1998), pp. 552-556 (5).

[91] Gupta B D, Khijwania S K, Experimental studies on response of the fiber optic evanescent field absorption sensor, Taylor and Francis Ltd., volume 17, Number 1, 1January 1998, pp. 63-73 (11).

[92] Y Zaatar, D. Zaouk, J Bechara, A Khoury, C zlinaress and J P Charles, Fabrication and characterization of an evanescent wave fiber optic sensor for air pollution control, Elsevier Science SA, Material science and Engineering B, volume 74, issues 1-3, 1 may 2000, pages 296-298.

[93] S. Sekimoto, H Nakagawa, S. Okazaki, K Fukuda, S Asakura, T Shigemori and S Takahashi, A fiber optic evanescent wave hydrogen gas sensor using palladium supported tungsten, Elsevier science S A, sensors and actuators B, vol. 66, issues 1-3, 25 July 2000, pages 142-145.

[94] A Kishen, M S John, C S Lim and A Asundi, Elsevier science B V, Biosensors and Bioelectronics, volume 18, issue 11, October 2003, pages 1371-1378.

[95] Wang, Chi – chang, Chia – I, Lin, Yi – Hua, Chau, Lai – kuwan, Detection of riboflavin based on fluorescence evanescent of evanescent wave excited beta – cyclodextrin complex in sol Gel derived porous coatings, society for applied spectroscopy, vol. 54, issue 1, pages 9A-41A and 1-158 (January 2000), pp. 15-19 (5).

[96] Karlowatz M, Kraft M, Eitenberger E, Mizaikoff B, Katzir A, Chemically tapered silver halide fibers: An approach for increasing the sensitivity of Mid Infrared evanescent

wave sensors, society for applied spectroscopy, volume 54, issue 11, pages 373A-385A and 1549-1718 (November 2000), pp. 1629-1633 (5).

[97] Woerdeman, Dara L, Parnas, Richard S, Model of a fiber optic evanescent wave fluorescence sensor, society for applied spectroscopy, volume 55, issue 3, pages 106A-128A and 241-370 (March 2001), pp. 331-337 (7).

[98] S Thomas Lee, B Neeshkumar, P Radhakrishnan, C P G Vallabhan and V P N Nampoori, A microbentfiber optic pH sensor, Elsevier science BV, Optics communications, volume 205, issues 4-6, 1 May 2002, pages 253-256.

[99] Yeh, Ta – chuan, Tien, Pei, Chau, Lai – Kwan, Fiber optic evanescent wave absorption copper (II) sensor based on sol gel derived organo functionalized silica cladding, Applied spectroscopy, volume 55, issue 10, pages 319A-350A and 1287-1433 (October 2001), pp. 1320-1326 (7).

[100] P Suresh kumar, S Thomas Lee, C P G Vallabhan, V P N Nampoori and P Radhakrishnan, Design and development of an LED based fiber optic evanescent wave sensor for simultaneous detection of chromium and nitrite traces in water, Elsevier science BV, optics communications, volume 214, issues 1-6, 15 December 2002, pages 25 – 30.

[101] Preejith P V, Lim C S, Kishen A, John M S, Asundi A, Total protein measurement using a fiber optic evanescent wave based biosensor, Biotechnology letters, volume 25, Number 2, January 2003, pp. 105-110 (6).

[102] S. Okazaki, H Nakagawa, S Asakura, Y Tomiuchi, N Tsuji, H Murayame and M Washiya, Sensing characteristics of an optical fiber sensor for hydrogen leak, Elsevier science BV, sensors and actuators B: Chemical, volume 93, issues 1-3, 1 August 2003, pages 142-147.

[103] Mitsuhiro iga, Atsushi seki, yuzurukubota and kazuhiro watanabe, Acidity measurements based on a heterocore structured fiber optic sensor, Elsevier B V, Sensors and actuators B: Chemical, volume 96, issues 1-2, 15 November 2003, pages 234-238.

[104] Kharat, Hridas J, Kakade, Kishor P, shirale, Dhammanand, Gade, Vikas K, Gaikwad, Pradeep D, Savale, Padmakar A, Shirsat, Mahendra D, Designing of optical fiber sensing probe, Fiber and integrated optics, volume 25, Number 6, November – December 2006, pp. 411 – 422 (12).

[105] Petr Tobis Ka, Miroslav chomat, V lastimil Mate jec, Daniela Berkova and ivan Huttel, Investigation of fiber optic evanescent wave sensors for detection of liquid hydrocarbons, Elsevier science SA, sensors and actuators B: chemical, volume 51, issue 1-3, 31 August 1998, pages 152-158.

[106] Marasu Mrrsushio and Morihide Higo, Simplification and Evaluation of a gold – deposited SPR optical fiber sensor, Analytical sciences, April 2004, vol. 20, The Jpan society for analytical sciences, April 2004.

[107] W B Lyons, H Ewald, C Flanagan and E Lewis, An optical fiber sensor for in situ measurement of external species in fluids based on artificial neural network pattern recognition, physiological measurements, issue 3, March 2001.

[108] D. King, W B Lyons, C Flanagan and E Lewis, Interpreting complex data from a three sensor multipoint optical fiber ethanol concentration sensor system using artificial neural network pattern recognition, Measurement science and Technology, July 2004.

[109] S P Reily, S W James and R P Tatam, Tunable and switchable dual wavelength lasers using optical fiber Bragg grating external cavities, Electronics Letters, August 2002, vol. 38, No. 18.

[110] D King, W B Lyons, C Flanagan and E Lewis, A multipoint optical fiber sensor system for use in process water systems based on artificial neural network pattern

recognition technique, sensors and actuators A: Physical, The 17th European conference on solid state transducers, volume 115, issues 2-3, 21september 2004, pages 293-302.

[111] Y. Raichlin, L Fel, and A Katzir, Evanescent wave infrared spectroscopy with flattened fibers as sensing elements, Optics letters, vol. 28, issue 23, pp. 2297-2299.

[112] Chen chun ye, Stephen E Stains, Stephen W James and Ralph P Tatam, A polarization system for multi axis strain sensing, Measurement science and technology, 13, 1446-1449, August 2002.

[113] Jan Turan, Edward F Carome, Lubos ovsenik, Fiber optic refractometer for liquid index of refraction measurements, 19-21 September 2001 IEEE.

[114] K Ilev, Simple fiber optic autocollimation refractometer, CLEO / EUROPE 1994 / 328.

[115] F. H. Zhang, P J Scully, E Lewis, An optical fiber yeast concentration sensor based on inter fiber distributed coupling, CLEO / EUROPE 1994 / 329.

[116] J Arrue, J Zubia, G Fuster, D Kalymnios, Light power behaviour when bending plastic optical fibers, IEE Proc. Optoelectron, vol. 145, No. 6, December 1998.

[117] Anna Grazia Mignani and Francesco Baldini, In vivo biomedical monitoring by fiber optic systems, Journal of light wave technology, vol. 13, No. 7, July 1995.

[118] B Maisenholder, H P Zappe, M Moser, P Riel, R E Kunz and J Edlinger, Monolithically integrated optical interferometer for refractometry, Electronics letters, 22nd May 1997, vol. 33, No. 11.

[119] Joel villatoro and david Monzon – Hernandez, Low cost optical fiber refractive – index sensor based on core diameter mismatch, Journal of light wave technology, vol. 24, No. 3, March 2006.

[120] Ainhoa Gaston, Ibon Lozano, Fatima perez, Fernando auza and Joaquin Sevilla, Evanescent wave optical fiber sensing (Temperature, Relative Humidity and pH Sensors), IEEE sensors journal, vol. 3, No.6, December 2003.

[121] George P. Anderson, Joel P, Golden, Lynn K. Cao, Daya vijesuriya, Lisa C. Shriver – lake, Frances S. Ligler, Development of an evanescent wave fiber optic biosensor, IEEE Engineering in medicine and biology, June / July 1994.

[122] B. D. Mac Craith, G. Okeefe, C. Mc Donagh and A. K. Mc Evoy, LED – based fiber optic oxygen sensor using sol – gel coating, Electronics Letters, 26th May 1994, vol. 30. No.11.

[123] P V Preejith, C S Lim and T F Chia, Serum albumin measurement using a tapered fluorescent fiber optic evanescent wave – based biosensor, 81-904262-1-4/06/2006 research publishing services.

[124] S. V. Alekseenko, A. V. Bobylev, A. R. Evseev, V. M. Karsten, D. M. Markovich, and B. V. Tarasov, Measurements of the liquid film thickness by a fiber optic probe, Instruments and experimental techniques, vol. 46, No. 2, 2003, pp. 260-264.

[125] O. I. Katov, L. B. Liokumovich, V. M. Nicoleav, V. Yu. Petrun'kin, and Zekhrani buabid, Conversion of phase modulation of light into intensity modulation by means of an external fiber optic interferometer, Tech. Phy. Lett. 23(5), May 1997.

[126] David A Egan, Stephen W James and Ralph P. Tatam, Design note: a polarization based optical fiber vibrometer, Meas. Sci. Technol. 8(1997) 343 – 347.

[127] N. A. George, Fiber optic position sensitive detection of photothermal deflection, Appl. Phys. B77, 77-80 (2003).

[128] Stephen kreger, Sean calvert, Eric Udd, Density multiplexing of multi-axis fiber Bragg gratings, Blue road research, 376NE 219th Ave, Gresham OR97030.

[129] Saeed Pilevar, Christopher C. Davis, Alexander J. Fielding, Frank Portugal, Optical fiber evanescent field excited fluorosensor and method of manufacture, United States patent, patent number 6,103,535, date of patent August 15, 2000.

[130] Tomas B. Hirschfeld, Apparatus for improving the numerical aperture at the input of a fiber optics device, United states patent, patent number, 4,654,532, date of patent, Mar.31, 1987.

[131] Timothy J. Mc Intyre, steven W. Allison, L. Curt maxen, Michael R. Cates, Fiber optic temperature sensors for P E M fuel cells, D O E Hydrogen program, F Y 2004 progress report.

[132] Sarfraz khaliq, Stephen W James and Ralph P Tatam, Enhanced sensitivity fiber optic long period grating temperature sensor, Meas. Sci. Techno,. 13 (2002) 792 – 795.

[133] Martin J O'Dwyer, Chen – Chun ye, Stephen W James and Ralph Tatam, Thermal dependence of the strain response of optical fiber Bragg gratings, Meas. Sci. Technol. 15 (2004) 1607 – 1613.

[134] Stephen W James, Ralph P Tatam, Andrew Twin, Rod Batman and paul noonan, Cryogenic temperature response of fiber optic long period gratings, Meas. Sci. Technol. 14 (2003) 1409 – 14511.

[135] Artur Olszak and Ralph P. Tatam, The calibration of the path length imbalance in optical fiber ESPI systems employing source wavelength mokulation, Meas. Sci. Technol. 8(1997) 759 -763.

[136] Paul Grems Duncan, Sean Michael Chriatian, Kevin Anthony shinpaugh, Fiber optic sensor and methods therefore, United States patents, patent No. US 6,496,265 B1, Dec. 17, 2002.

[137] Paul Grems Duncan, Sean Michael Christian, Kevin Anthony Shinpaugh, Fiber optic sensors system and method for measuring the pressure of media, United States patent application publication, pub. No. US 2003/0001082 A1, Jan. 2, 2003.

[138] J. Potter, A. Ezbiri, R. P. Tatam, A broad band signal processing technique for miniature low finesse Fabry perot interferometric sensors, Elsevier Science B.V., optics communications 140(1997) 11-14.

[139] Paul Grems Duncan, John Alan Schroeder, Sensor for optically measuring magnetic field; United States patent application publication, pub. No.: U S 2003/0146748 A1, Aug. 7, 2003.

[140] Paul G. Duncan, Seam Michael Christian, System and method for distributed monitoring using remote sensors, United States patent application publication, pub. No. U S 2002/004369 A1, Apr. 18, 2002.

CHAPTER 2

Theoretical Aspects of Sensors

2.1 Fiber Optic Communication (FOC)

Fiber optic communication system uses light wave as an information carrier and an optical fiber as a guiding medium. This system offers many advantages over the existing copper communication system. First, since light is effectively the same as radio frequency radiation, but at a very much higher frequency of about 300THz, or 3,000,000GHz, the information carrying capacity of a fiber is very much greater than both microwave and radio systems. Next, the material used in fibers is silica glass, or silicon dioxide, which is one of the most abundant materials on earth, resulting in much lower material costs than with wire lines. The fibers are not electrically conductive, so they may be used in areas where isolation from electrical and electromagnetic interference is a problem. With much higher information capacities, multiple channel routes using optic fibers can be compressed into much smaller cables, greatly reducing congestion in over crowded cable ducts. The optical fiber communication system revolutionized human life in many ways as the computers and transistors revolutionized in earlier decades.

The subject of communication begins really with the situation as shown in Fig. 2.1. We have here the two entities one called the user and the other called the source. From the source, the user is located remotely in terms of distance. The user desires to learn what the information is

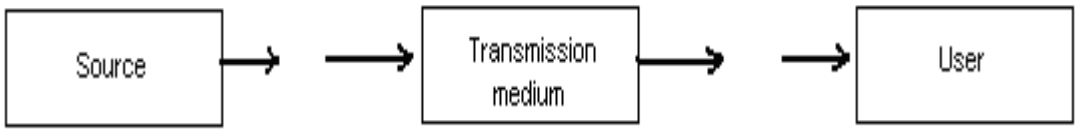

Fig.2.1: Source, Transmission medium, User in a communication system.

To transport the information from the source to the user, a transmission medium is employed. A transmission medium is some physical entity which is located between the Source and the User and is accessible to both. The Transmission medium has a set of properties described by physical parameters. The set of properties exist in a quiescent state initially. However, at least one of these properties can be stressed or disturbed at the Source end. This is accomplished by somehow imparting energy in order to stress the property. This disturbance does not stay still, but affects the parts of the Transmission medium around it. This disturbance then travels from the Source end to the User end. Consequently, energy imparted in creating the disturbance is thereby transferred from the Source end to the User end. Finally, this disturbance or stressed property can be sensed at the User end and it can be measured.

The medium of transmission could be an electromagnetic field set up in space by the applying current to an antenna, could be air, a wireless or a radio system. The stressed property can be the voltage between the conductors, being the potential difference on an electrical transmission line, for which the transmission medium could be a pair of electrical conductors. The stressed property could be the light-dark pattern on the paper, which can be a letter, for which the transmission medium could be a sheet of paper. The stressed property can be the intensity, polarization, wavelength, or the phase of the light in the glass rod, a fiber optic cable, to which the transmission medium could be a cylindrical glass rod. In accordance with the information, the source can generate a disturbance in the medium of transmission. The disturbance generated by the source varies with respect time exactly as the information. The disturbance which is encoded will be transmitted to the end user.

The generating process of a disturbance by the source, which is in accordance with that of the information and the launching of the signal into the transmission medium is referred as the modulation and the transmission. The sensing process of the received disturbance and confirming what the information it represents by the user is referred to as reception and demodulation. The device which carries out transmission and modulation is called the transmitter. The device which carries out the demodulation and the reception is called the receiver. The entities used to transfer the information from the

Source to the User are the Transmitter, the Transmission medium and the Receiver. The fundamental problem of communications is to choose the terminal equipments i.e. the Transmitter and Receiver and to choose the Transmission medium so as to satisfy the requirements for a given Source-User pair. This combination is referred generally as a data link, as the limitation placed on the message to be a sequence of bits. The main constraints of the transmission medium are its performance and its operation. For the particular data link design, which transmission medium can be employed will be decided by these constraints.

2.1.1 Optical fiber as a guiding medium

Glass is a hard material normally fragile and transparent, and commonly used in daily life. The raw material for glass is sand, which is abundantly available throughout the world. Glass is composed mainly of sand (silicates- SiO_2) and an alkali. These materials at a high temperature i.e. molten viscous state, fuse together; then they are cooled rapidly forming a rigid structure, however not having enough time to form a regular crystalline structure. Glass is an amorphous solid that has been manufactured for human use since 12,000 BC. Glass is a strange substance, defying easy scientific categorization. It is not a solid, not a gas, and not quite a liquid either. Generally, it is classified as a rigid liquid, maintaining liquid properties while acting like a solid.

Glass is a manufactured material, formed when a mixture of sand (SiO_2 silica), soda ($Na2CO_3$), and lime ($CaCo_3$) is heated to a high temperature and assumes a molten or liquid state. The soda makes the glass water-soluble, soft and not very durable. Therefore lime is added to it to increase its hardness and chemical durability and to provide insolubility to the materials. It changes little over time and is not affected by corrosive materials, not even by most acids. Glass does not react with its contents, it does not retain odors, and it can be completely sterilized. Liquids and air cannot pass through it, but light easily penetrates it. Glass does not conduct electricity. Although glass is a manufactured material, there exist several forms of naturally formed glass. Volcanic glass, or obsidian, is formed when the intense heat of a volcano fuses sand. The characteristics of durability, inertness, and transparency make glass an ideal material for preparing light transmission medium.

2.1.2 Transparent cylinders as light guiding media

The transmission of light along transparent cylinders was demonstrated by John Tyndall, a British physicist at the Royal Society in England, in 1870. John Tyndall set up a tank of water with a pipe which ran out on one side. He shone a bright light into the water stream from inside the tank, allowing the water to flow from the pipe. An arc of the light followed the water down as the water fell. The principle that will be discussed in more detail later, demonstrates the total internal reflection. In 1910, Hondros and Debye conducted a theoretical study on the transmission of light via a dielectric waveguide structure, and experimental work was reported by Schriever in 1920. During the 1920s, John Logie Baird in England and Clarence W. Hansell in the United States patented the idea of using arrays of hollow pipes or transparent rods to transmit images for television or facsimile systems. However, a transparent dielectric rod, typically of silica glass with a refractive index of around 1.5, surrounded by air, proved to be an impractical waveguide due to its unsupported structure.

The areas of optical imaging and medical diagnosis led to the proposals for clad dielectric rod in the mid 1950s in order to overcome these problems. In 1954, Dutch scientist Abraham Van Heel and British scientist Harold H. Hopkins separately wrote papers on imaging bundles. Hopkins reported on imaging bundles of unclad fibers, whereas Van Heel reported on simple bundles of clad fibers. Van Heel covered a bare fiber with a transparent cladding of a lower refractive index. This protected the fiber reflection surface from outside distortion and greatly reduced interference between fibers. This structure is illustrated in Fig. 2.2, which shows a transparent core with a refractive index n_1 surrounded by a transparent cladding of slightly lower refractive index n_2.

Fig. 2.2: Optical fiber waveguide showing the core of refractive index n_1, surrounded by the cladding of slightly lower refractive index n_2

In essence, the light energy travels in both the core and the cladding allowing the associated fields to decay to a negligible value at the cladding –air interface. In 1961, Elias Snitzer of American Optical Society published a theoretical description of a fiber with a core so small it could carry light with only one waveguide mode.

The invention of the clad waveguide structure led to the first serious proposals by Kao and Hockham, in 1966, to utilize optical fibers as a communications medium, even though they had losses in excess of 1000dB km^{-1}. The new era started in 1970 when Dr. Robert Maurer, Donald Keck, and peter Schultz of Corning Incorporation, New York, came up with the first low loss optical fiber, with losses less than 20 dB /km (decibels per kilometer). These proposals stimulated tremendous efforts to reduce the attenuation by purification of the materials. This has resulted in improved conventional glass refining techniques giving fibers with losses of around 4.2 dB km^{-1}. The progress in glass refining processes such as depositing vapour-phase reagents to form silica has allowed fibers with losses below 1 dB km^{-1} to be fabricated.

Most of this work was focused on the 0.8 to 0.9μm wavelength band because the first generation optical sources fabricated from gallium aluminum arsenide alloys operated in this region. However, as silica fibers were studied in further detail it became apparent that transmission at longer wavelengths (1.1 to 1.6μm) would result in lower losses and reduced signal dispersion. This produced shift in optical fiber source and detector technology in order to provide operation at these wave lengths. Hence, at longer wavelengths, especially around 1.55μm, fibers with losses as low as 0.2 dB km^{-1} have been reported. Interest has grown in glass forming systems which can provide low loss transmission in the mid-infrared (2 to 5μm) and also the far-infrared (8 to 12μm) optical wavelength regions. At present the best developed of these systems which offer the potential for ultra-low-loss transmission of around 0.01 dB km^{-1} at a wavelength of 2.5μm are based on the fluoride glasses.

In the late 1960s that the laser was invented, could transmit information over longer distance. Alexander Graham Bell also plagued the laser, unfortunately with the same

experience of drawbacks. It did not work any time a building was erected in between the transmitter and the receiver, although it could be used at night.

.

In April 1977, General Telephone and Electronics tested and deployed the world's first live telephone traffic through a fiber-optic system running at 6 Mbps, in Long Beach, California. They were soon followed by Bell in May 1977, with an optical telephone communication system installed in the downtown Chicago area, covering a distance of 1.5 miles (2.4 kilometers). Each optical-fiber pair carried the equivalent of 672 voice channels and was equivalent to a DS3 circuit. Today more than 80 percent of the world's long-distance voice and data traffic is carried over optical-fiber cables.

2.1.3 Visible light as a carrier

According to spectroscopy, different materials emit energies in the form of electromagnetic radiation when they are excited. The radiation emitted by all the materials available are arranged in the systematic order with respect to their frequency, which forms a pattern of all the available electromagnetic radiation called the electromagnetic spectrum. It can be observed that the wave length of visible light ranges from around 400nm.to 700nm and the frequency is varies from 10^{14} to 10^{15} Hz. Light is composed of an elementary particle called a photon. Many experiments conducted on light proved that it exhibits dual nature of wave and particle. It exhibits the properties like total internal reflection, refraction, reflection, interference, polarisation and diffraction. The velocity of light is observed to be 2.998×10^{5}kms. Light is electromagnetic radiation of a wavelength that is visible to the eye (visible light). In a scientific context, the word "light" is sometimes used to refer to the entire electromagnetic spectrum.

The study of light, known as optics, is an important research area in modern physics. The use of visible light for communication is basic phenomena in human life. The objects in the nature, and their phenomena are made visible by the communication of light, making use of reflection phenomena. The necessity was about to see the long distant objects and their phenomena, with an artificially monitoring capacity and to get the information in the form of images. To communicate information Paul Revere used

lanterns. This was an early example of optical communication, although not sophisticated. Fire beacons in the night and reflected sunlight in the day time were used as video signals for communication in ancient days for shorter distances. With the same concept the signling lamps in railways, in navel transport, in aviation and in the vehicular traffic control are being used for shorter distance communication using visible light even today.

In 1880 Alexander Graham Bell reported the transmission of speech using a light beam in the open atmosphere. The photophone proposed by Bell transmitted the speech over a distance of 200m. He quoted at that time that "I have heard a ray of light laugh and sing. We may take by light to any visible distance without any conducting wire". Than his previous invention, the telephone, Bell considered this as a great discovery. With the photo-phone, which would cause a mirror to vibrate, Bell would speak into a microphone. The vibration of the mirror would transmit the light across as open distance of about 656 feet (200 meters). The noise would come out on the other end, caused by the selenium crystal vibration, as the receivers mirror would receive the light.

The photo-phone had a few drawbacks, although the photo-phone was successful over open space in allowing the conversation. It did not work if someone walked between the transmitter and the receiver, at night, in the rain. However, although some investigation of optical communication continued, the use was limited to low capacity communication links. This was due to both the lack of suitable light sources and the problem that light transmission in the open atmosphere is restricted by disturbances such as rain, snow, fog, dust, temp., and atmospheric turbulence.

The transmission of visible light through transparent cylinders was tried in the beginning of the 20^{th} century. Again the problem of lack of suitable light sources the information transfer even through the guided cylinders limitted the transmission only to short distance communications. The light sources during that time were polychromatic, non unidirectional, hence incoherent in character which property made them to be weak in travelling for longer distances, subjecting to absorption, scattering by either the guided medium or unguided medium.

The problem of availability of suitable light source continued till 1960, when the powerful light source in the name of LASER was put forwarded. LASER is the acronym for the Light Amplification by Stimulated Emission Radiation. These laser sources emit the powerful radiation which is highly monochromatic, highly directional, coherent in terms of temporal coherence and spatial coherence and all the emitted waves having the same polarization. The laser with these characters could able to withstand for the disturbances like scattering, absorption offered by the guided medium and traveling for thousands of kilometers almost without any loss. Most of the lasers emit radiation in the visible region of the electromagnetic spectrum consisting all the visible colors and further extending their wavelengths into the infra red region of the electromagnetic spectrum. Thus the combination of transparent cylinders as guiding medium and laser light as the information carrier, offered an efficient communication system for the present day use and the necessity.

2.2 Fiber construction and fiber dimensions

Optical fiber for telecommunications consists of three components: core, cladding & coating. The core is the central region of an optical fiber through which light is transmitted. In general, the telecommunications industry uses sizes from 8.3 micrometers (µm) to 62.5 micrometers. The standard telecommunications core sizes in use today are 8.3 µm (single-mode), 50µm and 62.5 µm (multimode). The diameter of the cladding surrounding each of these cores is 125 µm. To put these sizes into perspective, compare them to a human hair, which is approximately 70 µm or 0.003 inch.

2.2.1 Fiber manufacturing

Standard optical fibers are made by first constructing a large-diameter preform, with a carefully controlled refractive index profile, and then pulling the preform to form the long, thin optical fiber. The preform is commonly made by three chemical vapor deposition methods: inside vapor deposition, outside vapor deposition, and vapor axial deposition. With inside vapor deposition, a hollow glass tube approximately 40 cm in length known as a "preform" is placed horizontally and rotated slowly on a lathe, and gases such as silicon tetrachloride ($SiCl_4$) or germanium tetrachloride ($GeCl_4$) are injected with oxygen in the end of the tube. The gases are then heated by means of an

external hydrogen burner, bringing the temperature of the gas up to 1900 Kelvin, where the tetrachlorides react with oxygen to produce silica or germania (germanium oxide) particles. When the reaction conditions are chosen to allow this reaction to occur in the gas phase throughout the tube volume, in contrast to earlier techniques where the reaction occurred only on the glass surface, this technique is called modified chemical vapor deposition (MCVD).

2.3 Classification of optical fibers

Optical fiber types*:* On the basis of the material used to fabricate, optical fibers are classified into two categories, 1 Plastic fibers, and 2 Glass fibers. In the case of glass the raw material used is the sand and its chemical name is SiO_2. Glass optical fibers are almost always made from silica, but some other materials, such as fluorozirconate, fluoroaluminate, and chalcogenide glasses, are used for longer-wavelength infrared applications. Like other glasses, these glasses have a refractive index of about 1.5. And in the case of plastic fibers polysterene (PS) and polymethyle methacrylate (PMMA) are used as core and Teflon, Fluorocarbon, or a silicon resin may be used as cladding material. Plastic optical fiber (POF) is commonly step-index multimode fiber, with core diameter of 1 mm or larger. POF typically has much higher attenuation than glass fiber, 1 dB/m or higher, and this high attenuation limits the range of POF-based systems. By using these two material types, three categories of optical fibers can be prepared. They are, Glass core with glass cladding fiber, Plastic core with plastic cladding, Glass core with plastic cladding.

The glass optical fiber having glass core and glass cladding can be achieved by adding do-pants like germanium, phosphorous, and boron etc. into the bulk glass material. The characterization of optical fibers is decided by the structure and by the transmission properties. Optical fibers are classified basically into two types. Single mode fibers are the first type. Multimode fibers are the second type. The names of the optical fibers are assigned depending on the number of modes that propagate along the system. The propagation of modes along the fiber are restricted or permitted as mentioned earlier.

2.3.1 Multimode step index fiber

The fiber manufactured with core diameters as small as 50 microns and as large as hundreds of microns and which transmits many modes through its structure is called multimode fiber (Fig. 2.3).

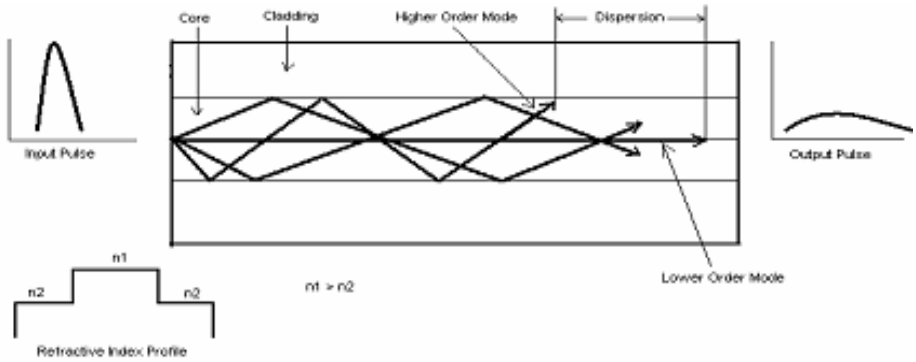

Fig.2.3: Multimode Step Index Fiber

Rays that meet the core-cladding boundary at a high angle, greater than the critical angle, are completely reflected. A high numerical aperture allows light to propagate down the fiber in rays both close to the axis and at various angles, allowing efficient coupling of light into the fiber. However, this high numerical aperture increases the amount of dispersion as rays at different angles have different path lengths and therefore take different times to traverse the fiber. This disparity between arrival times of the different light rays is known as dispersion, and the result the pulse, an aggregate of different modes, begins to spread out, losing its well-defined shape. The need to leave spacing between pulses to prevent overlapping limits bandwidth that is, the amount of information that can be sent. Consequently, this type of fiber is best suited for transmission over short distances and lower bandwidth applications.

2.3.2 Single-mode step index fiber

Fiber supporting only one mode is called single-mode or mono-mode fiber. The most common type of single-mode fiber has a core diameter of 8 to 10 μm and is designed for use in the near infrared. Single Mode Fiber with a relatively narrow diameter, only one mode will propagate through the fiber. Carries higher bandwidth than multimode fiber, but requires a light source with a narrow spectral width. Synonyms are mono-mode optical fiber, single-mode fiber, single-mode optical waveguide, uni-mode fiber.

2.3.3 Multimode–graded index fiber

In graded-index fiber, the index of refraction in the core decreases continuously between the axis and the cladding (Fig. 2.4). This causes light rays to bend smoothly as they approach the cladding, rather than reflecting abruptly from the core-cladding boundary. The resulting curved paths reduce multi-path dispersion because high angle rays pass more through the lower-index periphery of the core, rather than the high-index center.

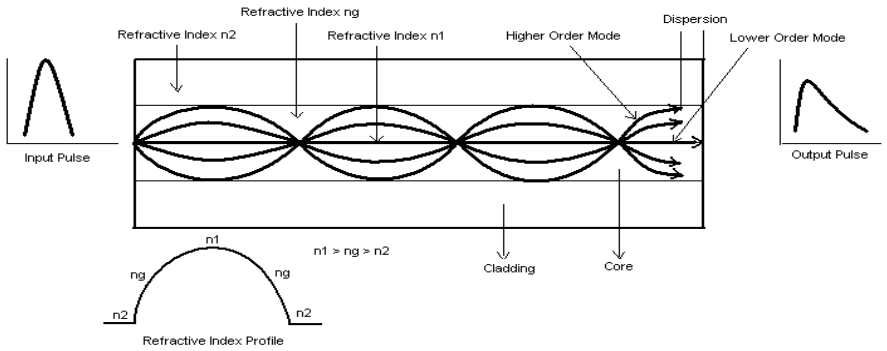

Fig.2.4: Multimode Graded Index Fiber

The shortened path and the higher speed allow light at the periphery to arrive at a receiver at about the same time as the slow but straight rays in the core axis. The result: a digital pulse suffers less dispersion. The index profile is chosen to minimize the difference in axial propagation speeds of the various rays in the fiber. This ideal index profile is very close to a parabolic relationship between the index and the distance from the axis.

2.4 light propagation through optical fibers

2.4.1 Total internal reflection

Total internal reflection is an optical phenomenon that occurs when a ray of light strikes a medium boundary at an angle larger than the critical angle with respect to the normal to the surface. If the refractive index is lower on the other side of the boundary no light can pass through, so effectively all of the light is reflected. The critical angle is the angle of incidence above which the total internal reflection occurs. When light crosses a boundary between materials with different refractive indices, the light beam will be partially refracted at the boundary surface, and partially reflected. However, if the angle of incidence is greater than the critical angle — the angle of incidence at which light is

refracted such that it travels along the boundary — then the light will stop crossing the boundary altogether and instead totally reflect back internally. This can only occur where light travels from a medium with a higher refractive index to one with a lower refractive index. For example, it will occur when passing from glass to air, but not when passing from air to glass. When a light ray traveling in one material hits a different material and reflects back into the original material without any loss of light, total internal reflection occurs.

2.4.2 Optical fiber parameters

Light that can be seen by the unaided human eye is said to be in the visible spectrum. In the visible spectrum, wavelength can be described as the color of light. Optical fiber transmission uses wavelengths which are above the visible light spectrum, and thus undetectable to the unaided eye. Typical optical transmission wavelengths are 850 nanometers (nm), 1310 nm, and 1550 nm. Both lasers and LED's (light-emitting diodes) are used to transmit light through optical fiber. Lasers are usually used for 1310 or 1550 nanometer, single-mode applications. LED's are used for 850 or 1300 nanometer multimode applications. There are ranges of wavelengths at which the fiber operates best (Table 2.1). Each range is known as an operating window. Each window is centered about the typical operational wavelength.

Window	Operating Wavelength
800nm - 900 nm	850 nm
1250 nm - 1350 nm	1310 nm
1500 nm - 1600 nm	1550 nm

Table: 2.1: Fiber best operating wavelengths of E.M. spectrum

These wavelengths were chosen because they best match the transmission properties of available light sources with the transmission qualities of optical fiber. The frequency of a system is the speed of modulation of the digital or analog output of the light source; in other words, the number of pulses per second emitted from the light source. Frequency is measured in units of hertz (Hz), where 1 hertz is equal to 1 pulse or cycle per second. A more practical measurement for optical communications is megahertz (MHz) or millions of pulses per second.

2.4.3 Light propagation through optical fiber – ray theory

The change in the wave direction will takes place if the light wave travels from one medium into the other medium having different velocity of travel. When the wave enters into the second medium a change in the direction occurs, called refraction. When the wave travels through the interface between the two media, it can bend nearer of away from the normal to the boundary. The angle of refraction is more than the angle of incidence and the wave bends away from the normal, when the wave travels from a high dense medium to a less dense medium. The angle of refraction is smaller than the angle of incidence and the wave bends nearer to the normal, when the wave travels from a less dense medium to a high denser medium. The light transmission through the fiber will be affected by these properties.

The basic optical property of a material, relevant to optical fibers, is the index of refraction. The index of refraction (n) measures the speed of light in an optical medium. The index of refraction of a material is the ratio of the speed of light in a vacuum to the speed of light in the material itself. The speed of light (c) in free space (vacuum) is 3 X 10^8 meters per second (m/s). The speed of light is the frequency (*f*) of light multiplied by the wavelength of light (λ). When light enters the fiber material (an optically dense medium), the light travels slower at a speed (v). Light will always travel slower in the fiber material than in air.

The concept of light propagation, the transmission of light along an optical fiber, can be described by two theories. According to the first theory, light is described as a simple ray when $\lambda \rightarrow 0$. This theory is the ray theory, or geometrical optics, approach. The advantage of the ray approach is that it provides a clearer picture of the propagation of light along a fiber. The ray theory is used to approximate the light acceptance and guiding properties of optical fibers. According to the second theory, light is described as an electromagnetic wave. This theory is the mode theory, or wave representation, approach. The mode theory describes the behavior of light within an optical fiber. The mode theory is useful in describing the optical fiber properties of absorption, attenuation, and dispersion. The light rays which propagate along the fiber are of two kinds. Meriodinal rays are of the first kind. The rays which propagate along the fiber axis are

the meridional rays. For the description of the propagation character of the optical fiber the meridional rays are used. The second kind of rays called skew rays. The rays which do not pass through the axis of the optical fiber are the skew rays. Bound and unbound are the two kinds of meridional rays. The rays which travel along axis of the fiber and confine within the core are the bound rays. By the phenomena of total internal reflection the bound rays travel through the fiber. The rays which refract out of the fiber core are the unbound rays. The bound rays travel through the fiber by the phenomena of total internal reflection. The entering rays into the fiber must intersect the core and cladding interface at an angle more than the critical angle (θc). The rays which enter only with these angles will travel through the optical fiber (Fig. 2.5). The definition for index of refraction n can be recalled as: s:

$$n = \frac{c}{v} \tag{1}$$

and for free space, n=1. For the silica glass SiO_2, n=1.5. By adding dopants (impurities) into the material, n can be modified. Optical fibers have a thick cladding surrounding the small core whose refractive index is slightly less than that in the core. Let n_0, which denote the nominal value of n of the core, and n_c of the cladding. Let a as the radius of the core medium. It is called step index fiber, if n is a constant within the core otherwise it is a graded index fiber. For a step index fiber, the value of n as a function of r is:

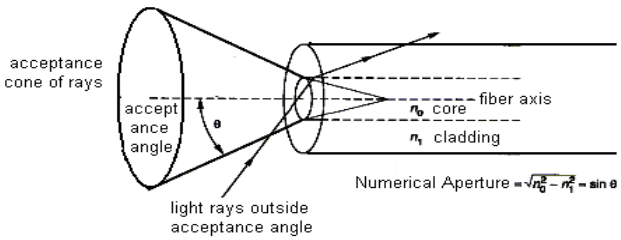

Fig. 2.5 Light rays to be guided in the core fall within a fiber's acceptance angle.

$$n = \begin{cases} n_0, & r \le a \\ n_c, & a \le r \le b \end{cases} \tag{2}$$

and which is graphed in the bellow figure, while for a graded index fiber, the value of n as function of r is:

$$n = \begin{cases} n_0\left(1 - 2\Delta(r/a)^x\right)^{1/2}, & r \le a \\ n_c, & a \le r \le b \end{cases} \tag{3}$$

Where x = 2.

we define, [pic], typically as $\Delta = \frac{n_0 - n_c}{n_c}$; which is usually not more than a few percent.

The approximated numerical aperture can be:

$$NA = \sqrt{n_0^2 - n_c^2} \approx n_0 \sqrt{2\Delta} \tag{4}$$

The typical value corresponding to a maximum entry angle is NA = 0.2 $\theta = 11^\circ$. The distortion of propagating wave is referred to as the dispersion. The constant group velocity in general is required by the dispersionless transmission. Dispersions are of several types. If a propagating wave is consisting of several kinds of modes with various transmission characters, modal dispersion is caused. Using single mode fibers, the modal dispersion can be avoided in principle having the cross section close to λ, and are common at 850 nm and 1300 nm. Typically, the core has a diameter of $8-12\mu m$ and the diameter of cladding as $125\mu m$. The diameter core of multimode fibers is $50-100\mu m$ and the diameter of the cladding $125-140\mu m$.

Reduction of modal dispersion is the main purpose of graded index fibers in multimode fibers. For the propagation of waves if we use the ray modal, at the core and cladding boundary, different modes correspond to a different angle of incidence; the steeper angle rays propagate with lower group velocity. In the graded index fibers, however, away from the center, the index of refraction decreases, hence as the cladding is approached, the speed of light increases, and this compensates for the different modes taken by different paths. The fibers of single mode have $\Delta = 0.2-1\%$ and the multimode fibers have $\Delta = 1-3\%$. Imperfect materials cause material dispersion whose n depends on λ. This effect is generally comparing modal dispersion an order of magnitude smaller, qualified typically in terms of:

$$\frac{d^2 n}{d\lambda^2} \tag{5}$$

Waveguide dispersion is the third type of dispersion, caused by the non constant group velocity which is a function of λ for a mode fixed. The propagation pulse broadening is the main consequence of dispersion. In terms of the variance σ^2 of waveform, the pulse

broadening can be quantified. Thus considering a light pulse whose intensity as function of time can be $I(t)$; by normalizing the intensity so that:

$$\int_{-\infty}^{\infty} I(t)dt = 1 \tag{6}$$

Defining the mean time as:

$$\bar{t} = \int_{-\infty}^{\infty} tI(t)dt \tag{7}$$

and variance as:

$$\sigma^2 = \int_{-\infty}^{\infty} (t-\bar{t})I(t)dt \tag{8}$$

Inputing the pulse with variance σ^2 into a dispersive system, output has variance $\sigma^2 out$ given by:

$$\sigma_{out}^2 = \sigma_{in}^2 + \sigma_{\mathrm{modal}}^2 + \sigma_{waveguide}^2 + \sigma_{material}^2 \tag{9}$$

The spectral width of the light pulse is an important consideration in the quantification of dispersion. The spectral width σ_λ as a function of wavelength is a measure of the purity of light signal. Cosidering intensity as a function of the wavelength, $I(\lambda)$, the spectral width then is defined as:

$$\sigma_\lambda^2 = \int_0^{\infty} (\lambda - \bar{\lambda})^2 I(\lambda)d\lambda \tag{10}$$

where:

$$\bar{\lambda} = \int_0^{\infty} \lambda I(\lambda)d\lambda \tag{11}$$

and the normalized intensity as:

$$\int_0^{\infty} I(\lambda)d\lambda = 1 \tag{12}$$

Since the dispersion is the cause for the pulse broadening, too many pulses are attempted to be placed per second, spreading takes place and they interfere each other. Thus the possible limitation is measuring the available bandwidth in MHz or Mbps. As we shall see soon, the bandwidth distance product in units of $MHz-km$ is roughly constant as the bandwidth is inversely proportional to distance. For step index multimode fiber, this is $20MHz-km$, for a multimode graded index fiber it is $2.5GHz-km$, and it can be larger $10GHz-km$ or more for single mode optical fibers.

2.5 Material dispersion

Consider the group delay to understand the effect of dispersion. Through a transmission system, for energy propagation, this is the time delay per unit length. It can be assumed that each spectral component undergoes its own time delay τ_g and travels independently. Let v_g be the group velocity and L, be the transmission distance. Then:

$$\frac{\tau_g}{L} = \frac{1}{v_g} = \frac{1}{c}\frac{d\beta}{dk} = -\frac{\lambda^2}{2\pi}\frac{d\beta}{d\lambda} \tag{13}$$

Where: $$k = 2\pi/\lambda \tag{14}$$

when the spectral width is σ_λ not very big, over the range of the wavelengths consisting the light energy the delay difference can be approximated by $d\tau_g/d\lambda$ at the wavelengths $\bar{\lambda} \pm \sigma_\lambda / 2$. Thus, between two such spectral components, the delay difference is:

$$\sigma_g = \frac{d\tau_g}{d\lambda}\sigma_\lambda = -L\frac{\sigma_\lambda}{2\pi C}\left(2\lambda\frac{d\beta}{d\lambda} + \lambda^2\frac{d^2\beta}{d\lambda^2}\right) \tag{15}$$

Dispersion constant D is: $$D = \frac{1}{L}\frac{d\tau_g}{d\lambda} \tag{16}$$

Its units are typically given as picoseconds per kilometer per the nanometer. We use the approximation of ray modal, to quantify the material dispersion, which particularly yields, $\beta = \frac{2\pi n}{\lambda}$, where $n = n(\lambda)$ is a function in wavelength. Which yield,

$$\tau_{mat} = \frac{L}{c}\left(n - \lambda\frac{dn}{d\lambda}\right) \tag{17}$$

And hence: $$\sigma_{mat} = -\frac{L}{c}\lambda\frac{d^2n}{d\lambda^2}\sigma_\lambda \tag{18}$$

Material dispersion constant D_{mat}: $D_{mat} = -\frac{\lambda}{c}\frac{d^2n}{d\lambda^2}$ (19)

Then: $$\sigma_{mat} = D_{mat}L\sigma_\lambda \tag{20}$$

2.5.1 Waveguide dispersion

we now quantify waveguide dispersion, $b = 1 - \left(\frac{ua}{V}\right)^2$ (21)

For a small Δ, we get: $\beta \approx n_2 k(b\Delta + 1)$

(22)

when [pic] not a function of λ, $\tau wg = \frac{L}{c}\frac{d\beta}{dk}$ (23)

Now, $V = kan_2\sqrt{2\Delta}$ and hence: $\tau wg = \frac{L}{c}\left(n_2 + n_2\Delta\frac{d(Vb)}{db}\right)$ (24)

the computation yields: $\frac{d(Vb)}{db} = b\left(1 - \frac{2J_v^2(ua)}{J_{v+1}(ua)J_{v-1}(ua)}\right)$ (25)

Then: $\sigma_{wg} = \sigma_\lambda L D_{wg} = -\frac{n_2 L\Delta\sigma_\lambda}{c\lambda} V\frac{d^2(Vb)}{d\lambda^2}$ (26)

At lower wavelengths: $\frac{\sigma_{wg}}{L} \approx \frac{0.003\sigma_\lambda}{c\lambda}$ (27)

And: $\frac{\sigma_{mat}}{L} \approx \frac{0.02\sigma_\lambda}{c\lambda}$ (28)

And hence the domination of material dispersion take place. At the higher wavelengths (about $1.3\mu m$), domination of waveguide dispersion takes place.

2.5.2 Model dispersion

the approximated modal dispersion in the multimode fibers is:

$$\sigma_{\text{mod}} = \frac{n_1\Delta L}{c} \quad (29)$$

now attenuation can be considered. Any propagating signal can be attenuated by the optical fiber. Given the input power P_{in} over a length of the fiber L and power output P_{out}, the mean constant of attenuation α of a fiber, in terms of units of dB/km, defined as:

$$\alpha = \frac{10}{L}\log\left(\frac{P_{in}}{P_{out}}\right) \quad (30)$$

The unit of decibel (dB) is used for the power ratio representation. However, it is convenient sometimes the representation of power levels on the logarithmic scale. The dBm is the most commonly used unit, which corresponds to 10Mw power reference:

$$P_{dBm} = 10\log\frac{P}{10\times10^{-3}} \quad (31)$$

Absorption of photons or energy is one of the main causes of the attenuation. When fiber is exposed to radiation atomic defects result, which cause atomic absorption, impurity atoms cause extrinsic absorption, and constituent atoms of the material cause intrinsic absorption. Extrinsic absorption is the dominant absorption mechanism, causes primarily by metallic ions like iron, cobalt, etc. and OH^- ions. The propagation distance was limited primarily by absorption by OH^- ions in early optical fibers. During the manufacture process these ions were introduced into the material from the water vapor or from the presence of water. Leaving the windows for the transmission between the wavelengths, attenuation caused by this ion is grater at 1400, 950 and 725 nm. With the advent of the vapor axial deposition (VAD) fabrication method, tremendous reduction in the OH^- concentration in fibers observed.

In modern fibers, the losses are caused by infrared loss, ultraviolet absorption and scattering losses. Modeled by the Rayleigh scattering, the scattering losses are caused by the light wave interaction with the constituent molecules which are in the light wavelength order. The loss of Rayleigh scattering is $\approx 1/\lambda^4$, so by increasing the wavelength it can be reduced. Infrared absorption losses tend to increase with λ on the other hand, and which is usually worst above $1.5\mu M$. By doping the halides, the point where the loss starts to increase to a unacceptably large levels can be pushed out. The combined effect of such losses in general is minimum at about $1.3\mu M$.

Losses also caused by microbends and bends; in the surface of the fiber, a microbend is a tiny crinkle or an imperfection, on several wavelength dimensions, and responsible for a perturbation within the field. Thus microbends causes power loss, not having the desered propagation characteristics, lead to coupling to higher order modes. Microbending and bending can result in the manufacturing process, especially during the spooling process. When we consider the very lengthy continuous fibers, of lengths of 1km or more, for the manufacturing, then spooling the fiber to minimixe the bends and microbends is of a not trivial. Significant losses are introduced by the splicing or coupling the fiber segments together which is the reason for manufacturing such a long fibers. All the ouput power of one segment is not inserted to the other as the faces of the

two segments are not properly aligned, which is the basic reason for the loss. Losses can be kept down to as small as 0.01dB/km, in the modern fibers.

The bandwidth length product is constant approximately, when L denotes the length of the fiber and the BW the signal bandwidth. On overall system parameters, such as the total power loss, and the BER, etc this constant depends. An empirical result more precisely is:

$$BW \times L^{\gamma} \tag{32}$$

is more or less constant, and the parameter γ is of some value between 0.5 and 0.9. Generally, for L<1km, $\gamma = 0.9$ whereas for L>1km. $\gamma = 0.5$. Actually, it is not entirely an empirical result. Over long distances the modes are strongly couple one another and do not propagate independently and energy at one mode tend to couple or induce the energy at the other mode, the light travels over a longer and very longer distances. In any case, the applications of optical fibers propagation into long haul and short haul links are separated by the length of 1km usually.

2.6 Light propagation through optical fiber – mode theory

The mode theory is used to explain the transmission of light along the optical fiber. The properties of light in fiber are described by using the mode theory where the ray theory is unable to explain. A set of electromagnetic waves which are guided is called as the modes in the optical fiber. A light wave can be represented as a plane wave, as suggested by the mode theory. By its amplitude, direction, and wavelength of propagation a plane wave is described. The wavelength of the plane wave is given as:

$$wavelength(\lambda) = \frac{c}{fn}$$

c is the light speed in the vacuum, f is the light frequency, and n is the plane wave medium refractive index.

Wave-fronts may undergo a change in phase that prevents the successful transfer of light along the fiber. Only those wave-fronts fall on the optical fiber at less than or equal to the critical angle only may travel through the fiber. As the wave travels through the fiber the wave-front suffers a gradual phase change in the fiber. If propagating wave-

fronts which are not in same phase, and they disappear eventually. Because of the destructive interference, the wave-fronts disappear. The in phase wave fronts interfere with the wave-fronts that are out of phase. The reason for why along the optical fiber only a finite number of modes can transmit is this interference.

It is assumed that the direction of transmission of the plane wave is in the z direction. The repetition of the plane wave is at a distance of $\lambda/\sin\theta$. The repetition of plane waves also can be observed at a distance of $\beta=2\pi\sin(\theta)/\lambda$. B is defined as the propagation constant along the fiber axis. The value of the propagation constant also must change as the wave length λ changes. A change in the wavelength can obstruct the mode from traveling along the fiber for a particular mode. Then such mode is said to be cut off and it no longer bound to the fiber. If the mode is defined with a particular wavelength may not exist at any other longer wavelengths. The cut off wavelength of the mode is the wavelength at which the mode ceases to be bound within the fiber. The optical fiber is however supports at least one mode to propagate along the fiber. This is called the fundamental mode of the optical fiber. And it can never be cut off from the optical fiber. The cut off wavelength of the fiber is the wavelength which stops the next higher order modes from traveling through the fiber. The single mode fiber is the one which operates above the cut off wavelength of the fiber. A multimode fiber is one which operates below the cut off wavelength of the optical fiber. The propagation constant of a plane wave in a fiber is a function of the wave's mode and the wavelength of the wave. For different waves the change in the constant of propagation is called dispersion. For different waves of different wavelengths the change in the propagation constant is called the chromatic dispersion. And for different modes the change in the propagation constant is called the modal dispersion. As the wave goes down the fiber, these dispersions cause the light pulse to spread. Dispersion occurs in all types of fibers.

2.6.1 Modes of guided waves

Consider a plane electromagnetic wave of frequency f in the z-direction through a refracting medium by writing the amplitude of its electric field component in the y-direction as the real part of E_y,

$$E_y = E_0 \exp\{-j(\omega t-\beta z)\} \quad (1)$$

Here, E0 is the field constant; $\beta = \frac{2\Pi}{\lambda m}$ is the propagation constant in the medium; $\omega = \frac{2\Pi}{t}$, is the angular frequency of the wave; and j^2=-1.

Eqn (1) represents a plane view traveling through a bulk dielectric material and we may imagine it to be plane polarized so that the electric vector is confined to the y-z plane.

The phase velocity of this wave is, $vp = \frac{\omega}{\beta}$

Thus, $$vp = \lambda_m f = \frac{\omega}{\beta} = \frac{c}{n} \text{ and } n = \left(\frac{c}{\omega}\right)\beta .$$

Because optical fibers are cylindrical in structure, we need to find guided wave solutions that are subjected to radial symmetric variation. The solutions are conveniently expressed in cylindrical polar coordinates and have the form

$$E = E(r,\phi)\exp\{-j(\omega t - \beta z)\}$$

In general the field components at any (r,ϕ) vary in phase as well as in amplitude and it is convenient to treat $E(r,\phi)$ as a complex phase or representing both the phase and the amplitude of the oscillating field component at that point.

The boundary conditions imposed by the fiber structure and geometry on the solutions to the E-M wave give rise to Eigen value solutions for $E(r,\phi)$. Each $E(r,\phi)$ has a particular β value for any given optical angular frequency ω. It is this discrete propagating electro magnetic field patterns $E(r,\phi)$ are referred to as modes. The step index and the graded index fibers are able to support many such modes. They are the examples of multi mode fibers. Because the propagation constant β varies from mode to mode, each mode propagates with its own characteristic phase and group velocity. This property is called as multimode dispersion.

In a typical fiber, as many as thousand modes may propagate. The actual number is proportional to the core area and to $(NA)^2$. If the product of these two parameters is decreased sufficiently, a situation is reached eventually in which only one mode can propagate. Multimode dispersion is then totally eliminated. Fibers designed to operate like this are known as single mode fibers or mono mode fibers.

In an optical fiber, a set of guided electromagnetic waves which propagates through it is called modes of an optical fiber. Modes having two components can be described by Maxwell's electromagnetic equations. The magnetic field, H(x, y, z), and the electric field E(x, y, z) are the two components of the wave modes. The magnetic field, H, and the electric field, E, are at right angles to each other in the wave. In an optical fiber, the traveling modes are said to be transverse in nature. In TE modes, the Electric field direction is perpendicular to the propagation direction and the magnetic field direction is in the direction of the travel.

Transverse magnetic (TM) mode is another kind of transverse mode. The TM modes and the TE modes are opposite to one another. The electric field is in the travel direction and magnetic field is perpendicular to the travel direction in the TM modes. Within the core of the fiber, the order of each mode is indicated by the number of field maxima. TE0 has one field maxima for example. The electric field decays towards the cladding and core boundary and is a maximum at the center of the waveguide. The TE0 is considered as the lowest order standing wave or as the fundamental mode of the waveguide. The order of the wave mode is higher, if the number of the field maxima increases. The higher order modes are referred as modes with more than a few field maxima, generally.

The determination of the order of the mode is also done by the angle the wave front makes with the fiber axis. Modes of higher order cross the fiber axis at steeper angles. It is to be noted that the modes are actually not confined fully to the fiber core. The modes partially penetrate into the cladding material. The lower order modes only slightly penetrate into the cladding material. The electric and magnetic fields of the lower order modes concentrate at the center of the optical fiber. The higher order modes however extend further into the cladding material. The electric and magnetic fields of the higher order modes distributed in greater extent towards the outer edges of the fiber. Because of the penetration of the higher order and lower order modes into the cladding some portion of the light is refracts out of the core of the fiber. Because of the dimensions of the cladding region the refracted rays will be trapped in the cladding of the fiber. Cladding modes are the modes that are trapped in the cladding region. Coupling of modes occur when the core and cladding modes propagate through the optical fiber. The exchange of

power between two modes are called mode coupling in the fiber. Loss of power from the core modes occur when modes couple to the cladding. Leaky modes also present in the fiber in addition to the refracted and bound modes of the fiber. Clear cut similarity can be noticed between leaky modes and leaky rays. When they travel through the fiber, the leaky modes will loss their optical power accordingly. The mode must satisfy certain boundary conditions to remain within the core. The propagation constant β of the mode must satisfy the following boundary conditions to remain within the core of the fiber.

$$\frac{2\pi n_2}{\lambda} < \beta < \frac{2\pi n_1}{\lambda}$$

The leakage of the power from the core entry into the cladding takes place when the propagation constant becomes less than the 2ΠIn2/λ. In a few centimeters into the cladding, the leaked modes are entirely lost.

2.6.2 Normalized frequency

By the fiber's normalized frequency, the electromagnetic waves of normalized frequency bound to an optical fiber are described. The number of modes an optical fiber supports can be determined by the normalized frequency. And it is a dimensionless quantity. It is also related to the cutoff wavelength of the fiber. The normalized frequency 'V' can be defined as:

$$V = \frac{2\pi a}{\lambda}(n_1^2 - n_2^2)^{\frac{1}{2}}$$

Where '*a*' is the core diameter, and λ is the wavelength of light in air. The number of modes that can exist in a fiber is a function of V. As the value of V increases, number of modes supported by the fiber increases. Optical fibers, singe mode and multimode, can support a different number of modes.

The core size of single mode fibers is small. A core of this size of the fiber allows the lowest order mode to propagate or allows only fundamental mode around a 1300 nm wavelength. When the operational wavelength (λ) approaches the core size of the fiber, single mode fibers propagate only one mode. Thus the mode propagation in the fiber is related with the value of the normalized frequency parameter (V) and the size of the core. V is equal to or less than the value 2.405, in the single mode fibers. The higher order

modes are lost in the fiber cladding, while the fundamental mode propagates down the fiber core, in single mode fibers as the level of V is 2.405. The propagation of the power takes place mostly in the cladding material for low V values (level 1.0). At the fiber bends the power transmitted by the cladding is lost easily. The V value should remain at the level of 2.405.

2.6.3 Bessel functions

Optical fiber composed of dielectric material consists of basically a two layered structure. Along the straight longitudinal axis it has a uniform circular cross-section. To derive several important propagation characteristics, we analyze first the electromagnetic fields present in optical fibers. With the radian (operating) frequency ω, we study fields in phasor form. The core is assumed to be characterized by a perfect dielectric by ε, μ, and the parameter k can be defined as:

$$k = \omega\sqrt{\mu\varepsilon} \tag{1}$$

We assume also that along the longitudinal axis, the power flow is occurring. The electric field has the form by setting this to be the z-axis:

$$\vec{\mathrm{E}} = \vec{e}(r,\phi)e^{-j\beta z} + e_z(r,\phi)e^{-j\beta z}\hat{a}_z \tag{2}$$

Where, $\vec{e}$, lies in the transverse plane which has no component of z, and (r,ϕ) are the transverse plane polar coordinates. The magnetic field similarly is given by;

$$\vec{H} = \vec{h}(r,\phi)e^{-j\beta z} + h_z(r,\phi)e^{-j\beta z}\hat{a}_z \tag{3}$$

The parameter β is called the constant of phase. When β positive and real it can be shown that power flow in the positive –direction occurs. The velocities of phase and group of the field, v_p and v_g, respectively, are defined as:

$$v_p = \frac{\omega}{\beta}, v_g = \frac{1}{\frac{d\beta}{d\omega}} \tag{4}$$

moreover, the information along the optical fiber or the speed of propagation of energy is the group velocity. Let q is defined as:

$$q = \sqrt{k^2 - \beta^2} \tag{5}$$

Then, equations of Maxwell for $\vec{\mathrm{E}}$ and $\vec{H}$ are:

$$\frac{\partial^2 e_z}{\partial r^2}+\frac{1}{r}\frac{\partial e_z}{\partial r}+\frac{1}{r^2}\frac{\partial^2 e_z}{\partial \phi^2}+q^2 e_z=0,$$

$$\frac{\partial^2 h_z}{\partial r^2}+\frac{1}{r}\frac{\partial h_z}{\partial r}+\frac{1}{r^2}\frac{\partial^2 h_z}{\partial \phi^2}+q^2 h_z=0 \tag{6}$$

and

$$e_r=-\frac{j}{q^2}\left(\beta\frac{\partial e_z}{\partial r}+\frac{\omega\mu}{r}\frac{\partial h_z}{\partial \phi}\right),$$

$$e_\phi=-\frac{j}{q^2}\left(\frac{\beta}{r}\frac{\partial e_z}{\partial \phi}-\omega\mu\frac{\partial h_z}{\partial r}\right),$$

$$h_r=-\frac{j}{q^2}\left(\beta\frac{\partial h_z}{\partial r}-\frac{\omega\varepsilon}{r}\frac{\partial e_z}{\partial \phi}\right),$$

$$h_\phi=-\frac{j}{q_2}\left(\frac{\beta}{r}\frac{\partial h_z}{\partial \phi}+\omega\varepsilon\frac{\partial e_z}{\partial r}\right) \tag{7}$$

Superposition of several types of fields is represented by the method of modal analysis. Modes are of several types. Since, in this situation no (nonzero) TEM modes lead to real flow of power, we must first outright reject TEM (transverse electric and magnetic) modes, in which both $e_z=0$, and $h_z=0$. The transverse electric (TE) modes have $e_z=0$, while transverse magnetic (TM) modes have, $h_z=0$. There are several important fields which can't be represented as the superposition of such modes, although TM or TE modes lead to a analysis somewhat simplified. The more general hybrid modes must also we must therefore consider; modes HE have, $|h_z|\rangle\rangle|e_z|\rangle 0$, [pic], and EH modes have $|e_z|\rangle\rangle|h_z|\rangle 0$. To seek functions periodic in the situation leads us is the geometry ϕ . We assume therefore -the form has the dependence $e^{jv\phi}$ where v is an integer (positive, negative, or 0). Thus:

$$e_z(r,\phi)=AF_V(r)e^{jv\phi} \tag{8}$$

and hence:

$$\frac{\partial^2 F_v}{\partial R^2}+\frac{1}{r}\frac{\partial F_v}{\partial r}+\left(q^2-\frac{v^2}{r^2}\right)F_v=0 \tag{9}$$

This is moreover in the core region, that we impose, $F_v(r)$ to stay finite as $r\to 0$. The solution is the v^{th} Bessel function of the first kind, $J_v(qr)$. And a result that is similar holds for h_z. Let us now distinguish between the core $(r\langle a)$, characterized by ε_1,μ_0, and

cladding $(r\rangle a)$ characterized by ε_2, μ_0. A similar result holds for. Now let us distinguish between the core, characterized by, and the cladding characterized by. Define:

$$k_1 = \omega\sqrt{\varepsilon_1\mu}\,, \qquad k_2 = \omega\sqrt{\varepsilon_2\mu}\,,$$
$$w = \sqrt{\beta^2 - k_2^2}$$
$$u = \sqrt{k_1^2 - \beta^2}\,, \qquad (10)$$

Imposing the function of the core stays finite at r=0, the function of the cladding decay to 0 at $r \to \infty$, and that at r = 0, for flow of real power, we have u>0 and w>0. Particularly this requires, $k_1\rangle\beta\rangle k_2$, which can be a case in the real fibers. It is at this time may be convenient to express k_1 and k_2 in terms of the respective refractive indices n_1 and n_2 and the wavelength λ in free space:

$$k_1 = 2\pi n_1/\lambda, k_2 = 2\pi n_2/\lambda \qquad (11)$$

The core longitudinal components are given by:

$$E_Z = AJ_v(ur)e^{jv\phi}e^{j(\omega t-\beta z0}, \quad H_z = BJ_v(ur)e^{jv\phi}e^{j(\omega t-\beta z)} \qquad (12)$$

and those in the cladding are:

$$E_z = CK_v(wr)e^{jv\phi}e^{j(\omega t-\beta z)}$$
$$H_z = DK_v(wr)e^{jv\phi}e^{j(\omega t-\beta z)} \qquad (13)$$

particularly, same value can be imposed v characterize the fields in the cladding and core. Which is the compulsory condition for acheiving phase match at r=a; for example, E_z continuous at r=a. also, K_v is the v^{th} order Bessel function of the second kind. It is shown as $K_v(wr) \approx e^{-wr}$ asymptotically as $r \to 0$. It can be shown that asymptotically as. In fact, $|J_v(j\alpha)| = K_v(\alpha)$ for real α.

2.6.4 Mode cutoff

Mode cutoff we must have to have the field in the cladding decay:

$$\beta\rangle k_2 \qquad (14)$$

The $\beta = k_2$ is called cutoff condition. In addition if $F_v(ur)$ not real valued, if $u^2\langle 0$, then there is no flow of real power. Hence we must also have:

$$\beta\langle k_1 \qquad (15)$$

with a condition of corresponding cutoff $\beta = k_1$. Summarizing:

$$n_2 k \langle \beta \langle n_1 k \tag{16}$$

where, $k = 2\pi/\lambda$ is the wave- number of free space. We must impose the appropriate boundary conditions at r=a are:

$$E_{z1} = E_{z2}, E_{\phi 1} = E_{\phi 2} \tag{17}$$

The equations correspond to the condition that along the tangential component of the electric field should be continuous. The boundary condition first leads to:

$$AJ_v(ua) - CK_v(ua) = 0 \tag{18}$$

and the second to:

$$\frac{-j}{u^2}\left(A\frac{jv\beta}{a}J_v(ua) - B\omega\mu uJ'_v(ua)\right) - \frac{j}{w^2}\left(C\frac{jv\beta}{a}K_v(wa) - Dw\mu\omega K'_v(wa)\right) = 0 \tag{19}$$

We also impose:

$$H_{z1} = H_{z2}, H_{\phi 1} = H_{\phi 2} \tag{20}$$

These refers to the fact that if there is no surface current present, then along the dielectric boundary the tangential magnetic field is continuous. A total of four homogeneous equations we have in A, B, C, D:

$$M\begin{bmatrix} A \\ B \\ C \\ D \end{bmatrix} = \begin{bmatrix} 0 \\ 0 \\ 0 \\ 0 \end{bmatrix} \tag{21}$$

Since as we seek nonzero fields, all four constants A, B, C, and D can't have equal to zero; hence:

$$\det .M = 0 \tag{22}$$

For a field to be present this condition must be met. Define:

$$\mathrm{J}_v = J'_v(ua)/uJ_V(ua), \mathrm{H}_v = K'_V(wa)/wK_v(wa) \tag{23}$$

Equation (22) becomes: $$(\mathrm{J}_v + \mathrm{H}_v)(k_1^2\mathrm{J}_v + k_2^2\mathrm{H}_v) = \left(\frac{\beta v}{a}\right)^2\left(\frac{1}{u^2} + \frac{1}{w^2}\right)^2 \tag{24}$$

for a given k, that is ω, values u, w are known functions of β. Hence, (24) specifies β β as a frequency function ω, and a function of the parameter v. The solutions of this equation are only discrete, and for each v there will be many roots defined as:

$$\beta_{v1}, \beta_{v2} \ldots, \beta_{vN} \tag{25}$$

The modes corresponding are denoted as TE, TM_{vm}, HE_{vm}, as is appropriate. In particular let us examine the TM and TE modes. By setting A=B=0, we obtain TE and we seek nonzero C, D; similarly TM is obtained by setting C=D=0 and we seed nonzero A, B. This requires in each case, a 2×2 sub-matrix of M for nonzero determinant, and can be shown to require in particular:

$$v = 0 \tag{26}$$

Thus, there is no ϕ variation for TM and TE modes. Which the equation determining β for TM $TE\ om$ is:

$$\frac{J_1(ua)}{uJ_0(ua)} + \frac{K_1(wa)}{wK_0(wa)} = 0 \tag{27}$$

Similarly, the equation determining β for $TM\,om$ is:

$$\frac{k_1^2 J_1(ua)}{uJ_0(ua)} + \frac{k_2^2 K_1(wa)}{wK_0(wa)} = 0 \tag{28}$$

If, $v \neq 0$, we don't have TM or TE modes, and the corresponding analysis becomes complex. If $n_1 \approx n_2 (n_1 - n_2 \langle\langle 1)$, we can apply approximations of an important class which lead to weakly guided waves.

The condition of cutoff is $w^2 \to 0$ for lower order modes given in the bellow table.

Table: 2.2: The condition of cutoff for lower order modes

v	*Mode*	*Cutoff condition*
0	TE_{om}, TM_{om}	$J_0(ua) = 0$
1	HE_{1m}, EH_{1m}	$J_1(ua) = 0$
≥2	EH_{vm},	$J_v(ua) = 0$
	HE_{vm}	$\left(\frac{n_1^2}{n_2^2}+1\right) J_{v-1}(ua) = \frac{ua}{v-1} J_v(ua)$

We now discuss the V-parameter also called the V-number or the normalized frequency. The V value is defined as:

$$V^2 = (u^2 + w^2)a^2 = \left(\frac{2\pi a}{\lambda}\right)^2 (n_1^2 - n_2^2) \tag{29}$$

which is the dimensionless number. Noting the value $2\pi/\lambda$ which is proportional to frequency (a factor equal to the speed of light), therefore V is called as the normalized frequency. The V value is corresponds to the number of modes a particular fiber can support. The normalized propagation constant also defined as:

$$b = \frac{a^2 w^2}{V^2} = \frac{(\beta/k)^2 - n_2^2}{n_1^2 - n_2^2} \tag{30}$$

Noting that 0<b<1 corresponds to light travel. Graph of b or β/k versus v shows, for a fixed V, only that several number of modes are possible. Particularly, the HE_{11} mode correspond to a value of b within the range 0 to 1 for all V, down to V = 0. None of the other modes exists until V = 2.405 (which is the smallest root of J_0). Hence, all modes other than the HE_{11} are cutoff below this value of V. HE_{11} is called the dominant mode for this reason. The numerical aperture of a fiber can be defined as:

$$NA = \sqrt{n_1^2 - n_2^2} \tag{31}$$

so that:

$$V = \frac{2\pi a}{\lambda} NA \tag{32}$$

For the wave propagation, using the approximation of ray theory, the physical importance of the numerical aperture can be obtained. According to total internal reflection (TIR), it can be assumed that the light propagates in the optical fiber like a plane wave reflecting back at the bottom and at the top core cladding boundaries. When the incident angle at dielectric boundary exceeds the critical angle, then TIR occurs. That is when:

$$\sin\theta_i \geq \frac{n_2}{n_1} \tag{33}$$

It can be proved that the cladding has no real power flow associated with it when TIR occurs, which is called evanescent. Let us assume the launching of light wave into the optical fiber core from air medium, with the entry angle, θ_{entry}, then:

$$\cos\theta_{entry} = \sin\theta_i \tag{34}$$

Thus, we define the numerical aperture in terms of the maximum angle, with which the light power will be launched into the optical fiber as:

$$NA = \sin\theta_{entry,\max} \tag{35}$$

The coincidence of two numerical apertures take place when $n_1 - n_2 \langle\langle 1$. According to equation (32), V is increased by two basic factors, thereby increase the number of modes exist in light transmission in optical fiber. First V is increased, if relative to wavelength, the diameter a, is increased. Hence, single mode optical fibers permit only one mode the HE_{11} mode to propagate which have narrow core diameter. Multimode optical fibers permit many modes, which have large core diameters. In the multimode fibers the large core diameters enlarge V additionally. Equation (1.35) represents a large NA relating to the ability of the optical fiber to permit a larger beam width of the inputting light signal. LED sources are used with large NA multimode fibers, as LED light sources generate much broader light beams comparing to semiconductor laser diodes.

Consider multimode fibers of large number of modes M with a laser beam input. Approximated $\sin\theta$ by θ, the light input solid acceptance angle specified by (1.35) is:

$$\Omega = \pi\theta^2 = \pi(n_1^2 - n_2^2) \tag{36}$$

For a laser with radiation or a waveguide at [pic], the unit solid angle number of modes is approximately:

$$2A/\lambda^2 \tag{37}$$

Where, $A = \pi a^2$ can be the area; the two polarized orientations are referred by factor 2. Then:

$$M \approx \frac{2A}{\lambda^2}\Omega = \frac{2\pi a^2}{\lambda^2}(n_1^2 - n_2^2) = \frac{V^2}{2} \tag{38}$$

2.6.5 Weakly guiding approximation

Now let us return to the approximation of weakly guiding optical fibers. Represent Δ as:

$$\Delta = \frac{n_1}{n_2} - 1 \tag{39}$$

and assuming $\Delta \langle\langle 1$. Two modes are said to be degenerate, if they are same value for [pic]. Although they have different distributions of field, we associate the degenerate modes as together, since the degenerate modes have the identical transmission characters. We consider all the linear combinations of a category of degenerate modes, in

other words to be a mode into itself. As per their degeneracies we group primary lower order modes:

$$\begin{aligned} &HE_{11} \\ &TE_{01}, TM_{01}, HE_{21} \\ &HE_{31}, EH_{11} \\ &HE_{12} \\ &HE_{41}, EH_{21} \\ &TE_{01}, TM_{02}, HE_{22} \end{aligned} \tag{40}$$

Numerically, $\Delta \approx 1$ implies:

$$K_1^2 \approx K_2^2 \approx \beta^2 \tag{41}$$

and we get:

$$\mathrm{J}_\nu + \mathrm{H}_\nu = \pm \frac{\nu}{a}\left(\frac{1}{u^2} + \frac{1}{w^2}\right) \tag{42}$$

The positive sign correspond to EH modes:

$$\frac{J_{\nu+1}(ua)}{uJ_\nu(ua)} + \frac{K_{\nu+1}(wa)}{wK_\nu(wa)} = 0 \tag{43}$$

and the HE modes correspond to negative sign:

$$\frac{J_{\nu-1}(ua)}{uJ_\nu(ua)} - \frac{K_{\nu-1}(wa)}{wK_\nu(wa)} = 0 \tag{44}$$

summarizing:

$$\frac{uJ_{j-1}(ua)}{J_j(ua)} = -\frac{wK_{j-1}(wa)}{K_j(wa)} \tag{45}$$

where:

$$j = \begin{cases} 1, & TE \text{ and } TM \\ \nu+1, & EH \\ \nu-1, & HE \end{cases} \tag{46}$$

hence all modes are degenerate which have same j and m; as an example $HE_{\nu+1,m}$, and, $EH_{\nu-1,m}$. Since the degenerate modes can be combined to give a fixed orientation, this pair of modes are called, LP (linearly polarized) modes. That means only one H component and one E component are significant in a set of modes, say $\vec{\mathrm{E}}$ polarizes along one of the axes and $\vec{\mathrm{H}}$ perpendicular to the axis. If the polarizations are reversed, then

equivalent solutions can be obtained. Combining the two cases, $\cos j\phi$ and $\sin j\phi$ so the mode patterns of four form one LP_{vm} mode.

2.7 Applications of optical fibers

Telecommunications applications are widespread, ranging from global networks to local telephone exchanges to subscribers' homes to desktop computers. These involve the transmission of voice, data, or video over distances of less than a meter to hundreds of kilometers, using one of a few standard fiber designs in one of several cable designs. Optical fiber is also used extensively for transmission of data signals. Because of various advantages of optical fibers for data transmission, they are used in Local Area Network (LAN), Metropoliton Area Network (MAN), and Wide Area Network (WAN). Optical fibers are used transmit information for the protection, supervision and control of the system, which are extremely important in large scale modern power plants.

Military applications of optical fibers include, communication, command and control links in battlefield, on ships and aircraft. Lighter weight is important for the military services as it allows faster deployment of communication cables on battlefields. A noves application is the fibre-guided missile. They are used as light guides in medical and other applications where bright light needs to be shone on a target without a clear line-of-sight path. Fiber optic endoscope is used to view the internal organs of the human body which is otherwise inaccesible. LASER enhanced Transluminal Angioplasty system system is used to transmit optical energy through the fiber to evaporate the built up plaque that is blocking an artery. Fiber optic devices are also used to treat the cancer in the human body. In a non transmission application of optical fiber, tremendous progress has been made over the last decade in using fibers as a versatile sensing medium both in science and industry.

2.8 Optical sources and detectors

The fiber optic data link must convert an electrical signal to an optical signal permitting the transfer of data along an optical fiber. The fiber optic device responsible for that signal conversion is a fiber optic transmitter. It launches optical signals into the fiber after converting the electrical signals into optical signals. Fiber optic transmitter consists

of a source drive circuit, an interface circuit and an optical source. Accepting the incoming electrical signal and processing it to make compatible with signal drive circuit is done by the interface circuit. By varying the current through the source, the source drive circuit modulates the intensity of the optical source. The conversion of electrical energy into optical energy is done by an optical source. Then for the propagation, the light emitted by an optical source will be launched into an optical fiber. The launched optical power into the optical fiber will decide the performance of the fiber optic data link.

2.8.1 Optical source properties

Semiconductor optical sources have the physical characteristics and performance properties necessary for successful implementations of fiber optic systems. Be compatible in size to low-loss optical fibers by having a small light-emitting area capable of launching light into fiber. They are required to

- Launch into the optical fiber the sufficient optical power.
- Emit light at wavelengths that minimize optical fiber loss and dispersion.
- Should have a narrow spectral width.

The source must maintain stable operation in changing environmental conditions such as temperature. For the optical fiber systems the suitable semiconductor sources range from more expensive semiconductors to inexpensive light emitting diodes (LED's). The principal light sources used in optical fibers are the semiconductor LED's and laser diodes (LD's). Optical sources produce the power range from tens of milliwatts (mW) for semiconductor (LD's) to microwatts for (LED's). All the available optical power is not possible to couple into the optical fiber for the transmission. The coupled amount of optical power into the fiber depends on the factors following:

- Over the light emitted angles
- The light emitting area of the source relative to the fiber core size.
- The source and fiber alignment
- The characters of coupling of the fiber, such as the refractive index profile and the NA.

The emitted light by the semiconductor lasers spread over an angle of 10 to 15 degrees. The light emitted by semiconductor LED's spread out at even larger angles. Especially with LED's losses of coupling of several decibels easily can result, when light coupled from an optical source to a fiber. The efficiency of the coupling depends on the coupling technique and also on the attached fiber to the optical source. The coupling of source to fiber depends on centering a flat fiber – end face over the light source emitting region. The coupling is referred as the butt coupling when the fiber end face is placed directly over the emitting region of the source. The efficiency of the source to fiber coupling may be improved, when the output light pattern of the source is larger than the acceptance pattern of the source.

2.8.2 Operating wavelength

The operating windows of wavelengths of fiber optic communication systems lies in the range of 850-nm, the 1300-nm, the 1550nm. The sources of semiconductor are so designed that they operate at maximum system bandwidth and at wavelengths that minimize absorption of optical fiber. Absorption can be minimized from the impurities such as hydroxyl ions (OH-), by constructing the optical source to operate at specified wavelengths. At the required operational wavelength the maximization of system bandwidth, depends on the designing of the sources and optical fiber that minimize inter modal and chromatic dispersion.

An 850-nm operational wavelength avoids fiber absorption loss from OH^- impurities near the 900-nm wavelength. Light sources for 850-nm systems were originally semiconductor LED's and lasers. Currently, most 850-nm systems use LED's as a light source. LED's operating at 850-nm provide sufficient optical power for short-distance, low-bandwidth systems. However, multimode fiber dispersion, the relatively high fiber attenuation, and the LED's relatively low optical output power prevent the use of these devices in longer-distance, higher bandwidth systems. The first development allowing the operational wavelength to move from 850 nm to 1300 nm was the introduction of multimode graded-index fibers.

Multimode graded-index fibers have substantially lower inter-modal dispersion than multimode step-index fibers. Systems operating at 850 nm cannot take full advantage of the fiber's low inter-modal dispersion because of high chromatic dispersion at 850 nm. However, the use of multimode graded-index fibers allow 850-nm LED's to operate satisfactorily in short-distance, higher bandwidth systems. Following the enhancements in multimode fiber design, next generation LED's were designed to provide optical emission in the 1300-nm region. Multimode graded-index fiber systems using these LED's can operate over longer distances and at higher bandwidths than 850-nm systems. Longer distances and higher bandwidths are possible because fiber material losses and dispersion are significantly reduced at the 1300-nm region.

2.8.3 Semiconductor material and device operating principles

Device operating principles and semiconductor material requires the knowledge of semiconductor material and device properties for the understanding of the optical emission in semiconductor lasers and LED's. The diodes with all of the characteristics typical diodes are the semiconductor diodes. Their construction however includes a special layer which emits photons (light particles) when a current passes through the layer. By the layering of the materials within the semiconductor and the material used, the particular properties of the semiconductor are determined. The two most common semiconductor materials used in electro optic devices and electronic are the Silicon (Si) and gallium arsenide (GaAs). To modify the semiconductor properties, other elements, such as aluminum (Al), indium (In) and phosphorus (p), are added to the base semiconductor in some cases. They are called dopant elements. The production of light is caused by the flow of current through a semiconductor optical source. When a current is passed through them, the LEDs generally produce light through spontaneous emission. The random generation of photons within the active layer of the LED is the spontaneous emission. The photons that emitted are move in random directions. The photons that exit the semiconductor which couple into the fiber are limited in percentage. The LED material absorbs the many of the photons and the energy dissipates as heat. The output from an LED to be incoherent and have a wide output pattern, and have a broad spectral width due to this process.

2.8.4 Light emitting diodes

When a current is passed through it a semiconductor diode emits incoherent light through spontaneous emission is called a light emitting diode (LED). Using GaAs and AlGaAs, the LED's for the 850-nm region typically can be fabricated. Using InGaAsP and InP, the LED's for the 1300-nm and 1550-nm regions can be fabricated. The surface-emitting LED (SLED), the edge-emitting LED (ELED), and the super luminescent diode (SLD) are the basic LED typed used for the fiber optic communication systems. The SLED's and ELED's are the preferred optical sources for the short-distance (0 to 3 km), low-data-rate fiber optic systems. For the bit rates up to 250 megabits per second (Mb/s), the SLED's operates typically and efficiently. SLED's are almost exclusively used in multimode systems, because they emit light over a wide field angle (wide area). ELED's are preferred for medium-distance, medium data system rates. The modulation rates up to 400 Mb/s achieved using ELED's. For both multimode and single mode fiber systems the ELED's may be used. For the achievement of high-data-rate and for long-distance systems both SLD's and ELED's can be used. The diodes designed to operate in the super-luminescence mode are SLDs which are ELED based diodes. The modulation of SLD's may be at bit rates of over 400 Mb/s.

2.8.5 Laser diodes

The device that generates optical radiation through the process of stimulated emission is a laser device. The production of stimulated emission within the laser active region should contain photons necessarily. Fig. 4.2 shows the formation of an optical cavity by replacing one mirror at each end of an amplifying medium (Fig. 4.2) to contain the emitted photons. To escape some radiation from the cavity for the coupling to an optical fiber, one of the mirrors is made partially reflecting. Part of the optical radiation is only amplified. There are only certain wavelengths that will be amplified by the laser with a particular structure. When the selected wavelengths or laser modes reflect back and forth the cavity, then amplification occurs. During one round trip through the cavity, the optical gain of the selected modes must exceed the optical loss for lasing to occur. The corresponding process is called optical feedback. The laser output results mainly from the stimulated emission rather than the spontaneous emission, when the lasing threshold is the lowest drive current level. The threshold current is the lowest current at which the

stimulated emission exceeds the spontaneous emission. With small increase in drive current, the optical output power increases only slightly before the threshold current is reached. The optical output power increases greatly with small changes in the drive currents, after the threshold current is reached, however. The lasing medium can be formed by many types of materials including gases, liquids, and semiconductors. The primary lasers used in the optical fiber are the semiconductor laser diodes. The highly monochromatic and very directional light is emitted by laser diode. Means that the LD's output has a small output beam angle and a narrow spectral beam width.

The device that generates optical radiation through the process of stimulated emission is a laser device. The production of stimulated emission within the laser active region should contain photons necessarily. Fig. 4.2 shows the formation of an optical cavity by replacing one mirror at each end of an amplifying medium (Fig. 4.2) to contain the emitted photons. To escape some radiation from the cavity for the coupling to an optical fiber, one of the mirrors is made partially reflecting. Part of the optical radiation is only amplified. There are only certain wavelengths that will be amplified by the laser with a particular structure. When the selected wavelengths or laser modes reflect back and forth the cavity, then amplification occurs. During one round trip through the cavity, the optical gain of the selected modes must exceed the optical loss for lasing to occur. The corresponding process is called optical feedback.

The laser output results mainly from the stimulated emission rather than the spontaneous emission, when the lasing threshold is the lowest drive current level. The threshold current is the lowest current at which the stimulated emission exceeds the spontaneous emission. With small increase in drive current, the optical output power increases only slightly before the threshold current is reached. The optical output power increases greatly with small changes in the drive currents, after the threshold current is reached, however. The lasing medium can be formed by many types of materials including gases, liquids, and semiconductors. The primary lasers used in the optical fiber are the semiconductor laser diodes. The highly monochromatic and very directional light is emitted by laser diode. Means that the LD's output has a small output beam angle and a narrow spectral beam width.

2.8.6 Optical detectors

A device which converts the input form of energy into output energy of another is called a transducer. The transducer that converts optical signal into an electrical signal is called an optical detector. This is done by generating an electrical current proportional to the incident optical radiation intensity. The relation between the output electrical current and the input optical radiation is given by the responsivity of the detector. The optical detectors of the fiber optic communication systems required to meet specific performance and compatibility requirements. To those optical sources many of the requirements are of similar nature. The optical detectors of the fiber optic systems require:

- To allow for the efficient coupling and easy packaging, they can be compatible to low-loss optical fibers.
- At the operating wavelength of the optical sources, they have a high sensitivity.
- To handle the system data rate, they have a sufficiently short response time (sufficiently wide bandwidth)
- Low amounts of noise contribution to the system.
- In changing environmental conditions, such as temperature, they maintain stable operation.

Semiconductor photodiodes are the optical detectors which meet many of these requirements and suitable for fiber optic systems. Avalanche photodiodes (APD's) and positive intrinsic negative (PIN) photodiodes are the principal optical detectors used in fiber optic systems.

2.9 Attenuation in optical fibers

The AT & T in the year, 1934, obtained the first patent on guided optical communications through glass. The attenuation of fiber optic cable made from glass is decreased from a value of 1000 dB/km to a value of 20 dB/km, the years of 1968 and 1970. The process for its fabrication was patented by the world famous corning company immediately. Then after, the guided light communications with the optical fiber cable allowed the take off, as there was a continuous decrease in the attenuation. This momentum increased in the late 1980's and 1990's with the lower cost plastic clad silica (PCS) fibers and plastic fiber optic cable. The performance consideration comes to answer three questions:

1) Through the external acceptance angle, how much light can be coupled into the core?
2) In propagating down the fiber, how much of attenuation will a light ray experience?
3) In propagating down the core, how much time dispersion will light rays representing?

The BER is lower, if more light reaches the receiver by coupling more light into the core of the fiber. Also, the BER is lower, if more light reaches the receiver on account of lower attenuation in propagating down the core of the fiber. The higher end to end rate from the source to user is obtained, if the signaling rate is faster with less time dispersion in propagating down the core of the fiber. On many factors the answers to these questions really depend. The mode propagation, the size of the fiber, and the composition of the fiber are the major factors.

It is known that the transmission of light depends on the structure of the optical fiber and the nature of light. In terms of bandwidth and signal loss how optical fibers affect the system performance will be described. The amount of data transmitted over a particular length of fiber can be described by signal loss and system bandwidth. The increase in signal loss and reduction of system bandwidth can be decided by many optical fiber properties. Fiber dispersion and fiber attenuation are the most important properties which affect the system performance. The distance an optical signal (pulse) can travel and the reduction of amount of optical power transmitted by the fiber can be decided by the attenuation. An error occurs when the power of an optical signal is reduced to a point where the receiver is not able to detect the pulse.

The result of attenuation is mainly due to absorption, scattering, and bending losses. As the optical signal travels along the fiber, dispersion spreads the optical pulse. The reduction system bandwidth or the fiber information carrying capacity and limiting of the information transfer occurs due to the spreading of the signal pulse. When the receiver is not able to distinguish between the input pulse caused by the each pulse spreading, an error occurs. Other optical fiber properties also affect the performance of the system in addition to fiber attenuation and dispersion. The system performance can be reduced by properties of the fiber, such as modal noise, pulse broadening, and polarization.

2.9.1 Absorption losses

The portion of the attenuation resulting from the change of optical power into another energy form, such as heat is defined as absorption. In optical fibers absorption is explained by three factors:

- The intrinsic or basic fiber-material properties
- The presence of extrinsic impurities in fiber material
- Imperfections in the atomic structure of the fiber material

Intrinsic absorption: The cause to the intrinsic absorption is basic material properties of the fiber. All the absorptions would be intrinsic, when optical fiber with no imperfection or impurities is absolutely pure. The minimal level of absorption is set by intrinsic absorption. In optical fibers, silica (pure glass) fibers are used at the wavelengths of operation because of their low intrinsic material absorption. The range of operation of wavelengths are from 700 nanometers (nm) to 1600 nm, in silica glass fibers. At the wavelengths of operation Figure 2-8 shows the level of attenuation. This wavelength of operation is occurring between the two intrinsic absorption regions. Ultraviolet region is the first region (λ=below 400nm). The second region (λ=above 2000nm) is the infrared region.

Electronic absorption bands cause the intrinsic absorption in the ultraviolet region of the E.M. spectrum. Absorption occurs basically when a photon (light particle) interacts with an electron and excites it to a level of higher energy. The ultraviolet absorption band tails and infrared pattern of absorption are shown (Fg. 2.2). The vibration of atomic bonds of silicon oxygen (Si-O) causes the intrinsic absorption in the region of infrared in silica glass. The interaction between the electromagnetic field of the optical signal and the vibrating bond causes the intrinsic absorption. The transfer of light energy takes place from the electromagnetic field to the bond. The main cause of the intrinsic absorption in ultraviolet region is caused by the vibration of electronic charge of the individual atoms of silicon present in the material.

Extrinsic Absorption: Extrinsic absorption causes in the fiber due to the presence of the external material such as impurities, do-pants, introduced into the fiber material.

Extrinsic absorption takes place by the electronic transition of these metal ions from one energy level to another.

2.9.2 Loss due to resonance

The electronic, and atomic resonances, which are responsible for the 'dispersive properties' of a dielectric material also give rise to 'absorption' in the vicinity of the resonance frequencies. For materials of interest to us these are resonances in the ultra-violet region, associated with the electronic structures of the crystal atoms and resonances in the infra red region associated with the lattice vibrations of the atoms themselves.

Although these resonance frequencies are well away from the optical frequencies we wish to use, the absorption they produce is very strong and the tails of their absorption bands do exist into the very low lever attenuation region we are concerned. The absorption band-edges show an exponential variation of the absorption coefficient associated with photon energy. Thus the absorption coefficient associated with the u. v. band edge, α_{uv}, may be expressed as

$$\alpha_{uv} = A_{uv} \exp(\varepsilon / \varepsilon_{uv}) = A_{uv} \exp(\lambda_{uv} / \lambda)$$

Where A_{uv}, ε_{uv}, and λ_{uv} are constants. If λ increases, α_{uv} decreases (Fig. 2.6).

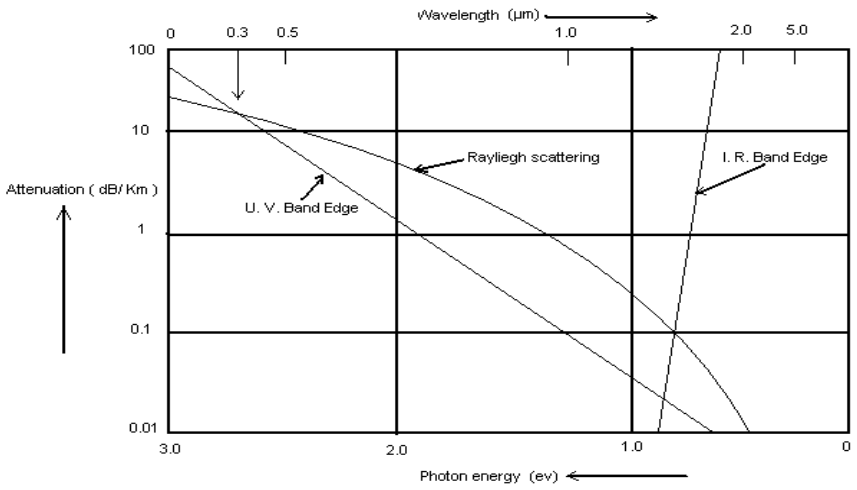

Fig. 2.6 Fundamental loss limits in glasses with high silica content.

The absorption coefficient associated with the infrared band-edge may likewise be expressed as

$$\alpha_{ir} = A_{ir} \exp(-\varepsilon / \varepsilon_{ir}) = A_{ir} \exp(-\lambda_{ir} / \lambda)$$

Again A_{ir}, ε_{ir}, and λ_{ir} are constants. α_{ir} increases as λ increases (figure 2.3).The window between the two edges corresponding to low loss should be greatest at about 1.5μm, but it is considerably reduced by another fundamental loss mechanism called Rayleigh's scattering which dominates the u.v. absorption band-edge at wavelength longer than 0.3 μm. The u.v. absorption takes place if the window width of the fiber is above 0.3 μm. But the usual window width of optical fiber is of the order of 1.5 μm. Hence loss in energy takes place. The I.R. band-edge becomes significant at wavelengths longer than 1.5 μm.

2.9.3 Loss due to dopants

This I.R. edge absorption takes place due to the stretching vibrations of the oxide bonds which have the following fundamental frequencies. The resonance frequencies for some of the dopants are, Si-O --- 9 μm, Ge-O --- 11 μm, P-O --- 8 μm, B-O --- 7.3 μm. From the data, we notice that Germania is the most favourable impurity because of longer wavelength associated with Ge-O stretching vibrations. This is observed by the measurements plotted in Fig. 2.7.

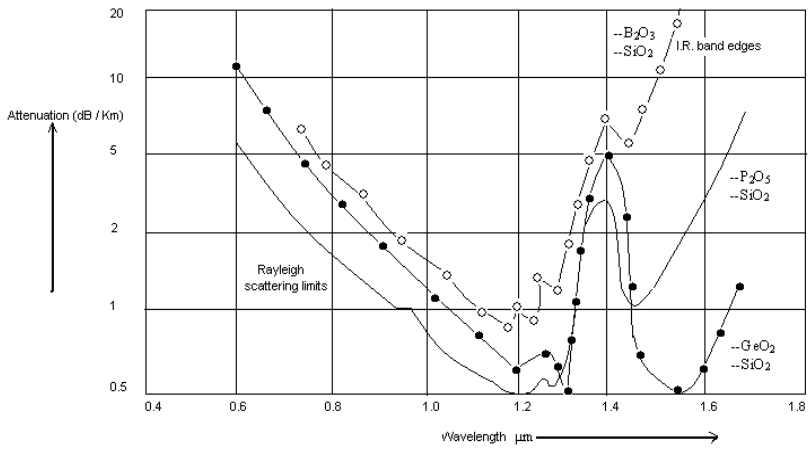

Fig. 2.7: Effects of dopants on the infra-red band edges and Rayleigh scattering loss.

The absorption peaks near 1.4 and 1.5 μm are caused by residual water vapour.

The figure 2.7 shows that the I.R. band edge move toward shorter wavelengths when P_2O_5 and B_2O_3 are used as dopants. That is the I.R. absorption is reduced to a wavelength of 1.4 μm when P_2O_5 and B_2O_3 are used as dopants. These dopants have little effect on the attenuation level of 0.85 μm. Therefore this rules out the use of these materials as dopants in fibers which are designed to be used at 1.55 μm. The band edge absorption is inherent in the materials used to make the fiber.

2.9.4 Loss due to impurities

Another cause for absorption is that the material may also contain impurity atoms and molecules which can cause absorption at wavelengths of interest. The most harmful impurities present in the silica fibers are hydroxyl ions, Hydrogen and the first row of transition materials. That is vanadium, chromium, iron, manganese, cobalt and nickel. The metals occur in the glass as ions give rise to broad band absorption by virtue of their elelctronic structure at the wavelengths of interest for us. The concentration of these transition metal ionic impurities have to be kept bellow about 1 part in 10^9 parts (PPM) of the fiber material to maintain the attenuation 1Db / km at the wavelengths of 1 μm.

If the hydroxyl ions (OH-) are introduced into the fiber, absorption occurs. A silicon-hydroxyl (Si-OH) bond will be formed by the water vapour in silica. The fundamental absorption of this bond is at 2700nm. In the region of operation, however, the overtones or the harmonics of the fundamental absorption occur.

The extrinsic absorption increases these harmonics at 1383 nm, 1250 nm, and 950 nm. The three windows or regions of preferred operation, is defined by these absorption peaks. At 850 nm, the first window is centered. At 1300 nm, the second window is centered. And at 1550 nm, the third window is centered. At wavelengths defined by one of these windows, fiber optic systems operate. The absorption caused by hydroxyl ions (water vapour) arises from the stretching vibrations of the O – H bond. The following Table 2.3 gives an approximate relation between the resonance wavelength and absorption caused due to O – H bond vibration.

Table 2.3 O-H bond absorption at different wavelengths

Approximate resonance wavelength (μm)	Absorption caused due to O – H bond vibration (dB / km)
1.39	65.0
1.24	2.3
1.13	0.1
0.95	1.0
0.88	0.1
0.72	0.05

For fibers designed to be used in the wavelength range of 0.8 μm to 0.9 μm, a water vapour concentration of 1 in 10^6 parts have the negligible effect. But fibers designed to have windows around 1.2 to 1.6 μm require a concentration of less than 1 part in 10^8 parts. However this is difficult to achieve.

Hydrogen is evolved from the polymers and other materials used in cable fabrication. Hydrogen molecules diffuse in silica, occupying interstitial positions in the glass matrix and form weak chemical bonding with the silica. It is impossible to take steps to prevent the fiber being exposed to this hydrogen. This problem can be solved by good cable design. Fig. 2.8 Represents the behavior of attenuation with wavelength for a typical low – loss mono-mode fiber. The only significant impurity absorption is caused by hydroxyl ions.

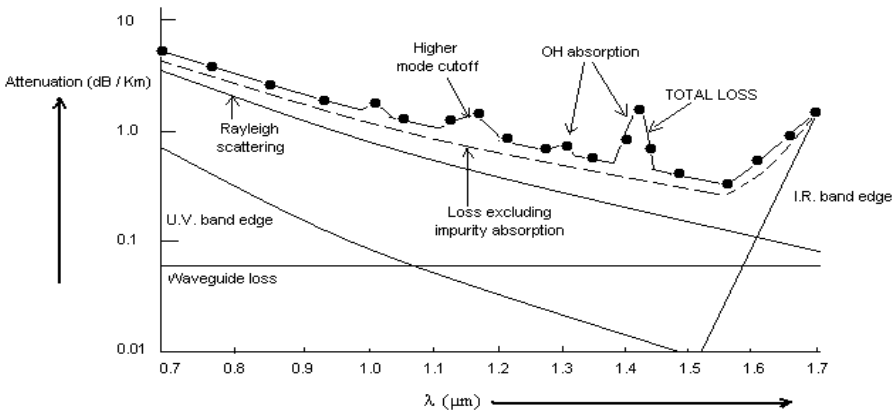

Fig. 2.8: Variation of attenuation with wavelength for a mono-mode fiber.

Fig. 2.9 illustrates the behavior of attenuation with the wavelength taken over an ensemble of optical fiber cable material types. It is indicated the operation of three windows, and propagation through a cable. These correspond to a receiver to carry out detection, wavelength regions where attenuation is low and matched to the ability of a transmitter to generate the light efficiently. The presence of Hydroxyl radicals in the material of the cable cause a bump in the attenuation represented by OH symbols at particular wavelengths. From the presence of water these radicals result. In the manufacturing process, they enter through the either a chemical reaction or as humidity in the environment into the fiber optic cable material.

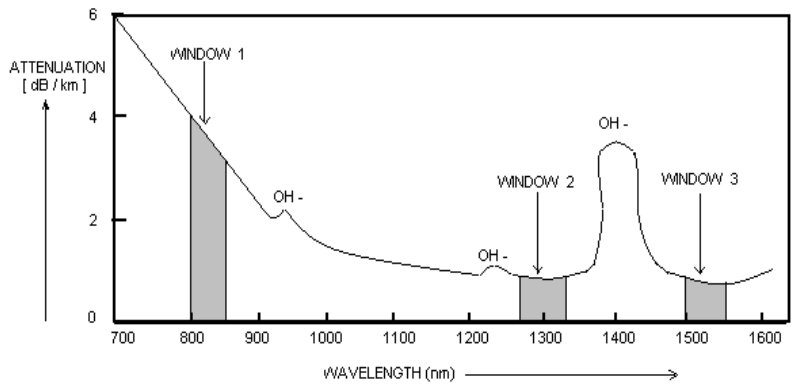

Fig. 2.9: Attenuation vs. Wavelength

2.9.5 Scattering losses

Glass by its nature is a disordered structure. Gases and liquids are disordered throughout their structure. Almost all solids are crystalline in their structures. Glass is the main solid that is not crystalline in structure. That is why it has microscopic variations in its density. Each of these variations gives rise to variations of R.I. This is the fundamental property of any glassy material, however carefully it is made. It causes the light to be scattered as in Rayleigh scattering and the intensity of light diminishes along the length of the fiber. The light is then lost from the fiber.

2.9.6 Rayleigh's scattering loss

When the frequency of the scattered light is same as that of the original light, then it is called Rayleigh's scattering of light. In this scattering, the light energy is absorbed by the molecules of the matter and then re-radiated by them as scattered light. The interaction of

light with the density fluctuations within a fiber causes the scattering losses basically. When the optical fibers are manufactured, the density changes are produced. Relative to the average density of the fiber, regions of lower and higher density areas are created during manufacturing. The light is partially scattered in all directions, when light traveling through the optical fiber interacts with the density areas. The important loss mechanism between the infrared regions and the ultraviolet regions is the Rayleigh scattering. If the size of the density fluctuation (fiber defect) is less than one-tenth of the light operating wavelength, then Rayleigh scattering occurs. The Rayleigh scattering caused by loss is proportional to the fourth power of the wavelength ($1/\lambda 4$). Rayleigh scattering loss decreases, as the wavelength increases. The scattering mechanism is Mie scattering, if the size of the defect is greater than one-tenth of the wavelength of light. Mie scattering scatters light out of the fiber core, if it caused by these large defects in the fiber core.

The loss of intensity of light is higher in multi-component glasses because of compositional variations. For multi-component glasses, the scattered power and hence the attenuation is inversely proportional to the wavelength. It is observed in the earlier section that it is Rayleigh scattering rather than the U.V. absorption band edge that is the principal cause of loss in silica fibers at wavelengths less than 1.5μm.

For glasses with high silica content, a typical value for the Rayleigh scattering attenuation is 1 dB / km at 1 μm. Germanium doping usually causes a slight increase and phosphorus pentoxide a slight decrease. This effect is observed in the figure of earlier section. Very carefully made single mode fibers with only a lightly doped core (Δn = 0.003) can show as little as 0.9dB/ km Rayleigh scattering loss at 1μm. In single mode fibers made with a core of pure silica, this value has been reduced to 0.7dB / km. The h higher doping levels used in multimode fibers lead to values in the range 1-1.6 dB / km at 1 μm. With sodium borosilicate glasses 2 dB / km is more typical. In general, a Rayleigh scattering loss coefficient α_R, may be defined such that

$$\alpha_R = A_R / \lambda^4$$

Where, A_R is a constant for any given material.

2.9.7 Macro-bending loss

Bending loss also causes attenuation by bending the fiber. According to the radius of the bend the bending losses is classified: loss due to micro-bend or loss due to macro-bend. So far we have assumed that the geometry of any fiber is perfect from one end to the other end and the fiber itself is straight. In practice, this is not the case and the bends and imperfections that do occur, lead to the guided rays being scattered and radiated away from the core cladding interface. Major disturbances to the fiber geometry steps, offsets, inclusions and large imperfections within the fiber core (bubbles, impurities) each give rise to a large local scattering loss. Similarly tight bends and tight joints will also cause some light not to be internally reflected but to propagate into the cladding and be lost. Theoretically, the optical power scattered from a fiber at a major bend depends exponentially on the bend radius R.

The bending loss is proportional to $\exp(-R / R_C)$

Where R_C is critical radius = $a / (\text{Numerical aperture})^2$

$= a / (NA)^2$

$= A / 2n.\ \Delta n$

'a' is the radius of the fiber core.

Because of the exponential function, the loss decreases rapidly for less tight bends. Infact it is the mechanical property of the fiber rather than bending losses that will determine the minimum allowable bending radius. It is observed that if a fiber is bent so tightly so that its surface strain exceeds about 0.2%. Then stress cracking likely to develop during its life time. This can be prevented by enclosing the fiber in a suitable rigid cable.

2.9.8 Micro-bending loss

Micro-bending losses are caused by imperfections in the fiber or small discontinuities in the fiber. The micro-bend loss is increased by uneven coating applications and improper cabling procedures. The sources of micro-bends are the external forces work on the fiber. The external force causes only a small bend in the fiber and deforms the cabled jacket surrounding the fiber. The path taken by the modes of propagation is changed by the micro-bends (fig. 2-5). The naturally lossy lower order modes coupled with high-order

modes leading to increase in the micro-bend loss. Compared to the fiber diameter, if fiber bend radius of curvature is large, macro-bend losses are observed. Macro-bend losses will occur, if fibers are bent too sharply, during installation. When the radius of curvature is less than several centimeters, these bends become great source of loss. At the outer side of the bend the light propagates greater distance than the inner side of the bend. The phase velocity of the mode must increase to maintain the phase of the light wave. The phase velocity of the mode must increase to a speed greater than the speed of light, when the fiber bend is less than critical radius.

The speed of the light however is impossible to exceed. Some of the light converted to higher-order modes within the fiber by this condition. The modes of higher order then radiated out of the fiber or lost. The bending losses due to fiber sensitivity can be reduced. The fiber sensitivity decreases, when the core refractive index is increased. As the overall fiber diameter increases, the sensitivity also decreases. However, the fiber sensitivity increases if the fiber core diameter increases. Propagation of modes will be more with the large core size of the fiber. Modes that are additional tend to be lossy. Apart from the above bending losses, small bends may cause significant rise in fiber attenuation. This is known as the micro-bending loss.

2.9.9 Waveguide loss

Anther type of loss known as “waveguide loss” arises because of small variations in core diameter of the fiber during manufacture. The bending and, micro-bending and waveguide losses are wavelength independent. These losses can be kept bellow 0.1dB / km with proper protection and cushioning of the fiber and preventing from the over tight bending.

2.9.10 Loss due to ionizing radiation

In some industrial, space and military applications, communication links may be required to be resistant to high levels of radioactivity. The effects of ionizing radiation on glasses are very complex and quite severe. The chemical bonds in glasses get disrupted and new energy levels are created and transitions take place between them and this gives rise to absorption in the visible and near infrared region. The fiber is not directly susceptible to

α particles or β particles, which are absorbed in the protective layers of the cable. We are concerned with r – radiation which penetrates into the fiber.

At low levels of irradiation the additional radiation induced attenuation rises in direct proportion to the irradiation reaching the fiber. But the radiation induced attenuation varies for different types of fibers from 10 – 1000 dB / km / Gy at an optical wavelength of 0.82μm. There is some evidence that the radiation induced attenuation increase is less at longer wavelengths. The bonds in multi-component glasses are particularly vulnerable. Fibers having cores made from silica doped with GeO_2 or B_2O_3 are more sensitive to the effects of radiation than those having cores of synthetic silica. Most fibers required to be radiation hard are used in relatively short links so that a very high level of attenuation is acceptable and additional radiation induced attenuation is less critical.

2.9.11 Fiber coupling loss

Idially, the transmission of optical signals at the coupling between the optic components, occur with no loss of light. However, at the fiber optic connections, there is always some type of imperfection present, which causes come loss of light. The fiber optic system design depends on how much optical signal is coupled between fiber optic components i.e. from one fiber to another and how much light is injected into an optical fiber from an optical source. The launched power amount from a source into a fiber depends on the properties of both the fiber and the source.

The launched amount of optical power depends on the optical source radiance. The radiance of an optical source or the brightness, is the measure of its launching capability of optical power. The amount of emitted optical power in a specific direction by a unit area of emitting surface per unit time is called the radiance. Only a fraction of the emitted power by the source will be launched into the fiber for most of optical sources. Similar to that of to that of attenuation of signal through a fiber, the loss of optical power through a connection also can be defined. The log relationship can be used for the losses in the optical fibers. The optical power loss through a fiber connection is defined as:

$$loss = 10 \log_{10} \frac{P_i}{P_o}$$

For example in a fiber to fiber connection, P_o is the emitted power from the source fiber. P_i is the accepted power by the connector fiber. P_o and P_i are the measured optical power levels before and after the joint, respectively in any fiber optic connection. The intrinsic and extrinsic coupling losses affect the fiber to fiber connection loss in a fiber joint. The inherent fiber characteristics cause the intrinsic coupling losses in optical fibers. The fiber jointing techniques cause the extrinsic coupling losses in optical fibers. By the following sources of extrinsic and intrinsic coupling loss increases the fiber to fiber connection loss: poor fiber end parameters, index of refraction profile difference, numerical aperture mismatch, cladding and core diameter mismatch, angular misalignment, fiber separation and lateral misalignment, and reflection losses etc. by reducing the mismatches between the fibers connected, the intrinsic coupling losses can be limited. This can be achieved by procuring the fibers which meet stringent optical and geometrical specifications. By the following procedures of proper connection, the extrinsic coupling losses can be limited.

To reduce the coupling losses between the components, some fiber optic components designed are modular devices. From any fiber optic system, the modular components can be removed or inserted. The fiber optic receivers and transmitters are the modular components for example. The devices which are generally manufactured with fiber optic connectors or fiber optic pigtails are the fiber optic transmitters and receivers. A short length optical fiber (usually 1 meter or less) fixed permanently to the optical source or optical detector is called fiber pigtail.

As fiber coupling to detectors and sources must be done during fabrication, therefore manufacturers supply transmitters and receivers with pigtails. In a controlled manufacturing environment, when source to fiber and fiber to detector coupling is done, then such connectorization reduced coupling loss results. From one fiber to another, the launching optical power is reduced to coupling light, when optical sources and detectors are pigtailed or connectorized. The most fiber optic connections are of fiber to fiber in fact.

2.9.12 Reflection losses

The optical power may reflect back into the source fiber, when optical fibers are connected one another. The light power is lost that is reflected back into the source fiber. At every fiber interface, this reflection loss occurs which is called the Fresnel reflection. By a step change that occurs at the fiber joint in the refractive index causes the Fresnel reflection. In most cases, a small gap at the each fiber separation causes the step change in the refractive index. Usually this small gap is an air gap between the two fibers. In the Fresnel reflection, at the fiber interface, a small portion of the light incident is reflected back into the source. The ratio (R), which approximates the portion of incident light (normal incidence of light) that reflects back into the source fiber is shown below.

$$R = \left(\frac{n_1 - n_o}{n_1 + n_o} \right)^2$$

n1 is the refractive index of the core of the fiber and R is the fraction of the reflected incident light at the fiber. And n0 is the medium refractive index between the two fibers. In a fiber to fiber joint the Fresnel refraction occurs twice.

When the light exits first the source fiber, a portion of optical power reflects back. Thus as the optical signal enters the receiving optical fiber, light then reflects back. At each interface the Fresnel reflection must be calculated to account for the total fiber to fiber coupling loss. Then the losses are significant from the Fresnel reflection. An index matching gel can be used to fill the air gap to reduce the loss amount from the Fresnel reflection. The index matching gel should have the refractive index that should match with the refractive index of the core of the optical fiber. Index matching gel reduces the Fresnel refraction, reducing at the fiber interface, the step change in the refractive index.

In any system, the index matching gel are used to reduce the Fresnel reflection or used to eliminate the Fresnel reflection. it is to be noted that the choice of the index matching gel is very important. The fiber to fiber joints are required no maintenance and are designed to be permanent. The index matching material must meet the mechanical requirements and the specific optical requirements over the lifetime of the fiber connection. The transparency should be maintained by the index matching liquids throughout. They should be viscous for resisting flow or dripping. Some of the index

matching gels leak out of the fiber joints or darken over time while others settle. The fiber to fiber joint losses will increase over time, if these requirements are not met.

2.9.13 Fiber alignment loss

Poor fiber alignment is the main source of the extrinsic coupling loss in fiber to fiber joint. Angular misalignment, lateral misalignment and the fiber separation (longitudinal misalignment) are the three basic coupling losses that occur during fiber alignment. The mechanical imperfections introduce by fiber joints result the most of the alignment errors. With fiber separation, a small gap remains between fiber-end faces after completing the fiber connection.

Lateral, or axial, misalignment: occurs when the axes of the two fibers are offset in a perpendicular direction. Angular misalignment: occurs when the axes of two connected fibers are no longer parallel. At some angle (θ), the axes of each fiber intersect. Typically, coupling losses caused by angular and lateral misalignments is more than the losses caused by separation of the fiber. Because of ease in limiting the fiber separation distance, losses are less critical caused by fiber separation. However, fiber optic joints prevent the fiber from actual contact, in some cases. By a small gap, these optical fiber connectors separate the fibers. During connection, this gap between fibers will eliminate the damage to fiber end face. The coupling losses will be reduced by using the index matching gel for connectors with an air gap.

Most joints are designed so that when connector is mated, the connector ferrule end faces contact. The assembly of the connector onto the fiber is such a way that when mated, the fibers come in contact with each other. However, the connector also can be assembled onto the fiber, so that they can't come in contact with each other. Depending on whether the fiber sticks slightly out from the ferrule, or is increased inside the ferrule, the fiber contact can be determined. By using the connector polishing technique, the fiber position can be controlled. For most connectors, the technique of physical contact (PC) was developed, so that the fibers would touch each other when mated. To reduce the reflections, the index matching gel is not needed in these types of connectors.

The losses in lateral misalignment, does not affected when index matching gel reduce the coupling losses from the separation of the fibers. Additionally, the increase in the fiber's coupling loss which is sensitive to the angular misalignment, results due to the index matching gel. The index matching gel reduce the light launching angle from the source fiber, although the angular misalignment involves the fiber separation. The light to be coupled into the receiving fiber will be lessened by the index matching gel. The angle and theta should be less than 1°, to reduce the coupling losses from the angular misalignment. The fiber alignment coupling losses depend on fiber core diameter, on fiber type, and the optical power distribution among the propagating modes. Fibers with large NAs increase the loss from the fiber separation and reduce the loss from angular misalignment. Because of their smaller core size, the single mode fibers are more sensitive to the alignment losses than multimode fibers. However, the alignment losses in multimode fibers joints may increase the coupling losses and may disturb the distribution of optical power in the modes of propagation.

2.9.14 Polarization dependent loss

Polarization dependent loss (PDL) refers to the difference in the maximum and minimum variation in transmission or insertion loss of an optical device over all states of polarization (SOP) and is expressed in decibels. A typical PDL for a simple optical connector is less than .05 dB and varies from component to component. Typically, the PDL for an optical add/drop multiplexer (OADM) is around 0.3 dB. The complete polarization characterization of optical signals and components can be determined using an optical polarization analyzer.

2.10 Sensing mechanism and classification

2.10.1 Intensity modulated fiber optic sensors

The advantage of intensity modulated sensors lies in their simplicity of construction and their being compatible to the multimode fiber technology. The general feature of the intensity modulated sensor in depicted in the fig. 2.10.

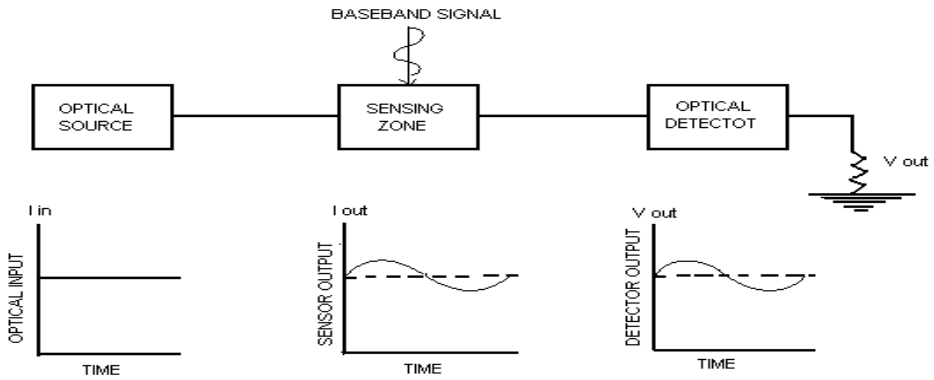

Fig. 2.10: General configuration of an intensity modulated sensor**.**

As shown in figure above, the baseband signal (the measurand) in the form of a sinusoidal varying quantity is seen to modulate the intensity of the light transmitted through the sensor. The envelope is reflected in the voltage output of the detector, which upon calibration, can be used to retrieve measure of the measurand.

Intensity modulation can be achieved through a variety of schemes, e.g., displacement of one fiber relative to the other, shutter type, i.e. variable coupling of light between two axially aligned fibers, intensity modulation through reflection using Y-guide or bifurcated fiber probe and modulation of light in the core or in the cladding through bending, microbending or evanescent coupling to another fiber.

2.10.2 Intensity modulation through light interruption

Optical fibers can be configured by interrupting direct optical interconnection between an optical source and a detector. The coupled light intensity across a fiber joint can be varied through either, transverse, longitudinal or angular misalignments or through a combination of them between the axes of two fibers. Here the loss on dB scale is calculated relative to intensity transmitted across the joint for zero misalignment between the fiber axes. The longitudinal displacement of one fiber relative to the other can be used to measure axial displacement.

This phenomenon can be exploited to configure an a.c. pressure or an acoustic sensor in which two fiber end faces are kept close to each other with 2-3 μm separation between them, whose axes are otherwise well aligned by maximizing optical power

across the joint. If the output fiber is free to move relative to the input fiber which is kept fixed and an external force field is applied in a direction transverse to their axes, it will induce motion to the free end of the output fiber relative to the fixed fiber, thereby creating an intensity modulation of the light coupled across the joint. The device was found to detect deep sea noise levels in the frequency range 100 Hz to 1 kHz and transverse static displacements down to a few Angstrom. Sensitivity of such fibers still can be increased by cleaving and polishing the two fibers at a slant angle so as to produce total internal reflection of the guided light from the slant fiber air interface.

2.10.3 Intensity modulation through shutter

In this type a shutter being actuated by the measurand resulting in an interruption of the optical beam between two opposed multimode fibers. The concept of shutter induced interruption of light between opposed fibers can also form the basis of an optical microswitch. Several optical fiber microswitch devices are used to detect displacements in hazardous environments. In a pressure operated switch, a correct amount of pressure is applied then only the optical coupling between the fibers. Acoustic field / pressure sensor based on a moving grating across the joint between two multimode fibers works making use of the principle of shutter induced loss mechanism. Acoustic pressures less than 60 dB relative to 1 micropascal over the frequency range 100 Hz to 3 kHz and it could resolve relative displacements as small as few Angstrom with a dynamic range of 125 dB.

2.10.4 Reflective type fiber optic sensors

A Y-coupler fiber optic probe consisting of two multimode fibers cemented / fused along some portion of their length, to form a power divider would constitute a reflective fiber fiber optic sensor. If the cemented end of the Y-power divider is made to face a light reflecting diaphragm and light is injected through port 1, the intensity of back reflected light that will exit through port 3 will depend on the distance of the reflecting target from the fiber probe. Pressure sensitive sensors can be developed with the help of the principle of light reflected from the Y- fiber probe. Such Y- coupler fiber probes as reflective sensors have reportedly been used to determine surface texture, pressure over a range of

100 psi, and in medical catheters as intercardiac pressure transducer with a sensitivity of 1 mm Hg.

2.10.5 Evanescent – wave fiber sensors

The guided light in a fiber waveguide penetrates into the cladding to a distance a few wavelengths as the evanescent wave. This evanescent wave is precisely responsible for the working of a fiber optic directional coupler. Such a device is formed if two fibers are laid side by side along some portion of their length in which cladding has been depleted to almost negligible thickness. If light is injected into port 1, it will split into ports 2 and 3 with negligible light appearing on pot 4. The amount of light that will be distributed between ports 2 and 3 is a function of coupling length (L), core to core spacing(d), and refractive index (n_2). A somewhat similar idea was exploited in the so called cross – talk fiber sensor for detection of oil film on the surface of water and for analog measurement of liquid levels and temperatures and R. I.

In this configuration the cores of two multimode fibers are exposed to each other over a small length with a small air gap, which constitutes the sensing region. If this sensing region is immersed in a liquid of refractive index less than the core refractive index, part of the light injected into port 1 will get coupled to the second fiber due to cross talks through this sensing zone will be a function of the refractive index of this liquid. The cross talk signal which travels down through fiber 2 is made to undergo reflection at the end of the fiber which is eventually detected by a photodiode. The principle is can be exploited to constrict a thermometer by immersing the cross talk zone in a suitable liquid of refractive index 1.45. The small change in refractive index of the liquid as a function of temperature would lead to a corresponding change in the cross talk signal level.

In the same configuration, it can be used as an analog liquid level sensor by partially filling the sensing region lengthwise with the liquid, because cross talk signal will be a function of the length of the liquid column within the sensing zone. By reducing the sensing zone, i.e., the cross talk region to a bare minimum length, it can be alternatively used as a digital on off sensor for detecting the threshold level of a liquid by suspending

the sensor in the liquid container so that the sensing zone coincides with the threshold level. This way it can be used, for example to trigger an alarm signal if a hazardous liquid like petrochemical is found to ever cross the danger lever in its storage tank.

An alternative mode of digital liquid level sensing involves connecting two independent fibers to the base of a 90° glass micro-prism. The ray paths are such that when the prism is surrounded by air, the detector will pick up relatively large signal due to total internal reflection at the sides of the prism. If the prism touches the liquid, the light suffers attenuation due to frustrated total internal reflection which, in fact, results in a drop in the signal level at the detector end. In a modified version of the above principle, a Y-coupler made out of plastic fibers in which the single end of the fiber coupler was cut into a conical shape was used to detect liquid levels or configure a fiber optic spirit level. This configuration of a Y- fiber coupler tip can also be exploited to construct a fiber optic refractometer.

2.10.6 Microbend optical fiber sensors

It works on the microbend induced transmission loss of an optical fiber which measures displacement, acoustic pressure, strain and temperature. If a portion of a fiber lay is forced by a deformer, a continuous succession of small bends can be created on a microscopic scale; thereby the fiber would exhibit excess loss. The fiber may be sandwiched between a pair of toothed or serrated plates to induce microbending. Such regular or random meandering of fiber axis, results in redistribution of guided power between modes of the fiber, and also coupling of power from one mode / mode group to another. If the spatial wavelength (Λ) of periodic deformation satisfies the condition:

$$\beta_A - \beta_B = \frac{2\pi}{\Lambda},$$

Where β_A and β_B represent modal propagation constants of two modes, power transfer will take place from A-th to B-th mode. If the B-th mode happens to be a radiation mode, this transfer of power will result in a net transmission loss of the guided modes. In the case of a step index fiber of core radius a, core index n_1, and relative core cladding index difference Δ, critical spatial wavelength (Λ_{cri}) of a deformer required to induce transfer of power from highest order guided mode to radiation modes will be,

$$\Lambda cri = \frac{\pi a}{\sqrt{\Delta}} = \frac{\sqrt{2}}{N.A.}\frac{\pi an1}{}$$

And in the case of a parabolic index fiber, adjacent guided modes are separated from each other by a constant difference in wave number, given by

$$\Lambda cri = \frac{2\pi}{\Delta\beta} = \frac{2\pi an1}{N.A.},$$

The spatial wavelength of a deformer required to couple power between adjacent modes. Where

$$\Delta\beta = \frac{\sqrt{2\Delta}}{a}$$

Initially, microbend fiber optic sensors were mainly used to detect acoustic fields as hydrophones and displacement sensors. However, depending on the construction of the deformer the same concept can be exploited as a generic sensor to determine several other environmental changes like temperature, acceleration and electric and magnetic fields.

2.10.7 Intensity modulated fiber optic thermometers

Metal clad optical fibers exhibit high attenuation at optical frequencies. Longer the length of the metal cladding, larger will be the attenuation. This fact has been exploited to construct a fiber optic thermometer. It works like an ordinary mercury thermometer. A plastic clad silica fiber was used from which a portion of the plastic cladding was removed. The fiber was run through a capillary tube of 1 mm in diameter having a bulb at one end of mercury. It must be taken care that the lower end of the unclad portion of the fiber touches the upper level of mercury at the ambient temperature. As the temperature surrounding the mercury reservoir is raised, the mercury level rises in accordance with conventional thermometer principle and thereby becomes the cladding for the bare portion of the fiber. As the temperature rises, more and more length of the fiber becomes metal clad which leads to more and more attenuation of the guided light due to absorption by the metallic mercury. The variation of normalized power

$$P_N = \frac{P}{P_0},$$

With P_0 as the initial power detected at the fiber end with respect to the length (l) of the mercury cladding in the capillary. A functional dependence for P_N with l as

$$P_N = \frac{b}{l + l_0},$$

was found and in good agreement to the experimental data. In another version, a fiber optic thermometer especially for medical applications can be constructed by using a plastic clad silica fiber whose cladding is removed at its one of the ends for a small length. In this region a thermo sensitive liquid is maintained which acts as a cladding in that portion of the fiber. Light injected into the PCS fiber is reflected back from one end of the fiber and the returned light intensity is monitored at the other end. Since the refractive index of the liquid cladding around the sensing zone is temperature dependent, effective N. A. of the fiber for collecting the reflected signal gets modulated in accordance with variations in temperature used to construct the thermometer. The reported sensitivity of such a thermometer was 0.1°C, and the response time of 1sec.

2.10.8 Fluorescent temperature sensor

Another approach of measuring temperature involves the use of a fiber optic probe tipped with rare earth phosphors which fluoresce under excitation with UV light. The fluorescent radiation appears in the visible range (hence, does not interfere with the exciting UV light) and is collected by the same fiber for detection. In practice, relative intensities of two fluorescent emission lines are measured, the ratio of which is a measure of the temperature of the phosphor. The emitted lines are a direct function of temperature. A phosphor which has been successfully employed in such sensors is known as europium-activated gadolinium oxysulfide. The sensor can work over the temperature range of -50°C to 250°C.

2.10.9 Fiber optic fluorimetric sensors

Optical fibers have been used in a variety of ways for chemical analysis. Flourimetric techniques have been extensively exploited in this domain of optical fiber sensors. A high intensity light beam is injected into a typically large core quartz fiber. The output end of the fiber is immersed in the sample to stimulate fluorescence, which is collected by the same fiber (often referred to as an “optrode”) for detection and processing by an on line computer. This technique has been reported to have been used to monitor

contamination of ground water with pollutants like toluene, xylene etc. RFF (Remote Fiber Fluorimetry) technique has been also used to measure partial pressure of oxygen in a given environment by measuring fluorescence due to chemical reaction of oxygen with a fluorescent dye attached to a fiber probe. Remote fiber fluorescence quenching technique has been extended to measure concentration of glucose, halides and pH over the range 3 to 8.

2.10.10 Distributed fiber optic sensors

Distributed sensing is used in particular to determine thermal distribution and location of hot spots, local stress, and local pressure distribution using fiber optics. The technique is essentially based on the well known time domain reflectometry (OTDR) concept, which was extensively used for the measurement of fiber loss and its location due to any discontinuity e.g. break, splice along a fiber length. In the first implementation, a liquid core fiber was employed to detect the Rayleigh backscatter signal from a long length of the fiber.

Any localized temperature rise led to an increase in backscatter signal which could be detected and processed at the input end of the fiber to locate the measurand as well as obtain its temperature. There were, however, doubts about the life and stability of liquid core fibers. This technique was later on modified in which solid core germano silicate multimode fibers were used and the signal processing was based on detection of anti stokes Raman line of the backscattered light. The OTDR can also be employed to locate local stresses along a pipeline by bonding a continuous length of fiber to the walls of the pipe.

2.10.11 Fiber optic refractometers

1. Fiber optic refractometers are classified into four categories.
2. Misalignment fiber optic refractometers.
3. Tapered fiber optic refractometers.
4. Temperature sensitive refractometers
5. U-shaped fiber optic refractometers.

2.10.12 Misalignment fiber optic refractometers

Optical fibers can be used to measure refractive index of liquids through intensity modulation, in a number of ways. In fig. 2.11, light is partially coupled to fiber 2 from fiber 1 through a fixed small air gap.

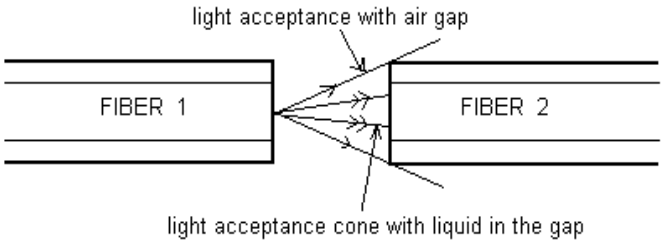

Fig. 2.11: Longitudinal misalignment fiber refractometer.

Due to the air gap, only a fraction of the light emitted into a cone will be collected by the fiber 2. Emitted light cone is a function of refractive index of the liquid maintained in the gap between the two fibers. If a liquid of refractive index greater than n of air fills up the gap between the fibers, a greater fraction of the light emitted by fiber 1 will be picked up and guided by fiber 2 as shown in the figure due to an effective decrease in fiber N.A. The power collected by fiber 2 through the liquid is a linear function of the refractive index of the liquid. This fiber optic refractometer configuration, can also be used to detect acid levels in batteries and as a threshold liquid level sensor because, with and without the liquid in the gap between the two fibers, the signal level at the output of fiber 2 will be different.

2.10.13 Tapered fiber optic refractometer

Fig. 2.12 represents a bare tapered multimode fiber refractometer.

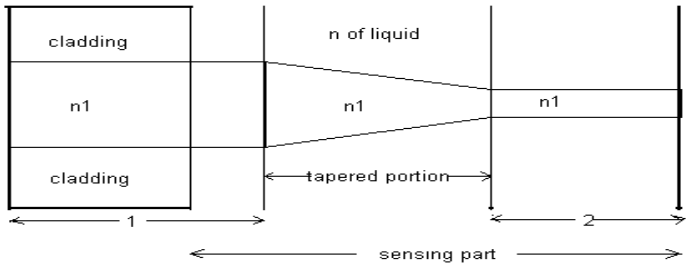

Fig. 2.12: Geometry of a tapered multimode fiber refractometer.

A plastic clad silica core fiber is used in which a small portion of plastic has been removed. This bare portion of the fiber is then converted into a taper by heating and pulling and immersing the taper zone in a liquid of refractive index n_l,($‹n_1$). Immersing the taper subsequently in a number of other liquids and monitoring the corresponding power reaching the fiber 2, one can generate a calibration curve for a given fiber taper. Thus by measuring the power exiting from fiber 2 when the taper is immersed in a liquid of unknown refractive index, one can use this calibration curve to determine the refractive index of the unknown liquid. The tapered portion can be thought of as interconnection between two fibers. One is of core dia $2a_i$, and another of core dia $2a_0$ ($a_0‹ a_i$). Fibers 1, 2 and tapered interconnecting zone all having the same core and cladding refractive indices n_1 and n_2 , respectively except for the initial section of fiber 1 in which the cladding index is n_{cl}. If P_0 represents the total power injected into the guided modes of fiber 1, then the power in the guided modes of fiber 2 is given by,

$$P_b = P_0 \frac{n_1^2 - n_l^2}{R^2(n_1^2 - n_{cl}^2)} \quad (1)$$

It is evident from this equation that power coupled to fiber 2 through the taper increases linearly with proportional decrease in n_l^2.

2.10.14 Temperature sensitive refractometers

In principle, the same technique can be used to construct a temperature sensor as explained above by encapsulating the taper with a metallic encapsulation filled with a liquid whose refractive index is temperature sensitive.

2.10.15 U – shaped fiber optic refractometers

In U – shaped fiber optic refractometer, a plastic clad silica fiber has been bent into the form of a U – shape by removing plastic cladding from a section of the fiber as shown in Fig. 2.13.

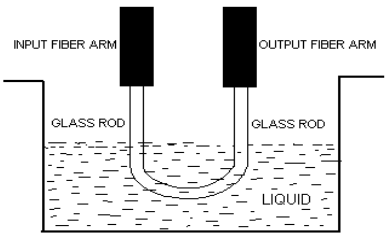

Fig. 2.13: Schematic of a U – shaped fiber refractometer

The bent section of the fiber, when immersed in a liquid of refractive index $n_l (\rangle n_{cl})$ yields a signal different from that in a bare fiber in the same manner as in a tapered fiber refractometer.

Theory: Consider a multimode step index optical fiber in which the cladding has been replaced locally by the absorbing fluid. When [pic] is the transmitted power by the fiber in the absence of the absorbing fluid, then in the presence of the fluid the power transmitted by the fiber is given by:

$$\mathrm{P} = \mathrm{P}_0 \exp(-\gamma L) \tag{2}$$

Where, γ is evanescent coefficient of absorption of the fluid and L is the length of the uncladded portion of the fiber. At the sensing region γ in the case a ray making an angle, θ, with normal to the cladding interface is given by:

$$\gamma(\theta) = \frac{\alpha \lambda n_2 \cos\theta \cot\theta}{2\pi\rho n_1^2 \cos^2\theta_c (\cos^2\theta_c - \cos^2\theta \sin^2\theta_\phi)^{1/2}} \tag{3}$$

Where, θ_ϕ is the angle of skewness, α is the fluid bulk absorption coefficient and ρ is radius of the core of the fiber. It may be noted for a fixed value of θ, from equation (3), when the ray is meridional (i.e. $\theta_\phi = \pi/2$) the evanescent coefficient of absorption is maximum. With the increase in skewness, it decreases. It can be shown that the sensitivity $[-1/\mathrm{P}(d\mathrm{P}/dc]$ of the sensor is proportional to $L\gamma/\alpha$, when the index of refraction of the absorbing fluid does not vary with c, the concentration of the fluid within the range of desired concentration. Thus, γ/α for a given L, directly defines the sensitivity. It means, when the meridional rays are launched in the fiber, the sensitivity will be maximum. For the propagation of meridional rays in the optical fiber, using a microscope objective, the light is lauched into the optical fiber from a laser which is a collimated source. At the axial point, to focus the beam onto the end face of the fiber, the objective is used. To excite all the boundary rays in the fiber, it is assumed that the numerical aperture of the objective is greater than that of the fiber. The power, $d\mathrm{P}$, for such an illumination, arriving at the axial point of the fiber end face between the angles, θ_0 *and* $\theta_0 + d\theta_0$ is proportional to $(\tan\theta_0 / \cos^2\theta_0) d\theta_0$, where θ_0 is the angle of the ray

with the axis outside the fiber. Using Snell's law and $\theta = 90^\circ - \theta_1$, where θ_1 is the angle of the same ray with the axis of the fiber inside the core, we can write:

$$dP \propto \frac{n_1^2 \sin\theta\cos\theta}{(1-n_1^2\cos^2\theta)^2} d\theta$$

Hence, for the launched meridional rays into the sensing region, the effective evanescent absorption coefficient for the angles in the range (θ_1, θ_2) with respect to the normal to the core cladding interface is given by:

$$\gamma_{eff}(\theta_1,\theta_2) = \left[\int_{\theta_1}^{\theta_2} \frac{\sin\theta\cos\theta}{(1-n_1^2\cos^2\theta)} \gamma(\theta) d\theta \Big/ \int_{\theta_1}^{\theta_2} \frac{\sin\theta\cos\theta}{(1-n_1^2\cos^2\theta)^2} d\theta\right] \quad (4)$$

for the propagation of all bound rays in the sensing region, $\theta_1 = \sin^{-1}(n_{cl}/n_1)$ *and* $\theta = 90^\circ$. As shown in figure 2.14, let us consider a U – shaped sensing region. We consider a two dimensional approach to simplify the theoretical treatment of the probe. The rays in the region of sensing will be mainly meridional under this approach and will confine in the plane of bending.

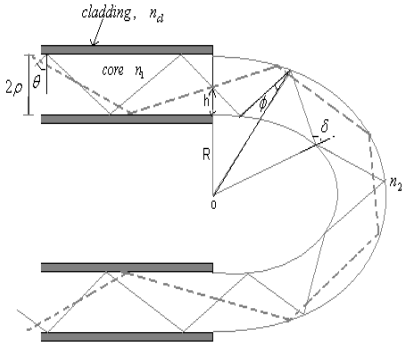

Fig. 2.14: Geometry of the U-shaped sensing region and the representation of a meridional ray travel in it.

In the case of a two dimensional approach as mentioned above, the sensitivity calculated will be more than with the actual case, with decreasing skewness the sensitivity increases. The ray angle with the normal to the cladding core interface within the sensing region should be greater than the sensing region critical angle for the transmission through the sensing region. The ray can undergoes TIR at the outer surface and will not reach the inner surface at all (dotted ray) or a ray can undergo the total internal reflection (TIR) both at the inner and at the outer surfaces (continuous ray), which are the two possibilities in a U – shaped optical fiber. When θ defines in the

straight fiber, the angle which a guided ray makes with the normal to the cladding core interface, then the corresponding angle ϕ at the bent core outer surface is given by the equation:

$$\sin\phi = \left[\frac{R+h}{R+2\rho}\right]\sin\theta \tag{5}$$

Where R is the bending radius, h, is from the cladding and core boundary, is the distance at which the ray is incident on the entrance of the sensor. Similarly, the angle δ of the ray of the bent core at the inner surface and is given by:

$$\sin\delta = \left(\frac{R+h}{R}\right)\sin\theta \tag{6}$$

Hence the angle θ is transformed to angles ϕ *and* δ from equations 5 and 6 respectively. Hence, for the sensing region outer surface, the effective evanescent coefficient of absorption will be given by:

$$\left[\gamma_{eff}(\theta_1,\theta_2)\right]_{outer} = \frac{\alpha\lambda n_1}{2[2\pi\rho(n_1^2-n_1^2)]}\times\left[\begin{array}{l}\int_0^{2\rho}\int_{\phi_1}^{\phi_2}\dfrac{\cos^3 d\theta\, dh}{(1-n_1^2\cos^2\theta)^2(n_{12}^2\sin^2\theta-1)^{1/2}}\\ \div\int_0^{2\rho}\int_{\phi_1}^{\phi_2}\dfrac{\sin\theta\cos\theta\, d\theta\, dh}{(1-n_1^2\cos^2\theta)^2}\end{array}\right] \tag{7}$$

$$\phi_1 = \sin^{-1}\left[\frac{(R+h)n_{cl}}{(R+2\rho)n_1}\right], \text{ And}$$

$$\phi_2 = \sin^{-1}\left(\frac{R+h}{R+2\rho}\right)$$

Similarly, for the inner surface of the sensing region, the effective evanescent coefficient of absorption can be written as:

$$[\gamma_{eff}(\delta_1,\delta_2)]_{inner} = \frac{\alpha\lambda n_1}{2[2\pi\rho(n_1^2-n_2^2)]}\times\left[\begin{array}{l}\int_0^{2\rho}\int_{\delta_1}^{\delta_2}\dfrac{\cos^3\theta\, d\theta\, dh}{(1-n_1^2\cos^2\theta)(n_{12}^2\sin^2\theta-1)^{1/2}}\\ \div\int_0^{2\rho}\int_{\delta_1}^{\delta_2}\dfrac{\sin\theta\cos\theta\, d\theta\, dh}{(1-n_1^2\cos^2\theta)^2}\end{array}\right] \tag{8}$$

Where

$$\delta_1 = \sin^{-1}\left[\frac{(R+h)n_{cl}}{Rn_1}\right], \text{ And}, \delta_2 = 90^\circ.$$

Thus in the case of a U – shaped region of sensing, the total effective evanescent coefficient of absorption is given by:

$$\gamma_{eff} = [\gamma_{eff}(\phi_1, \phi_2)]_{outer} + [\gamma_{eff}(\delta_1, \delta_2)]_{inner} \quad (9)$$

The second term in the equation 9 vanishes, when only from the outer surface the total internal reflection occurs. As already mentioned above, the sensitivity is proportional to γ / α, for a given sensing region length, to evaluate the characteristics of the sensor, we calculate this ratio.

2.10.16 Phase modulated fiber optic sensors or Interferometric fiber optic sensors

The term interferometer is originated from the interference phenomena that take place in this mechanism. Interference of coherent waves takes place in the interferometric optical fiber sensors. The device in which interference of two coherent waves take place is called interferometer. This device senses through the principle of interference. Most of these sensors are single mode fibers optic sensors, because interference can not be observed with multimode fiber optic sensors as they carry many modes. In these sensors interaction takes place between the measurand and the light propagating through the fiber, thereby causing the phase delay in the signal.

The physical mechanism is the interference between the signal and the reference signal that will be provided externally in the system. The light transmitting through the fiber will be exposed to the measurand and the reference signal will be kept insulated from all sorts of the parameters of the system including from the measurand. The interference pattern produced by the signal in the sensing arm and signal in the reference arm will be observed once with exposing the sensing arm to the measurand and other time without exposure to the measurand. Thus the phase of the signal is modulated by the measurand and the system works as an interferometric sensor which is shown in Fig. 2.15.

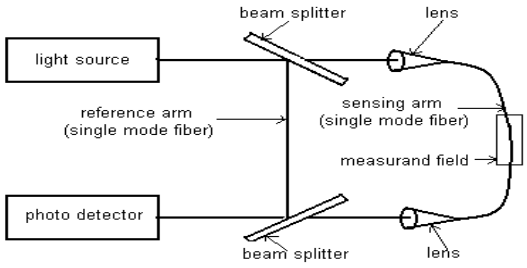

Fig. 2.15: A fiber optic interferometer

An interferometric optical fiber sensor operates by measuring induced change in the signal delay along a fiber as a change in optical phase. The change in the delay may be introduced by changes in ambient temperature or pressure, longitudinal or radial strain etc. The most important among the interferometric sensors are the optical fiber gyroscope, magnetometers and hydrophones. In all the cases the phase change is detected using one or other design of an optical fiber interferometer. The output from one port of such an interferometer in which the splitting ratios of the coupler are exactly 50% is related to the phase difference ϕ between the two paths through:

$$P = \frac{P_0}{2}\{1 + \cos\phi\} \quad (1)$$

the measurand introduces a change in the value of ϕ, between the two paths of the interferometer by differentiating the above expression. This sensitivity is clearly a maximum when the phase angle ϕ is 90° or odd multiples thereof. The perceived phase change $\delta\phi$ may be expressed as

$$\delta\phi = \frac{2\pi\Lambda L}{\lambda}\left\{\frac{\delta L}{L} + \frac{\delta f}{f}\right\} \quad (2)$$

Where L is the physical path difference between the two interferometer arms and f is the operating frequency of the optical source.

With increasing the path difference between the two arms of the interferometer, reduction in the signal to noise ratio of the output signal observed. The reduction in the signal level is due to the fact that the source is becoming less coherent with the delayed version of itself. The increase in noise level also due to phase to amplitude conversion induced by the delays in the interferometer. This fact is one of the principle limitations of interferometric fiber optic sensors. The noise penalties become substantial when the path difference between the two signals increases. The sensitivity of the interferometer to the desired measurand and of course, to undesired measurands depends upon two basic criteria. The first is the efficiency of the interface between the measurand and the optical delay in the fiber and the ability of this interface to reject interfering measurands. The second is the relative spectral occupancy of the desired and undesired signals. The phase sensitivities of fiber optics interferometers to external measurands are in the region of 10

radians per micro strain per meter, 10 radians per bar per meter and 100 radians per degree centigrade per meter at the operating wavelength of 850 nanometers.

2.10.17 Polarization modulated fiber optic sensors

In many types of OFS, another valuable and very interesting technique is polarization modulation for the signal recovery and measurand encoding. Through an appropriate interactive effect, for example the elasto-optic effect or the electro-ooptic (Faraday), the relevant physical quantity is to be measured can be transduced into a change in the polarization as the basic operation. The measured field can be outside the fiber (extrinsic sensor), or inside the fiber (intrinsic sensor), or the situation of both may apply in one system. In the last few years many new sensors based on polarization modulation have been developed, but historically, these were some of the first modulation schemes to be developed. In particular, these are sensors for measuring magnetic field and current, temperature and stress, and others amongst, many of which in detail have been reported in the literature.

2.10.18 Wavelength modulated fiber optic sensors

Using optical fibers, a number of intensity dependent measurements can be made with wavelength encoding/modulation techniques which are very much useful as a means. The wavelength division multiplexing (WDM), which depends on the encoding of the measured information in specific wavelength terms from the transducer, has been discussed by a number of others. In a real sensor, this frequency means, depending on the external parameter perturbation, the wide band optical source with the transducer acts as a wavelength encoder. Using filters or gratings, which are moved in a linear fashion or rotated mechanically to yield necessary output for testing in the environment of aerospace, several rotation / displacement transducers have been developed recently.

In interferometric sensors, further, there are two kinds of wavelength modulation in common use. The frequency modulation continuous wave (FMCW) is the first technique. In this case in an unbalanced interferometer, the output wavelength (frequency) varied with the change in the drive current, and a single mode diode laser is driven by a ramp of linear current. The intensity received from the interferometer changes which yield the

information on the measurand and yield optical path difference information in the interferometer, as the variation of the wavelength of the output of the diode causes changes in the phase. The modulation either by the frequency modulator in the experimental optical arrangement such as a Bragg cell or by the Doppler shifts from a moving body is the second example. Using optical fibers wherever appropriate, for the development of such systems, in recent years a considerable amount of effort has been extended, and for the measurement of the surface velocity, fluid flow, and often in the application of medical measurement e.g. blood flow, it has become established as an important technique. A number of different applications of wavelength modulation using Bragg gratings for strain sensor have been discussed by Dunphy et al.

2.11 Theory of refractive index

One of the most important constants in physics is the speed of electromagnetic waves in vacuum, given by c = 2.99792458 m/s. A range of 360 nm (violet color) to (750 nm (red color) electromagnetic waves are able to be detected by human eye. This light range is called the visible range of the light. The electric field of the light interacts with the electrons of the medium and causes them to vibrate, when light waves travel through an optical medium. The electrons of the medium thus act as secondary light sources for the radiation of the light waves. However, according to the optical properties of the particular medium, the speed of new waves, v, changes. Comparing to the speed of the light in vacuum, it is always smaller, i.e. $v < c$. Refractive index is a way of measuring the speed of light in a material.

Light travels fastest in a vacuum, such as outer space. The actual speed of light in a vacuum is 300,000 kilometers per second, or 186,000 miles per second. Index of Refraction is calculated by dividing the speed of light in a vacuum by the speed of light in some other medium. The Index of Refraction of a vacuum by definition has a value of 1. The typical value for the cladding of an optical fiber is 1.46. The core value is 1.48. The larger the index of refraction, the more slowly is light travels in that medium. According to the ability to slow down the light waves, all the materials are characterized, known as optical index of refraction, n, given by,

$$n = \frac{c}{v}$$

The index of refraction is larger than 1 for any material (e.g. n = 1.33 for water) and equal to 1 for a vacuum, and a unitless parameter. The refractive index of air is of 1.0003, the speed of light in air is only slightly less than c. It is typically reduced to 1. The change in direction of the light propagation due to the difference in the light speed in different media is called refraction. Except when the light approaches normally to the boundary between the two media, refraction occurs if light passes from one medium to that into a medium with a different index of refraction. Accordingly, light portion approaching the at an incident angle α to the interface, is reflected back to the first medium whereas the remaining part propagates into the second medium with an angle of refraction β. The angles between the particular ray and the normal to the interface between the two media are defined as angles of incident, angle of reflection and angle of refraction. The angle of reflection is always equal to the angle of incidence. The angle of refraction is determined by the Snell's law on the other hand,

$$n_1 \sin\alpha = n_2 \sin\beta$$

Where n1 is the index of refraction of the medium 1 and n2 is the index of refraction of medium 2. for the media of different indices of refraction, it is possible to define an optical density. The refractive index of medium 1 is higher than that of medium 2, when medium 1 has a higher optical density than that of medium 2. If the optical density of the medium is higher, then according to the Snell's law, the light rays bend towards the normal to the interface. The light ray bends away from the normal to the interface if it enters the medium with a lower optical density (β<α). The double prism refractometer introduced by Abbe can be used to measure the refractive index.

Abbe's refractometer consists of two optical prisms both refracting and illuminating and when measuring it costs with a thin layer of a liquid sample between them. It allows to measure the refractive indices up to n1 < 1.75, as the measuring prism is made with a glass of high index of refraction (n2>1.75). From the left side of the illuminating prism, the light enters the refractometer at many different angles. The prism's (AB) bottom part is rough; i.e. the prism consists of several small areas orienting in various directions. The surface of the prism can be assumed to be a source of shining the light into all the directions. Part of this light enters the refracting prism through the sample, where the α

max, the biggest possible angle of incident, correspond to the propagated ray from point A to point B. The refraction of this ray is described by the angle of maximum refraction β max.

All other rays enter the refracting prism end up to the left of point C, which make smaller angles. The refracting prism detects the dark region to the right of the point C and the illuminated region to the left of point C, consequently. It is straight forward to determine the index of refraction of liquid measured, n1, since the α max, the maximum angle, and the index of refraction of the refracting region, n2, are known constants. The changes in the interface between an illuminated and dark region i.e. point C position results as a function of angle β max, which for samples with different refractive indices n1 is different. The refractive index can be determined readily using a conversion table or can be read out from the scale of refractometer. As the speed of the light depends on their wavelength, the index of refraction depends on the wavelength of light. Therefore in the Abbe's refractometer, smearing of an interface between the dark and illuminated regions causes using the white light. Therefore it is preferable to use a monochromatic light to increase the measurement precision i.e. light of a single wavelength. Sodium light of wavelength equal to 589.3 nm is the most commonly used source.

The index of refraction is affected by the temperature of the sample and depends on the density of the measured sample. The refractive index typically increases with temperature and decreases with the decreasing of the density. The refractive index measurement therefore is reported together with wavelength of the light used and the temperature. Symbol [pic] using the sodium D line light, represents the index of refraction at t = 20°C. The index of refraction is widely used in chemistry which is an important physical parameter. It is used commonly for the purity and for the identity of the liquid. It is often used for the determination of the solutions concentration.

2.11.1 Refractive index in bulk media

The refractive index of bulk media varies with the frequency of the light wave propagating through it, and hence with the wave length. During the course of the interaction of light wave with the medium, electrical charges of medium particles get

displaced from one another resulting polarization of charges within the medium. Polarization varies with respect to the wavelength of the wave and hence the refractive index. Thus the refractive index changes with changing the wavelength of the wave. We represent an E.M. wave propagating along z-direction through a refractive a refractive medium as

$$E_x(z,t) = E_0 \exp\{-j(wt - \beta z)\} \quad (1)$$

Where, $E_x(z, t)$ = Amplitude of the electric field component

E_0 = Field constant (maximum field)

$\beta = 2\pi / \lambda_m$, the propagation constant in the medium

Now the phase velocity of the wave is given by

$$v_p = \frac{\omega}{\beta} = \frac{c}{n} \quad (2)$$

The free space wavelength is defined as, $\lambda = \frac{c}{f}$ or $c = \lambda f$, using this equation (2) can be written as

$$v_p = \frac{\lambda f}{n}, \text{ or } v_p = \lambda_m f \quad (3)$$

Where, $\lambda_m = \frac{\lambda}{n}$, i.e. within a refractive medium, the wavelength is reduced to λ_m.

Thus $$v_p = \frac{\omega}{\beta} = \lambda_m f = \frac{c}{n} \text{ or } n = \frac{c\beta}{\omega}$$

Or $$n = \frac{c\beta}{\omega} \quad (4)$$

Hence from equations (2) & (4), it can be observed that the speed of the optical pulses through dispersive medium is proportional to the frequency to the pulse. If the wave is attenuated as it passes through the medium, we may then introduce an attenuation coefficient, a, in equation (1), so that

$$E_x(z,t) = E_0 \exp(-az) \exp\{-j(\omega t - \beta z)\}$$
$$= \exp[-j\{\omega t - (\beta + ja)z\}] \quad (5)$$

This behavior may be represented by defining a complex refractive index, n*, so that

$$n^* = \frac{c}{\omega}(\beta + ja) = n + jn' \quad (6)$$

This is the more general relation between the refractive index and frequency of the wave. The real part n is still equal to $\frac{c\beta}{\omega}$ and the imaginary part, $n' = \frac{ca}{\omega}$, which is a measure of loss of energy of the E. M. wave due to the material medium. Thus the refractive index of a dispersive medium is both a function of frequency and complex. At resonance frequency, the attenuation coefficient 'a' will by very high contributing more to the refractive index reducing the speed of the wave.

The effect of an electrical field of the medium in polarizing a dielectric material is expressed in terms of dielectric constant or permittivity, 'ϵ_r' of the material. The phase velocity of E. M. wave is given by

$$v_p = \frac{1}{\sqrt{(\mu_0 \mu_r \varepsilon_0 \varepsilon_r)}} = \frac{c}{\sqrt{(\mu_r \varepsilon_r)}} \tag{7}$$

Since $\mu_0 = 1$, and $\epsilon_0 = 1$ for free space. Comparing equations (2) and (7),

$$v_p = \frac{c}{\sqrt{(\mu_r \varepsilon_r)}} = \frac{c}{n}$$

Or
$$n = \sqrt{(\mu_r \varepsilon_r)}$$

Or
$$n = \sqrt{\varepsilon_r} \tag{8}$$

Hence all that is needed is ϵ_r and hence n as a function of frequency at optical frequencies. And ϵ_r even can be represented in terms of the still fundamental parameter i.e. polarizability, denoted by α. Polarizability is defined as, $p_x = \alpha E_x$, where p_x is the dipole moment. If the material has N molecules / unit volume, then the volume polarization, P_x is

$$P_x = Np_x = N\alpha E_X \tag{9}$$

Equation (9) is the more general relation and changes with state of the material medium. The permittivity ϵ_r defined as

$$\varepsilon_r \varepsilon_0 E_x = \varepsilon_0 E_x + P_x,$$

$$\text{Or} \quad \varepsilon_r = \frac{\varepsilon_0 E_x + P_x}{\varepsilon_0 E_x},$$

$$\text{Or} \quad \varepsilon_r = 1 + \frac{P_x}{\varepsilon_0 E_x}$$

$$\text{Hence, } \varepsilon_r - 1 = \frac{P_x}{\varepsilon_0 E_x} \tag{10}$$

Substituting the value of P_x from equation (9) in equation (10), we get,

$$\varepsilon_r = 1 + \frac{N\alpha E_x}{\varepsilon_0 E_x}$$

$$\text{Or } \varepsilon_r = (1 + \frac{N\alpha}{\varepsilon_0}) \tag{11}$$

Which is the relation between €r and α, which again is the more generalized equation. In a solid dielectric the effect of polarization of all the surrounding molecules on any one molecule is given by $1+\frac{P_x}{3\varepsilon_0 E_x}$. Therefore the local field increases by a factor $(1+\frac{P_x}{3\varepsilon_0 E_x})$ over the average field E_x. Thus, the polarization becomes from equation (9),

as $$P_x = N\alpha E_x\left[1+\frac{P_x}{3\varepsilon_0 E_x}\right]$$

$$= N\alpha E_X + \frac{N\alpha E_X P_X}{3\varepsilon_0 E_X},$$

Or $$P_x\left[1-\frac{N\alpha}{3\varepsilon_0}\right] = N\alpha E_X$$

Therefore, $$P_x = \frac{N\alpha E_X}{\left[1-(\frac{N\alpha}{3\varepsilon_0})\right]} \tag{12}$$

Substituting equation (12) in equation (10), we get,

$$(\varepsilon_r - 1) = \frac{N\alpha E_X / \varepsilon_0 E_X}{\left(1-\frac{N\alpha}{3\varepsilon_0}\right)}$$

$$\text{Or} \quad (\varepsilon_r - 1) = \frac{N\alpha/\varepsilon_0}{\left(1-\frac{N\alpha}{3\varepsilon_0}\right)} \tag{13}$$

$$(\varepsilon_r - 1) = \frac{N\alpha/\varepsilon_0}{\left(\frac{3\varepsilon_0 - N\alpha}{3\varepsilon_0}\right)}$$

$$= \frac{3N\alpha\varepsilon_0}{\varepsilon_0(3\varepsilon_0 - N\alpha)},$$

Or
$$\frac{(\varepsilon_r - 1)}{(\varepsilon_r + 2)} = \frac{N\alpha}{3\varepsilon_0} \qquad (14)$$

Equation (13) is expressed in the alternative form as equation (14), obtained by Claussius and Mossotti. Here α is defined as dipole moment per unit electric field $\alpha = p_x/E_X$. But E_x can have different frequencies. Thus 'p_x' depends on the frequency of E.M. wave and hence α depends on the frequency. Again as α changes with frequency $€_r$ also depends on frequency. As $n^2 = €_r$, if $€_r$ changes with frequency n also varies with frequency. As $v_p = c/n$, if n changes with frequency, v_p also varies.

Hence the phase velocity of E.M. wave traveling through the dielectric medium is a function of frequency. For a typical dielectric, the polarizability (α), variation with the frequency of the applied electric field is shown in Fig. 2.16.

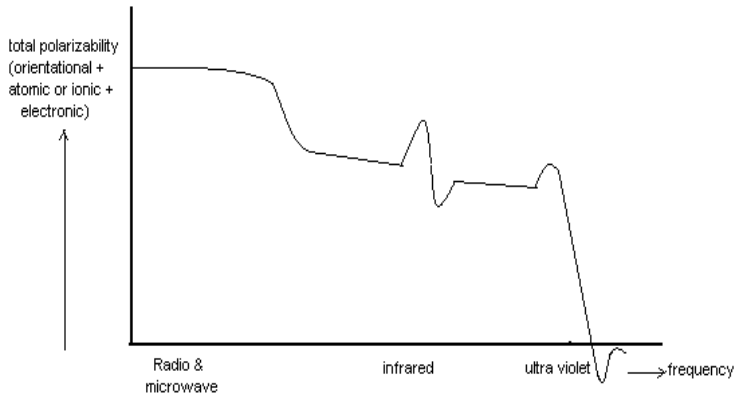

Fig. 2.16: Variation of polarizability with frequency of the wave.

α the polarizability decreases in general with frequency and hence velocity, v_p, of the wave increases with frequency. The high frequency resonances arising from the response of the electronic structure of the molecules are needed to be discussed for the purpose as

they are offering very low loss at the frequency between infrared and ultra violet regions of the wave. At this optical frequency, under resonance, the charge gets displaced with the applied field and the restoring force arises due to inertia of the molecules which is proportional to the displacement. Then the charge motion is that of the harmonic oscillator.

The origin for 'n' is the presence of atoms in the medium and hence their charges. During the interaction of electric field of the light with the charges of the atoms of the medium, the charges get displaced and gives rise to polarization. The charge is subjected to restoring force which is proportional to displacement. Then the charge motion is that of harmonic oscillator. Apart from the restoring force the charge may be subjected to damping force and external cyclic force. Thus three forces act on the charges. The equation of motion of the charge subjected to free, forced and damped oscillations is given by,

$$\frac{dx^2}{dt^2} + \gamma_k \frac{dx}{dt} + \omega_{0k}^2 x = \frac{e}{m} \mathrm{E}_1 \exp(-j\omega t) \tag{15}$$

Where the external force $eE_1\exp(-j\omega t)$, forces the oscillation of the field. ω_{0k} is the resonant frequency of a particular interaction represented by k, and γ_k is the damping factor. Damping is directly proportional to the velocity of the charge or $\text{damping} = \gamma_k \frac{dx}{dt}$. The solution of the above equation is

$$x = \frac{(e/m)\left[\mathrm{E}_1 \exp(-j\omega t)\right]}{\omega_{0k}^2 - \omega^2 - j\omega\gamma_k} \tag{16}$$

The complex polarizability is give by

$$\alpha^* = \frac{p_x}{\mathrm{E}_x} = \frac{xe}{\mathrm{E}_x} = \frac{(e^2/m}{(\omega_{0k}^2 - \omega^2 - j\omega\gamma_k)} \tag{17}$$

Substituting equation (17) in equation (13) we get the permittivity as

$$\varepsilon_r^*(\omega) = \left[1 + \frac{(Ne^2/m\varepsilon_0)}{(\omega_{0k}^2 - \omega^2 - j\omega\gamma_k)}\right] \tag{18}$$

If we take into account of all possible resonances and represent the strength of each by a factor, g_k, then ϵ_r becomes as a function of frequency as

$$\varepsilon_r^*(f) = 1 + k\sum_k \frac{g_k}{f_{1k}^2 - f^2 - j\gamma_k f} \tag{19}$$

Where

$$f_{1k}^2 = \frac{1}{4\pi^2}\left[\omega_{0k}^2 - \frac{Ne^2}{3m\varepsilon_0}\right]$$

And

$$k = \frac{Ne^2}{4\pi^2 m\varepsilon_0}$$

Now refractive index is also a complex given by n* = n + jn' and

$$(n^*)^2 = n^2 - n'^2 + 2jnn' = \varepsilon_r^*$$

In fiber optic materials, the attenuation is very small, because the E.M. waves selected as carriers are having frequencies well away from the resonance frequencies as the loss is very high near the resonance frequencies. Therefore away from the resonances, the effect of the imaginary part of ε_r^* may be neglected in equation (19) and hence the refractive index may be expressed as $n^2 = \varepsilon_r^*$. Thus

$$(n^2 - 1) = \sum_k \frac{kg_k}{(f_{1k}^2 - f^2)}$$

From this equation it is observed that 'n' increases as the frequency 'f' of the wave increases in the region between infrared and ultraviolet especially from the middle of theses two bands and towards ultraviolet.

Or

$$(n^2 - 1) = \sum_k \frac{G_K \lambda^2}{(\lambda^2 - \lambda_{1K}^2)} \tag{20}$$

where,

$$\lambda_{1k} = \frac{c}{f_{1k}} \text{ and } G_k = \frac{kg_k \lambda_{1k}^2}{c^2}$$

From equation (20), it is observed that the 'n' decreases as the wave length of the wave increases. Equation (20) gives the variation of R.I. of optical materials with wavelength between i. r. and u.v., and it is also called Selmeier dispersion formula.

References

[1] Gowar, John, Optical Communication Systems, 2 ed., Prentice-Hall, Hempstead U K, 1993.

[2] Gerd Keiser, Optical Fiber Communications, 2 ed., McGraw-Hill Book Co., Singapore, 1991.

[3] Ernsberger, F. M. *In* Glass: Science and Technology; (Edited) D.R. Uhlmann, N.J. Kreidle,; Vol. V, Chapter 1, Acad. New York, 1980.

[4] Hecht, Jeff, City of Light, the Story of Fiber Optics, Oxford University Press, New York,

[5] Hecht, Jeff, Understanding Fiber Optics, 4th ed., Prentice-Hall, Upper Saddle River, NJ, USA 2002.

[6] Mirabito, Michael M.A; and Morgenstern, Barbara L., The New Communications Technologies: Applications, Policy, and Impact, 5th. Edition. Focal Press, 2004.

CHAPTER 3

Experimental methods and techniques

3.1 Designing of Optical Sensors

As is known the properties of glass can be modified or changed with the addition of other compounds or heat treatment. The most obvious characteristic of ordinary glass is that it is transparent to visible light, of course not all glassy materials are. This transparency is due to an absence of electronic transition states in the range of visible light, and because ordinary glass is homogeneous on all length scales greater than about a wavelength of visible light. Pure SiO_2 glass, also called fused quartz, does not absorb UV light and is used for applications that require transparency in this region, although it is more expensive. This type of glass can be made so pure that when made into fiber optic cables, hundreds of kilometers of glass are transparent at infrared wavelengths. Amorphous SiO_2 is also used as a dielectric material in integrated circuits due to the smooth and electrically neutral interface it forms with silicon.

Glass appears colorless to the naked eye when it is thin, though it can be seen to be green when it is thick, or with the aid of scientific instruments. However, metals and metal oxides can be added to glass during its manufacture to change its color. From a more commonsense point of view, glass should be considered a solid since it is rigid according to everyday experience. Although glass has properties of a supercooled liquid, it is generally classed as solid at room temperature. Thus, the properties of quartz glass is a colorless solid having the overall refractive index about 1.5, molecular weight of 60.08 g/mole, boiling point of 2230°C, and the density about 2.50g/ml having different crystalline structures like hexagonal, rhombohedral, amorphous, cubic or tetragonal. A U-shaped glass rod is proposed to be used as sensing probe in the present investigation. Sensing elements are designed by selecting highly pure ordinary glass as the purity defines transparency and transparency decides the transmission efficiency of the glass rod.

3.1.1 Fabrication of the sensor

Designing of sensor is the one of the crucial aspects in constructing any sensing device used to measure an environmental parameter. The geometry, the assembly of components, the external feature of the structure and the construction of sensor varies from sensor to sensor. The design depends mainly on the two interacting factors in the sensor system, i.e. one the measurand to be measured and the second the measuring standard that measures the measurand. In most of the standard units that are used in the determination of any parameter, only one of their properties i.e. for example mass, time, length is exploited to construct a measuring device for the determination of certain parameter. In the case of fiber optic sensors, four of the important characters of light i.e. intensity, phase, polarization, and wavelength of the light are exploited to construct various sensing devices to detect and to record several quantities.

Thus light as a standard unit playing a versatile role in the determination of numerous parameters around us. To measure any parameter with the use of light wave, light alone has to be made to interact with the particular measurand. In order to achieve this interaction between the light and the measurand, light must be guided through some medium, and its characters must be protected from the other environmental quantities. For performing this role an optical fiber prepared from the silica glass in the form of a wire or rod can be employed. The design and construction of any sensor relies on that what type of character of the light is intended to be exploited, and also on the parameter that is to be detected with the sensor.

In the present work, as it is proposed to study and develop a light intensity based optical fiber sensor to determine the refractive index of liquids, a new, unique and a novel design approach has been introduced. Initially are adopted the basic ideas of light propagation through pure silica glass rods and selected them as sensing elements of very fine diameters and implemented them through using several design considerations. The central idea behind in selecting various geometries of glass rods is to check, which design can offer highest efficiency with respect to its reproducibility, precision, accuracy and sensitivity corresponding to the determination of refractive index of liquids in the range of 1.3 to 1.5. The diameters of different sensors are chosen about 0.25 mm and 0.5

mm thick. In designing the sensing elements, eight of the most probable shapes have been worked out and used to study in the finalization of an effective and an efficient sensor. The eight sensor designs selected have been shown in Fig. 3.1.

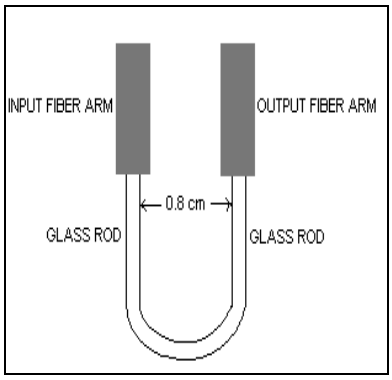

Fig.3.1a: U-shaped glass rod (0.25mm dia).

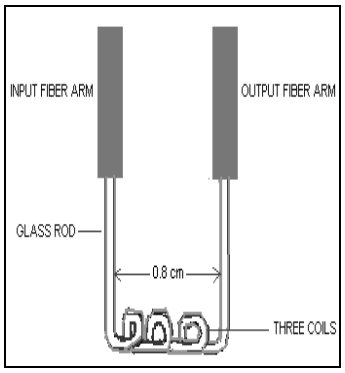

Fig.3.1b: Coiled neck U-shaped. (0.25mm dia)

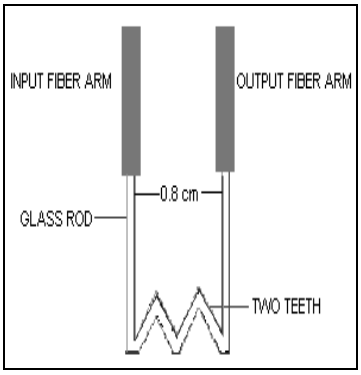

Fig.3.1c: Saw tooth neck U-shaped. (0.25mm dia)

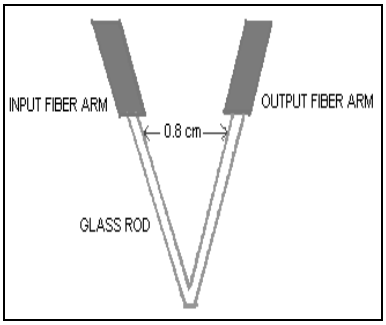

Fig. 3.1d: V-shaped. (0.25mm dia)

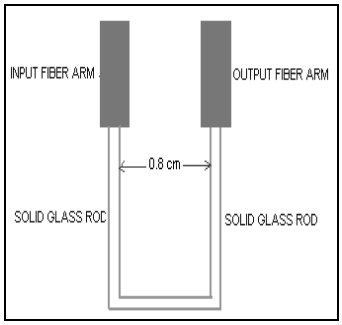

Fig.3.1e: Square shaped. (0.25mm dia)

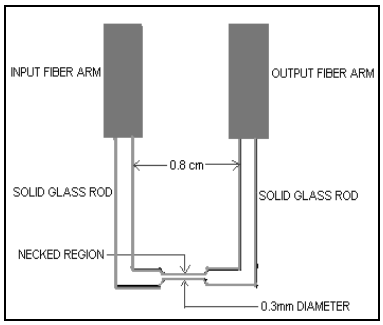

Fig.3.1f: Shrinked neck U-shaped. (0.25mm dia)

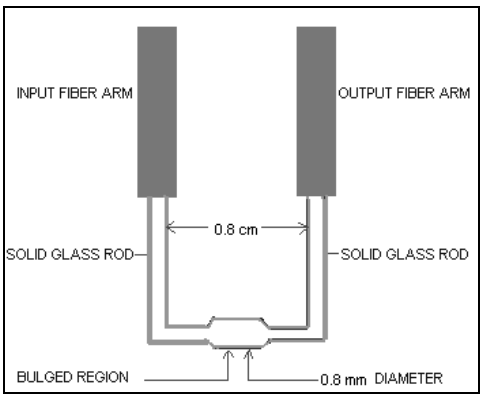

Fig.3.1g: Bulged neck U-shaped (0.25mm dia).

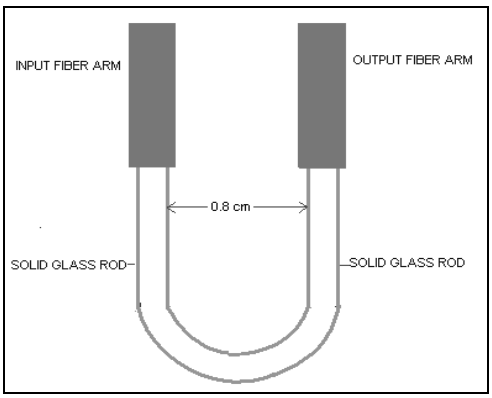

Fig.3.1h: U-shaped (0.5mm dia).

Fig. 3.1: Various designs and geometries of the sensing elements used in the experimental work for deciding as efficient sensor among them.

Proper care had been taken in the purity of the glass material by procuring the raw silica glass rods from the reliable brand supplier in the market. Sufficient care also has been taken in the preparation of the sensor elements by obtaining them from a skilled and genuine glass rod manufacture in and around the vicinity of the research laboratory. With respect to the dimensions and other parameters of the rods, the compatible sizes and diameters in correspondence with the fibers used have been selected. Suitable PCS fibers are used in the sensor design to couple the light to and from the sensor. The responses of the various elements are observed to be very effective in showing the values instantaneously and decisively in the output without and with the test liquids, and hence are proved to be having tremendous sensing characters. The comparative study of all the designs considered enabled in the conclusion of deciding the effective sensing element from among them.

The connection between the glass rod and optic fiber needs some proper preparation of both glass rod and plastic fiber. Quick identification of the exact size and type of a given piece of optical fiber is a routine but necessary task. If one has access to the fiber itself, the first step in identification is to remove any outer jacket material that may exist and carefully to remove the plastic buffer from the fiber. Fiber has tremendous strength in tension but is very weak in all other directions. The ends of optic fibers and the glass sensors are properly cleaned and dried before they are glued using instant fixing glues available in the market. The joints are then sealed using m-seal to provide a proper grip and strength to the joints.

3.1.2 Parameters of U-shaped glass rods

Thin borosilicate glass rods have been bent in the form of U shape, such that the separation between its two arms is given by 2x, and the depth of its curve by y as shown in Fig. 3.2.

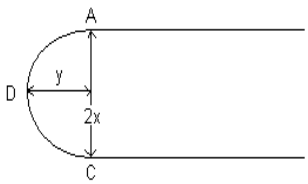

Fig. 3.2: U-shaped glass rod used for sensing liquid R.I.

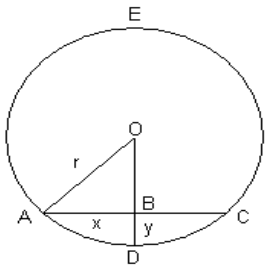

Fig. 3.3: Bend ADC of the U-shaped glass rod as an arc of the circle ADCE.

Let the ADC of the U-shaped glass rod is the arc of the circle ADCE, as shown in Fig. 3.3. Also let the radius of this circle be given by AO = OD = r, the length of the chord AC = 2AB = 2BC, and the depth of the curvature BD = r - OB = y. Radius of the sensor bend of the U-shaped rod can then be evaluated from the geometry of Fig. 3.3. Therefore, from the relation,

$$r^2 = OB^2 + AB^2 = (r - y)^2 + x^2 \quad (1)$$

It is that

$$r = (x^2 + y^2)/2y \quad (2)$$

The depth of curvature y and the separation 2x, between the two arms of the five U-shaped glass rods of diameter 1 mm fabricated in the laboratory have the corresponding radius of curvature r which can be evaluated with the help of equation (2). Thus the glass rod can be characterized by the following specifications: 2x, y, and r.

3.1.3 Refractive index of the glass sensor

Sensing element specifications: 2x = 8.0 mm, y = 4.0 mm, r = 4.0 mm

The refractive index of the glass sensor is determined by using a microscope and sodium light. Initially the sensor is placed on a semitransparent plastic scale with fine lines on it. The scale is illuminated by a monochromatic source of light (Na-5893 °A). The microscope can be focused on the surface of the glass sensor, and then the lines on the scale are seen through the sensor, and then finally on the lines on the scale directly. The readings on the vertical scale of the microscope are noted as A, B, and C respectively. The refractive index is then determined by the formula

RI = real depth / apparent depth = (A-C) / (A-B)

The above procedure is repeated at many places on the sensor and an average value of refractive index is determined and used in the work. Thus the refractive index of the

glass rod is determined to be 1.5, which acts as a core in the sensing zone of the sensor system.

3.2 Description of the experimental setup

The experimental setup and the design of overall sensing macro-system have been shown in Fig. 3.4, and Plate 3.1.

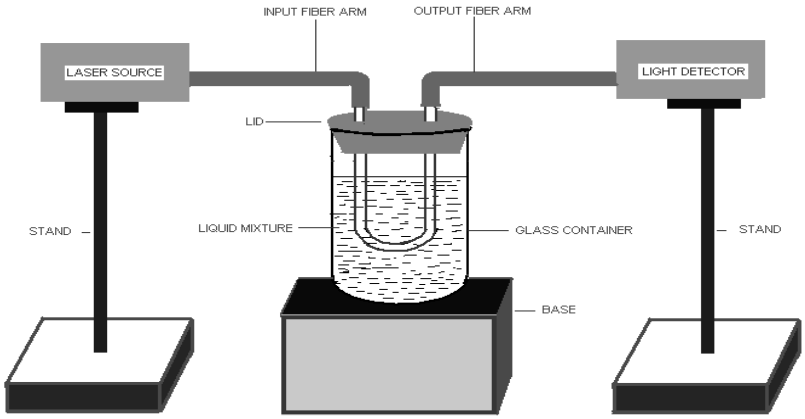

Fig. 3.4: Experimental arrangement of sensor

The sensor is basically an extrinsic type fiber optic intensity based refractive index sensor in which both the input fiber and the output fibers simply act as light conductors to couple the light from source to the sensing glass rod, and sensing rod to the power detector. The experimental arrangement consists of a light source of wavelength 633 nm fixed on a stand, and an optical power meter (bench mark) is fixed at the other side on another stand. The two fibers used as input arm and the output arm, are plastic clad silica fibers (PCS) of diameters ranging from 250μm to 500μm and lengths of about 25 cm each and accordingly the diameter also fixed to couple the light from one another.

The sensor consists of a solid glass rod bent in the form of U- shape. Light is injected at one end of the U- shaped rod through a plastic clad silica fiber coupled to a semiconductor laser diode. The selection of the solid glass rod bent in the U- shaped rod is essentially guided by the availability of the plastic clad silica fiber. The prong diameter of the glass rod is ranging from 0.25mm to 0.5mm, and heights are about 4 to 6 cm and prong diameter width is of 0.8 cm are used at different stages of the experimentation. The uniformity and the bending radius of U shaped rod were checked using traveling

International Journal of Engineering Research & Technology (IJERT)
ISSN: 2278-0181

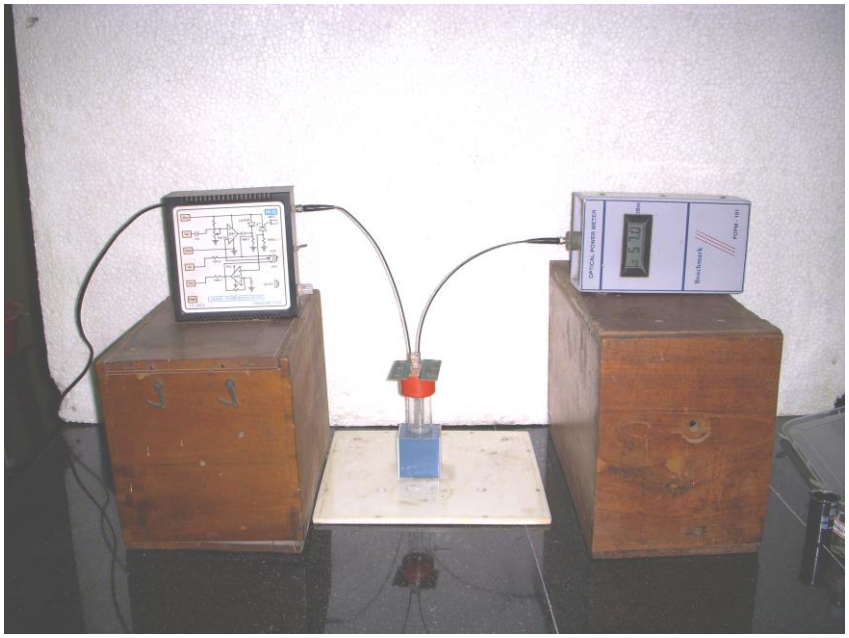

Plate 3.1 Experimental setup for the measurement of refractive index

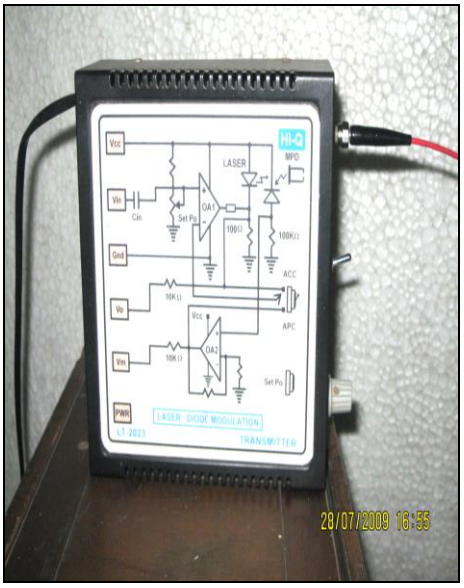

Plate 3.1 (a) Optical source

Plate 3.1 (b) Optical power Meter

microscope. Experiment was performed only on those probes that were uniform and bend was close to U-shape.

One end of the input fiber arm is connected to the light source by using a suitable SMA connector and other end of it is properly connected to the one of the ends of the U – shaped glass rod by using a glass to glass jointing adhesive available in the market and covered with m-seal and black insulation tape. The second end of the U – shaped glass rod is connected similarly to one of the ends of the output fiber having same dimensions as the input fiber, and the other end of the output fiber is connected to the light detector i.e. power meter, by using another SMA connector. At the point of coupling the PCS fiber to a glass rod sufficient care is taken to see that no light escapes at the joint.

The U – shaped glass rod so assembled is immersed into the glass container containing the liquid mixture which is placed on a rigid and stable base. The liquid container made of glass is placed in between the source and the detector. Stability is achieved throughout the experimentation to all the components and to the entire system as a whole as it is the one of the essential criteria for the effective working of the sensor. A black covering is used around the glass container to avoid the stray light from external environment around the container, with a view to expose the glass rod and the liquid mixture in the container only to the light from the input source. The light source and the power meter are connected to the respective power points as they are being active components in the entire sensor system assembly. A suitable cork lid is also used to prevent the liquid mixture and the sensing element exposure to the ambient atmosphere.

Another experimental arrangement is used in the measurement of quality liquids is the burette along with stand. Two burettes of same measuring ranges and two glass beakers have been used to take the required amount and ratios of liquids to be used for the experimentation. For the calibration of the scale of the new sensor, an Abbe's refractometer (Plate 3.3) has been used initially to standardize the relation between the refractive index and the optical power output of the sensor. Abbe's Refractometer is the most familiar and very much known to the research world.

The arrangement so made is now ready for experimentation. The U-shaped rod is immersed into a wide mouth beaker containing liquid mixtures of various volumes keeping the total volume of the mixture always at 10 ml and care is taken to see that the bottom ends of the U- shaped rod are properly immersed in the mixture of liquids without touching the bottom of the beaker. This is verified by noting the height of the liquid column using a traveling microscope. Light is injected into the PCS fiber from one end and collected through another PCS fiber, which is in turn connected to U-shaped glass rod. When the U–shaped rod is immersed in a liquid, some amount of light escapes into the liquid and the amount of light collected at the other end is reduced.

3.3 Measurement of attenuation or Optical-Power Measurement

The power level in optical communications is of too wide a range to express on a linear scale. A logarithmic scale known as decibel (dB) is used to express power in optical communications. The gain of an amplifier or attenuation in fiber is expressed in decibels. The decibel does not give a magnitude of power, but it is a ratio of the output power to the input power.

$$Loss\ or\ gain = 10\log_{10}(P_{out}/P_{input})$$

The decibel mill watt (dBm) is the power level related to 1 mill watt (mW). Transmitter power and receiver dynamic ranges are measured in dBm. A 1-mW signal has a level of 0 dBm. Signals weaker than 1 mW have negative dBm values, whereas signals stronger than 1 mW have positive dBm values.

$$dBm = 10\log_{10}(Power(mW)/1(mW))$$

The signal attenuation as a unit of length is defined by the following equation:

$$\text{attenuation} = \left(\frac{10}{L}\right)\log_{10}\left(\frac{P_i}{P_o}\right)$$

The attenuation of the signal is a log relationship. The signal length (L) can be expressed in kilometers. The unit of attenuation therefore is deciber/kilometer (dB/km). A decibel (dB) is a unit used to express relative differences in signal strength. A decibel is expressed as the base 10 logarithm of the ratio of the powers of two signals, as shown here

$$dB = 10 \text{ x } Log_{10}\ (P_1/P_2)$$

Where Log_{10} is the base 10 logarithm, and P_1 and P_2 are the powers to be compared. Log_{10} is different from the Neparian Logarithm or base e logarithm (ln). We can also express signal amplitude in dB. Power is proportional to the square of the amplitude of a signal. Therefore, dB is expressed as:

$$dB = 20 \times Log_{10} (V_1/V_2)$$

Where, V_1 and V_2 are the amplitudes to be compared.

1 Bell (not currently used) = Log_{10} (P1/P2)

1 decibel (dB) = 1 Bell / 10 = 10 * Log_{10} (P1/P2)

dBr = dB (relative) = dB = 10 * Log_{10} (P1/P2)

Decibels in Milliwatt (dBm)

dBm = dB milliwatt = 10 x Log_{10} (Power in mW / 1 mW)

Power/Voltage Gains: With this information, one can define the formulas for attenuation and gain:

Attenuation (dB) = 10 x Log_{10} (P in/P out) = 20xLog_{10} (V in/V out)

Gain (dB) = 10 x Log_{10} (P out/P in) = 20 x Log_{10} (V out/V in)

Mole fraction: Concentrations of various liquids in a liquid mixture can be expressed in terms of 'mole fractions'. Mole fraction is defined as the ratio of number of moles of a constituent to the total number of moles of all constituents present in the solution. Mole fraction has no units and at any case it is independent of temperature of the liquid mixture.

$$\text{Mole fraction, } X = \frac{Number\ of\ moles\ of\ a\ constituent}{Total\ no.of\ all\ constituents\ present\ in\ the\ solution}$$

Let, N_p moles of solute 'p' be dissolved in N_q moles of a solvent 'q'. Then the mole fractions of 'p' and 'q' are calculated as follows:

Total no. of moles in the solution = $N_p + N_q$.

$$\text{Mole fraction of p, } X_P = \frac{No.of\ moles\ of\ p}{Total\ no.of\ moles\ in\ the\ solution}$$

$$\text{Therefore, } X_p = \frac{N_p}{N_P + N_q}$$

$$\text{Similarly, mole fraction of q, } X_q = \frac{No.of\ moles\ of\ q}{Total\ no.of\ moles\ in\ the\ solution}$$

$$\text{Or, } Xq = \frac{N_q}{N_q + N_P}$$

The sum of the mole fractions of all constituents present in the solution is equal to unity. Thus,

$$X_p + X_q = \frac{N_P}{N_P + N_q} + \frac{N_q}{N_q + N_q} = 1.$$

Formula for mole fraction, M_f of liquid 1 in a liquid 2**:**

$$M_f = \frac{V_1(M_1/d_1)}{V_1(M_1/d_1) + V_2(M_2/d_2)}$$

Where,

V_1, volume of liquid 1, d_1, density of liquid 1, M_1 molecular weight of liquid 1,

V_2, volume of liquid 2, d_2, density of liquid 2, M_2 molecular weight of liquid 2.

3.4 Experimental Procedure

In the present work, binary mixtures, viz. Methanol mixed in Benzene, Propyle Alcohol mixed in Benzene, Butanol mixed in Benzene and Cyclohexane mixed in Benzene were selected for the study of refractive index (Table 3.1).

A volume of 10ml mixture is prepared from individual solutions of Methanol, Propyle Alcohol, Butanol and Cyclohexane in Benzene. The experimental arrangement consists of a solid thin glass rod bent in the form of U-shape attached with a Plastic clad silica (PCS) fiber (Plate 3.2). Light is injected from a laser source (λ = 633nm.) at one end of the U-shaped rod through a Plastic Clad Silica (PCS) fiber coupled to a laser diode. To an optical power meter the output end of the rod is connected through another similar PCS optical fiber. The whole arrangement of the U-shaped rod is immersed in a beaker containing methanol, propyle alcohol, butanol and benzene mixture of various volumes and the variation of the optical output power are noted. The output power is calibrated in terms of the refractive index of the liquid. The R.I. of the liquid is estimated with the help of output power which is in close agreement with the values given in literature.

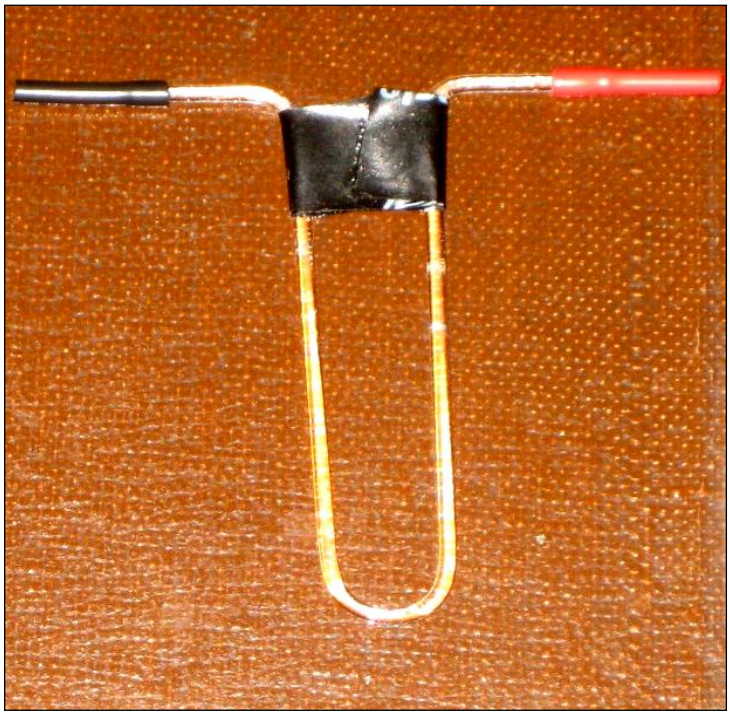

Plate: 3.2. U shaped glass sensor

With a view to check that which shape of the U shaped glass rod is more sensitive, a comparative experimental study of the evanescent field absorption sensor based on straight, U-shape, coiled neck shape U-shaped, shrinked neck U-shaped, bulged neck U-shaped, saw tooth neck U-shaped, V-shaped, square shaped probes is presented. The effect of power launching, radius and the shape of the fiber on the sensitivity of the sensor are experimentally investigated. Increase in the launching angle of the light (Numerical Aperture) of the fiber increase the sensitivity of the sensor. The effects of radius on the sensitivity, depends up on the bending radius of the probe. A U-shaped probe has high sensitivity having large fiber radius than that of a low fiber radius probe. In the case of straight probe (i.e. infinite bending radius), the fiber with small radius has high sensitivity. Thus which fiber (small or large radius) has matching sensitivity depends on the bending radius of the probe. For a given glass fiber, decrease in the bending radius increase the sensitivity of the U-shaped probe. An inverse power law relationship between bending radius and sensitivity is established according to literature.

To have negligible contribution of the adsorption on the response curve, the solution of methanol in benzene has been selected as the test fluid. The effect of the output power on the various shaped probes has been studied experimentally.

A theoretical mechanism for the variation of output power is proposed in this work. If the prism is immersed in a liquid, the light is no longer confined to the prism but some part of it enters into the liquid and as a result, the amount of light returned back is considerably reduced. This happens because the difference in refractive index between the prism and the liquid is reduced. A similar phenomenon can be observed if the experiment is done using a U–shaped glass rod. The present work is done on the basis of the above principle.

Binary mixtures of Methanol and Benzene were prepared by mixing ‘x’ cc of Methanol (or Propyle Alcohol, Butanol, Cyclohexane) in ‘y’ cc of Benzene. The composition of the binary mixture is varied by varying x and y in known steps keeping the sum ‘(x + y)’, a constant. The concentration of Methanol in the binary mixture is expressed in mole fraction as:

$$\text{Mole fraction of Methanol, } m_f = [x\,(M_1/d_1) / [(x\,(M_1/d_1) + y\,(M_2/d_2)]$$

M_1 = Molecular weight of Propanol, M_2 = Molecular weight of Benzene,
d_1 = Density of propanol and d_2 = Density of Benzene.

This procedure was repeated for Cyclohexane mixed in Benzene, Propanol mixed in Benzene, and Butanol mixed in Benzene.

To calibrate the more sensitive sensor of dimensions 0.25 mm diameter, the experiment is carried out by noting the refractive index of the mixture of methanol and benzene using Abbe's refractometer. At this RI value the power coming through the glass rod via PCS fiber is noted. The experiment is repeated for various RI values and various mixtures of methanol mixed in Benzene. An interesting observation noticed is that as the mole fraction of methanol in benzene increases, the output power also increases as stated in the theory. Another interesting observation is as the RI of the binary mixture is decreases, the output power increases. These two observations are depicted graphically in Figs. 3.6 & 3.7 respectively.

The sensors response for U-shaped with bending radius fixed and the diameter of the rod 0.25 is found theoretically to be linear which indicates the absence of adsorption. The variation of refractive index with the mole fraction of methanol in benzene and the power relation with change in R. I. of mixture from R. I. of the core is shown in Figs. 3.8 & 3.9. For a given concentration of a solution, it is in according to the results reported in the literature, that the value of the coefficient of absorption is larger in case of U – shaped probe. For the study of the effect of the power output on the thickness of the glass rod another U-shaped glass rod of 0.5mm is made use of and the experiment is repeated. Figs.3.25 & 3.26 indicate a graph between mole fraction of methanol in benzene and power output and behavior of power output with mole fraction. Interestingly, it was also observed that the output power is an inverse function of the Refractive Index (RI) of the binary mixture. Similar behavior was noticed for the mixture of Propanol in Benzene, Butanol in Benzene and Cyclohexane in Benzene.

It is evident from the above two graphs (Figs.3.25 & 3.26), that for a given concentration of a solution and fiber core radius, the value of the evanescent absorption coefficient is larger in the case of 0.5mm sized probe as compared to a 0.25mm U-

shaped probe (Fig. 3.1a). The experiment is further repeated as shown in figure (3.1b), with a coiled neck U-shaped glass rod dipped in the same binary mixer of the liquid and the corresponding graph is represented in figs.3.10 & 3.11.

Experiment was also carried out with saw tooth neck U-shaped glass rod as indicated in Fig.3.1c and dipped in the same binary mixture of the liquids. No power is recorded from beginning to the end of the experiment. This is due to the fact that multiple micro-bending (sharp bending) of the fiber results in total loss of power into the liquid which can not be retrieved. The experiment is further carried out with a V-shaped glass rod as indicated in Fig. 3.1d and straight neck U-shape (square shaped) glass rod as indicated in Fig. 3.1e and finally a shrinked neck U-shaped glass rod as indicated (3.1f) and bulged neck U-shaped glass rod in figure (3.1g) and corresponding graphs are presented in Figs. 3.13 & 3.14, 3.16 & 3.17, 3.19 & 3.20, and 3.22 & 3.23 respectively.

3.5 Sensitivity of the various glass elements

Sensitivity of any sensor can be defined as the change in the measurer for a particular change in the measurand value. If the change in the measurer value is more, corresponding to a small change in the measurand value. In the present study, the measurer is the light wave, and the character that change is its intensity (I). The measurand that is measured is the index of refraction (n) of the liquid. Therefore, when the sensors sensitivity is denoted as α, then the equation for sensitivity can be written as,

$$\alpha = dI / dn$$

1. *Sensitivity measurement of 0.25mm diameter and 2cm fang width, U-shaped solid glass sensor:* The free space power output i.e. when air surrounding the U-shaped sensor element, is -52.0 dBm. Power output when water surrounding the U-shaped sensor element, is -53.8 dBm.

Change in power output (dI) is -1.8 dBm.

Change in refractive index (dn) is $1.33 - 1.0 = 0.33\ n_D$.

Where 1.33 is the refractive index of the water and 1.0 is the refractive index of the air.

$$\alpha = -1.8\ dBm / 0.33 = -5.455\ dBm/n_D.$$

2. *Coiled U-shaped, 0.25mm diameter, and 2cm fang width solid glass sensor:* The free space power output i.e. when air surrounding the U-shaped sensor element, is -57.0 dBm. Power output when water surrounding the U-shaped sensor element, is -58.0 dBm.

Change in power output (dI) is -1.0 dBm.

Change in refractive index (dn) is 1.33 – 1.0 = 0.33 n_D.

α = -1.0 dBm / 0.33 = -3.030 dBm/n_D.

3. *Bulged neck U-shaped 0.25mm diameter, 2cm fang width solid glass sensor:* The free space power output i.e. when air surrounding the U-shaped sensor element, is -59.2 dBm. Power output when water surrounding the U-shaped sensor element, is -60.3 dBm.

Change in power output (dI) is -1.1 dBm.

Change in refractive index (dn) is 1.33 – 1.0 = 0.33 n_D.

Where 1.33 is the refractive index of the water and 1.0 is the refractive index of the air.

α = -1.1 dBm / 0.33 = -3.333 dBm/n_D

4. *Square neck U-shaped 0.25mm diameter, and 2cm fang width solid glass sensor:* The free space power output i.e. when air surrounding the U-shaped sensor element, is -51.0 dBm. Power output when water surrounding the U-shaped sensor element, is -51.2 dBm.

Change in power output (dI) is -0.2 dBm.

Change in refractive index (dn) is 1.33 – 1.0 = 0.33 n_D.

α = -0.2 dBm. / 0.33 = -0.606 dBm/n_D.

5. *Sensitivity measurement of V-shaped 0.25mm diameter, and 2cm fang width solid glass sensor:* The free space power output i.e. when air surrounding the U-shaped sensor element, is -48.1 dBm. Power output when water surrounding the U-shaped sensor element, is -48.4 dBm.

Change in power output (dI) is -0.3 dBm.

Change in refractive index (dn) is 1.33 – 1.0 = 0.33 n_D.

α = -0.3 dBm / 0.33 = -0.909 dBm/n_D.

6. *Shrinked neck U-shaped, 0.25diameter, and 2cm fang width solid glass sensor:* The free space power output i.e. when air surrounding the U-shaped sensor element, is -60.6 dBm. Power output when water surrounding the U-shaped sensor element, is -61.8 dBm.

Change in power output (dI) is -1.2 dBm.

Change in refractive index (dn) is 1.33 – 1.0 = 0.33 n_D.

α = -1.2 dBm / 0.33 = -3.636 dBm/n_D.

7. *Saw tooth (two teeth) neck U-shaped, 0.25mm diameter, and 2cm fang width solid glass sensor:* No response is noticed with this design of the sensor element and question of sensitivity does not arise.

8. *Sensitivity measurement of 0.5mm diameter and 2cm fang width, U-shaped solid glass sensor:* The free space power output i.e. when air surrounding the U-shaped sensor element, is -62.6 dBm. Power output when water surrounding the U-shaped sensor element, is -63.9 dBm.

Change in power output (dI) is -1.3 dBm.

Change in refractive index (dn) is 1.33 – 1.0 = 0.33 n_D.

α = -1.3 dBm / 0.33 = -3.939 dBm/n_D

Comparing the sensitivities of all the above eight sensing elements, it is observed that the one with 0.25mm diameter U-shaped solid sensing element is exhibiting the highest sensitivity i.e., -5.455 dBm/n_D. Therefore this element has been selected being efficient for the study of the refractive index of the liquids. Thus the glass rod of very small diameter used as a sensing probe in the present work and, is stood in forefront in finding the R.I. of even hazardous liquids, being insensitive to such type of materials. The following conclusion may be drawn on the basis of the experimental results obtained.

(a) The numerical aperture of the fiber and hence the launching angle effects the sensitivity of the sensor. Increase in numerical aperture of the fiber increases the sensitivity. This has been observed for U-shaped probes with a solution of methanol in benzene as a test fluid. The other important observation is that the sensitivity of the sensor based on U-shaped probe increases with the decrease in the thickness of the glass rod.

(b) In case of U-probe the sensitivity of the device depends on the core radius which, fiber (with small or large) has maximum sensitivity depends up on the bending radius of the fiber probe.

An interesting observation made is that the output power is a function, proportional to the mole fraction of Methanol in Benzene. In order to confirm the above behavior studies are made on another two binary mixtures of Propanol mixed in Benzene, and Butanol mixed in benzene for the same mixture volumes as before. The results are represented in Figs. 3.28 & 3.29, & 3.32 & 3.33. For further conformation of the sensor response with the surrounding medium, Cyclohexane mixed in Benzene has also been selected in study. The corresponding results are depicted in Figs. 3.36 & 3.37.

In the final calibration of the sensor response in terms of output power in dBm with respect to the refractive index of the surrounding liquid mixture, the results of all the four mixtures i.e. Methanol and Benzene, Propanol and Benzene, Butanol and Benzene and Cyclohexane and Benzene are considered and the data is tabulated in the Table 3.17. The relevant unified data also has been tabulated in the Table 3.18. Finally with the help of the unified data corresponding to refractive index of the liquid and the power output, a calibrated graph is drawn between refractive index recorded with the help of Abbe's refractometer (Plate 3.3) and the output power of the sensor (Fig. 3.40). A standard relation has been formulated between the refractive index and the output power of the sensor, which has been mentioned along with the graph (Fig. 3.40). Thus the sensor is calibrated using Abbe's refractometer for the refractive index study of liquids of a dynamic range from 1.32 to 1.50 at room temperature of 30°C.

The RI variation occurs within the height of the penetration depth of the evanescent field of the guided wave. As the volume of the benzene increases in the mixture, the RI of the liquid medium surrounding the glass rod also increases. When the sensor is surrounded by air (RI = 1), most of the light is confined to the medium (RI = 1.50)

International Journal of Engineering Research & Technology (IJERT)
ISSN: 2278-0181

Plate: 3.3 Abbe's Refractometer

within the sensor. The intensity of light collected at the other end is observed to be a maximum. When the sensor is dipped in media of higher refractive indices than that of air, light is no longer confined to the sensor, but some part of it starts escaping into the surrounding medium. This leads to a decrease in the optical power sensed at the receiver end. The glass sensor proposed is immune to chemical reaction and as such will be of immense use where there is a need for an instant check of RI of liquids.

Show in this experiment the glass rod used is sensitive to index of refraction changes within the range of 1.32 to 1.49. The observed sensitivity in refractive index change, according to the findings of susano et al and kumar et al is in agreement. The technique reported in this work for example, not a direct measurement of refractive index, as is in the Brewster's angle or the conventional methods which use critical angle. In this method the accuracy is entirely dependent on the reported values in index of refraction

In fact the U-shaped thin glass rod considered here would be far more, sturdy than either the cladded or the uncladded U-shaped optical fiber. For a given length of the glass rod, the evanescent field absorption depends on the evanescent field penetration depth in the sensing region, and on the number of reflections of ray per unit length of the glass rod. The depth of penetration is given by,

$$d_p = \frac{\lambda}{2\pi n_1(\sin^2\theta - \sin^2\theta_c)^{1/2}} \quad (1)$$

where λ is the wavelength of the free space for the launched light into the fiber, n1 is the index refraction of the core, $\theta_c = [\sin^{-1}(n_2/n_1)]$ is the sensing region critical angle with respect to the normal on cladding core interface, n_2 is the index of refraction of the absorbing cladding (fluid), and θ is the angle of the ray with the normal to the cladding core interface. As θ approaches θ_c, the depth of penetration increases, which results in the increase in the sensitivity of the sensor and hence the evanescent absorption. In general practice, $n_2 \langle n_{cl}, n_{cl}$ is the index of refraction of the cladding (plastic) and, hence the sensing region numerical aperture is higher than that of the optical fiber. The critical angle of the fiber in other words is higher than that of the region of sensing. Thus, θ of

propagated ray in the fiber will not approach θ_c of the region of sensing when the region of sensing is uniform and straight in the diameter.

Hence, in the sensing region, one can not achieve any significant penetration of the evanescent field in the region of sensing, and as such the sensors sensitivity is limited. It has been suggested, for the increase in sensitivity, the tapering of the region of sensing and the use of selective launching of the ray in the fiber. By launching only those rays which make close angles to the critical angle of the region of sensing, the sensitivity is increased in the selective launching. The angle of a ray approaches the critical angle, if it propagates in the case of a tapered fiber. When the sensing part of the fiber is bent, the angle of the light ray can also be brought very close to the critical angle of the region of sensing. The fiber optic refractive index sensors based on this with a U – shaped probe have been reported in the literature.

In the present work, a detailed experimental study has been carried out on the optical fiber evanescent wave absorption sensor selecting a U – shaped sensing region. With different concentrations of the solvent and refractive indices, the sensors performance has been studied. Theoretically it has been shown that the sensors sensitivity increases with the increase in refractive index of the liquid and also with decreasing the bending radius of the sensor probe. To compare the results of the experiment and to evaluate the sensors characteristics a two dimensional treatment with a geometrical approach can be adopted.

The light output passing through a silica glass rod is observed is the sensitive indicator of the refractive index of the liquid, in which the glass rod is immersed in liquid, or mixture of liquids. From the slope of the sensor, the refractive index change to the output signal has been investigated. We conclude that these sensing elements are easy to handle and fabricate, or to the refractive index change highly sensitive (3^{rd} decimal place in precision), the measurement can be done with a small liquid volume, sensitive to a wide range of refractive index values (1.32 – 1.49), and at the refractive index being measured are sensitive to light absorption, as a result of these investigations.

When the bulk refractometers are inconvenient, these features make them very useful in some applications.

3.6 Effect of temperature on refractive index

Study of refractive index of organic liquids or mixture of liquids is important to scientists, chemists and pharmacists. Though several methods are proposed in literature, we present a simple and reliable mechanism for the determination of refractive index of liquids or binary mixture of liquids at various temperatures using a simple glass rod bent in the form of U-shape. It was demonstrated that optical signals could be transmitted along the glass with extremely low losses.

Optical fiber sensors experienced a development with the advances in telecom technology and found applications in the sensing region. When organic liquids are heated above certain temperature, they may be explosive. The conventional refractive index detectors for such organic liquids in volatile conditions is little dangerous and should be handled carefully. One such answer in such a situation is the use of silica glass optical fibers or silica glass rods surrounding the optical fiber to sense the power passing through the fiber. The present work deals exclusively with using a silica glass rod for sensing mechanism at different temperatures.

Many of the chemical properties of liquids are attributed to the refractive index and density of liquids. Several methods for the determination of refractive index of liquids are mentioned in literature. In the present work we propose a simple, reliable, light weight, portable and cheap glass rod based sensor for the study of refractive index of liquids or binary mixtures of liquids at various temperatures.

3.6.1 Experimental arrangement

The experimental arrangement for the study of refractive index of liquids at various temperatures is shown in Fig. 3.5, and is similar to the earlier arrangements reported. The method involves in selecting a good silica glass rod bent in the form a rod of a U – shape. The length of the U-shaped rod is of 5cm and the diameter of the glass rod is 0.5mm. The two ends of the U-shaped rod are connected to a PCS fiber and glued at the

joints by using glass to glass adhesive and covered with m-seal. A laser source of 633 nm is connected with the one end of the PCS fiber, and the other end of the U-shaped rod is connected to a power meter through another PCS fiber.

Sample dimensions:

Shape of the glass sensor: U-shaped solid rod

Thickness (dia) of the glass rod: 0.5 mm

Height of the (prongs) glass rod immersed in the liquid: 2 cm

Width between the two prongs of the U-shaped glass rod: 0.8 cm

Depth of the curvature: 4.0 mm, Radius of the curvature: 4.0 mm

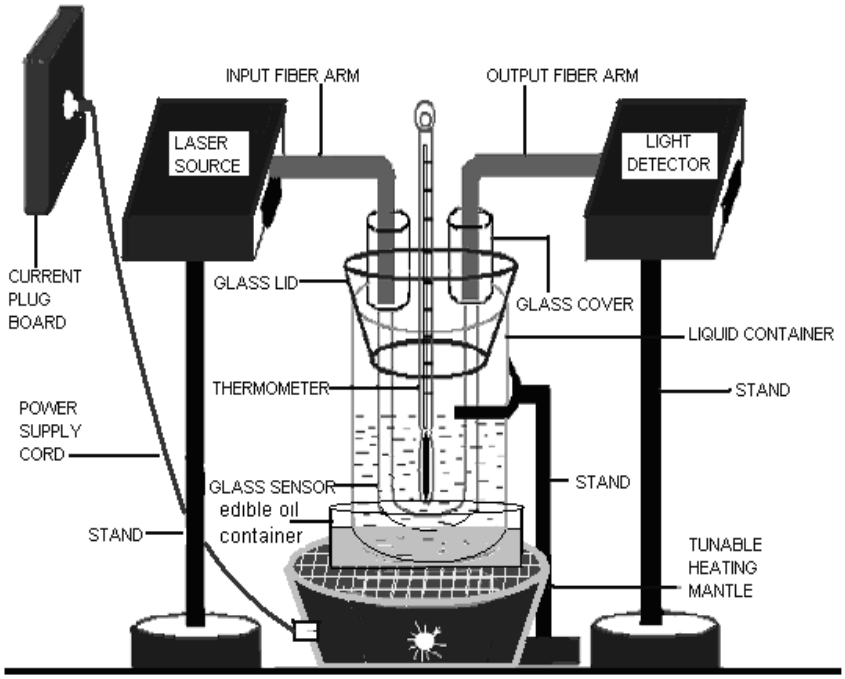

Fig. 3.5: Experimental arrangement and design of glass temperature sensor.

The U-shaped glass rod is then immersed into a beaker containing a mixture of benzene and methanol. The temperature of the glass beaker containing the mixture is then heated using an electric heating mantle by indirect heating method using edible oil. The purpose of using edible oil is to avoid the breakage of the liquid mixture container during direct heating. The boiling point (more than 350°C) and the other competent features of the edible oil best suited to raise the temperature in the beaker containing the liquid mixture.

A thermometer of a dynamic range of 20°C – 100°C is made stand in the liquid, immersing the mercury bulb into the liquid, which is used to record the temperature during the experimentation. Electrical power connections are taken for the heating mantle, laser source, and the power meter which are being active components in the sensor system. A glass lid is used to cover the liquid mixture exposing from the outside environment and a black tape is also used to prevent the stray light entering into the liquid mixture. The arrangement so assembled is now ready for the experimentation and to note down the readings.

3.6.2 Experimental Procedure

Every time the different liquid mixtures (Methanol mixed in Benzene, Propanol mixed in Benzene, Buatanol mixed in Benazene, and Cyclohexane in Benzene) are heated bellow their boiling points mentioned in the Table 3.1. Initially the beaker contains 10ml of methanol at room temperature. Keeping the total volume of the liquid as 10ml, 1 ml of methanol is removed from the beaker and 1ml benzene is added and thoroughly mixed. Thus the mixtures of different proportions are prepared from every binary combination and taken each of them in a separate glass container.

Now the arrangement of sensor element is immersed into the container containing the particular proportion of mixture of Methanol and Benzene. The power source is switched on and the power output is recorded at the room temperature. The temperature of the beaker containing benzene and methanol is slowly heated upto55°C and at each temperature the power output is recorded. At the same temperature the refractive index of liquid is determined by the Abbe's refractometer. Fig. 3.42 shows a variation in power output with the variation of the temperature of the binary mixture (benzene and methanol) of the liquid. Fig. 3.41 shows a relation between power output and the refractive index of the mixture of the liquids.

The experiment is further repeated using another binary mixture of the liquid namely propyle alcohol in benzene and the relevant graphs are shown in Figs. 3.43 and 3.44. To establish the trend, another two binary mixtures namely butanol mixed in benzene and

cyclohexane mixed in benzene, the experiment is further repeated at various temperatures and the results are plotted in Figs. 3.45, 3.46, 3.47, and 3.48. The consolidated data of all the four mixtures at room temperature (Methanol mixed in Benzene, Propanol mixed in Benzene, Butanol mixed in Benzene, and Cyclohexane mixed in Benzene) is tabulated in Table 3.27. The unified data of the same is also shown in Table 3.28.

A relation is established between the refractive index of the liquid mixtures surrounding the sensor and the corresponding power that is reached at the output power meter. This has been represented graphically by plotting a graph (Fig. 3.49) between refractive index and the output power of the sensor along with the equation that relates the refractive index and the power output. Thus the sensor is calibrated to determine the refractive index of any liquid mixture in terms of output power in the dynamic range of refractive index from 1.33 to 1.50 and within the temperature range of 30°C to 60°C. Thus by finding the output power values at different temperatures the corresponding refractive index values can be determined from the equation or with the help of the calibrated graph (Fig. 3.49).

From the above data, one can calculate the refractive index of any liquid or mixture of liquids at any given temperature. Figs 3.54, 3.55, 3.56, 3.57 indicate the variation of the refractive index of the liquids with the variation of the temperature of the liquid mixture. Fig. 3.49 gives the calibrated graph between refractive index versus power output for a range of temperatures of 30°C to 60°C at room temperature.

Thus by knowing the temperature of the liquid one can estimate the refractive index of the liquid at that temperature. The variation of the three parameters of the sensor i.e. temperature, output power and refractive index have been shown simultaneously in a single three dimensional graphs for the four mixtures selected (Methanol mixed in Benzene, Propanol mixed in Benzene, Butanol mixed in Benzene, and Cyclohexane mixed in Benzene) in Figs. 3.50,3.51,3.52, and 3.53 respectively. The calibrated graphs obtained at 35°C, 40°C, 45°C, 50°C, 55°C, and 60°C are represented in Figs. 3.62, 3.63,

3.64, 3.65, 3.66, and 3.67. The corresponding three dimensional graphs are also show in Figs. 3.58, 3.59, 3.60, 3.61 for all four binary mixtures.

Conclusions: The method presented is a simple glass based fiber optic sensor to determine the refractive index of liquids or mixtures of the liquids at any temperature. The present method is limited to a study of refractive index of liquids in the temperature range from room temperature to 60°C. The method can be extended to any temperature within the boiling point and volatile point of the liquid. The method proposed can be further extended for the study of online determination of refractive index of liquids, solvents at any temperature. Such an arrangement will be of immense use in chemical industries, pharmaceutical industries, and fragrant industry, food technology and processing where conventional methods fail to register the refractive index of liquids at higher temperatures.

Table 3.1: Properties of the Chemicals used in the experimentation

Name of the chemical	Color	Solubility	Refractive index (R.I.)	Molecular weight (g/mole)	Boiling point (^{0}C)	Density (ρ)g/ml
Benzene (C_6H_6)	colorless liquid		1.5011	78.11	80.1	0.8737
Methanol (CH_3OH)	colorless liquid	soluble in benzene	1.330	32.04	64.7	0.7866
Propanol (C_3H_8O)	colorless liquid	soluble in benzene	1.3850	60.10	82.3	0.7810
Butanol ($CH_3(CH_2)_3OH$)	colorless liquid	soluble in benzene	1.3993	74.12	117.7	0.8057
Cyclo-hexane (C_6H_{12})	colorless liquid	soluble in benzene	1.4266	84.16	80.7	0.7739

Benzene and Methanol study using U-shaped glass rod:

Shape of the glass sensor: U-shaped solid rod

Thickness (dia) of the glass rod: 0.25 mm

Height of the (prongs) glass rod immersed in the liquid: 2 cm

Width between the two prongs of the U-shaped glass rod: 0.8 cm

Depth of the curvature: 4.0 mm, Radius of the curvature: 4.0 mm

Table 3.2: Average R. I. values of Benzene and Methanol mixtures at various proportions

Benzene (C_6H_6) (ml.)	Methanol (CH_3OH) (ml.)	R.I. Trail-I	R.I. Trail-II	R.I. Trail-III	Average (R.I.)	Rounded off (R.I.)
0	10	1.325	1.325	1.326	1.3250	1.325
1	9	1.336	1.338	1.339	1.3376	1.338
2	8	1.350	1.352	1.353	1.3516	1.352
3	7	1.369	1.368	1.370	1.3690	1.369
4	6	1.386	1.388	1.389	1.3876	1.388
5	5	1.402	1.402	1.407	1.4036	1.404
6	4	1.430	1.420	1.410	1.4200	1.420
7	3	1.436	1.437	1.435	1.4360	1.436
8	2	1.450	1.452	1.453	1.4516	1.452
9	1	1.470	1.470	1.471	1.4703	1.470
10	0	1.488	1.487	1.486	1.4870	1.487

Table 3.3: Variation of output power and mole fraction with respect to R.I. value benzene and methanol mixtures using 0.25 mm dia U shaped glass rod (Free space power output -48.0dBm)

SL. No.	C_6H_6 (ml)	CH_3OH (ml)	R. I. of Mixture (R.I.)	Power output (dBm)	Mole fraction of CH_3OH	d (R.I.)/R.I. of glass rod
1	0	10	1.325	-48.0	1.0000	0.116670
2	1	9	1.338	-49.0	0.8039	0.108000
3	2	8	1.352	-50.2	0.6457	0.098670
4	3	7	1.369	-51.8	0.5153	0.087330
5	4	6	1.388	-53.0	0.4060	0.074670
6	5	5	1.404	-54.8	0.3130	0.064000
7	6	4	1.420	-55.7	0.2330	0.053330
8	7	3	1.436	-57.6	0.1634	0.042670
9	8	2	1.452	-59.1	0.1026	0.032000
10	9	1	1.470	-60.6	0.0482	0.020000
11	10	0	1.487	-62.0	0.0000	0.008670

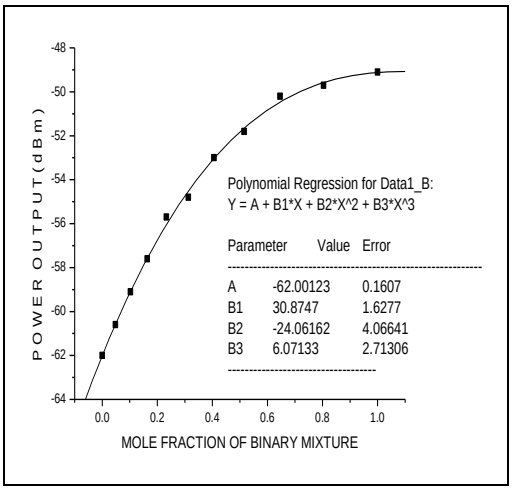

Fig.3.6: Relation bet. Mole fraction and Power For benzene and methanol using 0.25 mm dia U shaped glass rod

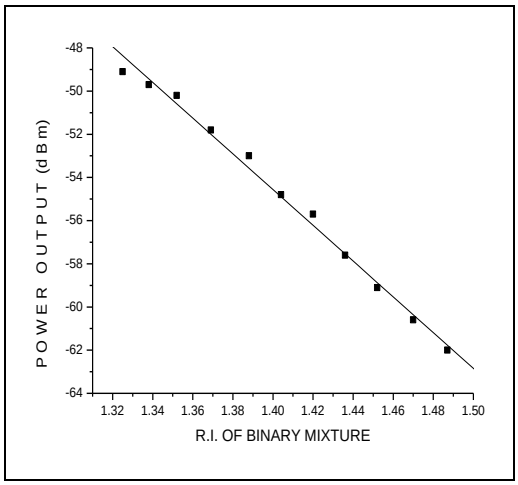

Fig. 3.7: Relation bet. R.I. and Power For benzene and methanol using 0.25 mm dia U shaped glass rod

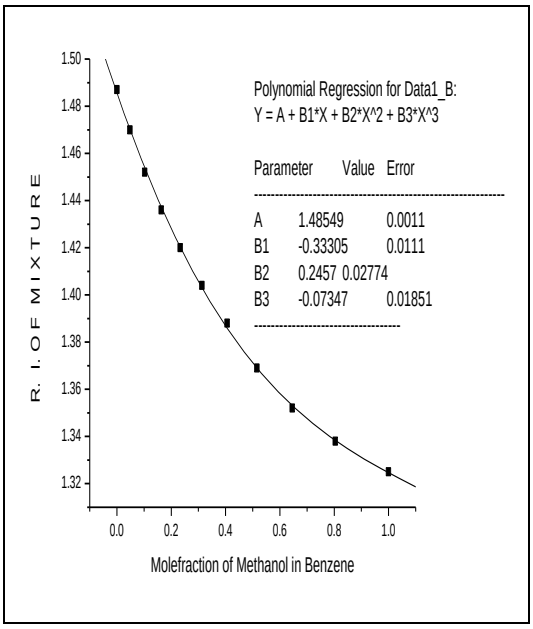

Fig.3.8: Relation between Mole fraction and R.I. for benzene and methanol using 0.25 mm dia U shaped glass rod

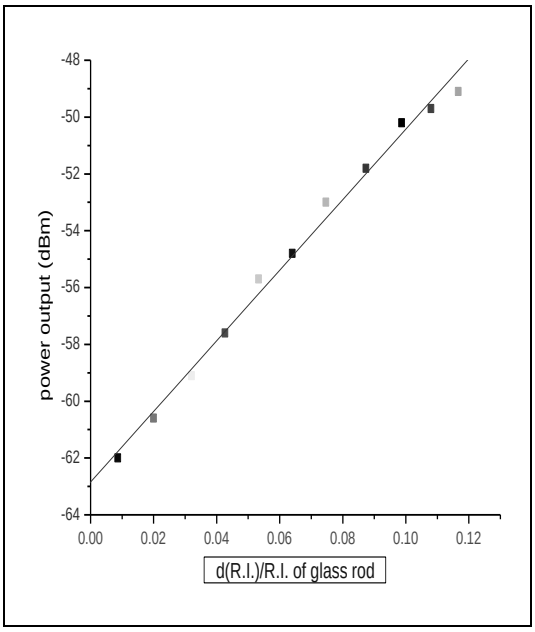

Fig.3.9: Relation between d (R.I.)/ R and Power for benzene and methanol using 0.25 mm dia U shaped glass rod

Benzene and Methanol study using coiled neck U-shaped glass rod:

Shape of the glass sensor: Coil-shaped solid rod

Thickness (dia) of the glass rod: 0.25 mm

Height of the (prongs) glass rod immersed in the liquid: 2 cm

Width between the two prongs of the U-shaped glass rod: 0.8 cm

Number of coils: 3**,** Coil dia: 0.5cm

Depth of the curvature: 4.0 mm, Radius of the curvature: 4.0 mm

Table 3.4: Change in output power with refractive index and mole fraction of benzene and methanol mixtures using coiled U shaped 0.25 dia mm rod (Free space power output -57.8dBm)

SL. No.	C_6H_6 (ml)	CH_3OH (ml)	R. I. of Mixture	Power output (dBm)	Mole fraction of CH_3OH
1	0	10	1.325	-64.0	1.0000
2	1	9	1.338	-64.5	0.8039
3	2	8	1.352	-65.0	0.6457
4	3	7	1.369	-65.6	0.5153
5	4	6	1.388	-66.6	0.4060
6	5	5	1.404	-67.4	0.3130
7	6	4	1.420	-68.3	0.2330
8	7	3	1.436	-69.2	0.1634
9	8	2	1.452	-70.1	0.1026
10	9	1	1.470	-70.7	0.0482
11	10	0	1.487	-71.3	0.0000

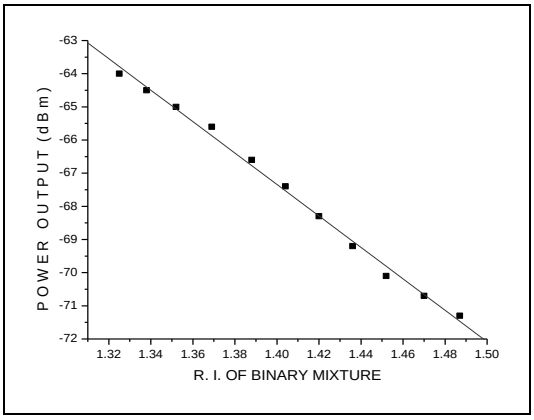

Fig.3.10: Relation between R.I. and Power for Benzene and methanol mixtures using Coiled U shaped 0.25 mm dia glass rod

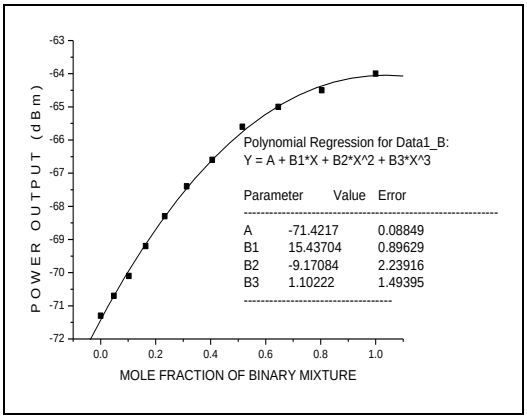

Fig.3.11: Relation between Mole fraction and Power for benzene and methanol mixtures using Coiled U shaped 0.25 mm dia rod

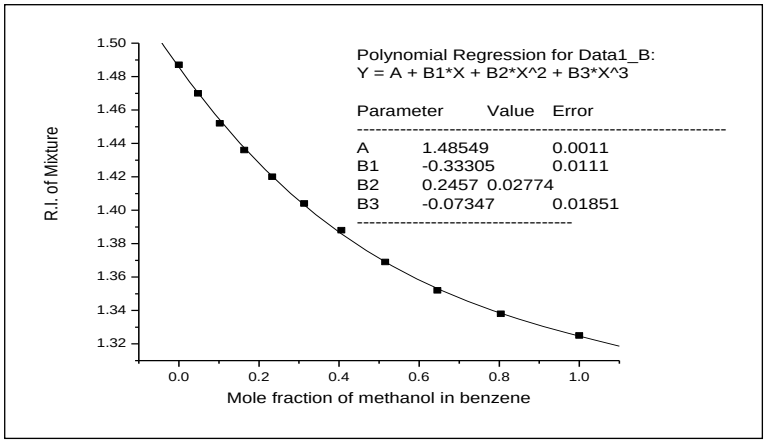

Fig. 3.12: Relation between Mole fraction of Methanol and R.I. of mixture using Coiled U shaped 0.25 dia mm glass rod

Benzene and Methanol study using saw tooth neck U-shaped glass rod:

Shape of the glass sensor: Saw tooth-shaped solid rod

Thickness (dia) of the glass rod: 0.25 mm

Height of the (prongs) glass rod immersed in the liquid: 2 cm

Width between the two prongs of the U-shaped glass rod: 0.8 cm

Number of Teeth: 2**,** Hight of the tooth: 2 mm

Depth of the curvature: 4.0 mm, Radius of the curvature: 4.0 mm

Table 3.5: variation in power with refractive index and mole fraction of benzene and methanol mixtures using saw toothed U shape 0.25 mm dia rod (Free space power output -50.0dBm)

SL. No.	C_6H_6 (ml)	CH_3OH (ml)	R. I. of Mixture	Power output (dBm)	Mole fraction of CH_3OH
1	0	10	1.325	N	1.0000
2	1	9	1.338	O	0.8039
3	2	8	1.352		0.6457
4	3	7	1.369	R	0.5153
5	4	6	1.388	E	0.4060
6	5	5	1.404	S	0.3130
7	6	4	1.420	P	0.2330
8	7	3	1.436	O	0.1634
9	8	2	1.452	N	0.1026
10	9	1	1.470	S	0.0482
11	10	0	1.487	E	0.0000

Benzene and Methanol study using V-shaped glass rod:

Shape of the glass sensor: V-shaped solid rod

Thickness (dia) of the glass rod: 0.25 mm

Height of the (prongs) glass rod immersed in the liquid: 2 cm

Width between the two prongs of the V-shaped glass rod: 0.8 cm

Depth of the curvature: 4.0 mm, Radius of the curvature: 4.0 mm

Table 3.6: Change in power with refractive index and mole fraction of benzene and methanol mixtures using V shaped 0.25 mm dia glass rod (Free space power output -65.0dBm)

SL. No.	C_6H_6 (ml)	CH_3OH (ml)	R. I. of Mixture	Power output (dBm)	Mole fraction of CH_3OH
1	0	10	1.325	-65.9	1.0000
2	1	9	1.338	-66.1	0.8039
3	2	8	1.352	-66.3	0.6457
4	3	7	1.369	-66.5	0.5153
5	4	6	1.388	-66.7	0.4060
6	5	5	1.404	-66.9	0.3130
7	6	4	1.420	-67.1	0.2330
8	7	3	1.436	-67.3	0.1634
9	8	2	1.452	-67.5	0.1026
10	9	1	1.470	-67.7	0.0482
11	10	0	1.487	-67.9	0.0000

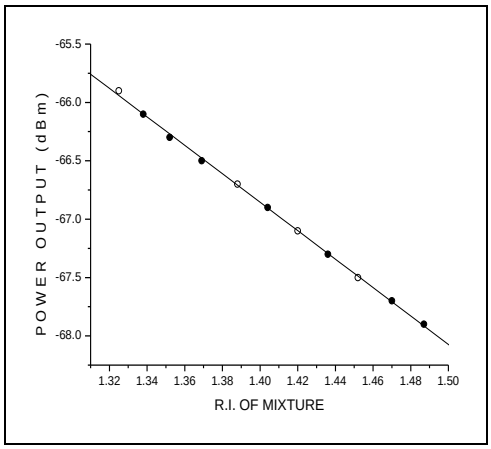

Fig.3.13: Relation between R.I. And Power output for Benzene and methanol mixtures using V shaped 0.25 mm dia glass rod

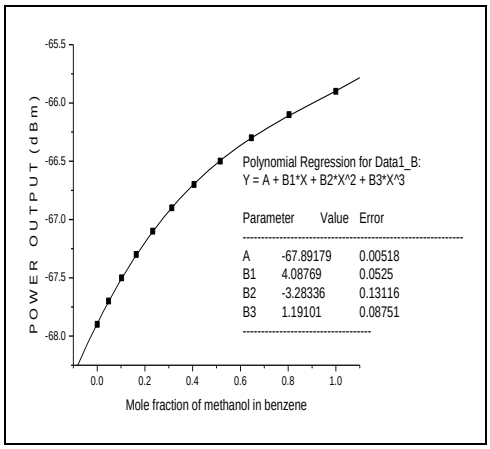

Fig.3.14: Relation between Mole fraction and Power for benzene and methanol mixtures using V shaped 0.25 mm dia glass rod

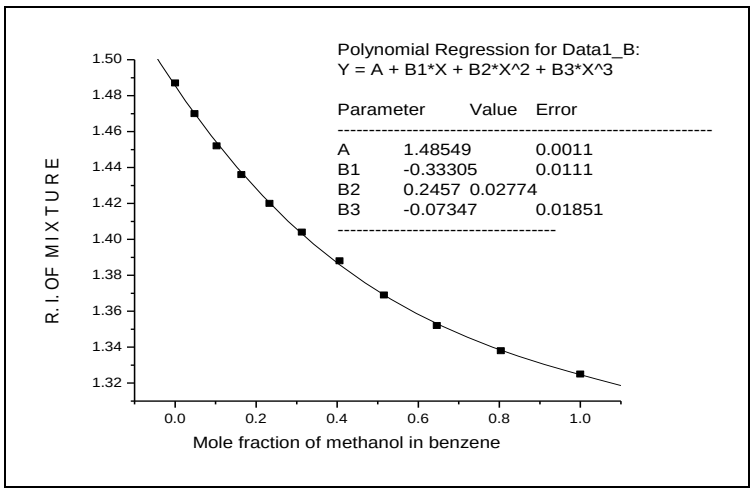

Fig. 3.15: Relation between Mole fraction and R.I. of benzene and Methanol mixtures using V shaped 0.25 mm dia glass rod

Benzene and Methanol study using straight neck U-shaped glass rod:

Shape of the glass sensor: Square-shaped solid rod

Thickness (dia) of the glass rod: 0.25 mm

Height of the (prongs) glass rod immersed in the liquid: 2 cm

Width between the two prongs of the U-shaped glass rod: 0.8 cm

Depth of the curvature: 4.0 mm, Radius of the curvature: 4.0 mm

Table 3.7: Change in power with refractive index and mole fraction of benzene and methanol mixtures using 0.25 mm dia straight neck U shaped rod (Free space power output -58.0dBm)

SL. No.	C_6H_6 (ml)	CH_3OH (ml)	R. I. of Mixture	Power output (dBm)	Mole fraction of CH_3OH
1	0	10	1.325	-61.2	1.0000
2	1	9	1.338	-62.0	0.8039
3	2	8	1.352	-63.1	0.6457
4	3	7	1.369	-64.0	0.5153
5	4	6	1.388	-64.8	0.4060
6	5	5	1.404	-65.5	0.3130
7	6	4	1.420	-66.3	0.2330
8	7	3	1.436	-67.2	0.1634
9	8	2	1.452	-67.9	0.1026
10	9	1	1.470	-68.7	0.0482
11	10	0	1.487	-69.4	0.0000

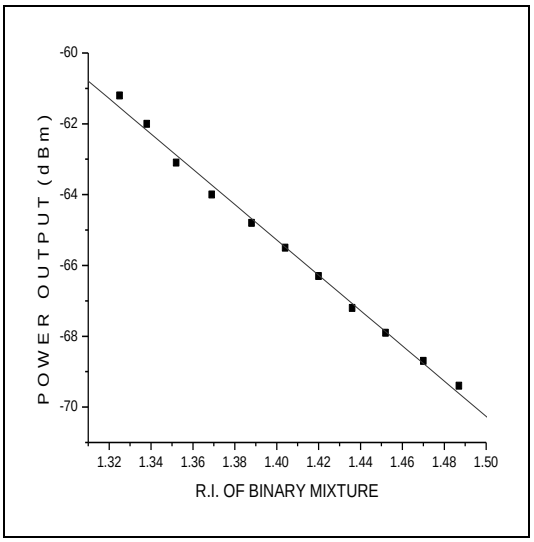

Fig. 3.16: Relation between R.I. and Power Output for benzene and methanol Mixtures using 0.25 mm Dia straight neck U shaped glass rod

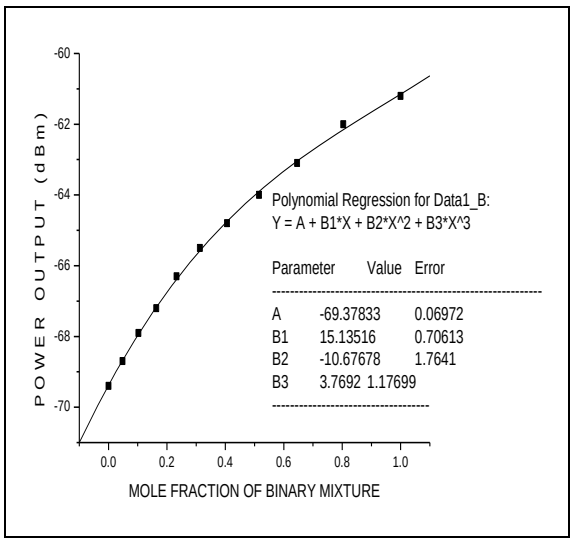

Fig.3.17: Relation between Mole fraction and Power for benzene and methanol mixtures using 0.25 mm dia straight neck U shaped rod

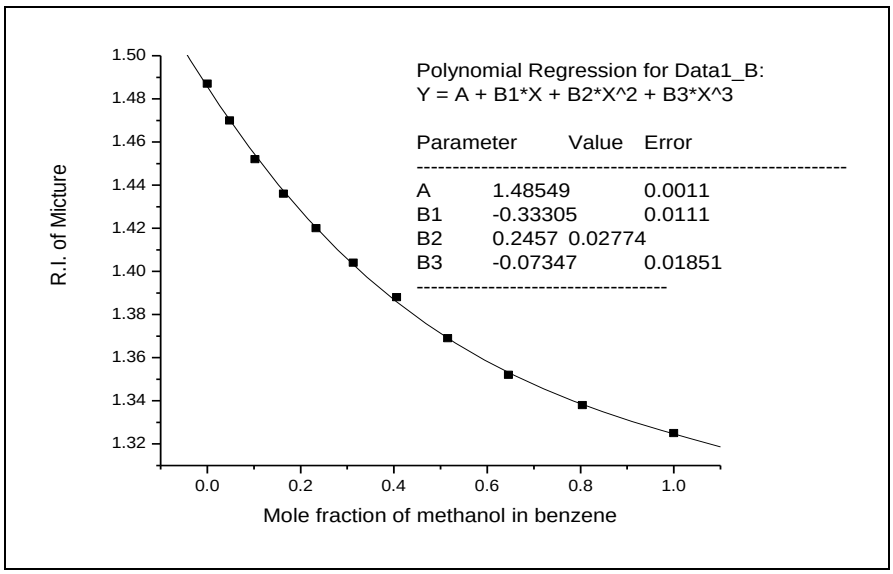

Fig. 3.18: Relation between Mole fraction and R.I. of benzene and methanol Mixtures using 0.25 mm dia straight neck U shaped glass rod

Benzene and Methanol study using shrinked neck U-shaped glass rod:

Shape of the glass sensor: Necked U-shaped solid rod

Thickness (dia) of the glass rod: 0.25 mm

Height of the (prongs) glass rod immersed in the liquid: 2 cm

Width between the two prongs of the U-shaped glass rod: 0.8 cm

Diameter of the necked region: 0.2mm

Length of the necked region: 0.4cm

Depth of the curvature: 4.0 mm, Radius of the curvature: 4.0 mm

Table 3.8: Change in power with refractive index and mole fraction of benzene and methanol mixtures using 0.25 mm dia shrinked neck U shaped rod (Free space power output -68.0dBm)

SL. No.	C_6H_6 (ml)	CH_3OH (ml)	R. I. of Mixture	Power output (dBm)	Mole fraction of CH_3OH
1	0	10	1.325	-69.3	1.0000
2	1	9	1.338	-69.4	0.8039
3	2	8	1.352	-69.5	0.6457
4	3	7	1.369	-69.6	0.5153
5	4	6	1.388	-69.7	0.4060
6	5	5	1.404	-69.8	0.3130
7	6	4	1.420	-69.9	0.2330
8	7	3	1.436	-70.0	0.1634
9	8	2	1.452	-70.1	0.1026
10	9	1	1.470	-70.2	0.0482
11	10	0	1.487	-70.3	0.0000

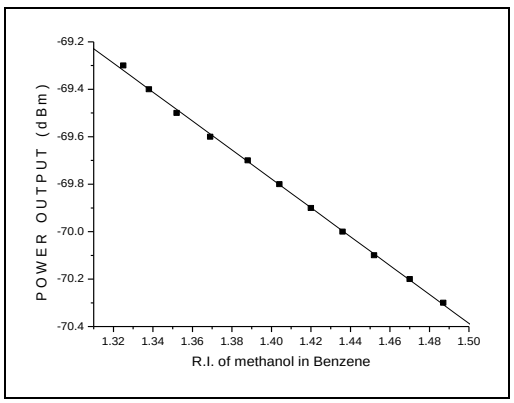

Fig. 3.19: Relation between R.I. and Power for Benzene and methanol mixtures using 0.25 mm dia shrinked neck U shaped glass rod

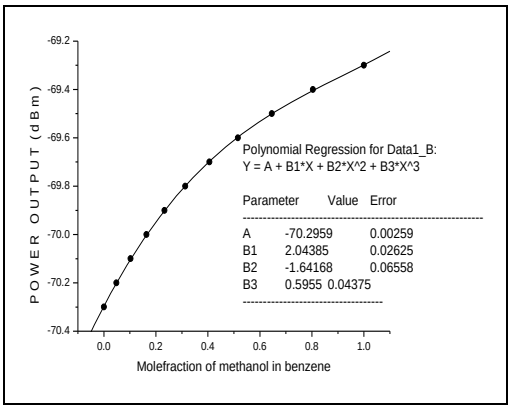

Fig. 3.20: Relation between Mole fraction and Power for benzene and methanol mixtures using0.25 mm dia shrinked Neck U shaped glass rod

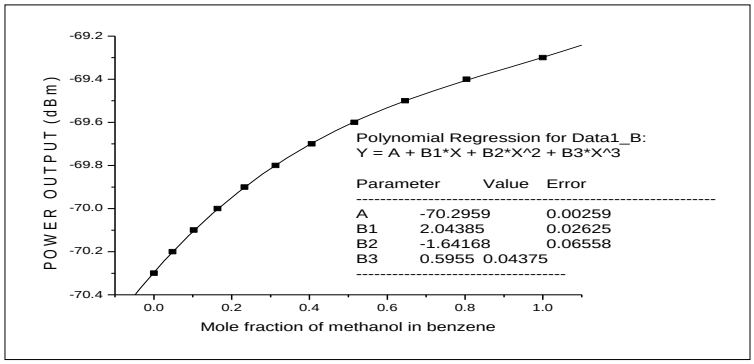

Fig.3.21: Relation between Mole fraction and R.I. of benzene and methanol Mixtures using 0.25 mm dia shrinked neck U shaped glass rod

Benzene and Methanol study using bulged neck U-shaped glass rod:

Shape of the glass sensor: Bulged U-shaped solid rod

Thickness (dia) of the glass rod: 0.25 mm

Height of the (prongs) glass rod immersed in the liquid: 2 cm

Width between the two prongs of the U-shaped glass rod: 0.8 cm

Diameter of the bulged region: 1.0 mm

Length of the bulged region: 0.4 cm

Depth of the curvature: 4.0 mm, Radius of the curvature: 4.0 mm

Table 3.9: Change in power with refractive index and mole fraction of benzene and methanol mixtures using bulged neck U shaped 0.25 mm dia rod (Free space power output -60.0dBm)

SL. No.	C_6H_6 (ml)	CH_3OH (ml)	R. I. of Mixture	Power output (dBm)	Mole fraction of CH_3OH
1	0	10	1.325	-64.0	1.0000
2	1	9	1.338	-64.1	0.8039
3	2	8	1.352	-64.2	0.6457
4	3	7	1.369	-64.3	0.5153
5	4	6	1.388	-64.4	0.4060
6	5	5	1.404	-64.5	0.3130
7	6	4	1.420	-64.6	0.2330
8	7	3	1.436	-64.7	0.1634
9	8	2	1.452	-64.8	0.1026
10	9	1	1.470	-64.9	0.0482
11	10	0	1.487	-65.0	0.0000

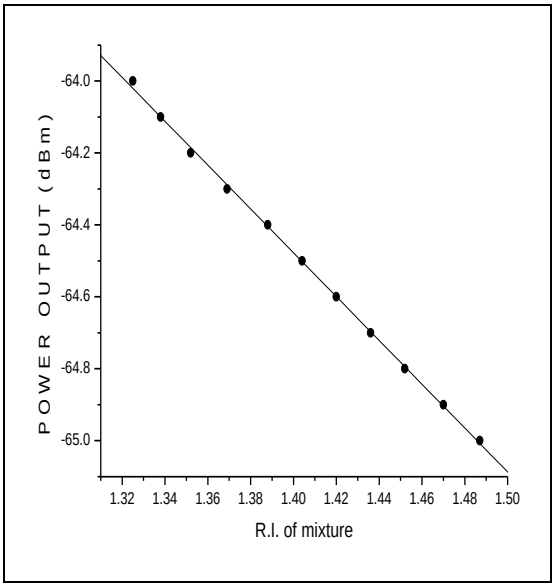

Fig.3.22: Relation between R.I. Power of benzene and methanol mixtures using bulged neck U shaped 0.25 mm dia glass rod

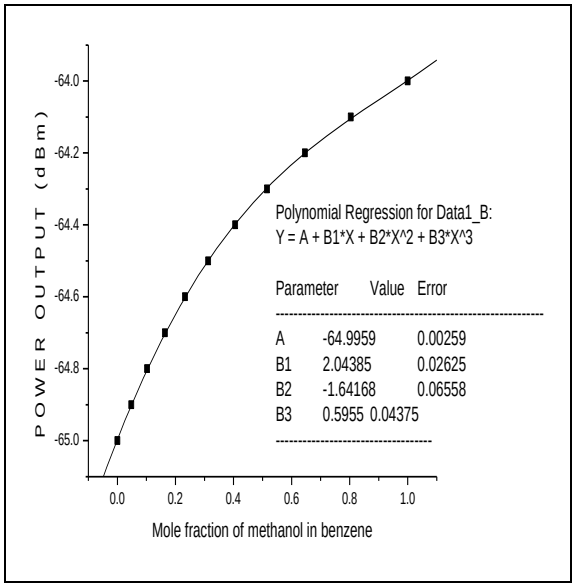

Fig.3.23: Relation between Mole fraction and Power of benzene and methanol mixtures using bulged neck U shaped 0.25 mm dia rod

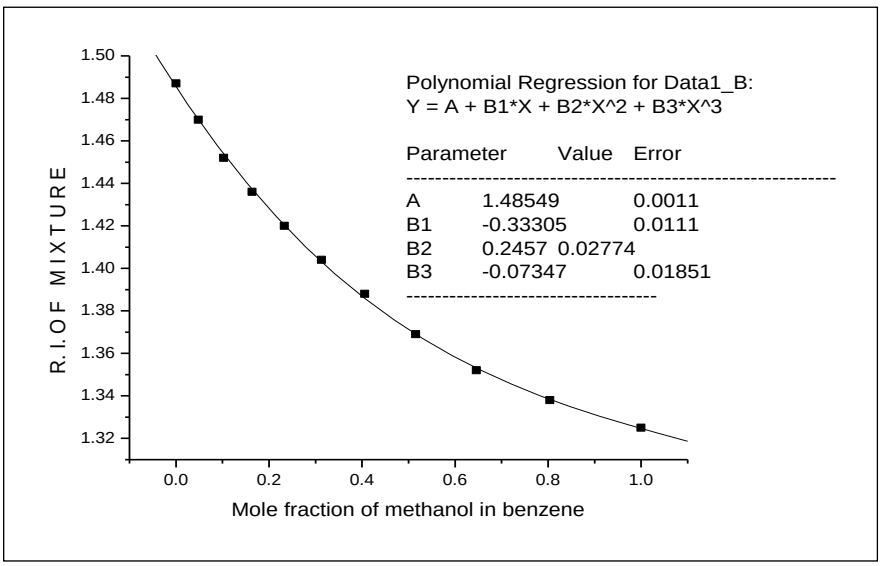

Fig. 3.24: Relation between Mole fraction and R.I. benzene and methanol Mixtures using bulged neck U shaped 0.25 mm dia glass rod

Benzene and Methanol study using large diameter U-shaped glass rod:

Shape of the glass sensor: U-shaped solid rod

Thickness (dia) of the glass rod: 0.5 mm

Height of the (prongs) glass rod immersed in the liquid: 2 cm

Width between the two prongs of the U-shaped glass rod: 0.8 cm

Depth of the curvature: 4.0 mm, Radius of the curvature: 4.0 mm

Table 3.10: Change in power with refractive index and mole fraction of benzene and methanol Mixtures using U shaped 0.5 mm dia glass rod (Free space power output -45.0dBm)

SL. No.	C_6H_6 (ml)	CH_3OH (ml)	R. I. of Mixture	Power output (dBm)	Mole fraction of CH_3OH
1	0	10	1.325	-46.4	1.0000
2	1	9	1.338	-47.0	0.8039
3	2	8	1.352	-47.4	0.6457
4	3	7	1.369	-47.8	0.5153
5	4	6	1.388	-48.2	0.4060
6	5	5	1.404	-48.7	0.3130
7	6	4	1.420	-49.0	0.2330
8	7	3	1.436	-49.4	0.1634
9	8	2	1.452	-49.7	0.1026
10	9	1	1.47	-50.2	0.0482
11	10	0	1.487	-50.5	0.0000

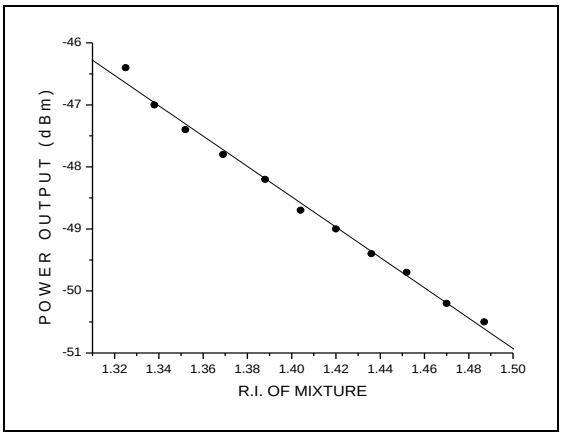

Fig. 3.25: Relation between R.I. and Power Of benzene and methanol mixtures Using U shaped 0.5 mm dia glass rod

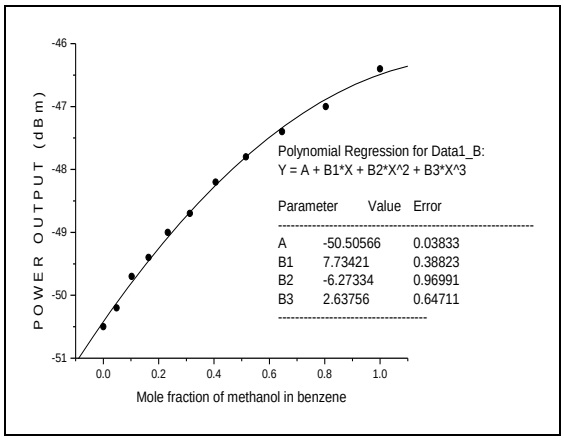

Fig. 3.26: Relation between Mole fraction and Power of benzene and methanol mixtures using U shaped 0.5 mm dia rod

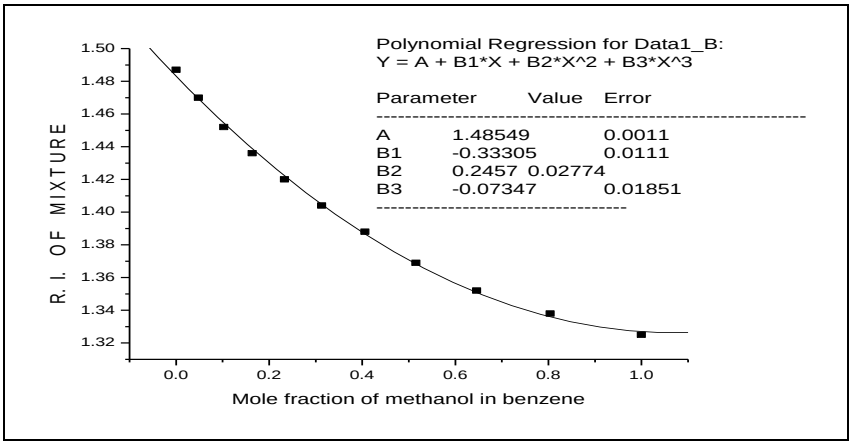

Fig. 3.27: Relation between Mole fraction and R.I. of benzene and Methanol mixtures using U shaped 0.5 mm dia glass rod

Benzene and propanol study:

Shape of the glass sensor: U-shaped solid rod

Thickness (dia) of the glass rod: 0.25 mm

Height of the (prongs) glass rod immersed in the liquid: 2 cm

Width between the two prongs of the U-shaped glass rod: 0.8 cm

Depth of the curvature: 4.0 mm, Radius of the curvature: 4.0 mm

Table 3.11: Average R. I. value of Benzene and Propanol mixtures of various proportions (Free space power output -45.0dBm)

Benzene (C_6H_6) (ml.)	Propanol (C_3H_8O) (ml.)	R.I. Trail-I	R.I. Trail-II	R.I. Trail-III	Average (R.I.)	Rounded off (R.I.)
0	10	1.369	1.368	1.370	1.3690	1.369
1	9	1.379	1.379	1.380	1.3793	1.379
2	8	1.391	1.392	1.391	1.3913	1.391
3	7	1.398	1.402	1.403	1.4010	1.401
4	6	1.413	1.412	1.413	1.4127	1.413
5	5	1.424	1.423	1.424	1.4237	1.424
6	4	1.438	1.436	1.435	1.4363	1.436
7	3	1.449	1.446	1.446	1.4470	1.447
8	2	1.459	1.461	1.461	1.4603	1.460
9	1	1.478	1.479	1.479	1.4786	1.479
10	0	1.489	1.489	1.488	1.4887	1.489

Table 3.12: Change output power with refractive index and mole fraction of Benzene and Propanol using 0.25 mm dia U shaped glass rod (Free space power output -48.0dBm)

C_6H_6 (ml)	C_3H_8O (ml)	R. I. of Mixture (R.I.)	Power output (dBm)	Mole fraction of C_3H_8O	d (R.I.)/R.I. of glass rod
0	10	1.369	-52.0	1.000	0.087333
1	9	1.379	-52.5	0.885	0.080667
2	8	1.391	-53.4	0.773	0.072667
3	7	1.401	-54.2	0.665	0.066000
4	6	1.413	-55.3	0.561	0.058000
5	5	1.424	-56.1	0.460	0.050667
6	4	1.436	-57.6	0.362	0.042667
7	3	1.447	-58.3	0.267	0.035333
8	2	1.460	-59.8	0.175	0.026667
9	1	1.479	-61.4	0.087	0.014000
10	0	1.489	-62.2	0.000	0.007333

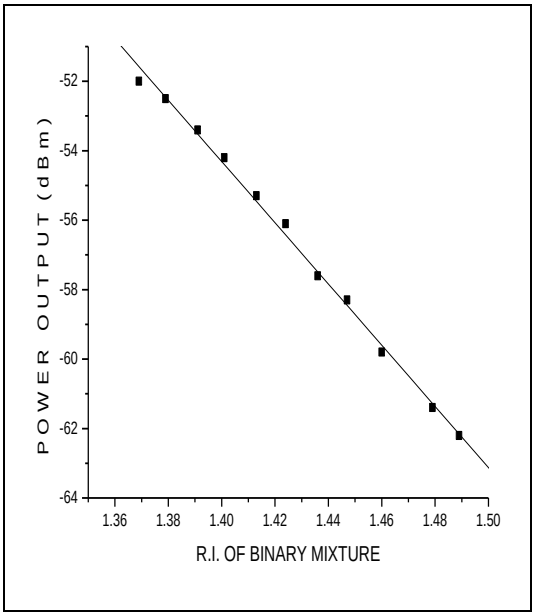

Fig.3.28: Relation between R.I. and Power of Benzene and Propanol using 0.25 mm dia U shaped glass rod

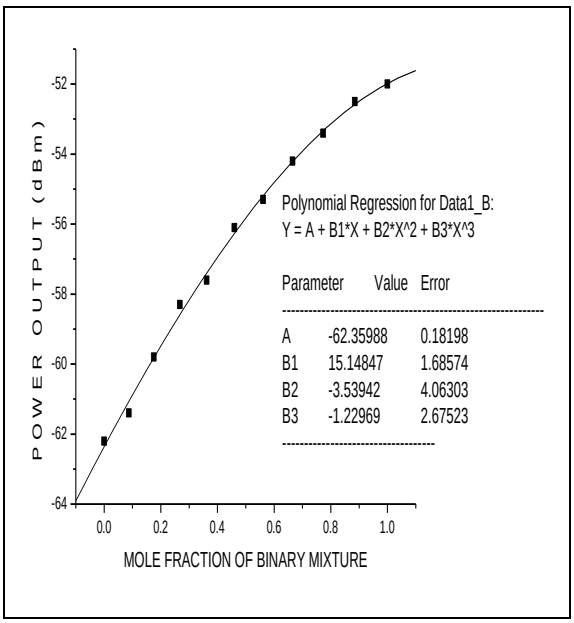

Fig.3.29: Relation between Mole fraction and Power of Benzene and Propanol using 0.25 mm dia U shaped glass rod

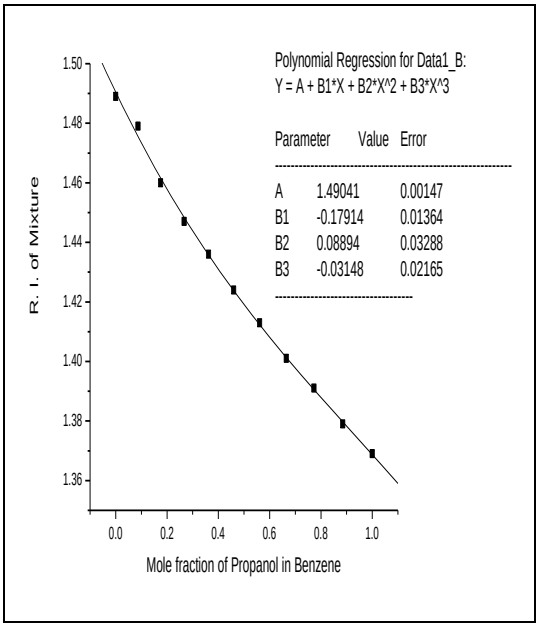

Fig.3.30: Relation between Mole fraction and R.I. Of Benzene and Propanol 0.25 mm dia U shaped glass rod

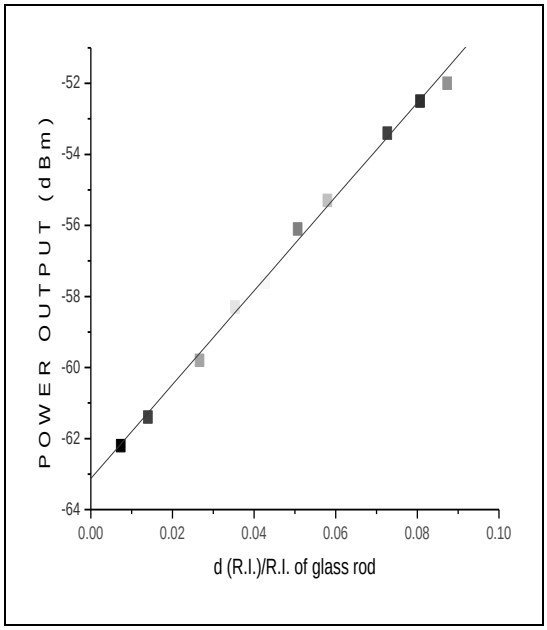

Fig.3.31: Relation between d (R.I.)/ R and Power of Benzene and Propanol using 0.25 mm dia U shaped glass rod

Benzene and Butanol study:

Shape of the glass sensor: U-shaped solid rod

Thickness (dia) of the glass rod: 0.25 mm

Height of the (prongs) glass rod immersed in the liquid: 2 cm

Width between the two prongs of the U-shaped glass rod: 0.8 cm

Depth of the curvature: 4.0 mm, Radius of the curvature: 4.0 mm

Table 3.13: Average value of Benzene and Butanol mixtures of various proportions

Benzene (C_6H_6) (ml.)	Butanol $CH_3(CH_2)_3OH$ (ml.)	R.I. Trail-I	R.I. Trail-II	R.I. Trail-III	Average (R.I.)	Rounded off (R.I.)
0	10	1.391	1.394	1.393	1.3927	1.393
1	9	1.403	1.402	1.402	1.4023	1.402
2	8	1.412	1.411	1.411	1.4113	1.411
3	7	1.418	1.420	1.421	1.4196	1.420
4	6	1.426	1.429	1.429	1.4280	1.428
5	5	1.442	1.438	1.441	1.4403	1.440
6	4	1.453	1.449	1.451	1.451	1.451
7	3	1.463	1.459	1.461	1.4610	1.461
8	2	1.472	1.473	1.473	1.4727	1.473
9	1	1.480	1.483	1.481	1.4813	1.481
10	0	1.491	1.491	1.492	1.4913	1.491

Table 3.14: Change in output power with refractive index and mole fraction for Benzene and Butanol mixtures using 0.25 mm dia U shaped glass rod (Free space power output -48.0dBm)

C_6H_6 (ml)	$CH_3(CH_2)_3OH$ (ml)	R. I. of Mixture (R.I.)	Power output (dBm)	Mole fraction of C_3H_8O	d (R.I.)/R.I. of glass rod
0	10	1.393	-53.5	1.000	0.071333
1	9	1.402	-54.3	0.902	0.065333
2	8	1.411	-55.2	0.804	0.059333
3	7	1.42	-55.7	0.705	0.053333
4	6	1.428	-56.4	0.605	0.048000
5	5	1.44	-57.9	0.506	0.040000
6	4	1.451	-59.0	0.406	0.032667
7	3	1.461	-59.9	0.305	0.026000
8	2	1.473	-60.9	0.204	0.018000
9	1	1.481	-61.7	0.102	0.012667
10	0	1.491	-62.5	0.000	0.006000

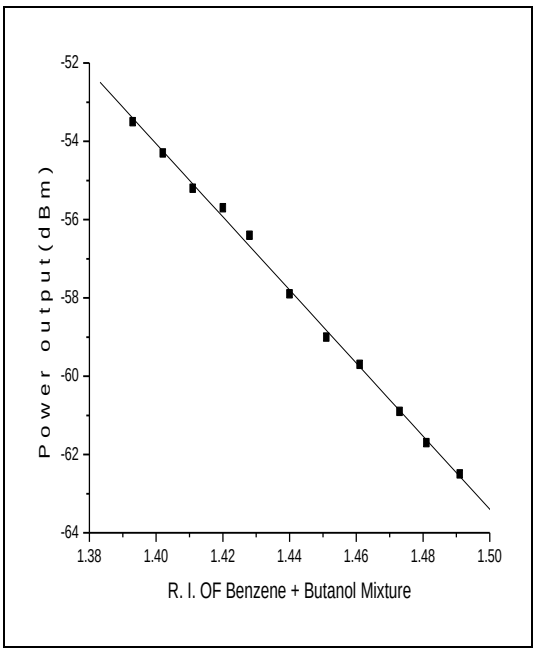

Fig.3.32: Relation between R.I. and Power For Benzene and Butanol mixtures Using 0.25 mm dia U shaped glass rod

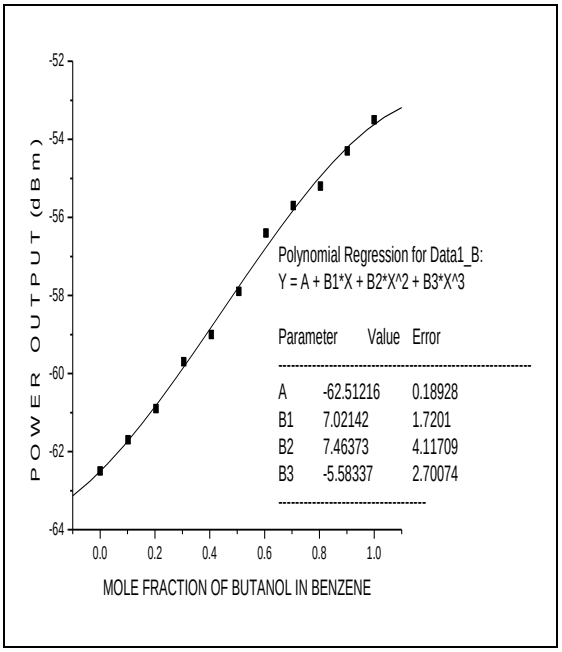

Fig.3.33: Relation between Mole fraction and Power for Benzene and Butanol mixtures using 0.25 mm dia U shaped glass rod

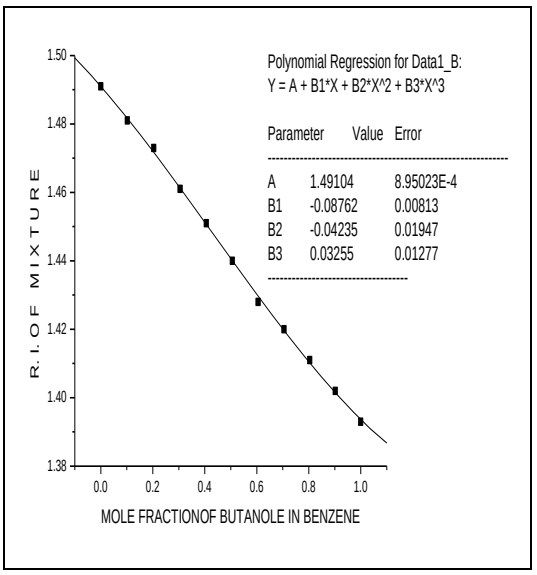

Fig.3.34: Relation between Mole fraction and R.I. For Benzene and Butanol mixtures Using 0.25 mm dia U shaped glass rod

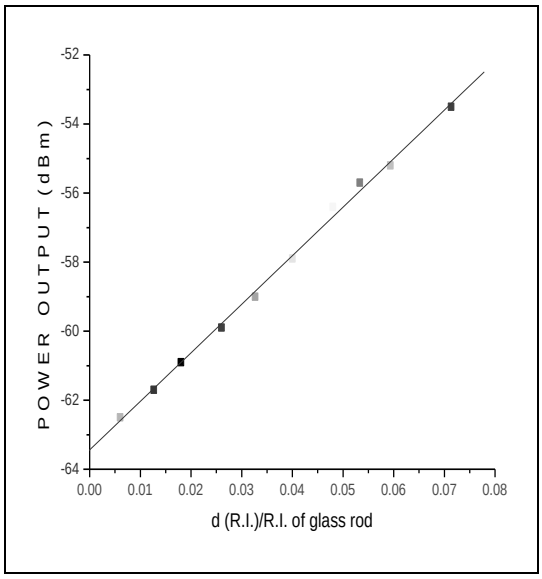

Fig.3.35: Relation between d (R.I.)/r and power for Benzene and Butanol mixtures using 0.25 mm dia U shaped glass rod

Benzene and Cyclohexane study

Shape of the glass sensor: U-shaped solid rod

Thickness (dia) of the glass rod: 0.25 mm

Height of the (prongs) glass rod immersed in the liquid: 2 cm

Width between the two prongs of the U-shaped glass rod: 0.8 cm

Depth of the curvature: 4.0 mm, Radius of the curvature: 4.0 mm

Table 3.15: Average R.I. value of Benzene and Cyclohexane mixtures of different proportions

(C_6H_6) ml.	(C_6H_{12}) ml.	R.I. Trail-I	R.I. Trail-II	R.I. Trail-III	Average (R.I.)	Rounded (R.I.)
0	10	1.422	1.418	1.419	1.4196	1.420
1	9	1.424	1.427	1.427	1.4260	1.426
2	8	1.435	1.432	1.433	1.4333	1.433
3	7	1.440	1.441	1.438	1.4396	1.440
4	6	1.446	1.448	1.446	1.4466	1.447
5	5	1.455	1.454	1.454	1.4543	1.454
6	4	1.463	1.460	1.459	1.4606	1.461
7	3	1.471	1.470	1.470	1.4703	1.470
8	2	1.476	1.478	1.478	1.4773	1.477
9	1	1.484	1.488	1.486	1.4860	1.486
10	0	1.496	1.494	1.496	1.4953	1.495

Table 3.16: Change in power with refractive index and mole fraction of Benzene and Cyclohexane mixtures using 0.25 mm dia U shaped rod (Free space power output -48.0dBm)

C_6H_6 (ml)	C_6H_{12} (ml)	R. I. of Mixture (R.I.)	Power output (dBm)	Mole fraction of C_3H_8O	d (R.I.)/R.I. of glass rod
0	10	1.420	-55.7	1.0000	0.053333
1	9	1.426	-56.2	0.9159	0.049333
2	8	1.433	-57.3	0.8288	0.044667
3	7	1.440	-57.9	0.7385	0.040000
4	6	1.447	-58.3	0.6448	0.035333
5	5	1.454	-59.4	0.5475	0.030667
6	4	1.461	-59.9	0.4465	0.026000
7	3	1.470	-60.6	0.3415	0.020000
8	2	1.477	-61.1	0.2322	0.015333
9	1	1.486	-61.9	0.1185	0.009333
10	0	1.495	-62.8	0.0000	0.003333

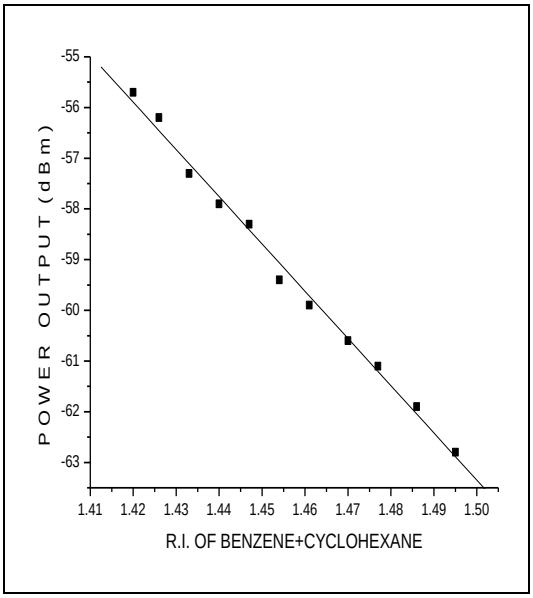

Fig.3.36: Relation between R.I. and Power Of Benzene and Cyclohexane mixtures Using 0.25 mm dia U shaped glass rod

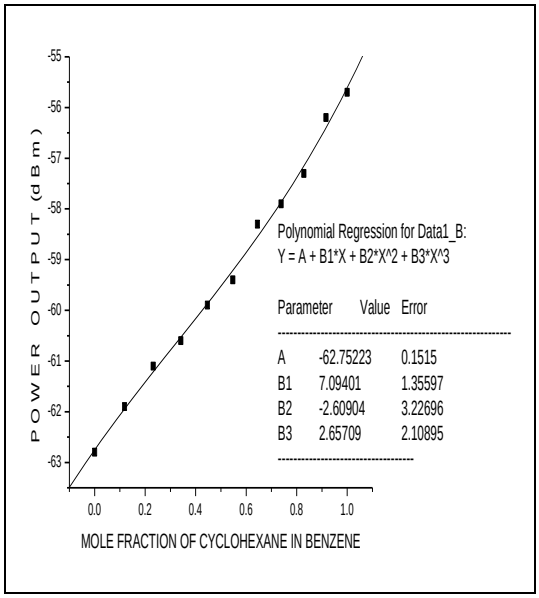

Fig. 3.37: Relation between Mole fraction and Power of Benzene and Cyclohexane mixtures using 0.25 mm dia U shaped rod

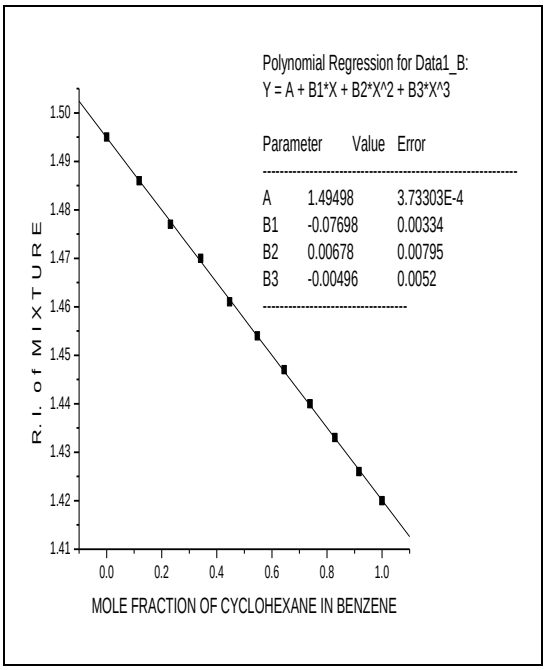

Fig.3.38: Relation between Mole fraction and R.I. Of Benzene and Cyclohexane mixtures Using 0.25 mm dia U shaped glass rod

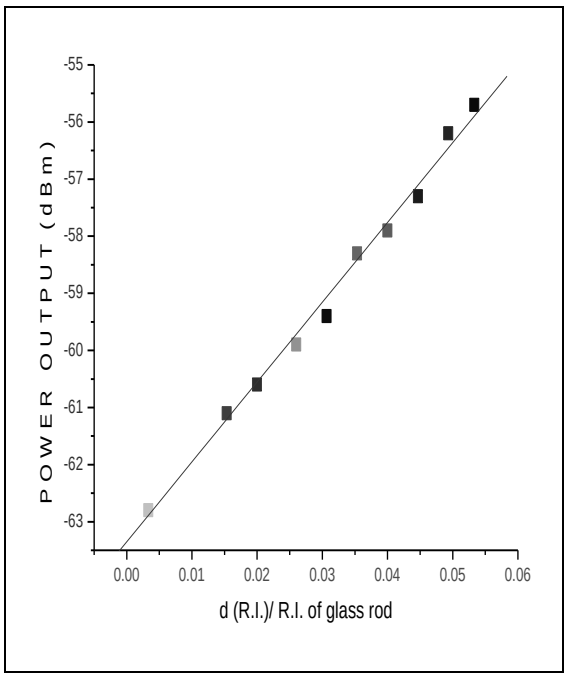

Fig.3.39: Relation between d (R.I.)/ R and Power of Benzene and Cyclohexane using 0.25 mm dia U shaped glass rod

Table 3.17: Consolidated refractive index and power output data with all the mixtures (benzene+methanol, benzene+butanol, benzene+propanol, benzene+cyclohexane) using 0.25 mm U shaped glass rod(Free space power output -45.0dBm)

Refractive index				Power output			
Benzene + Methanol (R.I.)	Benzene + Propanol (R.I.)	Benzene + Butanol (R.I.)	Benzene + Cyclohex (R.I.)	Benzene + Methanol (dBm)	Benzene + Propanol (dBm)	Benzene + Butanol (dBm)	Benzene + Cyclohexa (dBm)
1.325				-48.0			
1.338				-49.0			
1.352				-50.2			
1.369	1.369			-51.8	-52.0		
	1.379				-52.5		
1.388				-53.0			
	1.391				-53.4		
		1.393				-53.5	
	1.401				-54.2		
		1.402				-54.3	
1.404				-54.8			
		1.411				-55.2	
	1.413				-55.3		
1.420		1.420	1.420	-55.7		-55.7	-55.7
	1.424				-56.1		
			1.426				-56.2
		1.428				-56.4	
			1.433				-57.3
1.436	1.436			-57.6	-57.6		
		1.440	1.440			-57.9	-57.9
	1.447		1.447		-58.3		-58.3
		1.451				-59.0	
1.452				-59.1			
			1.454				-59.4
	1.460				-59.8		
		1.461	1.461			-59.9	-59.9
1.470			1.470	-60.6			-60.6
		1.473				-60.9	
			1.477				-61.1
	1.479				-61.4		
		1.481				-61.7	
			1.486				-61.9
1.487				-62.0			
	1.489				-62.2		
		1.491				-62.5	
			1.495				-62.8

Table 3.18: Unified R.I. and power data with all the mixtures (benzene+methanol, benzene+butanol, benzene+propanol, benzene+cyclohexane) using 0.25 mm U shaped glass rod (Free space power output -45.0dBm)

SL. No.	Refractive index of the four Mixtures together (Benzene+Methanol, Benzene+Propanol, Benzene+Butanol, Benzen+Cyclohexane) (R.I.)	Power output of the four Mixtures together (Benzene+Methanol, Benzene+Propanol, Benzene+Butanol, Benzen+Cyclohexane) (dBm)
1	1.325	-48.0
2	1.338	-49.0
3	1.352	-50.2
4	1.369	-51.8
5	1.379	-52.5
6	1.388	-53.0
7	1.391	-53.4
8	1.393	-53.5
9	1.401	-54.2
10	1.402	-54.3
11	1.404	-54.8
12	1.411	-55.2
13	1.413	-55.3
14	1.420	-55.7
15	1.424	-56.1
16	1.426	-56.2
17	1.428	-56.4
18	1.433	-57.3
19	1.436	-57.6
20	1.440	-57.9
21	1.447	-58.3
22	1.451	-59.0
23	1.452	-59.1
24	1.454	-59.4
25	1.460	-59.8
26	1.461	-59.9
27	1.470	-60.6
28	1.473	-60.9
29	1.477	-61.1
30	1.479	-61.4
31	1.481	-61.7
32	1.486	-61.9
33	1.487	-62.0
34	1.489	-62.2
35	1.491	-62.5
36	1.495	-62.8

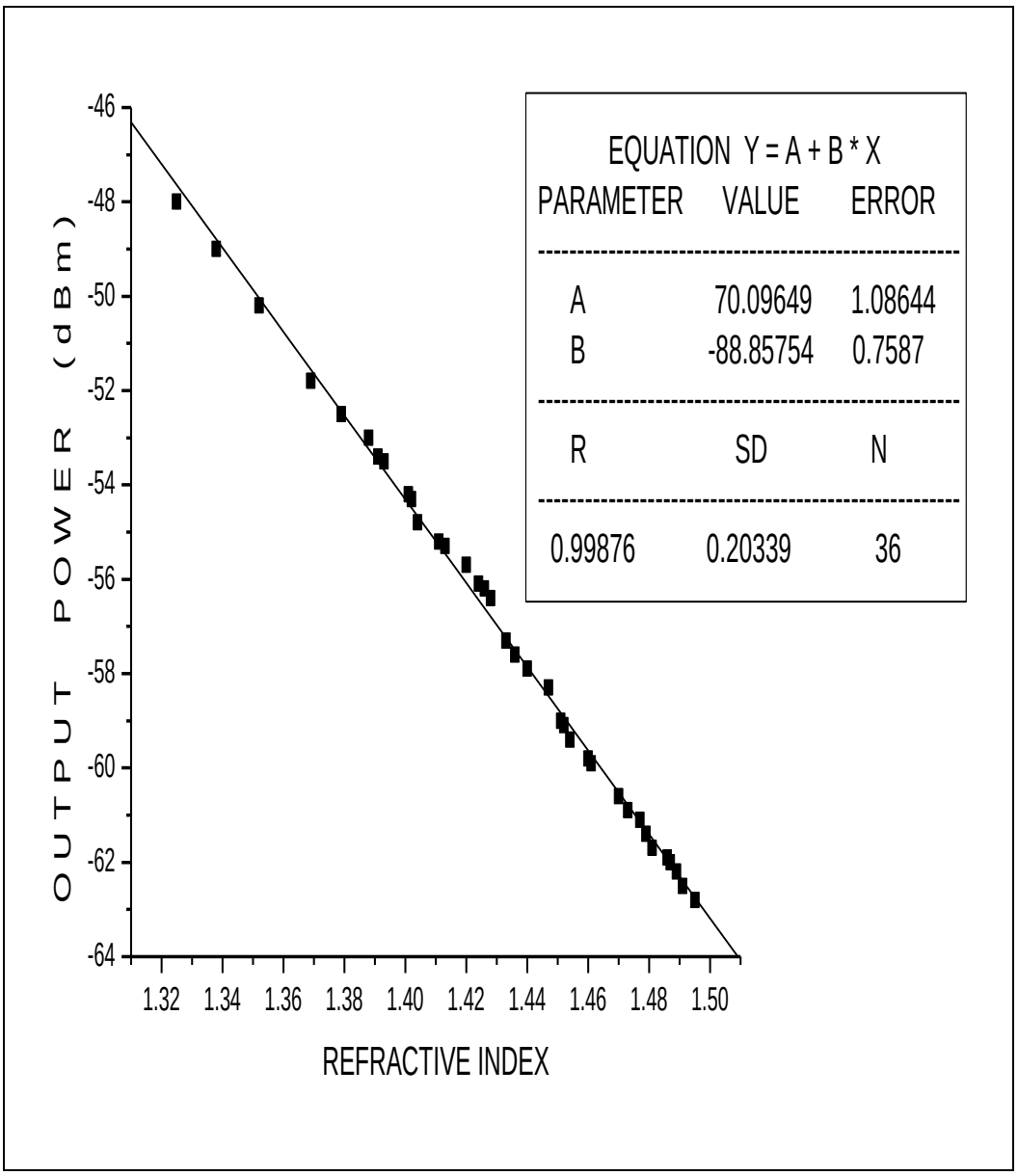

Fig.3.40: Calibration graph between R.I. and power with all the mixtures (benzene+methanol, benzene+butanol, benzene+propanol, benzene+cyclohexane)
Using 0.25 mm U shaped glass rod

DATA AT VARIOUS TEMPERATURES

Benzene and Methanol study:

Table 3.19: Variation of Power at different temperatures for Benzene and Methanol mixtures using 0.5 mm dia U shaped glass rod (Free space power output: -45.0dBm)

C6H6	CH3OH	Mixture	Power output (dBm) at different Temp. (°C)					
(ml)	(ml)	(R.I.)	30	35	40	45	50	55
0	10	1.325	-46.4	-46.1	-45.6	-45.2	-44.7	-44.4
1	9	1.338	-47.0	-46.4	-46.1	-45.6	-45.2	-44.7
2	8	1.352	-47.4	-47.0	-46.4	-46.1	-45.6	-45.2
3	7	1.369	-47.8	-47.4	-47.0	-46.4	-46.1	-45.6
4	6	1.388	-48.2	-47.8	-47.4	-47.0	-46.4	-46.1
5	5	1.404	-48.7	-48.2	-47.8	-47.4	-47.0	-46.4
6	4	1.420	-49.0	-48.7	-48.2	-47.8	-47.4	-47.0
7	3	1.436	-49.4	-49.0	-48.7	-48.2	-47.8	-47.4
8	2	1.452	-49.7	-49.4	-49.0	-48.7	-48.2	-47.8
9	1	1.470	-50.2	-49.7	-49.4	-49.0	-48.7	-48.2
10	0	1.487	-50.5	-50.2	-49.7	-49.4	-49.0	-48.7

Table 3.20: Dependence of power with temperature for Benzene and Methanol mixtures of different R.I. values using 0.5 mm dia U shaped glass rod(Free space power output: -45.0dBm)

Temp	Power output (dBm) at different R. I.										
(°C)	1.325	1.338	1.352	1.369	1.388	1.404	1.420	1.436	1.452	1.470	1.487
30	-46.4	-47.0	-47.4	-47.8	-48.2	-48.7	-49.0	-49.4	-49.7	-50.2	-50.5
35	-46.1	-46.4	-47.0	-47.4	-47.8	-48.2	-48.7	-49.0	-49.4	-49.7	-50.2
40	-45.6	-46.1	-46.4	-47.0	-47.4	-47.8	-48.2	-48.7	-49.0	-49.4	-49.7
45	-45.2	-45.6	-46.1	-46.4	-47.0	-47.4	-47.8	-48.2	-48.7	-49.0	-49.4
50	-44.7	-45.2	-45.6	-46.1	-46.4	-47.0	-47.4	-47.8	-48.2	-48.7	-49.0
55	-44.4	-44.7	-45.2	-45.6	-46.1	-46.4	-47.0	-47.4	-47.8	-48.2	-48.7

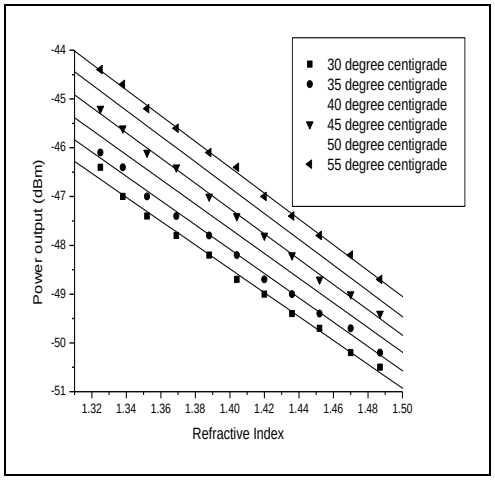

Fig.3.41: R.I. versus Power output For Benzene and Methanol mixtures Of different R.I. values using 0.5 mm Dia U shaped glass rod

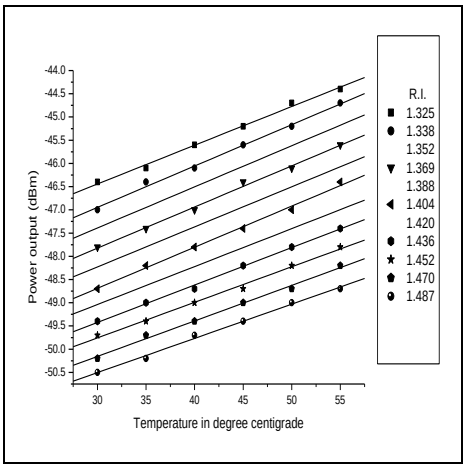

Fig. 3.42: between Temperature (^{0}C) versus Power output for Benzene and Methanol mixtures of different R.I. values using 0.5 mm dia U shaped glass rod

Benzene and Propanol study:

Table 3.21: Dependence of Power on refractive index at various temperatures for Benzene and Propanol mixtures using 0.5 mm dia U shaped glass rod(Free space power output:-45.0dBm)

C6H6	CH3OH	Mixture	Power output (dBm) at different Temp. (°C)						
			30	35	40	45	50	55	60
(ml)	(ml)	(R.I.)							
0	10	1.369	-47.8	-47.5	-47.3	-46.9	-46.7	-46.3	-46.0
1	9	1.379	-48.1	-47.8	-47.5	-47.3	-46.9	-46.7	-46.3
2	8	1.391	-48.4	-48.1	-47.8	-47.5	-47.3	-46.9	-46.7
3	7	1.401	-48.6	-48.4	-48.1	-47.8	-47.5	-47.3	-46.9
4	6	1.413	-48.9	-48.6	-48.4	-48.1	-47.8	-47.5	-47.3
5	5	1.424	-49.2	-48.9	-48.6	-48.4	-48.1	-47.8	-47.5
6	4	1.436	-49.4	-49.2	-48.9	-48.6	-48.4	-48.1	-47.8
7	3	1.447	-49.6	-49.4	-49.2	-48.9	-48.6	-48.4	-48.1
8	2	1.460	-50.0	-49.6	-49.4	-49.2	-48.9	-48.6	-48.4
9	1	1.479	-50.3	-50.0	-49.6	-49.4	-49.2	-48.9	-48.6
10	0	1.489	-50.6	-50.3	-50.0	-49.6	-49.4	-49.2	-48.9

International Journal of Engineering Research & Technology (IJERT)
ISSN: 2278-0181

Table 3.22: Dependence of power in temperature at various R.I. values for Benzene and Propanol mixture using 0.5 mm dia U shaped glass rod(Free space power output:-45.0dBm)

Temp. (°C)	Power output (dBm) at different R.I.										
	1.369	1.379	1.391	1.401	1.413	1.424	1.436	1.447	1.46	1.479	1.489
30	-47.8	-48.1	-48.4	-48.6	-48.9	-49.2	-49.4	-49.6	-50.0	-50.3	-50.6
35	-47.5	-47.8	-48.1	-48.4	-48.6	-48.9	-49.2	-49.4	-49.6	-50.0	-50.3
40	-47.3	-47.5	-47.8	-48.1	-48.4	-48.6	-48.9	-49.2	-49.4	-49.6	-50.0
45	-46.9	-47.3	-47.5	-47.8	-48.1	-48.4	-48.6	-48.9	-49.2	-49.4	-49.6
50	-46.7	-46.9	-47.3	-47.5	-47.8	-48.1	-48.4	-48.6	-48.9	-49.2	-49.4
55	-46.3	-46.7	-46.9	-47.3	-47.5	-47.8	-48.1	-48.4	-48.6	-48.9	-49.2
60	-46.0	-46.3	-46.7	-46.9	-47.3	-47.5	-47.8	-48.1	-48.4	-48.6	-48.9

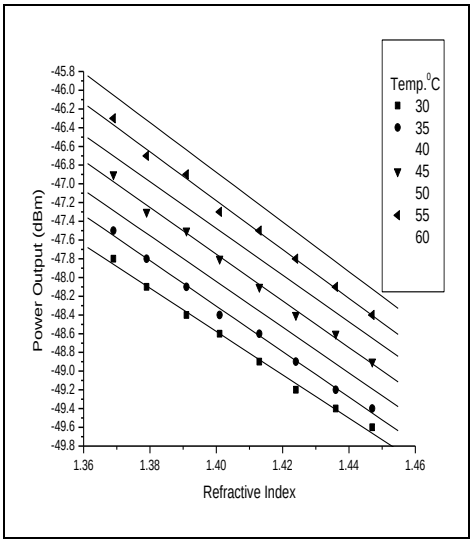

Fig.3.43: Relation between R.I. and Power output For Benzene and Propanol mixture Using 0.5 mm dia U shaped glass rod

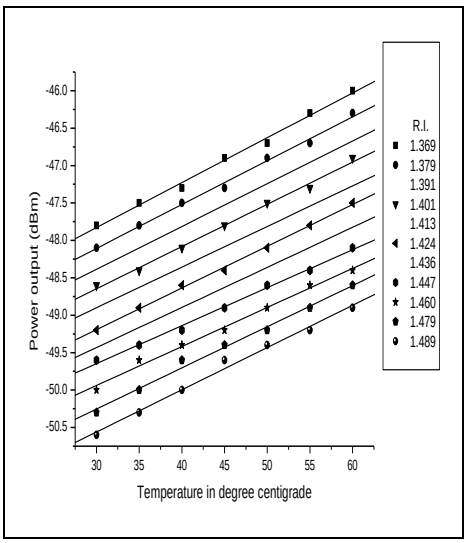

Fig.3.44: Temperature versus Power output for Benzene and Propanol mixture using 0.5 mm dia U shaped glass rod

Benzene and Butanol study:

Table 3.23: Dependence of power on R.I. at various temperatures for Benzene and Butanol mixtures using 0.5 mm dia U shaped glass rod(Free space power output:-45.0dBm)

C_6H_6	Butanol $CH_3(CH_2)_3OH$	Mixture	Power output (dBm) at different temp. (°C)						
(ml)	(ml)	(R.I.)	30	35	40	45	50	55	60
0	10	1.393	-48.5	-48.3	-47.9	-47.7	-47.3	-47.1	-46.7
1	9	1.402	-48.7	-48.5	-48.3	-47.9	-47.7	-47.3	-47.1
2	8	1.411	-48.9	-48.7	-48.5	-48.3	-47.9	-47.7	-47.3
3	7	1.420	-49.0	-48.9	-48.7	-48.5	-48.3	-47.9	-47.7
4	6	1.428	-49.2	-49.0	-48.9	-48.7	-48.5	-48.3	-47.9
5	5	1.440	-49.4	-49.2	-49.0	-48.9	-48.7	-48.5	-48.3
6	4	1.451	-49.7	-49.4	-49.2	-49.0	-48.9	-48.7	-48.5
7	3	1.461	-50.0	-49.7	-49.4	-49.2	-49.0	-48.9	-48.7
8	2	1.473	-50.2	-50.0	-49.7	-49.4	-49.2	-49.0	-48.9
9	1	1.481	-50.4	-50.2	-50.0	-49.7	-49.4	-49.2	-49.0
10	0	1.491	-50.7	-50.4	-50.2	-50.0	-49.7	-49.4	-49.2

Table 3.24: Dependence of power on temperature at various R. I. for Benzene and Butanol mixtures using 0.5 mm dia U shaped glass rod(Free space power output:-45.0dBm)

Temp.	Power output (dBm) at different R.I.										
	1.393	1.402	1.411	1.420	1.428	1.440	1.451	1.461	1.473	1.481	1.491
(°C)											
30	-48.5	-48.7	-48.9	-49.0	-49.2	-49.4	-49.7	-50.0	-50.2	-50.4	-50.7
35	-48.3	-48.5	-48.7	-48.9	-49.0	-49.2	-49.4	-49.7	-50.0	-50.2	-50.4
40	-47.9	-48.3	-48.5	-48.7	-48.9	-49.0	-49.2	-49.4	-49.7	-50.0	-50.2
45	-47.7	-47.9	-48.3	-48.5	-48.7	-48.9	-49.0	-49.2	-49.4	-49.7	-50.0
50	-47.3	-47.7	-47.9	-48.3	-48.5	-48.7	-48.9	-49.0	-49.2	-49.4	-49.7
55	-47.1	-47.3	-47.7	-47.9	-48.3	-48.5	-48.7	-48.9	-49.0	-49.2	-49.4
60	-46.7	-47.1	-47.3	-47.7	-47.9	-48.3	-48.5	-48.7	-48.9	-49.0	-49.2

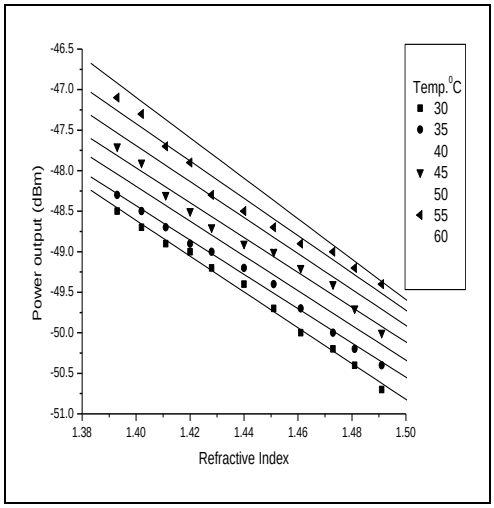

Fig.3.45: Relation between R.I. and Power output For Benzene and Butanol mixtures Using 0.5 mm dia U shaped glass rod

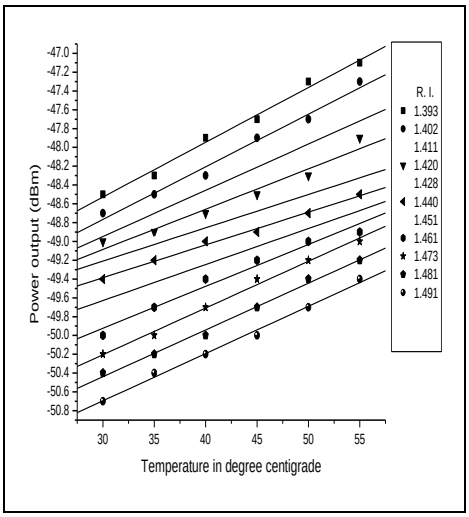

Fig.3.46: Temperature versus Power output for Benzene and Butanol mixtures using 0.5 mm dia U shaped glass rod

Benzene and Cyclo-hexane study:

Table 3.25: Dependence of power on R.I. at various temperatures for Benzene and Cyclohexane mixtures using 0.5 mm dia U shaped glass rod(Free space power output:-45.0dBm)

SL. No.	C6H6 (ml)	C6H12 (ml)	Mixture (R.I.)	Power output (dBm) at different temp. (°C)						
				30	35	40	45	50	55	60
1	0	10	1.420	-49.0	-48.7	-48.6	-48.3	-48.2	-48.0	-47.8
2	1	9	1.426	-49.2	-49.0	-48.7	-48.6	-48.3	-48.2	-48.0
3	2	8	1.433	-49.3	-49.2	-49.0	-48.7	-48.6	-48.3	-48.2
4	3	7	1.440	-49.4	-49.3	-49.2	-49.0	-48.7	-48.6	-48.3
5	4	6	1.447	-49.6	-49.4	-49.3	-49.2	-49.0	-48.7	-48.6
6	5	5	1.454	-49.8	-49.6	-49.4	-49.3	-49.2	-49.0	-48.7
7	6	4	1.461	-50.0	-49.8	-49.6	-49.4	-49.3	-49.2	-49.0
8	7	3	1.470	-50.2	-50.0	-49.8	-49.6	-49.4	-49.3	-49.2
9	8	2	1.477	-50.4	-50.2	-50.0	-49.8	-49.6	-49.4	-49.3
10	9	1	1.486	-50.6	-50.4	-50.2	-50.0	-49.8	-49.6	-49.4
11	10	0	1.495	-50.8	-50.6	-50.4	-50.2	-50.0	-49.8	-49.6

Table 3.26: : Dependence of power on temperature at various R. I. for Benzene and Cyclohexane mixtures using 0.5 mm dia U shaped glass rod(Free space power output:-45.0dBm)

Temp.	Power output (dBm) at different R.I..										
(°C)	1.420	1.426	1.433	1.440	1.447	1.454	1.461	1.470	1.477	1.486	1.495
30	-49.0	-49.2	-49.3	-49.4	-49.6	-49.8	-50.0	-50.2	-50.4	-50.6	-50.8
35	-48.7	-49.0	-49.2	-49.3	-49.4	-49.6	-49.8	-50.0	-50.2	-50.4	-50.6
40	-48.6	-48.7	-49.0	-49.2	-49.3	-49.4	-49.6	-49.8	-50.0	-50.2	-50.4
45	-48.3	-48.6	-48.7	-49.0	-49.2	-49.3	-49.4	-49.6	-49.8	-50.0	-50.2
50	-48.2	-48.3	-48.6	-48.7	-49.0	-49.2	-49.3	-49.4	-49.6	-49.8	-50.0
55	-48.0	-48.2	-48.3	-48.6	-48.7	-49.0	-49.2	-49.3	-49.4	-49.6	-49.8
60	-47.8	-48.0	-48.2	-48.3	-48.6	-48.7	-49.0	-49.2	-49.3	-49.4	-49.6

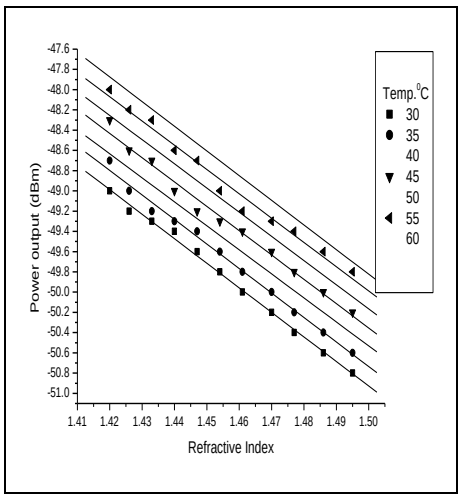

Fig.3.47: R.I. verses Power output
For Benzene and Cyclohexane mixtures
Using 0.5 mm dia U shaped glass rod

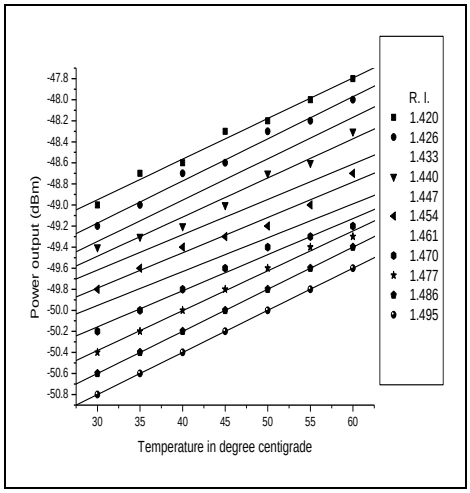

Fig. 3.48: Temperature verses Power output
for Benzene and Cyclohexane mixtures
using 0.5 mm dia U shaped glass rod

Table 3.27: Consolidated data of R.I. and power output at 30°C for all four (benzene+methanol, benzene+propanol, benzene+butanol, benzene+cyclohexane) mixtures using 0.5 mm dia U shaped glass rod(Free space power output:-45.0dBm)

Sl. No.	Refractive Index (R.I.)				Power output (dBm) at 30°C			
	C_6H_6 + CH_3OH	C_6H_6 + (C_3H_8O)	C_6H_6 + $CH_3(CH_2)_3OH$	C_6H_6 + (C_6H_{12})	C_6H_6 + CH_3OH	C_6H_6 + (C_3H_8O)	C_6H_6 + $CH_3(CH_2)_3OH$	C_6H_6 + (C_6H_{12})
1	1.325				-46.4			
2	1.338				-47.0			
3	1.352				-47.4			
4	1.369	1.369			-47.8	-47.8		
5		1.379				-48.1		
6	1.388				-48.2			
7		1.391				-48.4		
8			1.393				-48.5	
9		1.401				-48.6		
10			1.402				-48.7	
11	1.404				-48.7			
12			1.411				-48.9	
13		1.413				-48.9		
14	1.420		1.420	1.420	-49.0		-49.0	-49.0
15		1.424				-49.2		
16				1.426				-49.2
17			1.428				-49.2	
18				1.433				-49.3
19	1.436	1.436			-49.4	-49.4		
20			1.440	1.440			-49.4	-49.4
21		1.447		1.447		-49.6		-49.6
22			1.451				-49.7	
23	1.452				-49.7			
24				1.454				-49.8
25		1.460				-50.0		
26			1.461	1.461			-50.0	-50.0
27	1.470			1.470	-50.2			-50.2
28			1.473				-50.2	
29				1.477				-50.4
30		1.479				-50.3		
31			1.481				-50.4	
32				1.486				-50.6
33	1.487				-50.5			
34		1.489				-50.6		
35			1.491				-50.7	
36				1.495				-50.8

Table 3.28: Unified R. I. and power output data at 30°C for all four (benzene+methanol, benzene+propanol, benzene+butanol, benzene+cyclohexane) mixtures using 0.5 mm dia U shaped glass rod (Free space power output:-45.0dBm)

SL. No.	Refractive index of the four Mixtures together (Benzene+Methanol, Benzene+Propanol, Benzene+Butanol, Benzen+Cyclohexane) (R.I.)	Power output of the four Mixtures together (Benzene+Methanol, Benzene+Propanol, Benzene+Butanol, Benzen+Cyclohexane) (dBm)
1	1.325	-46.4
2	1.338	-47.0
3	1.352	-47.4
4	1.369	-47.8
5	1.379	-48.1
6	1.388	-48.2
7	1.391	-48.4
8	1.393	-48.5
9	1.401	-48.6
10	1.402	-48.7
11	1.404	-48.7
12	1.411	-48.9
13	1.413	-48.9
14	1.420	-49.0
15	1.424	-49.2
16	1.426	-49.2
17	1.428	-49.2
18	1.433	-49.3
19	1.436	-49.4
20	1.440	-49.4
21	1.447	-49.6
22	1.451	-49.7
23	1.452	-49.7
24	1.454	-49.8
25	1.460	-50.0
26	1.461	-50.0
27	1.470	-50.2
28	1.473	-50.2
29	1.477	-50.4
30	1.479	-50.3
31	1.481	-50.4
32	1.486	-50.6
33	1.487	-50.5
34	1.489	-50.6
35	1.491	-50.7
36	1.495	-50.8

International Journal of Engineering Research & Technology (IJERT)
ISSN: 2278-0181

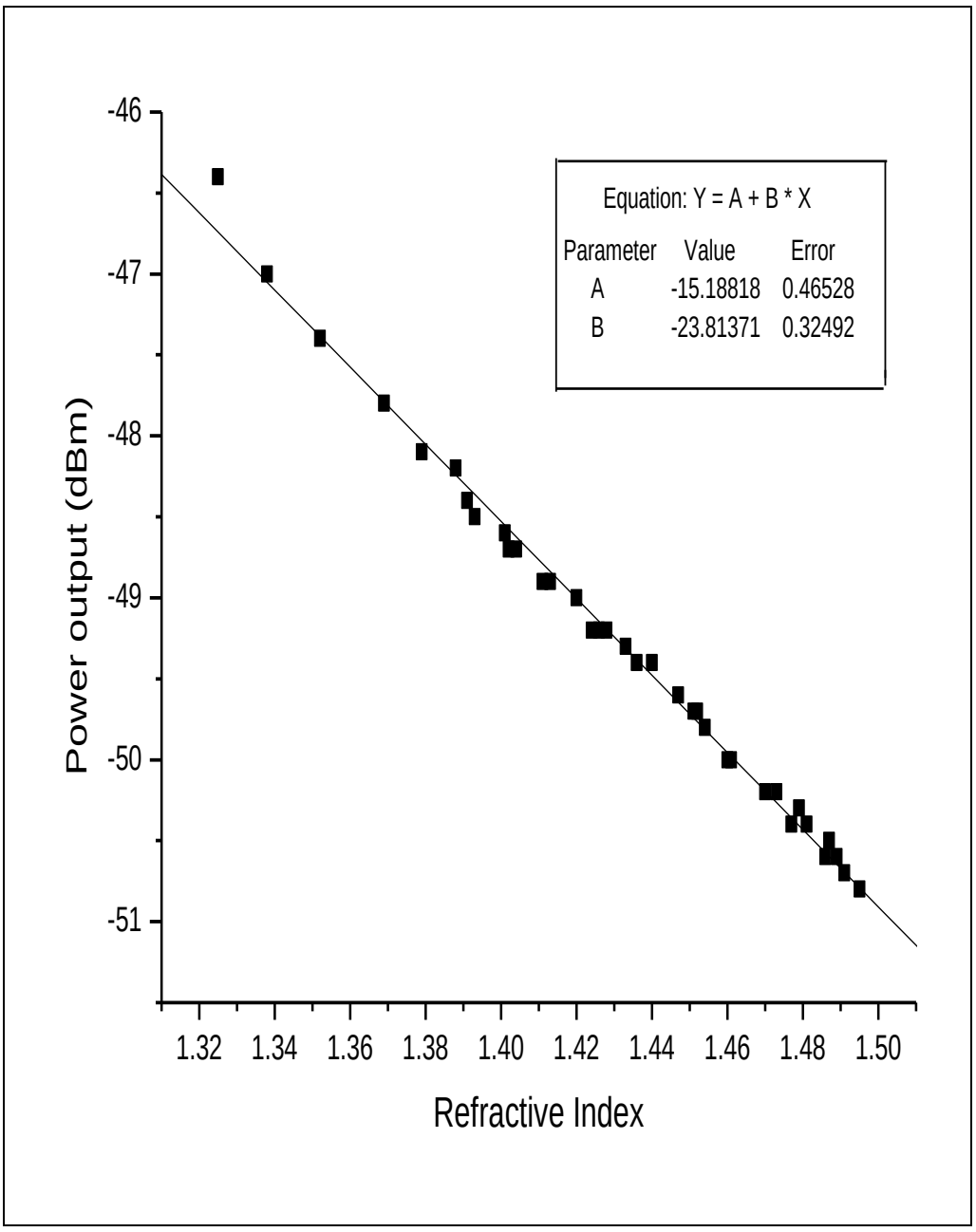

Fig.3.49: Calibrated graph between power output and refractive index at the temperature of 30°C for (benzene+methanol), (benzene+propanol), (benzene+butanol), (Benzene+cyclohexane) mixtures using 0.5 mm dia U shaped glass rod.

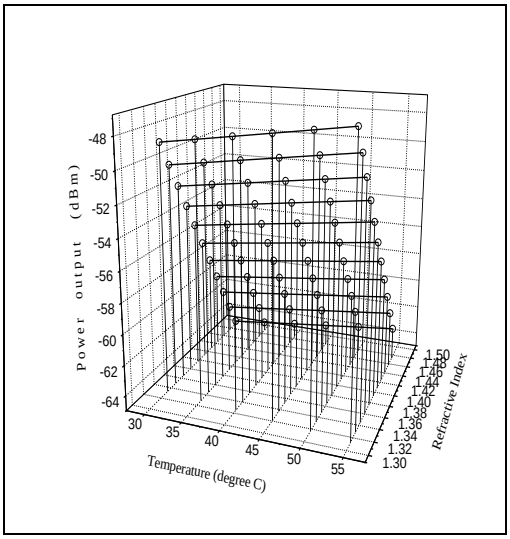

Fig.3.50: Variation of 3 parameters) for (benzene+methanol) Using 0.5 mm dia U shaped glass rod

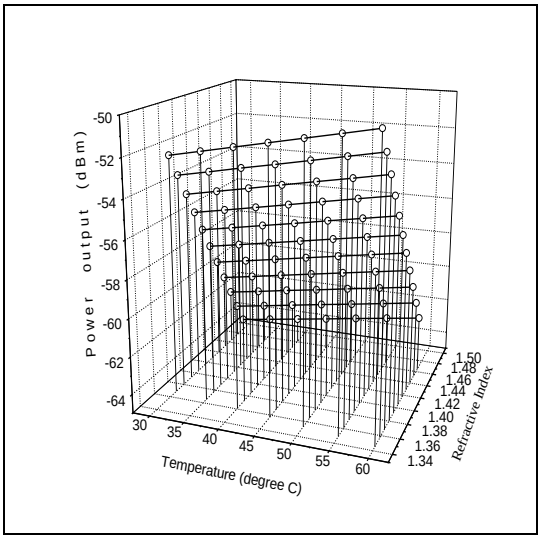

Fig.3.51: Variation of 3 parameters for (benzene +Propanol) using 0.5 mm dia U shaped glass rod

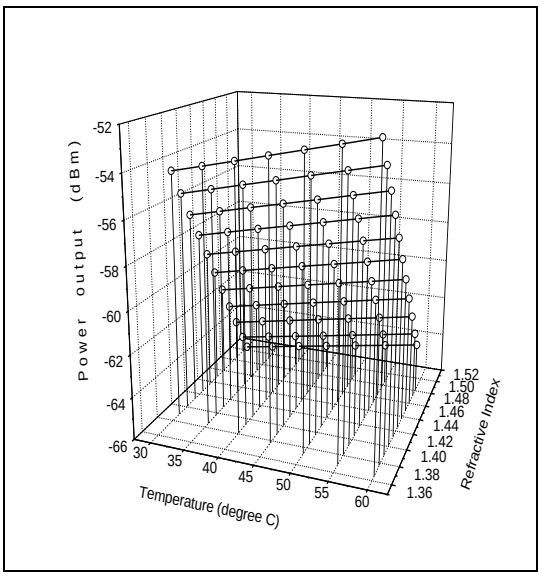

Fig.3.52: Variation of 3 parameters for (benzene+butanol). Using 0.5 mm dia U shaped glass rod

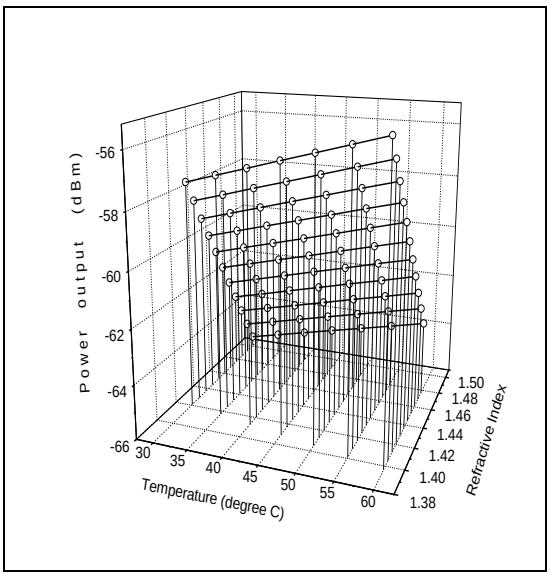

Fig.3.53: Variation of 3 parameters for (benzene+cyclohexane). using 0.5 mm dia U shaped glass rod

Benzene and Methanol:

Table 3.29: Refractive index obtained from Power data at various temperatures of the Benzene and Methanol (Free space power output: -45.0dBm) for 0.5 mm dia U shaped glass rod

C_6H_6 + CH_3OH	30°C		35°C		40°C		45°C		50°C		55°C	
	dBm	R. I.	dBm	R. I.	dBm	R. I.	dBm	R. I.	dBm	R. I.	dBm	R. I.
0+10	-46.4	1.325	-46.1	1.298	-45.6	1.277	-45.2	1.260	-44.7	1.239	-44.4	1.227
1+9	-47.0	1.338	-46.4	1.325	-46.1	1.298	-45.6	1.277	-45.2	1.260	-44.7	1.239
2+8	-47.4	1.352	-47.0	1.338	-46.4	1.325	-46.1	1.298	-45.6	1.277	-45.2	1.260
3+7	-47.8	1.369	-47.4	1.352	-47.0	1.338	-46.4	1.325	-46.1	1.298	-45.6	1.277
4+6	-48.2	1.388	-47.8	1.369	-47.4	1.352	-47.0	1.338	-46.4	1.325	-46.1	1.298
5+5	-48.7	1.404	-48.2	1.388	-47.8	1.369	-47.4	1.352	-47.0	1.338	-46.4	1.325
6+4	-49.0	1.420	-48.7	1.404	-48.2	1.388	-47.8	1.369	-47.4	1.352	-47.0	1.338
7+3	-49.4	1.436	-49.0	1.420	-48.7	1.404	-48.2	1.388	-47.8	1.369	-47.4	1.352
8+2	-49.7	1.452	-49.4	1.436	-49.0	1.420	-48.7	1.404	-48.2	1.388	-47.8	1.369
9+1	-50.2	1.470	-49.7	1.452	-49.4	1.436	-49.0	1.420	-48.7	1.404	-48.2	1.388
10+0	-50.5	1.487	-50.2	1.470	-49.7	1.452	-49.4	1.436	-49.0	1.420	-48.7	1.404

Table 3.30: Refractive index obtained from Power data at various temperatures of the Benzene and Methanol mixtures for 0.5 mm dia U shaped glass rod

(Free space power output: -45.0dBm)

Temp.	(0+10) ml		(1+9) ml		(2+8) ml		(3+7) ml		(4+6) ml		(5+5) ml	
	dBm	R.I.	dBm	R.I.	dBm	R.I.	dBm	R.I.	dBm	R.I.	dBm	R.I.
30°C	-46.4	1.325	-47.0	1.338	-47.4	1.352	-47.8	1.369	-48.2	1.388	-48.7	1.404
35°C	-46.1	1.298	-46.4	1.325	-47.0	1.338	-47.4	1.352	-47.8	1.369	-48.2	1.388
40°C	-45.6	1.277	-46.1	1.298	-46.4	1.325	-47.0	1.338	-47.4	1.352	-47.8	1.369
45°C	-45.2	1.260	-45.6	1.277	-46.1	1.298	-46.4	1.325	-47.0	1.338	-47.4	1.352
50°C	-44.7	1.239	-45.2	1.260	-45.6	1.277	-46.1	1.298	-46.4	1.325	-47.0	1.338
55°C	-44.4	1.227	-44.7	1.239	-45.2	1.260	-45.6	1.277	-46.1	1.298	-46.4	1.325

	(6+4) ml		(7+3) ml		(8+2) ml		(9+1) ml		(10+0) ml	
30°C	-49.0	1.420	-49.4	1.436	-49.7	1.452	-50.2	1.470	-50.5	1.487
35°C	-48.7	1.404	-49.0	1.420	-49.4	1.436	-49.7	1.452	-50.2	1.470
40°C	-48.2	1.388	-48.7	1.404	-49.0	1.420	-49.4	1.436	-49.7	1.452
45°C	-47.8	1.369	-48.2	1.388	-48.7	1.404	-49.0	1.420	-49.4	1.436
50°C	-47.4	1.352	-47.8	1.369	-48.2	1.388	-48.7	1.404	-49.0	1.420
55°C	-47.0	1.338	-47.4	1.352	-47.8	1.369	-48.2	1.388	-48.7	1.404

Benzene and Propanol:

Table 3.31: Refractive Index data obtained from corresponding Power data at various temp. of Benzene and Propanol using 0.5 mm dia U shaped rod(Free space power: -45.0dBm)

30°C		35°C		40°C		45°C		50°C		55°C		60°C	
dBm	R.I.	dBm	R.I.	dBm	R.I.	dBm	R.I.	dBm	R.I.	dBm	R.I.	dBm	R.I.
-47.8	1.369	-47.5	1.357	-47.3	1.349	-46.9	1.332	-46.7	1.323	-46.3	1.307	-46.0	1.294
-48.1	1.379	-47.8	1.369	-47.5	1.357	-47.3	1.349	-46.9	1.332	-46.7	1.323	-46.3	1.307
-48.3	1.391	-48.1	1.379	-47.8	1.369	-47.5	1.357	-47.3	1.349	-46.9	1.332	-46.7	1.323
-48.6	1.401	-48.3	1.391	-48.1	1.379	-47.8	1.369	-47.5	1.357	-47.3	1.349	-46.9	1.332
-48.9	1.413	-48.6	1.401	-48.3	1.391	-48.1	1.379	-47.8	1.369	-47.5	1.357	-47.3	1.349
-49.2	1.424	-48.9	1.413	-48.6	1.401	-48.3	1.391	-48.1	1.379	-47.8	1.369	-47.5	1.357
-49.4	1.436	-49.2	1.424	-48.9	1.413	-48.6	1.401	-48.3	1.391	-48.1	1.379	-47.8	1.369
-49.6	1.447	-49.4	1.436	-49.2	1.424	-48.9	1.413	-48.6	1.401	-48.3	1.391	-48.1	1.379
-50.0	1.460	-49.6	1.447	-49.4	1.436	-49.2	1.424	-48.9	1.413	-48.6	1.401	-48.3	1.391
-50.3	1.479	-50.0	1.460	-49.6	1.447	-49.4	1.436	-49.2	1.424	-48.9	1.413	-48.6	1.401
-50.6	1.489	-50.3	1.479	-50.0	1.460	-49.6	1.447	-49.4	1.436	-49.2	1.424	-48.9	1.413

Table 3.32: Refractive Index data obtained from corresponding Power data at various temp. of Benzene and Propanol (Free space power: -45.0dBm) mixture using 0.5 mm dia U shaped rod

Temp.	(0+10) ml		(1+9) ml		(2+8) ml		(3+7) ml		(4+6) ml		(5+5) ml	
	dBm	R.I.	dBm	R.I.	dBm	R.I.	dBm	R.I.	dBm	R.I.	dBm	R.I.
30°C	-47.8	1.369	-48.1	1.379	-48.4	1.391	-48.6	1.401	-48.9	1.413	-49.2	1.424
35°C	-47.5	1.357	-47.8	1.369	-48.1	1.379	-48.4	1.391	-48.6	1.401	-48.9	1.413
40°C	-47.3	1.349	-47.5	1.357	-47.8	1.369	-48.1	1.379	-48.4	1.391	-48.6	1.401
45°C	-46.9	1.332	-47.3	1.349	-47.5	1.357	-47.8	1.369	-48.1	1.379	-48.4	1.391
50°C	-46.7	1.323	-46.9	1.332	-47.3	1.349	-47.5	1.357	-47.8	1.369	-48.1	1.379
55°C	-46.3	1.307	-46.7	1.323	-46.9	1.332	-47.3	1.349	-47.5	1.357	-47.8	1.369
60°C	-46.0	1.294	-46.3	1.307	-46.7	1.323	-46.9	1.332	-47.3	1.349	-47.5	1.357

	(6+4) ml		(7+3) ml		(8+2) ml		(9+1) ml		(10+0) ml	
30°C	-49.4	1.436	-49.6	1.447	-50.0	1.460	-50.3	1.479	-50.6	1.489
35°C	-49.2	1.424	-49.4	1.436	-49.6	1.447	-50.0	1.460	-50.3	1.479
40°C	-48.9	1.413	-49.2	1.424	-49.4	1.436	-49.6	1.447	-50.0	1.460
45°C	-48.6	1.401	-48.9	1.413	-49.2	1.424	-49.4	1.436	-49.6	1.447
50°C	-48.4	1.391	-48.6	1.401	-48.9	1.413	-49.2	1.424	-49.4	1.436
55°C	-48.1	1.379	-48.4	1.391	-48.6	1.401	-48.9	1.413	-49.2	1.424
60°C	-47.8	1.369	-48.1	1.379	-48.4	1.391	-48.6	1.401	-48.9	1.413

Benzene and Butanol:

Table 3.33: Refractive Index data obtained from corresponding Power data at various temp. of Benzene and Butanol using 0.5 mm dia U shaped rod (Free space power: -45.0dBm)

30°C		35°C		40°C		45°C		50°C		55°C		60°C	
dBm	R.I.	dBm	R.I.	dBm	R.I.	dBm	R.I.	dBm	R.I.	dBm	R.I.	dBm	R.I.
-48.5	1.393	-48.3	1.391	-47.9	1.374	-47.7	1.365	-47.3	1.349	-47.1	1.340	-46.7	1.323
-48.7	1.402	-48.5	1.393	-48.3	1.391	-47.9	1.374	-47.7	1.365	-47.3	1.349	-47.1	1.340
-48.9	1.411	-48.7	1.402	-48.5	1.393	-48.3	1.391	-47.9	1.374	-47.7	1.365	-47.3	1.349
-49.0	1.420	-48.9	1.411	-48.7	1.402	-48.5	1.393	-48.3	1.391	-47.9	1.374	-47.7	1.365
-49.2	1.428	-49.0	1.420	-48.9	1.411	-48.7	1.402	-48.5	1.393	-48.3	1.391	-47.9	1.374
-49.4	1.440	-49.2	1.428	-49.0	1.420	-48.9	1.411	-48.7	1.402	-48.5	1.393	-48.3	1.391
-49.7	1.451	-49.4	1.440	-49.2	1.428	-49.0	1.420	-48.9	1.411	-48.7	1.402	-48.5	1.393
-50.0	1.461	-49.7	1.451	-49.4	1.440	-49.2	1.428	-49.0	1.420	-48.9	1.411	-48.7	1.402
-50.2	1.473	-50.0	1.461	-49.7	1.451	-49.4	1.440	-49.2	1.428	-49.0	1.420	-48.9	1.411
-50.4	1.481	-50.2	1.473	-50.0	1.461	-49.7	1.451	-49.4	1.440	-49.2	1.428	-49.0	1.420
-50.7	1.491	-50.4	1.481	-50.2	1.473	-50.0	1.461	-49.7	1.451	-49.4	1.440	-49.2	1.428

Table 3.34: Refractive Index data obtained from corresponding Power data at various temp. of Benzene and Butanol using 0.5 mm dia U shaped rod(Free space power : -45.0dBm)

Temp.	(0+10) ml		(1+9) ml		(2+8) ml		(3+7) ml		(4+6) ml		(5+5) ml	
	dBm	R.I.	dBm	R.I.	dBm	R.I.	dBm	R.I.	dBm	R.I.	dBm	R.I.
30°C	-48.5	1.393	-48.7	1.402	-48.9	1.411	-49.0	1.420	-49.2	1.428	-49.4	1.440
35°C	-48.3	1.391	-48.5	1.393	-48.7	1.402	-48.9	1.411	-49.0	1.420	-49.2	1.428
40°C	-47.9	1.374	-48.3	1.391	-48.5	1.393	-48.7	1.402	-48.9	1.411	-49.0	1.420
45°C	-47.7	1.365	-47.9	1.374	-48.3	1.391	-48.5	1.393	-48.7	1.402	-48.9	1.411
50°C	-47.3	1.349	-47.7	1.365	-47.9	1.374	-48.3	1.391	-48.5	1.393	-48.7	1.402
55°C	-47.1	1.340	-47.3	1.349	-47.7	1.365	-47.9	1.374	-48.3	1.391	-48.5	1.393
60°C	-46.7	1.323	-47.1	1.340	-47.3	1.349	-47.7	1.365	-47.9	1.374	-48.3	1.391

	(6+4) ml		(7+3) ml		(8+2) ml		(9+1) ml		(10+0) ml	
30°C	-49.7	1.451	-50.0	1.461	-50.2	1.473	-50.4	1.481	-50.7	1.491
35°C	-49.4	1.440	-49.7	1.451	-50.0	1.461	-50.2	1.473	-50.4	1.481
40°C	-49.2	1.428	-49.4	1.440	-49.7	1.451	-50.0	1.461	-50.2	1.473
45°C	-49.0	1.420	-49.2	1.428	-49.4	1.440	-49.7	1.451	-50.0	1.461
50°C	-48.9	1.411	-49.0	1.420	-49.2	1.428	-49.4	1.440	-49.7	1.451
55°C	-48.7	1.402	-48.9	1.411	-49.0	1.420	-49.2	1.428	-49.4	1.440
60°C	-48.5	1.393	-48.7	1.402	-48.9	1.411	-49.0	1.420	-49.2	1.428

Benzene and Cyclohexane:

Table 3.35: Refractive Index data obtained from corresponding Power data at various temp. of Benzene and Cyclohexane using 0.5 mm dia U shaped rod(Free space power : -45.0dBm)

30°C		35°C		40°C		45°C		50°C		55°C		60°C	
dBm	R.I.	dBm	R.I.	dBm	R.I.	dBm	R.I.	dBm	R.I.	dBm	R.I.	dBm	R.I.
-49.0	1.420	-48.7	1.407	-48.6	1.403	-48.3	1.391	-48.2	1.386	-48.0	1.378	-47.8	1.370
-49.2	1.426	-49.0	1.420	-48.7	1.407	-48.6	1.403	-48.3	1.391	-48.2	1.386	-48.0	1.378
-49.3	1.433	-49.2	1.426	-49.0	1.420	-48.7	1.407	-48.6	1.403	-48.3	1.391	-48.2	1.386
-49.4	1.440	-49.3	1.433	-49.2	1.426	-49.0	1.420	-48.7	1.407	-48.6	1.403	-48.3	1.391
-49.6	1.447	-49.4	1.440	-49.3	1.433	-49.2	1.426	-49.0	1.420	-48.7	1.407	-48.6	1.403
-49.8	1.454	-49.6	1.447	-49.4	1.440	-49.3	1.433	-49.2	1.426	-49.0	1.420	-48.7	1.407
-50.0	1.461	-49.8	1.454	-49.6	1.447	-49.4	1.440	-49.3	1.433	-49.2	1.426	-49.0	1.420
-50.2	1.470	-50.0	1.461	-49.8	1.454	-49.6	1.447	-49.4	1.440	-49.3	1.433	-49.2	1.426
-50.4	1.477	-50.2	1.470	-50.0	1.461	-49.8	1.454	-49.6	1.447	-49.4	1.440	-49.3	1.433
-50.6	1.486	-50.4	1.477	-50.2	1.470	-50.0	1.461	-49.8	1.454	-49.6	1.447	-49.4	1.440
-50.8	1.495	-50.6	1.486	-50.4	1.477	-50.2	1.470	-50.0	1.461	-49.8	1.454	-49.6	1.447

Table 3.36: Refractive Index data obtained from corresponding Power data at various temp. of Benzene and Cyclohexane using 0.5 mm dia U shaped rod(Free space power : -45.0dBm)

Temp.	(0+10) ml		(1+9) ml		(2+8) ml		(3+7) ml		(4+6) ml		(5+5) ml	
	dBm	R.I.	dBm	R.I.	dBm	R.I.	dBm	R.I.	dBm	R.I.	dBm	R.I.
30°C	-49.0	1.420	-49.2	1.426	-49.3	1.433	-49.4	1.440	-49.6	1.447	-49.8	1.454
35°C	-48.7	1.407	-49.0	1.420	-49.2	1.426	-49.3	1.433	-49.4	1.440	-49.6	1.447
40°C	-48.6	1.403	-48.7	1.407	-49.0	1.420	-49.2	1.426	-49.3	1.433	-49.4	1.440
45°C	-48.3	1.391	-48.6	1.403	-48.7	1.407	-49.0	1.420	-49.2	1.426	-49.3	1.433
50°C	-48.2	1.386	-48.3	1.391	-48.6	1.403	-48.7	1.407	-49.0	1.420	-49.2	1.426
55°C	-48.0	1.378	-48.2	1.386	-48.3	1.391	-48.6	1.403	-48.7	1.407	-49.0	1.420
60°C	-47.8	1.370	-48.0	1.378	-48.2	1.386	-48.3	1.391	-48.6	1.403	-48.7	1.407

	(6+4) ml		(7+3) ml		(8+2) ml		(9+1) ml		(10+0) ml	
30°C	-50.0	1.461	-50.2	1.470	-50.4	1.477	-50.6	1.486	-50.8	1.495
35°C	-49.8	1.454	-50.0	1.461	-50.2	1.470	-50.4	1.477	-50.6	1.486
40°C	-49.6	1.447	-49.8	1.454	-50.0	1.461	-50.2	1.470	-50.4	1.477
45°C	-49.4	1.440	-49.6	1.447	-49.8	1.454	-50.0	1.461	-50.2	1.470
50°C	-49.3	1.433	-49.4	1.440	-49.6	1.447	-49.8	1.454	-50.0	1.461
55°C	-49.2	1.426	-49.3	1.433	-49.4	1.440	-49.6	1.447	-49.8	1.454
60°C	-49.0	1.420	-49.2	1.426	-49.3	1.433	-49.4	1.440	-49.6	1.447

International Journal of Engineering Research & Technology (IJERT)
ISSN: 2278-0181

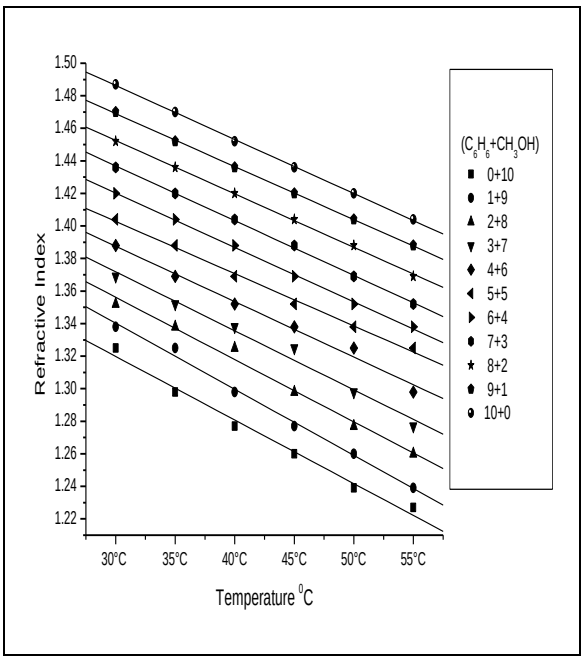

Fig.3.54: Temperature verses R. I. of Benzene and Methanol mixture Using 0.5 mm dia U shaped glass rod

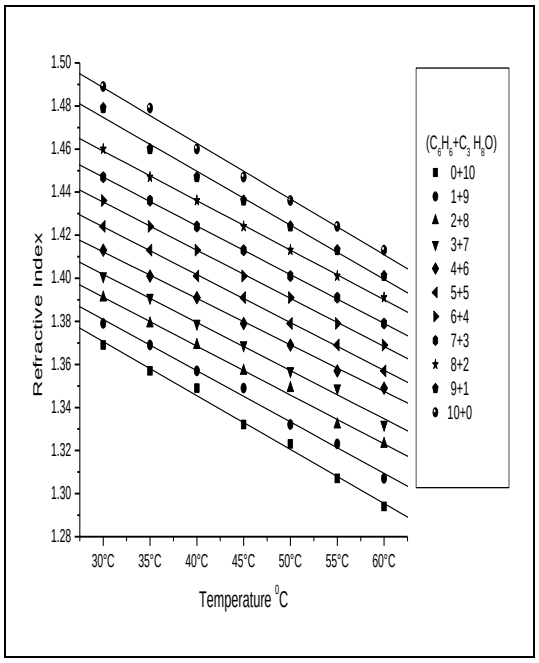

Fig.3.55: Temperature verses R. I. of Benzene and Propanol mixture using 0.5 mm dia U shaped glass rod

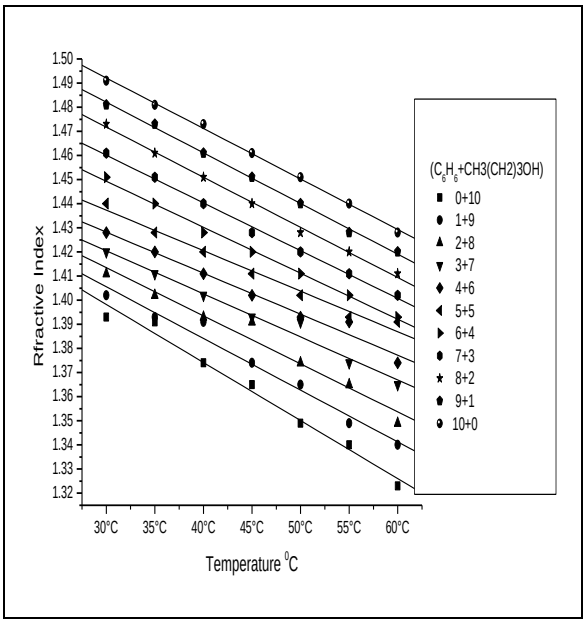

Fig.3.56: Temperature verses R. I. of Benzene and Butanol mixture Using 0.5 mm dia U shaped glass rod

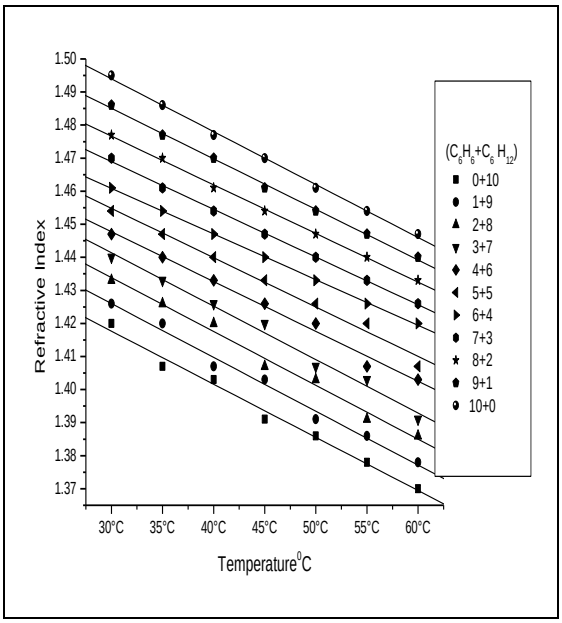

Fig.3.57: Temperature verses R. I. of Benzene and Cyclohexane mixture using 0.5 mm dia U shaped glass rod

]

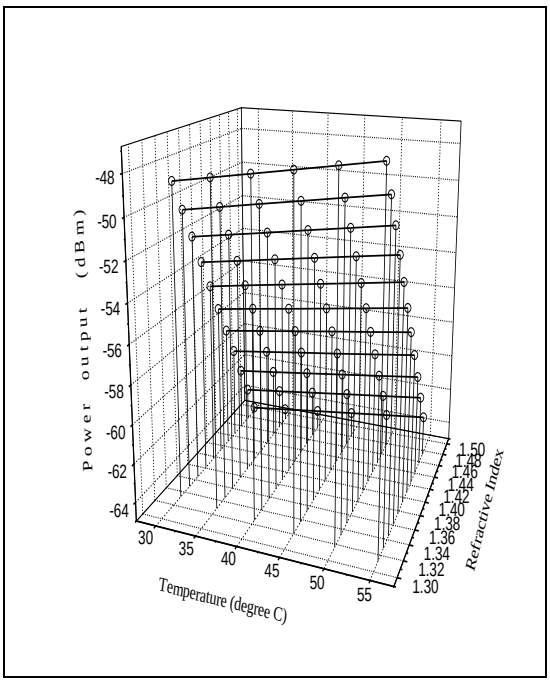

Fig.3.58: Variation of 3 parameters for (benzene+methanol) Using 0.5 mm dia U shaped glass rod

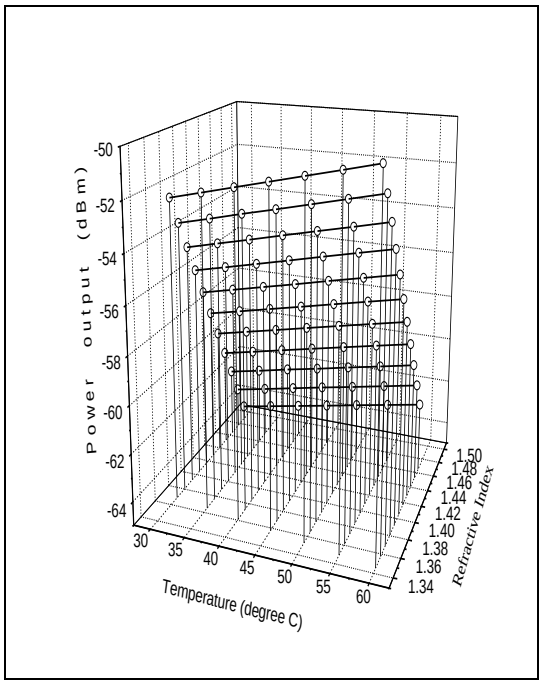

Fig.3.59: Variation of 3 parameters for (benzene +Propanol) using 0.5 mm dia U shaped glass rod

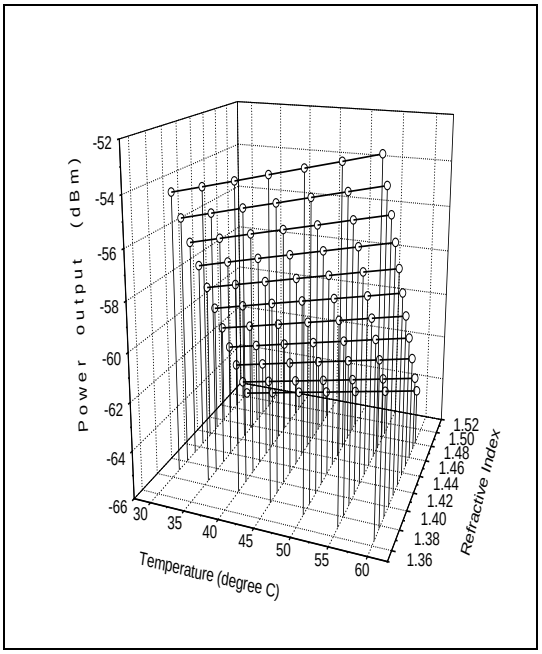

Fig.3.60: Variation of 3 parameters for (benzene+butanol). Using 0.5 mm dia U shaped glass rod

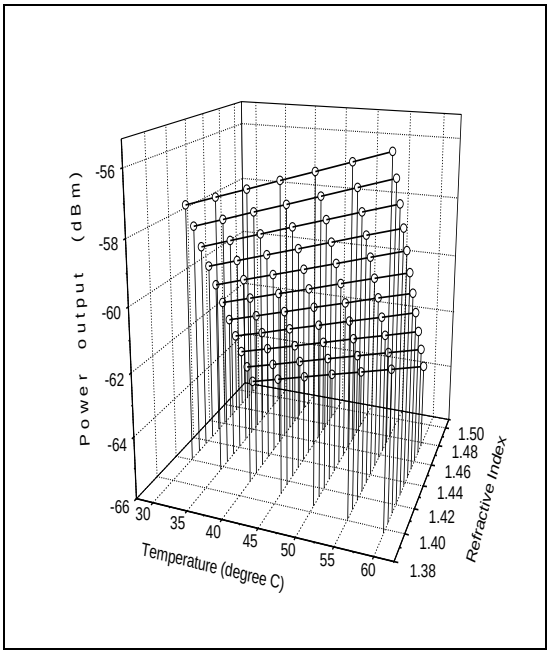

Fig.3.61: Variation of 3 parameters for (benzene+cyclohexane). using 0.5 mm dia U shaped glass rod

Table 3.37: Consolidated data of R.I. and power output at 35°C for all four (benzene+methanol, benzene+propanol, benzene+butanol, benzene+cyclohexane) using 0.5 mm dia U shaped glass rod (Free space power output:-45.0dBm)

SL. No.	Refractive Index				Power output at 35°C			
	C_6H_6 + CH_3OH	C_6H_6 + C_3H_8O	C_6H_6 + $CH_3(CH_2)_3OH$	C_6H_6 + C_6H_{12}	C_6H_6 + CH_3OH	C_6H_6 + C_3H_8O	C_6H_6 + $CH_3(CH_2)_3OH$	C_6H_6 + C_6H_{12}
1	1.298				-46.1			
2	1.325				-46.4			
3	1.338				-47.0			
4	1.352				-47.4			
5		1.357				-47.5		
6	1.369	1.369			-47.8	-47.8		
7		1.379				-48.1		
8	1.388				-48.2			
9		1.391	1.391			-48.4	-48.3	
10			1.393				-48.5	
11		1.401				-48.6		
12			1.402				-48.7	
13	1.404				-48.7			
14				1.407				-48.7
15			1.411				-48.9	
16		1.413				-48.9		
17	1.420		1.420	1.420	-49.0		-49.0	-49.0
18		1.424				-49.2		
19				1.426				-49.2
20			1.428				-49.2	
21				1.433				-49.3
22	1.436	1.436			-49.4	-49.4		
23			1.440	1.440			-49.4	-49.4
24		1.447		1.447		-49.6		-49.6
25			1.451				-49.7	
26	1.452				-49.7			
27				1.454				-49.8
28		1.460				-50.0		
29			1.461	1.461			-50.0	-50.0
30	1.470			1.470	-50.2			-50.2
31			1.473				-50.2	
32				1.477				-50.4
33		1.479				-50.3		
34			1.481				-50.4	
35				1.486				-50.6

Table 3.38: Consolidated data of R.I. and power output at 40°C for all four (benzene+methanol, benzene+propanol, benzene+butanol, benzene+cyclohexane) using 0.5 mm dia U shaped glass rod (Free space power output:-45.0dBm)

SL. No.	Refractive Index				Power output at 40°C			
	C_6H_6 + CH_3OH	C_6H_6 + C_3H_8O	C_6H_6 + $CH_3(CH_2)_3OH$	C_6H_6 + C_6H_{12}	C_6H_6 + CH_3OH	C_6H_6 + C_3H_8O	C_6H_6 + $CH_3(CH_2)_3OH$	C_6H_6 + C_6H_{12}
1	1.277				-45.6			
2	1.298				-46.1			
3	1.325				-46.4			
4	1.338				-47.0			
5		1.349				-47.3		
6	1.352				-47.4			
7		1.357				-47.5		
8	1.369	1.369			-47.8	-47.8		
9			1.374				-47.9	
10		1.379				-48.1		
11	1.388				-48.2			
12		1.391	1.391			-48.4	-48.3	
13			1.393				-48.5	
14		1.401				-48.6		
15			1.402				-48.7	
16				1.403				-48.6
17	1.404				-48.7			
18				1.407				-48.7
19			1.411				-48.9	
20		1.413				-48.9		
21	1.420		1.420	1.420	-49.0		-49.0	-49.0
22		1.424				-49.2		
23				1.426				-49.2
24			1.428				-49.2	
25				1.433				-49.3
26	1.436	1.436			-49.4	-49.4		
27			1.440	1.440			-49.4	-49.4
28		1.447		1.447		-49.6		-49.6
29			1.451				-49.7	
30	1.452				-49.7			
31				1.454				-49.8
32		1.460				-50.0		
33			1.461	1.461			-50.0	-50.0
34				1.470				-50.2
35			1.473				-50.2	
36				1.477				-50.4

Table 3.39: Consolidated data of R.I. and power output at 45°C for all four (benzene+methanol, benzene+propanol, benzene+butanol, benzene+cyclohexane) using 0.5 mm dia U shaped glass rod (Free space power output:-45.0dBm)

SL. No.	Refractive Index				Power output at 45°C			
	C_6H_6 + CH_3OH	C_6H_6 + C_3H_8O	C_6H_6 + $CH_3(CH_2)_3OH$	C_6H_6 + C_6H_{12}	C_6H_6 + CH_3OH	C_6H_6 + C_3H_8O	C_6H_6 + $CH_3(CH_2)_3OH$	C_6H_6 + C_6H_{12}
1	1.260				-45.2			
2	1.277				-45.6			
3	1.298				-46.1			
4	1.325				-46.4			
5		1.332				-46.9		
6	1.338				-47.0			
7		1.349				-47.3		
8	1.352				-47.4			
9		1.357				-47.5		
10			1.365				-47.7	
11	1.369	1.369			-47.8	-47.8		
12			1.374				-47.9	
13		1.379				-48.1		
14	1.388				-48.2			
15		1.391	1.391	1.391		-48.4	-48.3	-48.3
16			1.393				-48.5	
17		1.401				-48.6		
18			1.402				-48.7	
19				1.403				-48.6
20	1.404				-48.7			
21				1.407				-48.7
22			1.411				-48.9	
23		1.413				-48.9		
24	1.420		1.420	1.420	-49.0		-49.0	-49.0
25		1.424				-49.2		
26				1.426				-49.2
27			1.428				-49.2	
28				1.433				-49.3
29	1.436	1.436			-49.4	-49.4		
30			1.440	1.440			-49.4	-49.4
31		1.447		1.447		-49.6		-49.6
32			1.451				-49.7	
33				1.454				-49.8
34			1.461	1.461			-50.0	-50.0
35				1.470				-50.2

Table 3.40: Consolidated data of R.I. and power output at 50°C for all four (benzene+methanol, benzene+propanol, benzene+butanol, benzene+cyclohexane) using 0.5 mm dia U shaped glass rod (Free space power output:-45.0dBm)

SL. No.	Refractive Index				Power output at 50°C			
	C_6H_6 + CH_3OH	C_6H_6 + C_3H_8O	C_6H_6 + $CH_3(CH_2)_3OH$	C_6H_6 + C_6H_{12}	C_6H_6 + CH_3OH	C_6H_6 + C_3H_8O	C_6H_6 + $CH_3(CH_2)_3OH$	C_6H_6 + C_6H_{12}
1	1.239				-44.7			
2	1.260				-45.2			
3	1.277				-45.6			
4	1.298				-46.1			
5		1.323				-46.7		
6	1.325				-46.4			
7		1.332				-46.9		
8	1.338				-47.0			
9		1.349	1.349			-47.3	-47.3	
10	1.352				-47.4			
11		1.357				-47.5		
12			1.365				-47.7	
13	1.369	1.369			-47.8	-47.8		
14			1.374				-47.9	
15		1.379				-48.1		
16				1.386				-48.2
17	1.388				-48.2			
18		1.391	1.391	1.391		-48.4	-48.3	-48.3
19			1.393				-48.5	
20		1.401				-48.6		
21				1.403				-48.6
22			1.402				-48.7	
23	1.404				-48.7			
24				1.407				-48.7
25			1.411				-48.9	
26		1.413				-48.9		
27	1.420		1.420	1.420	-49.0		-49.0	-49.0
28		1.424				-49.2		
29				1.426				-49.2
30			1.428				-49.2	
31				1.433				-49.3
32		1.436				-49.4		
33			1.440	1.440			-49.4	-49.4
34				1.447				-49.6
35			1.451				-49.7	
36				1.454				-49.8
37				1.461				-50.0

Table 3.41: Consolidated data of R.I. and power output at 55°C for all four (benzene+methanol, benzene+propanol, benzene+butanol, benzene+cyclohexane) using 0.5 mm dia U shaped glass rod (Free space power output:-45.0dBm)

SL. No.	Refractive Index				Power output at 55°C			
	C_6H_6 + CH_3OH	C_6H_6 + C_3H_8O	C_6H_6 + $CH_3(CH_2)_3OH$	C_6H_6 + C_6H_{12}	C_6H_6 + CH_3OH	C_6H_6 + C_3H_8O	C_6H_6 + $CH_3(CH_2)_3OH$	C_6H_6 + C_6H_{12}
1	1.227				-44.4			
2	1.239				-44.7			
3	1.260				-45.2			
4	1.277				-45.6			
5	1.298				-46.1			
6		1.307				-46.3		
7		1.323				-46.7		
8	1.325				-46.8			
9		1.332				-46.9		
10	1.338				-47.0			
11			1.340				-47.1	
12		1.349	1.349			-47.3	-47.3	
13	1.352				-47.4			
14		1.357				-47.5		
15			1.365				-47.7	
16	1.369	1.369			-47.8	-47.8		
17			1.374				-47.9	
18				1.378				-48.0
19		1.379				-48.1		
20				1.386				-48.2
21	1.388				-48.2			
22		1.391	1.391	1.391		-48.3	-48.3	-48.3
23			1.393				-48.5	
24		1.401				-48.6		
25			1.402				-48.7	
26				1.403				-48.6
27	1.404				-48.7			
28				1.407				-48.7
29			1.411				-48.9	
30		1.413				-48.9		
31			1.420	1.420			-49.0	-49.0
32		1.424				-49.2		
33				1.426				-49.2
34			1.428				-49.2	
35				1.433				-49.3
36			1.440	1.440			-49.4	-49.4
37				1.447				-49.6
38				1.454				-49.8

Table 3.42: Consolidated data of R.I. and power output at 60°C for all four (benzene+methanol, benzene+propanol, benzene+butanol, benzene+cyclohexane) using 0.5 mm dia U shaped glass rod (Free space power output:-45.0dBm)

SL. No.	Refractive Index			Power output at 60°C		
	C_6H_6 + C_3H_8O	C_6H_6 + $CH_3(CH_2)_3OH$	C_6H_6 + C_6H_{12}	C_6H_6 + C_3H_8O	C_6H_6 + $CH_3(CH_2)_3OH$	C_6H_6 + C_6H_{12}
1	1.294			-46.0		
2	1.307			-46.3		
3	1.323	1.323		-46.7	-46.7	
4	1.332			-46.9		
5		1.340			-47.1	
6	1.349	1.349		-47.3	-47.3	
7	1.357			-47.5		
8		1.365			-47.7	
9	1.369			-47.8		
10			1.370			-47.8
11		1.374			-47.9	
12			1.378			-48.0
13	1.379			-48.1		
14			1.386			-48.2
15	1.391	1.391	1.391	-48.3	-48.3	-48.3
16		1.393			-48.5	
17	1.401			-48.6		
18		1.402			-48.7	
19			1.403			-48.6
20			1.407			-48.7
21		1.411			-48.9	
22	1.413			-48.9		
23		1.420	1.420		-49.0	-49.0
24			1.426			-49.2
25		1.428			-49.2	
26			1.433			-49.3
27			1.440			-49.4
28			1.447			-49.6

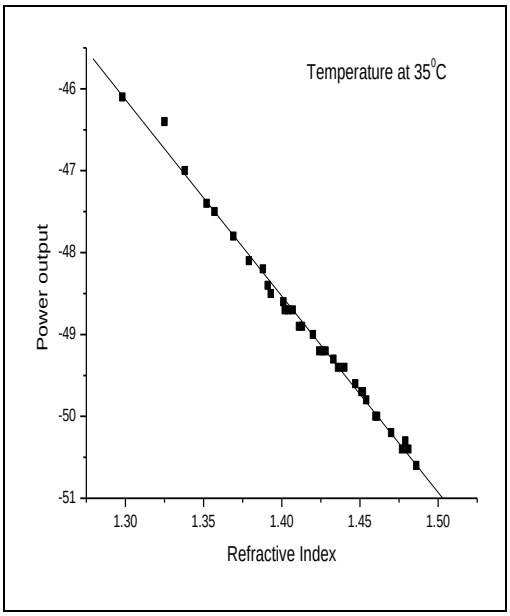

Fig.3.62: power output and refractive index
All of four mixtures at 35°C
Using 0.5 mm dia U shaped glass rod

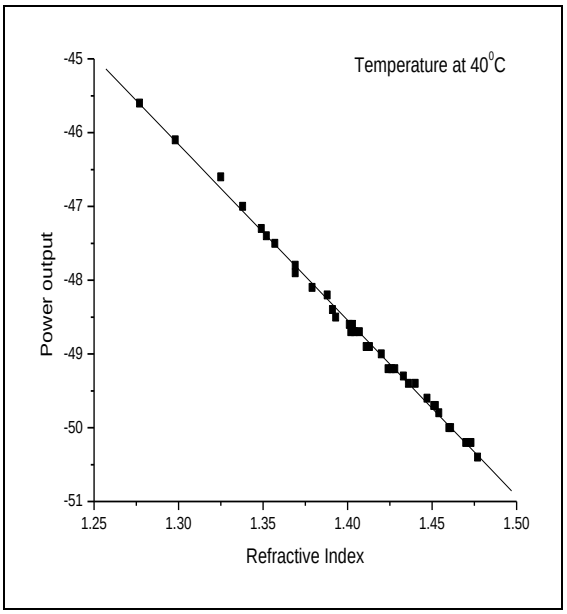

Fig.3.63: power output and refractive index
All of four mixtures at 40°C
using 0.5 mm dia U shaped glass rod

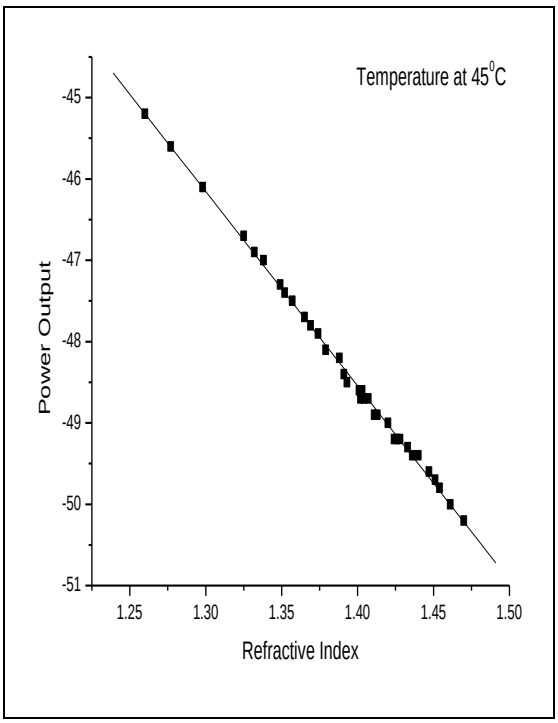

Fig.3.64: power output and refractive index
All of four mixtures at 45°C
Using 0.5 mm dia U shaped glass rod

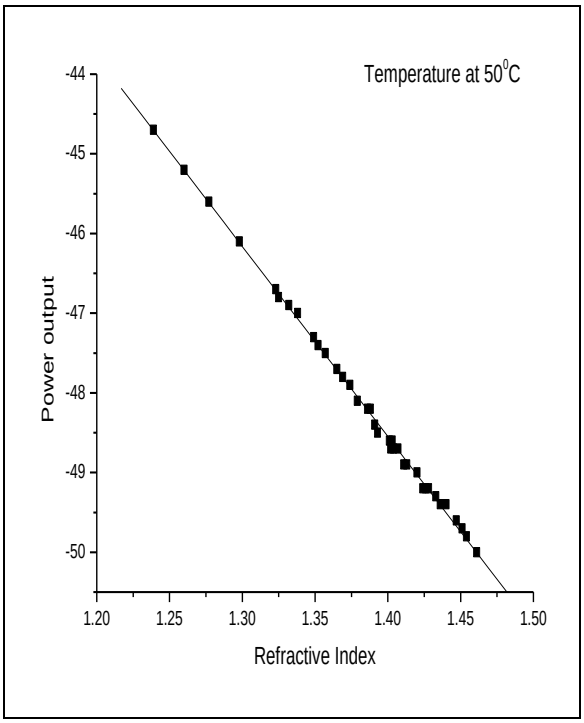

Fig.3.65: power output and refractive index
All of four mixtures at 50°C
using 0.5 mm dia U shaped glass rod

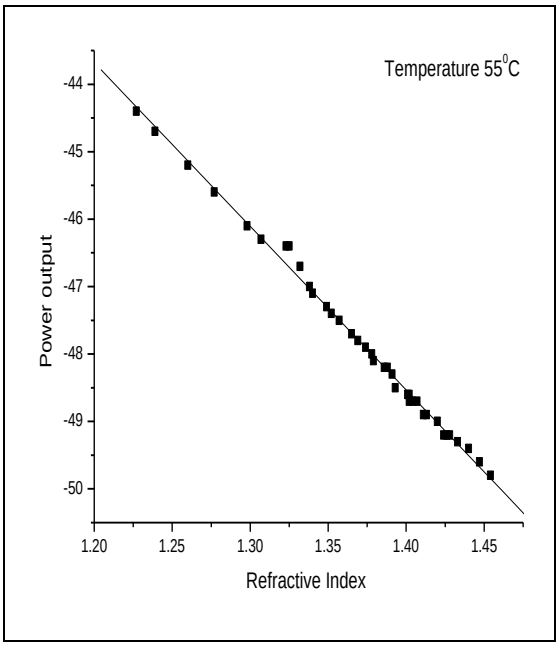

Fig.3.66: power output and refractive index Data of All four mixtures at 45°C Using 0.5 mm dia U shaped glass rod

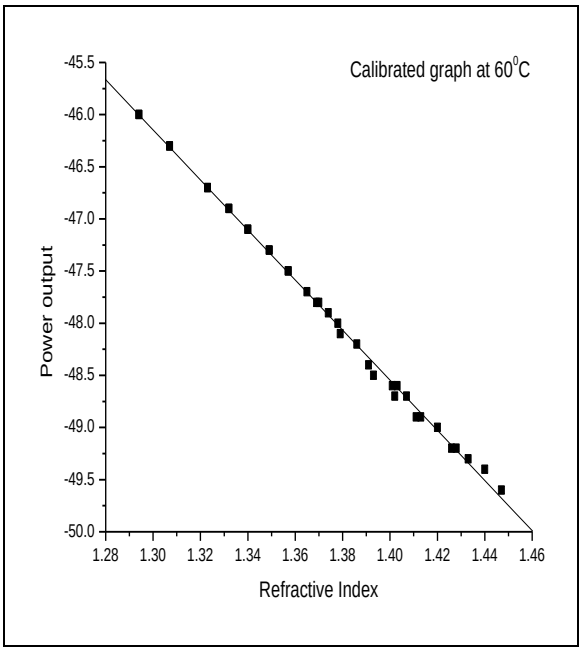

Fig.3.67: power output and refractive index data of All four mixtures at 50°C using 0.5 mm dia U shaped glass rod

CHAPTER 4

Refractive index of Edible and Medicinal Oils

4.1 Introduction

Any greasy substance that is liquid at room temperature and insoluble in water is called oil. It may be volatile or nonvolatile oil, essential oil, or mineral oil**.** An oil is any substance that is in a viscous liquid state at ambient temperatures or slightly warmer, and is both hydrophobic (immiscible with water) and lipophilic (miscible with other oils). This general definition includes compound classes with otherwise unrelated chemical structures, properties, and uses, including vegetable oils, petrochemical oils, and volatile essential oils. Oil is a non-polar substance. Any of the numerous plants, either under cultivation or growing wild, are used as sources of oil. Oil plants include trees such as palm, herbaceous plants such as flax, and even fungi.

Oil is a scientific term, and is used to refer to certain diverse and non related compounds sharing the same physical properties such as viscosity and a hydrophobic nature, while ignoring unrelated compounds. The compounds found in cooking oil are chemically very similar, almost identical, to those found in butter and very different from those found in diesel, but while diesel is oil, butter is not. Indeed diesel is once again very similar to natural gas, but gas is certainly not oil! This disparity stems partly from the fact that oils must be liquid at room temperature, and thus only certain liquid chemicals in many related families are recognized, collectively, as 'oil'. Scientists, instead of using the term 'oil', adopt the terms lipids and other terms such as alkanes and alkenes, to denote them instead.

Many edible vegetable and animal oils, and also fats, are used for various purposes in cooking and food preparation. In particular, many foods are fried in oil much hotter than boiling water. Oils are also used for flavoring and for modifying the texture of foods. Health advantages are claimed for a number of specific oils and some are known

to be harmful to the health. Almost all oils burn in air generating heat, which can be used directly, or converted into other forms of energy by various means. Electricity, for example, can be generated from the combustion of oils through a steam-powered generator. Oils are used as fuels for heating, lighting, powering combustion engines, and other purposes. Oils used for this purpose nowadays are usually derived from petroleum, biological oils such as biodiesel are gaining importance in the usage of many areas. Many oils have higher boiling points than water and are electrical insulators, making them useful for liquid cooling systems, especially where electricity is used.

Due to their non-polarity, oils do not easily adhere to other substances. This makes them useful as lubricants for various engineering purposes. Mineral oils are more suitable than biological oils, which degrade rapidly in most environmental conditions. Color pigments can be easily suspended in oil, making it suitable as supporting medium for paints. The slow drying process and miscibility of oil facilitates a realistic style. This method has been used since the 15th century. Crude oil can be processed into plastics and other substances. Oils have been used throughout history as a fragrant or religious medium. Oil is often seen as a spiritually purifying agent and is used in religious ceremonies.

Oils extracted from plants have been used in many cultures, since ancient time. Fatty acids play an important role in the life and death of cardiac cells because they are essential fuels for mechanical and electrical activities of the heart. Many vegetable oils are consumed directly, or used directly as ingredients in food - a role that they share with some animal fats, including butter and ghee. The oils serve a number of purposes in this role. Oils can serve to make other ingredients stick together less. Some oils oil may be chosen specifically for the flavor they impart. Oils can also carry flavors of other ingredients, since many flavors are present in chemicals that are soluble in oil.

Vegetable oils are used as an ingredient or component in many manufactured products. Many vegetable oils are used to make soaps, skin products, perfumes and other personal care and cosmetic products. Some oils are particularly suitable as drying agents, and are used in making paints and other wood treatment products. Dammar oil a mixture

of linseed oil and dammar resin, is used almost exclusively in treating the hulls of wooden boats.

Vegetable oils are increasingly being used in the electrical industry as insulators as vegetable oils are non-toxic to the environment, biodegradable if spilled and have high flash and fire points. However, vegetable oils have issues with chemical stability, so they are generally used in systems where they are not exposed to oxygen and are more expensive than crude oil distillate. A synthetic tetra ester, like a vegetable oil is found in a natural ester, and is manufactured by an alcohol plus acid reaction. Tetra esters generally have high stability to oxidation and have found use as engine lubricants. Vegetable oil is being used to produce bio-degradable hydraulic fluid and lubricant. Common vegetable oil has also been used experimentally as a cooling agent in PCs. One limiting factor in industrial uses of vegetable oils is that all such oils eventually chemically decompose turning rancid. Oils that are more stable, such as Ben oil or mineral oil, are preferred for some industrial uses. Vegetable-based oils, like castor oil, have been used as medicine and as lubricants for a long time. Castor oil has numerous industrial uses, primarily due to the presence of hydroxyl groups on the fatty acid chains. Castor oil, and other vegetable oils which have been chemically modified to contain hydroxyl groups, are becoming increasingly important in the production of polyurethane plastic for many applications. These modified vegetable oils are known as natural oil polyols. Vegetable oils are also used to make biodiesel, which can be used like conventional diesel. Some vegetable oil blends are used in unmodified vehicles but straight vegetable oil, also known as pure plant oil, needs specially prepared vehicles which have a method of heating the oil to reduce its viscosity. The vegetable oil economy is growing and the availability of biodiesel around the world is increasing.

4.2 About oils

All oils, with their high carbon and hydrogen content, can be traced back to organic sources. Mineral oils are, found in porous rocks underground. Through various geochemical processes, this material was converted to mineral oil, or petroleum, and its components, such as kerosene, paraffin waxes, gasoline, and diesel and such. These are

classified as mineral oils as they derived from underground geologic locations, ranging from rocks, to underground traps, to sands.

Other oily substances can also be found in the environment, the most well-known being tar, occurring naturally underground or, where there are leaks, in tar pits. Others include asphalt and bitumen. Petroleum and other mineral oils, specifically labelled as petrochemicals.

Oils are also produced by plants, animals and other organisms through organic processes. The scientific term for oils, fats, waxes, cholesterol and other oily substances found in living things and their secretions, is lipids. Lipids, repel, or refuse to dissolve, in water, and are however comfortably miscible in other liquid lipids. They also have a high carbon and hydrogen content, and are considerably lacking in oxygen compared to other organic compounds.

Vegetable fats and oils are substances derived from plants that are composed of triglycerides. Nominally, oils are liquid at room temperature, and fats are solid, a dense brittle fat is called a wax. Although many different parts of plants may yield oil, in actual commercial practice oil is extracted primarily from the seeds of oilseed plants. Triglyceride vegetable fats and oils include not only edible, but also inedible vegetable fats and oils such as processed linseed oil, tung oil, and castor oil, used in lubricants, paints, cosmetics, pharmaceuticals, and other industrial purposes.

Triglyceride-based vegetable fats and oils can be transformed through partial or complete hydrogenation into fats and oils of higher melting point. The hydrogenation process involves sparging the oil at high temperature and the oils viscosity and melting point increase with temperature. Fragrance oils, also known as aroma oils, aromatic oils, and flavor oils, are blended synthetic aroma compounds or natural essential oils that are diluted with a carrier like propylene glycol, vegetable oil, or mineral oil. Aromatic oils are used in perfumery, cosmetics, flavoring of food, and in aromatherapy.

The Fragrance wheel is a relatively new classification method created in 1983 by Michael Edwards, a consultant in the perfume industry, who designed his own scheme of fragrance classification. The new scheme was created in order to simplify fragrance classification and naming scheme. The five standard families consist of Floral, Oriental, Woody, Fougere, and Fresh, with the former four families being more "classic" while the latter consisting of newer bright and clean smelling citrus and oceanic fragrances that have arrived due to improvements in fragrance technology. With the exception of the Fougere family, each of the families are in turn divided into three sub-groups and arranged around a wheel.

The Fougere family is placed at the center of this wheel since they are a large family of scents that usually contain fragrance elements from each of the other four families; citrus from the fresh family, oak moss and woods from the woody family, coumarin and incense from the Oriental family, and lavender from the floral family. Perfume is a mixture of fragrant essential oils and aroma compounds, fixatives, and solvents used to give the human body, objects, and living spaces a pleasant smell.

An essential oil is any concentrated, hydrophobic liquid containing volatile aroma compounds from plants, which are called aromatic herbs or aromatic plants. The term essential indicates that the oil carries distinctive scent (essence) of the plant, not that it is an especially important or fundamental substance. Essential oils do not as a group needed to have any specific chemical properties in common, beyond conveying characteristic fragrances. Essential oils are generally extracted by distillation. Other processes include expression, or solvent extraction. They are used in perfumes and cosmetics, for flavoring food and drink, and for scenting incense and household cleaning products. Various essential oils have been used medicinally at different periods in history.

Today, most common essential oils, such as lavender, peppermint, and eucalyptus, are distilled. Raw plant material, consisting of the flowers, leaves, wood, bark, roots, seeds, or peel, is put into an alembic (distillation apparatus) over water. As the water is heated the steam passes through the plant material, vaporizing the volatile compounds.

The vapors flow through a coil where they condense back to liquid, which is then collected in the receiving vessel. Most citrus peel oils are usually expressed mechanically, or cold-pressed. Due to the large quantities of oil in citrus peel, prior to the discovery of distillation, essential oils were extracted by pressing.

Most flowers contain very little volatile oil to undergo expression and their chemical components are too delicate and easily denatured by the high heat used in steam distillation. Instead, a solvent such as hexane or supercritical carbon dioxide is used to extract the oils. Often ethyl alcohol, which only dissolves the fragrant low-molecular weight compounds, is used to extract the fragrant oil. Aromatherapy is a form of alternative medicine, in which healing effects are ascribed to the aromatic compounds in essential oils and other plant extracts. Many common essential oils have medicinal properties that have been applied in folk medicine since ancient times and are still widely used today. Essential oils are usually lipophilic compounds that usually are not miscible with water. Instead, they can be diluted in solvents like pure ethanol (alcohol), polyethylene glycol, or oils.

4.2.1 Sources

Essential oils are derived from various sections of plants. Some of the sources of essential oils are seeds, bark, wood, leaves, flowerss, peel, and roots. Plants have long been used in perfumery as a source of essential oils and aroma compounds. These aromatics are usually secondary metabolites produced by plants as protection against herbivores, infections, as well as to attract pollinators. Plants are by far the largest source of fragrant compounds used in perfumery.

Commonly used barks includes, cinnamon and cascarilla. The fragrant oil in sassafras root bark is also used either directly or purified for its main constituent, safrole, which is used in the synthesis of other fragrant compounds such as helional. Undoubtedly the largest source of aromatics includes the flowers of several species of rose and jasmine, as well as osmanthus, mimosa, tuberose, as well as the blossoms of citrus and ylang-ylang trees. Although not traditionally thought of as a flower, the unopened flower buds of the clove are also commonly used. Orchid flowers are not

commercially used to produce essential oils or absolutes, except in the case of vanilla, an orchid, which must be pollinated first and made into seed pods before use in perfumery.

Fresh fruits such as apples, strawberries, cherries unfortunately do not yield the expected odors when extracted; if such fragrance notes are found in a perfume, they are synthetic. Notable exceptions include litsea cubeba, vanilla, and juniper berry. The most commonly used fruits yield their aromatics from the rind; they include citrus such as oranges, lemons, limes, and grapefruit.

Commonly used for perfumery are lavender leaf, patchouli, sage, violets, rosemary, and citrus leaves. Sometimes leaves are valued for the "green" smell they bring to perfumes, examples of this include hay and tomato leaf. Resins have been widely used in incense and perfumery. Highly fragrant and antiseptic resins and resin-containing perfumes have been used by many cultures as medicines for a large variety of ailments. Commonly used resins in perfumery include labdanum, frankincense/olibanum, myrrh, Peru balsam, gum benzoin. Commonly used terrestrial portions in perfumery include iris rhizomes, vetiver roots, and various rhizomes of the ginger family. Commonly used seeds include tonka bean, coriander, caraway, cocoa, nutmeg, mace, cardamom, and anise. Highly important in providing the base notes to a perfume, wood oils and distillates are indispensable in perfumery. Commonly used woods include sandalwood, rosewood, agarwood, birch, cedar, juniper, and pine.

Animal sources: Ambergris Lumps of oxidized fatty compounds, whose precursors were secreted and expelled by the Sperm Whale. Ambergris is commonly referred to as amber in perfumery and should not be confused with yellow amber, which is used in jewelry. Civet also called Civet Musk, this is obtained from the odorous sacs of the civets, animals in the family Viverridae, related to the Mongoose. Honeycomb distilled from the honeycomb of the Honeybee. Musk originally derived from the musk sacs from the Asian musk deer; it has now been replaced by the use of synthetic musk.

Other natural sources Commonly used lichens include oakmoss and treemoss thalli. Seaweed: Distillates are sometimes used as essential oil in perfumes. An example of

commonly used seaweed is Fucus vesiculosus, which is commonly referred to as bladder wrack. Natural seaweed fragrances are rarely used due to their higher cost and lower potency than synthetics. Modern perfumes are almost exclusively made from synthetic odorants that are commonly synthesized from coal-tar and petroleum distillates, pine resins, or other relatively cheap organic feedstock.

4.2.2 Extraction

The modern way of processing vegetable oil is by chemical extraction, using solvent extracts, which produces higher yields and is quicker and less expensive. The most common solvent is petroleum-derived hexane. This technique is used for most of the newer industrial oils such as soybean and corn oils. Another way is physical extraction, which does not use solvent extracts. It is made the traditional way using several different types of mechanical extraction. This method is typically used to produce the more traditional oils. Expeller-pressed extraction is one type, and there are two other types that are both the screw press and the ram press.

Supercritical carbon dioxide can also be used for the extraction purpose and is non toxic Crude oil, straight from the crushing operation, is not considered edible in the case of most oilseeds. Researchers at Central Soya discovered that a trypsin inhibitor in soybeans could be deactivated by toasting the meal, and both licensed their invention, and sold soy meal augmented with vitamins and minerals as Master Mix, a product for farmers to mix with their own grain to produce a high quality feed. Some of the oil is further processed by carefully filtering the oil at near-freezing temperatures, winter oil is produced. This oil is sold to manufacturers of salad dressings, so that the dressings do not turn cloudy when refrigerated. The oil may be partially hydrogenated to produce various ingredient oils. Lightly hydrogenated oils have very similar physical characteristics to regular soy oil, but are more resistant to becoming rancid.

In the processing of edible oils, the oil is heated under vacuum to near the smoke point, and water is introduced at the bottom of the oil. The water immediately is converted to steam, which bubbles through the oil, carrying with it any chemicals which are water-soluble. The steam sparging removes impurities that can impart unwanted

flavors and odors to the oil. Before perfumes can be composed, the odorants used in various perfume compositions must first be obtained. Synthetic odorants are produced through organic synthesis and purified. Odorants from natural sources require the use of various methods to extract the aromatics from the raw materials. The results of the extraction are eitheressential oils, absolutes, concretes, or butters, depending on the amount of waxes in the extracted product.

The most used and economically important technique for extracting aromatics in the modern perfume industry is maceration. Raw materials are submerged in a solvent that can dissolve the desired aromatic compounds. Maceration lasts anywhere from hours to months. Fragrant compounds for woody and fibrous plant materials are often obtained in this manner as are all aromatics from animal sources. The technique can also be used to extract odorants that are too volatile for distillation or easily denatured by heat. Commonly used solvents for maceration/solvent extraction include hexane, and dimethyl ether. The product of this process is called a concrete. A relatively new technique for extracting fragrant compounds from a raw material, which often employs supercritical CO_2, supercritical fluid extraction. Due to the low heat of process and the relatively non-reactive solvent used in the extraction, the fragrant compounds derived often closely resemble the original odor of the raw material.

A type of solvent extraction used to extract fragrant compounds directly from dry raw materials, as well as the impure oily compounds materials resulting from solvent extraction or enfleurage. Ethanol extraction is not used to extract fragrance from fresh plant materials since these contain large quantities of water, which will also be extracted into the ethanol. A common technique for obtaining aromatic compounds from plants, such as orange blossoms and roses is Distillation. The raw material is heated and the fragrant compounds are re-collected through condensation of the distilled vapor. Steam from boiling water is passed through the raw material, which drives out their volatile fragrant compoundsis called steam distillation. The condensate from distillation is settled in a Florentine flask. This allows for the easy separation of the fragrant oils from the water. The water collected from the condensate, which retains some of the fragrant compounds and oils from the raw material is called hydrosol and sometimes sold. This is

most commonly used for fresh plant materials such as flowers, leaves, and stems. In dry/destructive distillation, the raw materials are directly heated in a still without a carrier solvent such as water. Fragrant compounds that are released from the raw material by the high heat often undergo anhydrous pyrolysis, which results in the formation of different fragrant compounds, and thus different fragrant notes. This method is used to obtain fragrant compounds from fossil amber and fragrant woods where an intentional burned or toasted odor is desired.

Raw material is squeezed or compressed and the oils are collected in the process of Expression. Of all raw materials, only the fragrant oils from the peels of fruits in the citrus family are extracted in this manner since the oil is present in large enough quantities as to make this extraction method economically feasible. Enfleurage is the absorption of aroma materials into wax and then extracting the odorous oil with ethyl alcohol. Extraction by enfleurage was commonly used when distillation was not possible due to the fact that some fragrant compounds denature through high heat. This technique is not commonly used in the present day industry due to its prohibitive cost and the existence of more efficient and effective extraction methods. Although fragrant extracts are known to the general public as the generic term essential oils, a more specific language is used in the fragrance industry to describe the source, purity, and technique used to obtain a particular fragrant extract. Of these extracts, only absolutes, essential oils, and tinctures are directly used to formulate perfumes. Absolute is the fragrant materials, that are purified from a pommade or concrete by soaking them in ethanol. By using a slightly hydrophilic compound such as ethanol, most of the fragrant compounds from the waxy source materials can be extracted without dissolving any of the fragrantless waxy molecules. Absolutes are usually found in the form of an oily liquid.

Fragrant materials that have been extracted from raw materials through solvent extraction using volatile hydrocarbons is called concrete. Concretes usually contain a large amount of wax due to the ease in which the solvents dissolve various hydrophobic compounds. As such concretes are usually further purified through distillation or ethanol based solvent extraction. Concretes are typically either waxy or resinous solids or thick oily liquids. Fragrant materials that have been extracted from a source material directly

through distillation or expression and obtained in the form of an oily liquid is essential oil. Oils extracted through expression are sometimes called expression oils.

Pomade is a fragrant mass of solid fat created from the enfleurage process, in which odorous compounds in raw materials are adsorbed into animal fats. Pommades are found in the form of an oily and sticky solid. Tincture is fragrant materials produced by directly soaking and infusing raw materials in ethanol. Tinctures are typically thin liquids. Natural ingredients vary by the times and locations where they are harvested. Perfume composed of only natural materials are more expensive. It's much more difficult to produce an equivalent odor over years. The perfumer has to equalize the natural variations of the ingredients, the user wants a steady product. Some natural aromatics contain allergens or even carcinogenic compounds. The use of some natural materials, like sandalwood or musk, can lead to species endangerment and illegal trafficking. Natural ingredients have aromas that are highly complex and are difficult or have been impossible to obtain through modern-day synthetics.

The production of synthetic materials may contribute to environmental problems, since their production involve known carcinogens such as aromatic hydrocarbons. Use of synthetic aromatics can make some perfumes available at widely-affordable prices. However, synthetic aromatics as a group are not necessarily cheaper than natural aromatics. There are many newly-created synthetic aromas that bear no olfactory relationship to any natural material. Synthetic aromatics are more consistent than natural aromatics.

Musk was traditionally taken from the male musk deer Moschus moschiferus. This requires the killing of the animal in the process. Although the musk pod is produced only by a young male deer, musk hunters usually did not discriminate between the age and sex of the deers. Due to the high demand of musk and indiscriminate hunting, populations were severely depleted. As a result, the deer is now protected by law and international trade of musk from Moschus moschiferus is prohibited.

4.3 Survey of literature

Charless et al [1] disclosed a fiber optic refractometer for the use in on line measurement of the hydrogenation state of edible oils during the hydrogenation process. It can also be used for the on line measurement of the refractive index of a process liquid.

Thompson et al [2] reported the quality of the oil of sunflower seed from plants infected with head rot caused by Rhizopus app. Free fatty acid content of this oil was 19.4%, compared with 0.8% for oil from seed of healthy plants.

Sheldon wishna et al [3] developed an instrument for the calibration of refractive index of sunflower sample for the identification of sunflower (linoleic, mid – oleic, or high oleic) prior to an NMR oil measurement.

Mayler et al [4] made the comparison between steam distillation and co_2 – extracted essential oils of celery seed (Apium graveolens L.), hop (Humulus lupulus L.), clove bud (syzygium aromaticum (L.) Merill.et L.M. perry), juniper berry (juniperus communis L.), mace (Myristica fragrant Houtt), and ginger (Zingiber officinale roscoe) using free choice odors profiling and standardized fingerprint analysis.

Gonzalez et al [5] proposed the determination of the triglyceride profile by liquid chrometography using propionitrile as the mobile phase to improve their quantification, together with a mathematical algorithm whose binary response determines the presence or absence of hazelnut oil.

Yunus et al [6] developed different methods to measure the refractive index of liquids and oils. Methods such as the Brewster angle, ellipsometry, attenuated internal reflection (ATR), and minimum deviation have been explained and the corresponding equations are derived.

Ingraham et al [7] explained a refractometric method for the determination of oil in coconut and sasame oil cake.

Kalemba et al [8] reviewed the classical methods commonly used for the evaluation of essential oils antibacterial and antifungal activities. This paper gives an overview on the susceptibility of human and food borne bacteria and fungi towards different essential oils and their constituents.

Toloza et al [9] reported the study of the fumigant and repellent properties of essential oils from 16 native and exotic plants in Argentina, and 21 chemical components against permethrin – resistant head lice from Argentine.

Bird et al [10] investigated the effect of a wide range of fragrance raw materials on skin irritation concluding that their inclusion into personal care products could improve product mildness.

Ashok kumar et al [11] explained agar disc diffusion method for antimicrobial action on staphylococcus aureus, bacillus cereus, salmonella typhi and shigella dysentery by using ethanol extract and essential oil of osmanthus fragrans (Lour) family (oleaccae).

Nagalakshmi et al [12] tested the essential oils of chukrasia tabularis and Melia dubia for their antimicrobial activity against ten different pathogenic micro-organisms responsible for human pathologies using standard antimicrobial assays.

Mondal et al [13] presented the investigation of the antifungal activity of essential oils obtained from fresh and dried leaves of O. Sanctum against clinical isolates of entieric bacteria i.e., Escherichia coli, shigella sp. and salmonella typhi and yeast (candida al bicans).

Rahman et al [14] studied the antifungal activity of the resulting essential oils against various pathogenic fungi (Aspergillus flavus, A. niger, candida albicans, Fusarium oxysporum var. lycopersici, Microsporum canis, psendallescheria boydii, Trichopyton mentagrophytes and T. simii).

Chianu et al [15] evaluated a method to determine the improved soybean varieties that if recommended to the farmers would have a high probability of adoption, a farmer participatory approach was used to evaluate 12 soybean varieties at full podding in five locations (oyani, riana, kasewe, akiites, and mabole) in western kenya.

Dexian et al [16] reviewed the root gravisensing structures and theories explaining root growth geotropism in directions of genetics, physilogy, biochemistry, and environmental influence.

Razavi et al [17] studied the respective physical properties of watermelon seeds of three major local iranian varieties, sarakhsi, kolaleh and red, at the moisture content of 4.55, 4.75 and 5.02% (w.b.).

Ashaye et al [18] reported the soybean quality attributes by processing it from four popular varieties and evaluated for chemical indexes and sensory characteristics by untrained male and female adults.

Muhammad et al [19] described the antimicrobial properties of essential oil of Foeniculum vulgare by using disk diffusion as well as minimum inhibitory concentration (MIC) method.

Ducel et al [20] reported the study of the interfacial properties of the plant proteins arabic gum coacervates, which are involved in encapsulation processes based on complex coacervation.

Foster et al [21] explained the efficiency boosting effect on water in oil microemulsions with droplet microstuctures which would provide confined comfortments in which chemical reaction of biological macromolecules can be performed on a single molecule level.

Joshi et al [22] reported a phytochemical study of the rhizome essential oils of four different Hedychium species by means of GC and GC/MS analysis.

Canakci et al [23] presented a review on both biodiesel productions from various feed stocks and their effects on the fuel properties.

Lin et al [24] emphesized the effect of oil phase transition on freeze/thaw – induced demulsification of water –in – oil emulsions.

Totani et al [25] proposed the weight reducing effect of the oil heated with gluten by removing traces of heated gluten from the oil. The gluten and heated oil groups showed no gross symptoms attributable to the experimental oils but had a slowed body weight increase.

Hassan et al [26] studied the physical and chemical characteristics of the bio oils by gas chromatography –mass spectrometry and Fourier transform infrared techniques.

Sing et al [27] investigated detoxify polychlorinated biphenyls (PCB) in transformer oils by gamma radiation using cobalt 60 source. The effect of radiation dose and destruction of PCB's in transformer oils was discussed in detail.

Ioan et al [28] studied the behaviour of two grade sunflower oil (pressing coars and extraction coarse sunflower oil, respectively) when using them as ecological lubricants by using the X-ray diffractomentry.

Mahadevan et al [29] reviewed the literature on fats, oils and detergents by studying the characteristics and comparing them from the already available sources.

Felib et al [30] reported the determination of concentration of As, Ba, Ce, Co, Cr, Cs, Eu, Fe, Hg, K, Na, Rb, Sb, Sc, Se, Sr and Zn in almond, sunflower, peanut, sesame, linseed, soy, corn and olive oils, as well as in three margarine brands by using instrumental neutron activation analysis.

4.4 Sample collection and maintenance

For the present investigation, 40 samples of edible and medicinal oils were selected. The oil samples were collected from "Munnalal Dawasaz" a reliable local medical store, which was established in the year 1844. Most of the aromatic or essential oils are volatile in character with reference to their odors and perfumery behavior. Samples were collected in a separate, non reactive plastic container. Throughout the experimentation the samples were stored in a cool and dark place to avoid the unnecessary exposure from sunlight and stray light from other sources. Special bottles (glass/plastic) were used to store them to avoid the chemical reaction of the oils with the containers for a long time. Care is taken to see that the oils are not interacted with the outside environment by making their lids as tight as possible and sealed properly. Care has been taken in terms of cleaning the apparatus immediately after experimentation. The details of oils studied such as scientific name, common name, botanical family, specific gravity, part used, and process of extraction are presented in Table 4.1.

4.5 Description of oils under investigation

1. Coconut oil*:* Coconut oil is tropical oil, with many applications. It is extracted from copra (the dried meat, or kernel, of the). Coconut oil has long been used by natives of the Pacific islands, becoming a valuable commercial product for merchants in the South Seas and South Asia in the 1860s.Coconut oil, also known as coconut butter, is a tropical oil with many applications. It is extracted from dried coconut. Coconut oil is a fat consisting of about 90% saturated fat. The oil contains predominantly medium chain triglycerides Unrefined coconut oil melts at 24-25°C (76°F) and smokes at 170°C (350°F), while refined coconut oil has a higher smoke point of 232°C (450°F).

2. Lavender*:* The Lavenders Lavandula are a genus of about 25-30 species of flowering plants in the mint family, Lamiaceae, native from the Mediterranean region south to tropical Africa and to the southeast regions of India. The genus includes annuals, herbaceous plants, subshrubs, and small shrubs. The native range extends across the Canary Islands, North and East Africa, south Europe and the Mediterranean, Arabia, and India. Because the cultivated forms are planted in gardens world-wide, they are occasionally found growing wild, as garden escapees, well beyond their natural range.

3. Rosemary: Rosemary is a woody, perennial herb with fragrant evergreen needle-like leaves. It is native to the Mediterranean region. It is a member of the mint family Lamiaceae, which also includes many other herbs. Forms range from upright to trailing; the upright forms can reach 1.5 m tall, rarely 2 m. The leaves are evergreen, 2-4 cm long and 2-5 mm broad, green above, and white below with dense short woolly hairs. The flowers are variable in color, being white, pink, purple, or blue. The name rosemary has nothing to do with the rose or the name Mary, but derives from the Latin name rosmarinus, which literally means "dew of the sea", though some think this too may be derived from an earlier name.

4. Moha (mahwa) oil: Madhuca longfolia, commonly known as mahwa or mahua, is an Indian tropical tree found largely in the central and north Indian plains and forests. It is a fast growing tree that grows to approximately 20 meters in height, possesses evergreen or semi-evergreen foliage, and belongs to the family Sapotaceae. It is adapted to arid environoments, being a prominent tree in tropical mixed deciduous forests in India in the states of Jharkhand, Uttar Pradesh, Bihar, Madhya Pradesh, Kerala, Gujarat and Orissa.

5. Almond oil: The Almond is a species of Prunus belonging to the subfamily Prunoideae of the family Rosaceae; within Prunus, it is classified with the Peach in the subgenus Amygdalus, distinguished from the other subgenera by the corrugated seed shell. An almond is also the seed of this tree. Despite what is commonly believed, the almond is not a nut.

6. Menthol: Menthol is a covalent organic compound made synthetically or obtained from peppermint or other mint oils. It is a waxy, crystalline substance, clear or white in color, which is solid at room temperature and melts slightly above. The main form of menthol occurring in nature is (-)-menthol, which is assigned the (1R,2S,5R) configuration. Menthol has local anesthetic and counterirritant qualities, and it is widely used to relieve minor throat irritation. There is evidence that menthol occurs naturally in peppermint oil (along with a little menthone, the ester menthyl acetate and other compounds), obtained from mentha *x* piperita.

7. Groundnut: Groundnut has an outer thick woody shell. Inside normally there are 2 or 3 embedded seeds (kernel). The seed consists of 2 cotyledons and the germ covered by an outer thin skin called the testa. The colour of the testa may be red, brown, purple or white depending upon the type and variety. The cotyledons constitute the bulk of the seed in the range of around 92 to 94 percent of the weight. The germ constitutes around 3 to 4 percent of the seed weight. The testa protects the seed against pests and diseases. Cotyledons are the storage organs, which supply food the germ during germination. As a result of these functional differences, the chemical make-up of the parts of the kernel also differ.

8. Eucalyptus(Nilgiri) oil: The leaves are leathery in texture, hang obliquely or vertically, and are studded with glands containing a fragrant volatile oil. The flowers in bud are covered with a cup-like membrane which is thrown off as a lid when the flower expands. The fruit is surrounded by a woody, cupshaped receptacle and contains numerous minute seeds. There are a great number of species of Eucalyptus trees yielding essential oils, the foliage of some being more odorous than that of others, and the oils from the various species differing widely in character.

9. Olive oil: Olive oil is a fruit oil obtained from the olive (Olea europaea; family Oleaceae along with lilacs, jasmine and ash trees), a traditional tree crop of the Mediterranean Basin. It is commonly used in cooking, cosmetics, pharmaceuticals, and soaps and as a fuel for traditional oil lamps. Olive oil is healthier than other sources of alimentary fat because of its high content of monounsaturated fat and polyphenols. This Light Grade of Olive retains the unique properties of olive with very low color & odor (most desirable for high end cosmetics & toiletries). Olive Oil is cold press & then refined from the fruit of olive. It is often found growing in European countries.

10. Pistha (pistachio) oil: The pistachio has a long history as a useful plant. The scientific name for the pistachio is Pistacia Vera L. It is native to the eastern Mediterranean region and central Asia which has cultivated for over 3000 years. Pistacia Vera is the most important genus of ten species in the sumac family (anacardiaceous). It

is small tall perennial woody plant. Pistachio nut trees, generally, are suited for areas where winters are cool enough to break bud dormancy and summers are long, hot and dry. It cannot grow in the shade the plant prefers light (sandy) and medium (loamy) soils, requires well-drained soil and can grow in nutritionally poor soil. Pistachio oil is a pressed oil, extracted from the fruit of Pistacia vera, the pistachio nut. Compared to other nut oils, it has a particularly strong flavor.

11. Mandara: Mandarin, sometimes referred to Mandarin orange, is considered a native of south-eastern Asia and the Philippines. It is most abundantly grown in Japan, southern China and India, and is esteemed for home consumption in Australia. Trees of Mandarin are evergreen, seldom exceeding 9 m (30 ft) in height. The leaves are oval and glossy and the flowers are white and fragrant. Although the terms Mandarin and Tangerine are used interchangeably, the two oils are quite different. Mandarin essential oil is generally preferred for therapeutic purposes. It is collected by cold pressing the outer peel of the fruits and is one of the safest oils often recommended for children and for use during pregnancy.

12. Citronella oil: Citronellal or rhodinal or 3, 7-dimethyloct-6-en-1-al ($C_{10}H_{18}O$) is a monoterpenoid, the main component in the mixture of terpenoid chemical compounds that give citronella oil its distinctive lemon scent. Citronellal is a major isolate in distilled oils from the plants Cymbopogon, lemon-scented gum, and lemon-scented teatree. Citronellal has insect repellent properties, and research shows high repellent effectiveness against mosquitoes. Research shows that citronellal has strong antifungal qualities. Citronella oil is one of the essential oils obtained from the leaves and stems of different species of Cymbopogon. The oil is used extensively as a source of perfumery chemicals such as citronellal, citronellol and geraniol. These chemicals find extensive use in soap, perfumery, cosmetic and flavouring industries throughout the world.

13. Til (sesame) oil: Sesame Oil is obtained from the seeds by a cold pressing process and is low in cholesterol. It has a very distinctive, nutty flavour and is a must in Asian, oriental cooking and excellent in dressings. Use very sparingly, as the flavour can be overwhelming. Sesame oil (also known as gingelly oil or til oil) is an edible vegetable oil

derived from sesame seeds. Besides being used as cooking oil in South India, it is often used as a flavor enhancer in Chinese, Taiwanese, Korean, and to a lesser extent, Southeast Asian cuisine. Sesame seeds were one of the first crops processed for oil as well as one of the earliest condiments. In fact, the word ennai that means oil in Tamil has its roots in the Prior to 600 BC, the Assyrians used sesame oil as a food, salve, and medication. Primarily by the rich, as the difficulty of obtaining it made it expensive.

14. Cajeput oil: A very useful oil during the winter months for its clearing and anti-viral properties. Regarded as valuable highly in the East, where it is used medicinally. A tall evergreen tree of thirty meters in height, belong to the Myrtaceae family. It has alternate, finely hairy, thick pointed leaves and small creamy white flowers. The trunk has a whitish papery thin, flaking bark and the tree is known in Malay as 'caju-puti' meaning white wood. Native to South Eastern Asia to Northern Australia and has been introduced to many countries including India closely related to eucalyptus, niaouli and tea tree. No pesticides or herbicides used produced from the leaves and buds from trees grown in the wild.

15. Kalonji (black seed) oil: The different names for Black Seed Oil. Black Seed Oil is referred to differently depending on where in the world you are. Variations can be found regionally, for example between places in India it is referred to as Kalonji or Kalwanji Oil. Researchers concluded that black seed oil could prove to be an effective ingredient to enhance mainstream treatment of allergic diseases. Black seed has a long tradition in the area of beauty care. Texts from the ancient Orient and from 1st century Europe, as recorded by Pliny, report extensive traditional use for black seed oil in hair and skin care. There are many well-established recipes for maintaining and restoring beauty with the help of black seed. Just like the skin, the hair also reflects the general condition of the body.

16. Ankola (Ankol): This is a very variable, small and deciduous tree with spinescent branchlets. The bark is grey, smooth, orange-yellow when young, and fibrous. The leaves are alternate, simple oblong-lanceolate, variable, entire and membranous, with prominent veins. The flowers are fragrant and white, in axillary fasicles. The fruit is a

purplish-red globose berry, with one seed. Shrubs or trees are deciduous up to 20 m high. Inflorescence is sessile, often clusters of 4 to 8 flowers, usually fewer, sometimes only a solitary flower, densely rusty tomentose. Flowers fragrant, cream-colored. Ankol has been used by traditional healers in the treatment of skin cancers by means of local application of the root. It is also used locally for the treatment of snakebite, scorpion bite as well as for dog bite. It also reduces blood pressure when taken orally due to its vasodilator ractivity.

17. Malkangani(Celastrus paniculatus): see-LAS-trus -- from the ancient Greek *kelastros*, the name of another tree pan-ick-yoo-LAY-tus or pan-ick-yoo-LAH-tus -- referring to the flower clusters (panicles) commonly known as black-oil plant, celastrus, oriental bittersweet, intellect tree, staff tree • Bengali: kijri, malkangani • Gujarati: malkangana • Hindi: malkangani • Kannada: bhavamga, jotishmati, kariganne, kougilu • Konkani: malkangoni • Marathi: kanguni,malkangoni • Oriya: korsana, pengu • Sanskrit: alavan, jyotishmati, kangu • Tamil: kuvarikuntal, mannai-k-katti, valuluvai • Telugu: kasara-tige, maneru • Urdu: ملکنگنی malkanguni

18. Mustard oil: The term mustard oil is used for two different oils that are made from mustard seeds. A fatty vegetable oil resulting from pressing the seeds, an essential oil resulting from grinding the seeds, mixing them with water, and extracting the resulting volatile oil by distillation. This oil has a strong smell, a little like strong cabbage, a hot nutty taste, and is much used for cooking in Bengal, Bihar, Kashmir, Punjab and other areas of India and Bangladesh. Due to its high content of erucic acid, which is considered noxious, mustard oil is not considered suitable for human consumption. In North India, mustard oil is also used for rub-downs and massages. Massage with the oil is thought to improve blood circulation, muscular development and good texture to human skin; the oil is also antibacterial.

19. Chemeli oil: Major Component**:**ß-farnesene, α-bisabolol oxide , chamazulene Aromatherapy Uses**:**Give relieve from allergies,arthritis,ha-ir,headache,inflamed skin, sores,strians stress,wounds.It include analgestic,anti-biotic,anti-inflammatory,digestive.It contains Azulene,a powerful anti-inflammatory in dark blue color.

Blending Property**:**Bergamot, Clary sage, Lavender, Geranium, Jasmine, Tea tree, Grapefruit, Rose, Lemon and Ylang Ylang. History**:** In the past Egypt era Egyptians were used this plant in large scale.Because of its cure fever and cooling ability, it was came as a part of life. Major Component**:**ß-farnesene, α-bisabolol oxide , chamazulene Aromatherapy Uses**:**Give relieve from allergies,arthritis,ha-ir,headache,inflamed skin, sores,strians stress,wounds.It include analgestic,anti-biotic,anti-inflammatory,digestive.It

20. Amla oil: Amla oil is prepared from Amla extract. Amla oil has a long tradition in being used for improving the health of hair and scalp. It is one of the world's oldest natural hair conditioners. This oil is light and gets absorbed easily within the hair producing no sticky impact. Amla oil contains vital and essential herbs; it nourishes hair and makes them stop falling.

21. Bawanchi: Scientifically known as Cymbopogon khasans, bawanchi refers to a small plant, which is generally of a pale yellowish color. The origin of bawanchi is in India and it is widely grown in areas like Chhattisgarh, Maharashtra, and Madhya Pradesh and also in the southern parts of the country. The bawanchi oil is extracted from the highly aromatic bawanchi seeds. This small sized plant is of hybrid origin, being a cross between the bawanchi and citronella. It is a plant which generally grows in the tropical region. The high quantities of ocimene and geraniol present in bawanchi impart it with the scents of mangoes and roses and this is how it differs from the bawanchi. Recently, the bawanchi products have seen a rise in demand and commercial cultivation of the grass on a larger scale is required.

22. Akhrot (walnut): The walnut is enclosed in a green, leathery, fleshy husk which is inedible. Removal of the husk reveals the wrinkly walnut shell, which is in two halves, and encloses the kernel, which is likewise in two halves separated by a partition (see Figures 2 and 3). The seed kernels are enclosed in a brown seed coat which contains antioxidants. The antioxidants protect the oil-rich seed from atmospheric oxygen so preventing rancidity (oxidative rancidity). Walnuts are shell fruit (nut types). Because of their similar characteristics with regard to transport, particularly their high oil content, their requirements regarding care during storage. It is a large deciduous tree attaining

heights of 25-35 m, commonly with a short trunk and broad crown, though taller and narrower in dense forest competition. It is a light-demanding species, requiring full sun to grow well. They are useful in herpes, eczema, scrofula and syphilis. Fruits are sweet and emollient, thermogenic and aphrodisiac.

23. Kaddu (pumpkin): Today the oil is an important export commodity of Austrian and Slovenian parts of Styria. It is made by pressing roasted, hulled pumpkin seeds (pepitas), from a local variety of pumpkin, the "Styrian oil pumpkin" (Cucurbita pepo var. styriaca, also known as *var*. oleifera). It has been produced and used in Styria's southern parts at least since the 18th century. The earliest confirmed record of oil pumpkin seeds in Styria (from the estate of a farmer in Gleinstätten) dates to February 18, 1697. The viscous oil is light green to dark red in colour depending on the thickness of the sample (dichromatic) colour. Used together with yoghurt, the colour turns to bright green and is sometimes referred to as "green-gold". Pumpkin seed oil has an intense nutty taste and is rich in polyunsaturated fatty acids. Brown oil has a bitter taste. Claims, based on local folk medicine, suggesting usefulness of the oil in the prevention and treatment of benign prostatic hyperplasia may be backed by some studies showing clinically proven efficacy (particularly along with Serenoa_repens, saw palmetto, and Pygeum africanum) according to the criteria of evidence-based medicine.

24. Lemon oil: The lemon is a hybrid in cultivated wild plants. It is the common name for the reproductive tissue surrounding the seed of the angiosperm lemon tree. The lemon is used for culinary and non culinary uses throughout the world. The fruit is used primarily for its juice, though the pulp and rind are also used, primarily in cooking and baking. Lemon juice is about acidic, which gives lemons a tart taste, and a pH of 2 to 3. This makes lemon juice an inexpensive, readily available acid for use in educational science experiments.

25. Soybean: The soybean or Soya bean is a species of legume native to East Asia. Soybeans occur in various sizes, and in several hull or seed coat colors, including black, brown, blue, yellow, and mottled. The hull of the mature bean is hard, water resistant, and protects the cotyledon and hypocotyls from damage. If the seed coat is cracked the

seed will not germinate. The scar, visible on the seed coat, is called the hilum (colors include black, brown, buff, gray and yellow) and at one end of the hilum is the micropyle, or small opening in the seed coat which can allow the absorption of water. To produce soybean oil, the soybeans are cracked, adjusted for moisture content, rolled into flakes and solvent-extracted with commercial hexane. The oil is then refined, blended for different applications, and sometimes hydrogenated. Soybean oils, both liquid and partially hydrogenated, are exported abroad, sold as vegetable oil, or end up in a wide variety of processed foods. The remaining soybean husks are used mainly as animal feed.

26. Khus khus (vetiver) oil: Vetiver grass oil as the name suggest is extracted from grasses. Vetiver is cultivated in south India, Indonesia and Sri Lanka. Vetiver requires tropical climatic conditions to grow henceforth very extensive grown in southern India. Vetiver is also termed as khus in India and treated as a wild plant. It belongs to the gramineae family. Vetivera is basically a Tamil word that means hatched up and mostly used. Vetiver became one of the main important medicines for the inflammation and joint pains. In other parts of the world, vetiver was used to stop soil erosion.

27. Turpent oil: This oil is commonly called spirit of turpentine. It is prepared by distillation from our common turpentine, though equally afforded by other varieties. It may be distilled either with or without water, but in the latter case a much higher temperature is required, and the product is liable to be empyreumatic. To obtain it quite pure it should be redistilled from a solution of potassium hydroxide. The turpentine of Pinus palustris is said to yield about 17 per cent. Of oil, while that from Pinus Pinaster affords 25 per cent., and that from Pinus sylvestris 32 per cent. Pure oil of turpentine is "a colorless liquid having a characteristic odor and taste, both of which become stronger and less pleasant on aging or exposure to the air. Soluble in 5 volumes of alcohol, Specific gravity: 0.860 to 0.870 at 25° C. Optical rotation variable. Distil 200 mils of the Oil, at the rate of two drops per second, from a 300 mil globe flask, having the side tube 8 cm. above the bulb.

28. Orange: Orange oil is an essential oil produced by glands inside the rind of an orange fruit. It is extracted or steam distilled as a by-product of orange juice production.

It is composed mostly of d-limonene, and is therefore often used in place of pure lemon, which can be further extracted from the oil by distillation. Limonene is what gives citrus fruit their familiar aroma, and is therefore used in perfume and household cleaners for its fragrance. It is also an effective, environmentally friendly, and relatively safe solvent, which makes it an active ingredient of choice in many applications, such as, but not limited to, adhesive and stain removers, cleaners of various sorts, and strippers.

29. Sunflower oil: Sunflower oil is the non-volatile oil expressed from sunflower seeds. Sunflower oil is commonly used in food as frying oil, and in cosmetic formulations as an emollient. Sunflower oil is liquid at room temperature having smoke point of (refined) 230 °C. The refined oil is clear and slightly amber-colored with a slightly fatty odor. Sunflower oil is light in taste and appearance and has a high Vitamin E content. Sunflower oil contains predominantly linoleic acid in triglyceride form. There are several types of sunflower oils produced, such as high linoleic, high oleic and mid oleic.

30. Karadi (kardi) oil: Safflower (karadi) is grown next to ground-nut among the oil-seeds in the district. It occupied an area of 67,095 hectares in 1971-72. The plant bears yellow flowers and thorny leaves. It is mainly a *rabi* crop and is sown in October-November. It is grown both as a rain-fed as well as an irrigated crop. The crop is grown on loam and black cotton soils as well as on light alluvial soils. Usually it is grown mixed with wheat and gram only in every fourth or eighth row of the main crop. Sometimes it is sown as a border crop to surround the main crops to protect it from stray cattle. The preparations are the same as the ones given to the crops along with which it is sown. When it is sown independently the land is ploughed twice and is harrowed once to give a fine tilth to the land. Sowing is done through three-coultered seed drill.

31. Neem oil: Neem oil is a vegetable oil pressed from the fruits and seeds of Neem (Azadirachta indica), an evergreen tree which is endemic to the Indian sub-continent and has been introduced to many other areas in the tropics. It is perhaps the most important of the commercially available products of neem. Characteristics: Neem oil is generally light to dark brown, bitter and has rather strong odors that is said to combine the odors of peanut and garlic. It comprises mainly triglycerides and large amounts of triterpenoid

compounds, which are responsible for the bitter taste. It is hydrophobic in nature and in order to emulsify it in water for application purposes, it must be formulated with appropriate surfactants.

32. Castor oil: Castor oil is a vegetable oil obtained from the castor bean. Castor oil is a colorless to very pale yellow liquid with mild or no odor or taste. Its boiling point is 313 °C (595.4 °F) and its density is 961 $kg \cdot m^{-3}$. It is a triglyceride in which approximately ninety percent of fatty acid chains are ricinoleic acid. Oleic and linoleic acids are the other significant components. Ricinoleic acid, a monounsaturated, 18-carbon fatty acid, is unusual in that it has a hydroxyl functional group on the twelfth carbon. This functional group causes ricinoleic acid and castor oil to be unusually polar, and also allows chemical derivatization that is not practical with most other seed oils. It is the hydroxyl group which makes castor oil and ricinoleic acid valuable as chemical feedstock's. Castor oil and its derivatives have applications in the manufacturing of soaps, lubricants, hydraulic and brake fluids, paints, dyes, coatings, inks, cold resistant plastics, waxes and polishes, nylon, pharmaceuticals and perfumes.

33. Alsi oil (linseed oil, niharti): Linseed oil, also known as flax seed oil or simply flax oil, is a clear to yellowish drying oil derived from the dried ripe seeds of the flax plant (Linum usitatissimum, Linaceae). It is obtained by pressing, followed by an optional stage of solvent extraction. Cold pressed oil obtained without solvent extraction is marketed as flaxseed oil. Linseed oil is the most commonly used carrier in oil paint. It can also be used as a painting medium, making oil paints more fluid, transparent and glossy. It is available in varieties such as Cold Pressed, alkali refined, sun Bleached, sun thickened, and polymerised oil.

34. Karanja: Plasma Power crushes seeds of the Pungam/Karanja tree, to extract Plasma Karanja™ Oil. The Karanja tree (Pongammia glabra syn Pongammia Pinnata) is found through out India and has been used for over a thousand years for its medicinal properties. Karanja Oil is widely used as a pesticide. Foliar sprays of karanja oil are effective against hosts of pests. Field trials of mixtures of Plasma Neem Oil and Karanja Oil have shown excellent results against pests and even viruses. Karanja oil-resin soap

sprays having a concentration of 2% have been reported to be effective against the nymph and adult stages of the green bug of coffee. Karanja Oil is also used in leather dressing, soap making and in the manufacture of lubricants. Pharmaceutical preparations based on Karanja oil are used for treating skin diseases including scales, herpes and leucoderma.

35. Nutmeg: Nutmeg oil is a volatile oil containing borneol and eugenol. The essential oil is obtained by the steam distillation of ground nutmeg and is used heavily in the perfumery and pharmaceutical industries. The oil is colorless or light yellow and smells and tastes of nutmeg. It contains numerous components of interest to the oleochemical industry, and is used as a natural food flavouring in baked goods, syrups (e.g. Coca Cola), beverages, sweets etc. It replaces ground nutmeg as it leaves no particles in the food. The essential oil is also used in the cosmetic and pharmaceutical industries for instance in tooth paste and as a major ingredient in some cough syrups. In traditional medicine nutmeg and nutmeg oil were used for illnesses related to the nervous and digestive systems. Myristicin in the essential oil is probably the agent responsible for the hallucinogenic properties of nutmeg oil.

36. Lemon Grass: Mainly consists of citral (neral and geranial) with the following terpenoids of nerol, limonene, linalool and β-caryphyllene. Lemongrass is known for its invigorating and antiseptic properties. It can be used used in facial toners as its astringent properties help fight acne and greasy skin. An excellent anti-depressant, Lemongrass tones and fortifies the nervous system and can be used in bath for soothing muscular nerves and pain. Lemongrass shares similar properties with citronella and has a great reputation for keeping insects away. Cymbopogon is a genus of about 55 species of grasses, native to warm temperate and tropical regions of the Old World and Oceania. It is a tall perennial grass. Common names include lemon grass, lemongrass, barbed wire grass, silky heads, citronella grass or fever grass amongst many others.

***37. Rosa (mehindi) oil*:** Scientifically referred to as Lawsonia Inermis, henna in the West is most commonly used to dye hair. But with the new popularity of tattoos, henna and the art of Mehndi is considered a safe, painless and non-permanent alternative form of body

ornamentation. Although henna is traditionally drawn only on the hands and feet, feel free to create your designs on arms, legs, around the belly button, and even may be behind the neck. Reaching a height of up to 6 meters, the plant has fragrant white or rose-red flowers. The reported life zone of henna is 19 to 27 degrees centigrade with an annual precipitation of 0.2 to 4.2 meters and a soil pH of 4.3 to 8.0. Henna is planted today primarily as an ornament hedge, but is probably best known for its dried, ground leaves (called henna) traditionally used to produce colorfast orange, red, and brown dyes.

38. Cedarwood oil: Cedar is a genus of coniferous trees in the plant family Pinaceae. They are most closely related to the Firs, sharing a very similar cone structure. They are native to the mountains of the western Himalaya and the Mediterranean region, occurring at altitudes of 1,500–3200 m in the Himalaya and 1,000–2,200 m in the Mediterranean. They are trees up to 30–40 m tall with spicy-resinous scented wood, thick ridged or square-cracked bark, and broad, level branches. The shoots are dimorphic, with long shoots, which form the framework of the branches, and short shoots, which carry most of the leaves. The leaves are evergreen and needle-like, 8–60 mm long, arranged singly in an open spiral phyllotaxis on long shoots, and in dense spiral clusters of 15–45 together on short shoots; they vary from bright grass-green to dark green to strongly glaucous pale blue-green, depending on the thickness of the white wax layer which protects the leaves from desiccation.

39. Clove oil: Cloves are the aromatic dried flower buds of a tree in the family Myrtaceae. It is native to Indonesia and used as a spice in cuisine all over the world. The name derives from French clou, a nail, as the buds vaguely resemble small irregular nails in shape. Cloves are harvested primarily in Zanzibar, Indonesia and Madagascar; it is also grown in Pakistan, India, and Sri Lanka. The clove tree is an evergreen which grows to a height ranging from 10-20 m, having large oval leaves and crimson flowers in numerous groups of terminal clusters. The flower buds are at first of a pale color and gradually become green, after which they develop into a bright red, when they are ready for collecting. Cloves are harvested when 1.5-2 cm long, and consist of a long calyx, terminating in four spreading sepals, and four unopened petals which form a small ball in the centre.

40. Cinnamon: Cinnamon is a small evergreen tree 10–15 meters tall, belonging to the family Lauraceae, native to Sri Lanka and South India. The bark is widely used as a spice due to its distinct odour. In India it is also known as Daalchini. The leaves are ovate-oblong in shape, and flowers, which are arranged in panicles, have a greenish color, and have a distinct odor. The fruit is a purple one-centimetre berry containing a single seed. Chemical components of the essential oil include ethyl cinnamate, eugenol, cinnamaldehyde, beta-caryophyllene, linalool and methyl chavicol. Its flavour is due to an aromatic essential oil which makes up its composition. This oil is prepared by roughly pounding the bark, macerating it in seawater, and then quickly distilling the whole. It is of a golden-yellow colour, with the characteristic odour of cinnamon and a very hot aromatic taste. The pungent taste and scent come from cinnamic aldehyde or cinnamaldehyde and, by the absorption of oxygen as it ages, it darkens in colour and develops resinous compounds.

4.6 Experimental

A study of refractive index of medicinal oils is carried out using a U-shaped glass probe as mentioned in chapter 3, one end of which is connected to a source and the other end to a power meter. Results are compared with Abbe's refractometer and are in good agreement.

Table 4.1: The necessary data on edible and medicinal oils used in the experimentation

SL. No.	*Name of the oil*	*Scientific name*	*Botanical Family*	*Specific gravity(30°C)*	*Part used*
1	Coconut	Cocos nucifera	Palmae Family	0.5	pulp
2	Levender	Lamiaceae	Lavandula Angustifolia Miller	0.885- 0.897	flower
3	Rose mary	Rosmarinus Officinalis	Lamiaceae	0.890-0.896	leaf
4	Moha(mahwa)	Bassia longifolia	Sapotaceae	0.925 - 0.0	kernel
5	Almond	Rosaceae	Prunus Amygdalus	0.910 – 0.915	kernels
6	Menthol	Cyamopsis tetragonoloba	Fabaceae	0.895- 0.899	leaf
7	Groundnut	Arachis hypogaea	Legume(bean)	0.916- 0.918	seed
8	Eucaliptus	Eucalyptus globules	N.O. Myrtaceae	0.905- 0.925	leaf
9	Olive oil	Olea europaea	Olea europaea	0.915-0.918	fruit
10	Pistha	Pistachia vera.L	Anacardiacea	0.910– 0.930	nut
11	Mandarin	Rutaceae	Citrus reticulata	0.848 – 0.855	peel
12	Citronela	Gramineae	Cymbopogon Nardus	0.893 to 0.910	grass

		family			
13	Til oil	Sesamum indicum L	Pedaliaceae Genus	0.919	seeds
14	Cajeput	Melaleuca cajuputi minor	Myrtaceae	0.912– 0.925	leaves
15	Kalonji	Nigella satica black cumin	Nigella sativa	0.910 – 0.915	seed
16	Ankola		Analgium decapetulum.Linn	0.895- 0.899	seeds
17	Malkangani	Celastrus paniculatus staff tree	Citrus peniculata	0.916- 0.918	seed
18	Mustard	Brassia Nigra	Mustard Family	0.905- 0.925	seed
19	Chemeli	Matricaria Chamomillai	Matricaria Recutita	0.915-0.918	flower
20	Amla	Embalica officinalis	Emblica officinalis	0.910– 0.930	seed
21	Bawanchi	Psoralea Rylifolia	Psoralea Rylifolia	0.848 – 0.855	seeds
22	Akhrot	Juglanduceae	Juglancs regia	0.893 to 0.910	bark
23	Kaddu(pumpkin)	Kukurbita pepo	Kukurbita	0.915– 0.925	seed
24	Lemon	Citrus Limonum	Magnoliopsida	0.915-0.918	Peel
25	Soyabean	Fabaceae	Legumes Family	0.927	seed
26	Khus khus	Vetiveria zizanoides L	Poaceae	0.915-0.918	seed
27	Turpent	Pinus pinaster	*Pinaceae*	0.860- 0.870	resin
28	Orange	Citrus Sinensis	Citrus Family	0.905- 0.925	Peel
29	Sunflower	Helianthus annuus	Composite Family (Aster)	0.915-0.918	seed
30	Karad oil			0.910– 0.930	seed
31	Neem oil	margosa	Azadirachta indica	0.848 – 0.855	seed
32	Caster oil	Linum usitatissimum	Ricinus cummunis	0.893 to 0.910	seed
33	Alsi(linseed)	Linum usitattisimum	Flax	0.915– 0.925	seed
34	Karanja	Pongamia glabra	Pongamia glabra	0.915-0.918	seed
35	Nutmeg	Myristica Fragrans	Myristicaceae	0.885- 0.915	seed
36	Lemon grass	Poaceae	Cymbopogon Flexuosus	0.873-0.897	grass
37	Rosa (mehindi)	Lawsonia alba/Innermis henna natura	Lawsonia Inermis	0.910– 0.930	leaf
38	Cederwood	Pinaceae	Cedrus Atlantica	0.848 – 0.855	wood
39	Clove oil	Eugenia Caryophyllata	Myrtaceae	0.893 to 0.910	bud
40	Cinnamon	Cinnamomum zeylanicum	Laurel Family	1.010 -1.030	bark

4.7 Results and discussion

As the study of refractive index of oils is very important in various applications, and in literature, several methods have been described for its measurement. In our earlier papers, the development of the alternative sensors for refractive index measurement based on optical fiber and silica glass relevance is reported. A silica fiber based refractive index sensor is very compact in weight and size and with slight modifications can be made suitable for remote sensing. It can be used for polymer composition or for liquids, can be adopted as a chemical sensor as it needs only a small volume of liquid. The fiber of silica glass has also been used as a sensor for absorption measurement. They are also used in experiments designed to detect refractive index, as light carriers, but not as a sensor directly of

In this chapter, the experimental results of refractive index on 40 samples of some medicinal and edible oils are presented. In chapter 3, binary mixture of organic liquids are used surrounding the U-shaped glass probe and the output power through the sensor is recorded as a function of refractive index of mixture of liquids. The refractive index of mixture of liquids (Benzene, Methanol, Propanol, Butanol, Cyclohexane) is determined by Abbe's refractometer and a graph is plotted with the power output as a function of index of refraction of the liquid (Fig.3.40). For a variation of 1.325 to 1.495 in R.I. of mixture of liquids, the output power through the sensor was observed to be from -49.1dBm to -62.6dBm.

Now, the earlier liquid surrounding the U-shaped probe is removed and the oils whose refractive index is to be determined are kept surrounding the U-shaped glass probe and the power through it is noted. About 40 oils, as listed in Table 4.1, have been selected for the study. Abbe's refractometer is made use to note the refractive index of these oils. Table 4.2 presents the data on refractive index of some edible oils and medicinal oils, totaling 40 samples, measured using the technique developed in the laboratory and also Abbe's refracto-metric technique for the verification. From Table 4.2 it can be noted that the values of refractive index of different oils range from 1.451 to 1.565. A study of refractive index of oils is important in a variety of applications. The following are some of the applications.

1. Hydrogenation state of edible oils during hydrogenation process.
2. Fatty acid content
3. Fatty acid profile
4. Triglyceride profile
5. Antimicrobial action
6. Antifungal activity

For this purpose, in the past, several methods, techniques and instruments were developed for the study of refractive index of bio-fluids and oils so as to understand their physiological alterations. Thus the methods developed and adopted for measurement of refractive index of oils are: Brewster's angle, ellipsometry, attenuated internal reflection (ATR) and minimum deviation. The optical glass sensor developed in the laboratory is simple, elegant and most suitable for the study of refractive index of oils. A variety of medicinal and edible oils have been selected for the study of refractive index for two reasons.

Table 4.2: Edible and medicinal oils under investigation – variation of refractive index obtained from the power recorded for various edible and medicinal oils using 0.25 mm U shaped rod

SL. No.	*Name of the oil*	*Power output (dBm)*	*R.I. from FO glass sensor (R.I.)*	*R.I. from Abbe's refractometer (R.I.)*	*Error percentage (R.I.)*	*Reported Values (R.I.)*
1	Coconut oil	-58.9	1.452	1.451	-0.069	1.448 – 1.4492
2	Levender	-59.4	1.458	1.455	-0.206	1.459 – 1.464
3	Rose mary	-59.8	1.462	1.460	-0.137	1.466 – 1.470
4	Moha	-60.1	1.466	1.464	-0.137	1.463 – 1.468
5	Almond	-60.2	1.467	1.465	-0.137	1.462 – 1.466
6	Menthol	-60.2	1.467	1.465	-0.137	1.462 – 1.469
7	Groundnut	-60.3	1.468	1.466	-0.136	1.462 – 1.464
8	Olive oil	-60.4	1.469	1.467	-0.136	1.468 – 1.471
9	Pistha	-60.4	1.469	1.467	-0.137	1.464 – 1.464
10	Mandara	-60.4	1.469	1.467	-0.137	1.465 – 1.471
11	Citronela	-60.4	1.469	1.467	-0.136	1.480 – 1.492
12	Til oil	-60.5	1.470	1.468	-0.136	1.465 – 1.468
13	Cajeput	-60.5	1.470	1.468	-0.136	1.464 – 1.482
14	Kalonji	-60.5	1.470	1.468	-0.136	1.460 – 1.470
15	Ankola	-60.5	1.470	1.468	-0.136	1.465 – 1.472
16	Malkangni	-60.5	1.470	1.468	-0.136	1.466 – 1.473
17	Mustard	-60.6	1.471	1.469	-0.136	1.527 – 1.529

18	Chemeli	-60.6	1.471	1.469	-0.136	1.468 – 1.475
19	Amla	-60.6	1.471	1.469	-0.136	1.466 – 1.470
20	Bawanchi	-60.6	1.471	1.469	-0.136	1.468 – 1.475
21	Akrot	-60.7	1.473	1.470	-0.204	1.475 – 1.478
22	Kaddu	-60.7	1.473	1.470	-0.204	1.472 – 1.474
23	Lemon	-60.7	1.473	1.470	-0.204	1.473 – 1.476
24	Soyabean	-60.7	1.473	1.470	-0.204	1.465 – 1.469
25	Khuskhus	-60.8	1.474	1.471	-0.204	1.469 – 1.473
26	Turpent	-60.8	1.474	1.471	-0.204	1.469 – 1.474
27	Orange	-60.8	1.474	1.471	-0.204	1.470 – 1.474
28	Sunflower	-60.8	1.474	1.471	-0.204	1.465 – 1.469
29	Eucaliptus	-60.9	1.475	1.472	-0.204	1.458 – 1.470
30	Karad oil	-60.9	1.475	1.472	-0.204	1.458 – 1.470
31	Neem oil	-61.0	1.476	1.474	-0.136	1.462 – 1.471
32	Caster oil	-61.1	1.477	1.475	-0.136	1.477 – 1.481
33	Alsi	-61.2	1.478	1.476	-0.136	1.475 – 1.479
34	Karanja	-61.2	1.478	1.476	-0.136	1.473 – 1.479
35	Nutmeg	-61.3	1.480	1.477	-0.203	1.469 – 1.472
36	Lemon grass	-61.4	1.481	1.480	-0.068	1.486 – 1.490
37	Rosa (mehindi)	-61.8	1.485	1.484	-0.067	1.474 – 1.486
38	Cederwood	-62.5	1.495	1.494	-0.067	1.495 – 1.510
39	Clove oil	-65.5	1.528	1.528	0.000	1.529 – 1.537
40	Cinnamon	-68.7	1.565	1.565	0.000	1.529 – 1.535

Standard deviation: ± 0.018

Mean value: 1.476

1. To assess the utility, applicability, suitability, sensitivity and accuracy of the sensor for the study of refractive index of bio turbid liquids and bio viscous fluids like oils which contain a variety of fatty-acids.
2. To have a comparative account on refractive index of a good number of edible and medicinal oils which may be of important in characterization, purity and applicability in the fields of food preparation and processing; Aroma therapy; pharmaceuticals; and cosmetics.

References

[1] Charles F. Cole, Jr., Fiber optic refractometer, United states patents 5311274, issued on may 10, 1994.

[2] T. E. Thompson, C.E. Rogers and D. C. Zimmerman, Sunflower oil quality and quantity as affected by rhizopus head rot, Journal of the American oil chemists society, vol. 57, No. 3/march 1980, pp. 106 – 108.

[3] Sheldon wishna, Using refractive index to improve sunflower oil measurements using nuclear magnetic resonance, American society of agricultural and biological engineering, Annual meeting 2004, paper number, 043131.

[4] David A. Moyler, Extraction of essential oils with carbon dioxide, Flavour and fragrance Journal, vol. 8, No. 5, pp. 235 – 247, 26 June 2006.

[5] Garcia Gonzalez, Diego L., Viera Maclas, Maria, Apaeicio – Raiz, Ramon, Morales, Maria T., Aparicio, Ramon, Validation of a method based on triglycerides for the determination of low percentages of hazelnut oil in olive oil by column liquid chromatography, Journal of AOAC international, september 1, 2007.

[6] Yunus, W. Mahmood mat, Fen, Yap wing, Yee, Lin Mei, Refractive index and fourier transform infrared spectra of virgin coconut oil and virgin olive oil, American journal of applied sciences, february, 2008.

[7] D. C. Ingraham and T. H. Simpson, The refractometric method for the determination of oils in coconut and sasame oil cake, Journal of the Americal oil chemists, vol. 13, No. 9, september 1936, pp. 222 – 224.

[8] Kalamba D., Kunicka A., Antibacterial and Antifungal properties of Essential oils, Current medicinal chemistry, vol. 10, No. 10, May 2003, pp. 813 – 829 (17).

[9] Ariel ceferino toloza, Julio zygadlo, Gaston mougabure cueto, Fernando Biurrun, Eduardo Zebra, and Maria Ines picollo, Fumigant and Repellent properties of essential oils and component compounds against permithrin – Resistant pediculus humanus lapitis (Anoplura: Pediculidea) from Argentina, Journal of medical Entomology, vol. 43, No. 5, september 2006, pp. 889 – 895.

[10] Katie bird, Anti irritant properties of essential oils in antiperspirants, International Journal of cosmetic science, vol. 29, pp 369 – 376, october 2007.

[11] Ashok kumar and deepak ganjewala, Antimicrobial properties of osmanthas fragrances (Lour), Research journal of medicinal plant 1(1): 21 – 24, 2007.

[12] M. A. H. Nagalaksmi, D. Thngadurai, T. Pullaiah, In vitro antimicrobial efficiency of leaf essential oils of chukrasia, Adr. Juss. And Melia dubia cav. (Meliaceae) Phytotherapy research, vol. 17, No. 4, pp. 414 – 416, April 2003.

[13] S. Mondal, S. C. Mahapatra, B. R. Mirdha, S. N. Naik, Antimicrobial activities of essential oils obtained from fresh and dried leaves of ocimum santuny (L) against enteric bacteria and yeast, International society for horticultural science, Acta Horticulture 756. International symposium on medicinal and nutraceutical plants 2008.

[14] Atta ur rahaman, M. Iqbal choudhary, Afgan farooq, Aftab Ahmed, M. Zafar Iqbal, Betul Demirci, Fatih Demirci and K. Huosnu cam baser, Antifungal activities and Essential oil constituents of some species from pakistan, Third International Electronic conference on synthetic organic chemistry (ECSOC – 3), september 1-30, 1999.

[15] Jonas chianu, Bernard vanlauwe, John Mukalama, Akin Adesina, Nteranya, Farmer evaluation of improved soybeans varieties being screened in five locations in kenya: Imlications for Agriculture research, vol. 1(5), pp.143 – 150, December 2006.

[16] Dexian He and David B South, A review on mechanism of plant geotropism: developing trend in research on pine root geotropism, African journal of Agriculture research, vol. 1(4), pp. 074 – 084, November 2006.

[17] Seyed M. A. Razavi and Elnaz Milani, Some physical properties of the watermelon seeds African journal of agricultural research, vol. 1(3), pp. 065 – 069, October 2006.

[18] Ashaye O. A. and Olusoji O. C., Evolution of some quality attributes of soybean oils in Ibadan African journal of agricultural research, vol. 1(1), pp. 017 – 019, august 2006.

[19] Muhammad Gulfraz, Sajid Mehmood, Nasir Minhas, Nyla Jabeen, Rehana Kausar, Kokab Jabeen and Gulshan Arshad, Composition and antimicrobial propeties of essential oil of Foeniculum vulgare, African journal of Biotechnology, vol. 7(24), pp. 4364-4368, 17 December 2008.

[20] V. Ducel, J. Richard, Y. Popineau, and Boury, Rheological interfacial properties of plant protein – Arabic gum coacervates at the oil – water interface, Biomacromolecules, 2005, 6(2), pp. 790 – 796.

[21] Foster T., Sottmann T., Schweins R, Strey R., Small angle nuetron – scattering from giant water –in-oil microemulsion droplets. II. Polymer –decorated droplets in a quaternary system The journal of chemical physics, 2008 Feb. 14; 128(6):064902.

[22] Joshi S, Chanotiya CS, Agarwal G, Pant AK, Mathela CS, Terpenoid compositions, and antioxidant and antimicrobial properties of the rhizome essential oils of different Hedychium species, journal of chemistry and biodiversity, 2008 Feb; 5(2): 299-309.

[23] Canacki M, Sanli H., Biodiesel production from various feedstocks and their effects on the fuel properties, Journal of industrial microbiology and biotechnology, 2008 May; 35(5): 431-41.

[24] Lin C, He G, Dong, Liu H, Xiao G, Liu Y, Effect of oil phase transition on freeze/thaw-induced demulsification of water –in –oil emulsions, The ACS Journal of surfaces and colloids, 2008 May 20;24(10):5291-8.

[25] Totani N, Burenjargal M, Tateishi S, Yawata M, Effects of oil heated with gluten on weight-loss dieting. II, Journal of oleo science, 2008;57(6):327-33.

[26] Hassan EB, Steele PH, Ingram L, Characterization of fast pyrolysis bio-oils produced from pretreated pine wood Journal of applied biochemistry and biotechnology, 2008 Dec. 3.

[27] Singh RK, Nayak P, Niyogi UK, Khandal RK, Singh G, Gamma radiation process for destruction of toxic polychlorinated biphenyls (Pcbs) in transformer oils, Journal of environmental science and engineering, 2006 Jan; 48(1):45-50.

[28] Ioan stefanescu, Camelia Calomir, Constantin gheorghies, Constantin Spanu, Study on tribological properties of vegetable sunflower oil used as possible ecological lubricant, The annals of university “Dunarea De Jos” of galati, Fascicle VIII, 2005, ISSN 1221-4590, Tribology.

[29] V. Mahadevan, Annual review of the literature on fats, oil, and detergents. Part I Journal of the American oil chemists society, vol. 40, number 8 / August, 1963.

[30] Felib Y. Iskander, Determination of seventeen elements in edible oils and margarine by instrumental neutron activation analysis, http://www.springerlink.com/content.

CHAPTER 5

Refractive index of Human Urine

5.1. Introduction

Urine is secreted by the kidneys in a process of filtration from the blood which is a waste product of the any zoological body and excreted through the urethra. In the process known as urination this waste is expelled eventually from the body. For the homeostasis fluids of the body and for the flushing of the waste molecules which are collected from the blood, the excretion of the urine mostly serves for. It is usually exists in light yellow color, and it is transparent solution that is clear to amber in color. Urine is a watery solution made up of organic materials, metabolic wastes such as urea, and dissolved salts. Materials and fluids come from interstitial fluid or from the blood, destined to become urine, being filtered by the kidneys.

When the body needed by the essential molecules, such as glucose, in the process of reabsorption the composition of urine is adjusted is reabsorbed back into the stream of the blood via carrier molecules. The remaining fluid will be released from the body through urination, which contains potentially toxic substances or high concentrations of urea and others. The flow of the urine will be through the ureter, kidney, bladder, and finally the urethra. By the process of re-absorption, filtration, and tubular secretion, the urine is produced. Large amounts of urine is contained in urea, is formed by the combination of cellular respiration (1 CO2 molecules) and the byproduct of deamination (2 NH3 molecules). Components of other category include various inorganic salts such as sodium chloride. Urea is an organic compound with the chemical formula $(NH_2)_2CO$. Urea is also known as carbamide, especially in the recommended International Nonproprietary Names in use. The other names include isourea, carbonyldiamine, carbonyl diamide, and carbamide resine.

The urea molecule is planar and retains its full molecular point symmetry, due to conjugation of one of each nitrogen's P-orbital to the carbonyl double bond. Each

carbonyl oxygen atom accepts four N-H-O hydrogen bonds, a very unusual feature for such a bond type. This dense hydrogen bond network is probably established at the cost of efficient molecular packing. The structure is quite open, the ribbons forming tunnels with square cross-section.

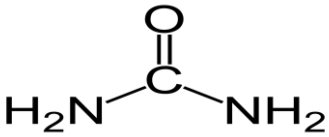

Fig.5.1. Structure of Urea

The individual atoms that make up a urea molecule come from carbon dioxide, water, aspartate and ammonia in a metabolic pathway known as the urea cycle, an anabolic process. This expenditure of energy is necessary because ammonia, a common metabolic waste product, is toxic and must be neutralized. Urea production occurs in the liver and is under the regulatory control of N-acetylglutamate. In this cycle, amino groups donated by ammonia and L-aspartate are converted to urea, while L-ornithine, citrulline, L-argininosuccinate, and L-arginine act as intermediates.

Urea also plays a very important role in that it helps set up the Countercurrent System in the nephrons, which allows for reabsorption of water and critical ions. Urea is reabsorbed in the inner medullary collecting ducts of the nephrons, thus raising the osmolarity in the medullary interstitium surrounding the thin ascending limb of the Loop of Henle. The greater the osmolarity of the medullary interstitium surrounding the thin ascending Loop of Henle, the more water will be resorbed out of the renal tubule back into the interstitium and thus back into the body. Some of the urea from the medually interstitium that helped set up the Countercurrent System will also flow back into the tubule, through urea transporter 2, into the thin ascending limb of the loop of Henle, through the collecting ducts, and eventually out of the body as a component of urine.

It is dissolved in blood and excreted by the kidney as a component of urine. In addition, a small amount of urea is excreted along with sodium chloride and water in sweat. Control of urea by anti diuretic hormone allows the body to create hyperosmotic urine. If the person’s body needs to save water in order to maintain a suitable

concentration of sodium ions in the blood plasma and to maintain a suitable blood pressure, preventing the loss of water in this manner is important.

Most organisms have to deal with amino acid catabolism and the excretion of nitrogen waste originating from protein. The land dwelling organisms convert the toxic ammonia to either uric acid or urea, while aquatic organisms the most common form of nitrogen waste is ammonia. Generally, the mammals, other remaining species excrete urea, while saurian reptiles and birds excrete uric acid. Remarkably, tadpoles excrete ammonia, and shift to urea production during metamorphosis. In veterinary medicine, Dalmatian breeds of dogs are noteworthy in that they excrete urea in the form of uric acid in the urine rather than in the urea form. This is due to a defect in one of the genes controlling expression of the conversion enzymes in the urea cycle. Despite the generalization above, the pathway has been documented not only in mammals and amphibians, but in many other organisms as well, including birds, invertebrates, insects, plants, yeast, fungi, and even microorganisms.

Urea can be irritating to skin and eyes. Too high concentrations in the blood can cause damage to organs of the body. Low concentrations of urea such as in urine are not dangerous. It has been found that urea can cause algal blooms to produce toxins, and urea in runoff from fertilizers may play a role in the increase of toxic blooms. Repeated or prolonged contact with urea in fertilizer form on the skin may cause dermatitis. The substance also irritates the eyes, the skin and the respiratory tract. The substance decomposes on heating above melting point producing toxic gases.

5.2. Chemical analysis

Substances non-organic in the urine: iodide, fluoride, bromide, sulphur, phosphorus, chloride, bicarbonate, iron, cagnesium, calcium, natron, potassium, rhodanide, mercury, lead, arsenium, selenium, cobalt, zinc, copper.

Substances that are nitrogenous in urine nitrogen: creatine, urea, piperidine, carnitine, choline, guanidine, creatinine, norepinephrine, epinephrine, dopamine, spermidine, bilirubin, levulinique amino-acid, tryptamine, serotonin and so on.

Amino acids in urine: carnosine, Alanine, methionine, lysine, leucine, histidine, glycine, hydroxyloproline, valine, tyrosine, serine, phenylalanine, xylosylserine, galactosylhy droxylyzine, and others.

Protein in urine: transferrin, haptoglobin, albumin, immunoglobulins IgM, IgA, IgG, and others.

Enzymes in urine: gamma-glutamyl transferase, Lactadehydrogenase, lysozyme, uropepsinogene, alpha amylase, protease, urokinase, beta N-acetylglucosaminidase, and others.

Sugars (carbohydrates in the urine: glucose, ketopentose, rhammose, fucose, xyloseribose, arabinose, sucrose, lactose, fructose, mannose, galactose, raffinose, fucosylglucose, and others.

Devoid of substances of nitrogen in urine: wide organic acids of assortment.

Vitamins in the urine: nicotinic acid, 4-pyridoxique acid, vitamin B6, riboflavin (vitamin B2), thiamine (vitamin B1), vitamine B12, ascirbic acid (vitamin C), biopterine and others.

Hormone in urine: corticotrophin, Gonadotropin, vasopressin, oxytocin, lactogeniques hormones, prolactin, catecholamines (dopamine, epinephrine, norepinephrine), thyroxine, corticosteroids (cortisone, corticosterone, aldosterone), erythropoietin, insulin, testosterone, estrogen progesterone and others.

Precipitines and agglutinins: the action of neutralization on the polio virus and the other viruses.

Antineoplaston: without affecting the healthy cells that selectively prevent the development of the cancer cells.

Allantoin: the substance of crystalline nitrogen that promotes healing from the uric acid oxidation. In the manufacture of many kinds of skin creams it is used.

Color: the color of the urine which of typical bright yellow is caused by the degradation products of urobilin and bilirubin, but also from the pigment urochrome. Clear colors and the preferred colors of urine are a sign of hydration of urine.

Unusual coloration: from the bloodstream, removal of excess B vitamins causes light orange / yellowing colors. Certain medications such as puridium and rifampin can cause orange urine.

Turbidity: Bacterial infection may be a symptom of turbid urine, can be due to the salt crystallization in urine (e.g. calcium phosphate), which dissolve if vinegar (acetic acid) is added.

pH: The urine pH can normally vary between 4.5 and 8, but is close to neutral, i.e. 7. Alkaline urine or strongly acidic may be a symptom of a disease

Amount: numerous factors will decide the amount of urine produced including activities, state of hydration, size, environmental factors, and health. The average production in adult humans is about 1-2 L per day. Producing too little or too much urine needs medical

5. 3. Renal physiology

Urination is the primary method for excreting toxins, chemicals and drugs from the body. These chemicals can be detected and analyzed by urinalysis. Cellular metabolism results in a buildup of toxic nitrogen compounds, or nitrogenous waste. Since this waste is toxic, most animals have excretory systems in humans this is known as the Urinary system, which consists of the Kidneys, Urinary bladder, Ureter, and Urethra) to rid themselves of this waste. The kidneys extract the nitrogenous wastes from the bloodstream, as well as excess water, sugars, and a variety of other chemicals.

In cases of kidney or urinary tract infection (UTI), the urine will contain bacteria, but otherwise urine is virtually sterile and nearly odorless when it leaves the body. However, after that, bacteria that contaminate the urine will convert chemicals in the urine into smelly chemicals that are responsible for the distinctive odor of stale urine, in particular, ammonia is produced from urea.

Some diseases alter the quantity and consistency of the urine, e.g., sugar in the urine is a sign of diabetes. Normal urine density values vary between 1.003-1.035 $g.cm^{-3}$, and any deviations may or may not be associated with urinary disorders.

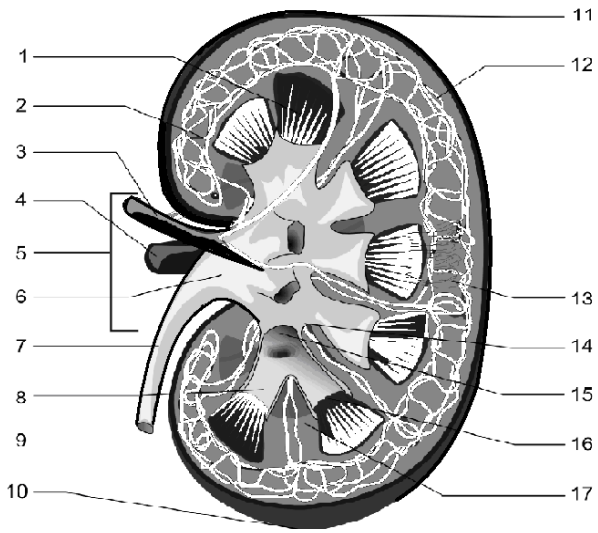

5.2. Parts of the kidney: Kidney parts: 1-renal pyramid, 2-efferent vessel, 3-renal artery, 4-renal vein, 5-renal hilum, 6-renal pelvis, 7-ureter, 8-monor calyx, 9-renal capsule, 10-inferior renal capsule, 11-superior renal capsule, 12-afferent vessel, 13-nephron, 14-minor calyx, 15-major calyx, 16-renal papilla, 17-renal column.

5.3.1. Nephron

The kidneys basic functional unit is the nephron, which present more than a million in number within each of the adult human kidney's cortex and medulla. In each normal adult human kidney, the water and the solute within the cortex and medulla are regulated by the nephrons. First filtering the blood under pressure, and reabsorbing the necessary fluid and while secreting other, unneeded molecules, molecules back into the blood, nephrons regulate the soluble matter, and water, electrolytes especially in the body. With

both counter transport and co-transport mechanisms established in the associated collecting ducts and in the nephrons, re-absorption and secretion are accomplished.

5.3.2. Collecting duct system

The fluid flows into the duct collecting system from the nephron. For the process of water conservation by the organism this segment of the nephron plays very crucial role. These ducts facilitate its re-absorption and become water permeable, in the presence of antidiuretic hormone (ADH), thus reducing its volume and concentrate the urine. Conversely, the collecting tubule becomes less permeable to water and the production of ADH is decreased, rendering urine dilute and abundant when the organism must eliminate excess water, such as after excess fluid drinking. To decrease the production of ADH appropriately due to failure of the organism, which condition is known as the syndrome of the inappropriate ADH (SIADH), may lead to dangerous dilution of the body fluids, and lead to water retention, in turn which causes the severe neurological damage. Excessive urination called diabetes insipidus (DI) due to the failure to produce ADH or collecting ducts inability. Acid-base homeostasis maintenance is the second major function of the collecting duct system. The urine, after the processing along the ducts and the collecting tubules, is drained via the ureter into the bladder, to be excluded finally from the organism.

Renal physiology: Waste products excretion: The a variety of waste products produced by nitrogenous wastes like uric acid from nucleic acid metabolism and water and urea from protein catabolism, including waste products produced by metabolism are excreted by kidneys.

Homeostasis: one of the major organs which involving the body whole homeostasis is the kidney. The regulation of blood pressure, control of blood volume, regulation of electrolyte concentrations, and the acid base balance are the homeostatic functions among its other functions. Through the coordination with other organs, especially those of endocrine system, homeostatic functions are accomplished by the kidneys. Through hormones secreted into the bloodstream, the kidneys communicate with these organs.

Acid-base balance: By eliminating water composition of the blood and H ions concentration which is called augmentation mineral ion concentration, the kidneys regulate the pH. The plasma of blood is maintained by the kidney acidic at pH 5 or alkaline at pH 8, on the other hand at a slightly alkaline pH of 7.4 by exchanging hydroxyl ions and hydronium ions. Through four main protein transporters the pH is maintained: an anion exchanger AE1 which exchanges chloride for bicarbonate, a sodium-hydrogen exchanger (NHE3), an isoform of the hydrogen ATPase, the V-type H-ATPase, and a sodium-bicarbonate cotransporter NBC1. The NHE3 and H-ATPase are exposed to the lumen due to the polar alignment of the cells in the renal epithelia, which is outside the body, on the cells apical side, which are responsible for excreting protons and hydrogen ions. Conversely, AE1 and NBC1 allow bicarbonate ions to move back into the extracellular fluid and which are on the basolateral side of the cells and are returned to the blood plasma.

Blood pressure: Renin – angiotensin system: by the aldosterone involved in the homeostatic process the sodium ions are controlled which in the distal convoluted tubules increase the sodium ion reabsorption. By the cells of the juxtaglomerular apparatus, a proteolytic enzyme called renin is secreted, when blood pressure becomes low.

Renin converts the blood protein, angiotensinogen to angiotensin I by acting on it. Angiotensin I, then in the lung capillaries converted into Angiotensin by the angiotensin enzyme (ACE), which then by the adrenal cortex, stimulates the secretion of aldosterone, which affects the tubules of the renal. An increase in the sodium ion reabsorption from the kidney tubules is stimulated by aldosterone, which in turn causes an increase of water volume that is reabsorbed from the tubule. The blood pressure will be raised by the increase in the volume of the blood, caused by the increase in the water reabsorption.

Volume of plasma: The hypothalamus detects significant rise or drop in plasma osmaolality, which communicates to the posterior pituitary gland. The gland for the secretion of antidiuretic hormone is caused by the osmolality resulting an increase in the urine concentration and water reabsorption by the kidney. For the return of the plasma

osmolality to its normal levels, the two factors work together. Secretion of the hormone: The hormones like erythropoietin, renin, urodilatin, and vitamin D are secreted by the kidneys.

Embryology: Development of the reproductive organs and urinary. From the intermediate mesoderm, the mammalian kidney will be developed. The nephrogenesis is the development of the kidney, proceeds through three successive phases of a series, and the development of each series is marked by a more advanced pair of kidneys: the mesonephros, the pronephros and the metanephros.

Pronephros: Towards the cranial end of the intermediate mesoderm the paired pronephroi appear, during about day 22 of human gestation. In a series of tubules called nephrotomes , epithelial cells arrange themselves in this region and with the pronephric duct join laterally, which does not reach the embryo's outside. As the pronephros cannot excrete the waste from the embryo, it is thus considered in mammals nonfunctional.

Mesonephros: the growth of each pronephric duct takes place towards the tail of the embryo, and in doing so induces mesonephric tubules, which is intermediate mesoderm in the thoracolumbar area. The blood supply from the branch of the aorta is received by each mesonephric tubule, ending in a capillary tuft which is analogous to the definitive nephron glomerulus. Allowing for the filtration of the blood, around the capillary tuft, the mesonephric tubule forms a capsule. This filtrate called the mesonephric duct flows through the mesonephric tubule and is drained into the pronephric duct. While the mesonephric duct extends towards the embryo's most caudal end, the nephrotomes of the pronephros degenerate, ultimately attaching to the cloaca. The kidneys of the aquatic amphibians and fishes are similar to the mesonephros of the mammalian.

Metanephros: the mesonephric duct develops the ureteric bud, an outpouching, near its attachment to the cloaca during the fifth week of the gestation. The metanephrogenic diverticulum, also called the bud, grows posteriorly towards the head of the embryo. The metanephric duct, the elongated stalk of the ureteric bud, later forms the ureter. As the bud's cranial end extends into the intermediate mesoderm, for the formation of the

collecting duct system of the kidney, it undergoes a series of branching. It also forms the renal pelvis and the major and the minor calyces. The part of the undifferentiated intermediate mesoderm is known as the metanephrogenic blastema which is in contact with the tips of the branching ureteric bud. Into the renal tubules the differentiation of the metanephrogenic blastema is induced by the signals released from the ureteric bud. Renal tubules come into contact and join with the collecting duct system tubules, forming to the collecting duct a continuous passage for the flow from the renal tubule as the renal tubules grow. Simultaneously at the tips of the renal tubules, the precursors of vascular endothelial cells begin to take their position. Then into the cells of the definitive glomerulus these cells differentiate.

Renal capsule: The kidneys membranous covering is called the renal capsule.

Cortex: The outer layer of the internal medulla is called the cortex. It contains glomeruli and blood vessels and is supported by a fibrous matrix and urine tubes.

Hilus: to pass into the renal sinus for blood vessels and nerves it is the opening in the middle of the concave medial border.

Renal column: the supporting structures of the cortex. They consist of fibrous material, urinary tubes and lines of blood vessels.

Renal sinus: the housing of the cavity which houses the renal pyramid.

Calyces: the pyramids holding recess in the internal medulla. Calyces are used kidney sections into subdivisions.

Papillae: along the wall of the renal sinus, these are the small conical projections. They have openings into the calyces through which the urine passes.

Renal pyramids: these are the segments in the conical shape within the internal medulla. They are also called malpighian pyramids, which contain the tubules and the secreting apparatus.

Renal artery: these are the two renal arteries each connecting to a kidney which come from the aorta. The artery will be divided into the five branches, each leads to a ball of capillaries. The blood to the kidneys will be supplied by the arteries. The left kidney receives the bloodflow of about 60%.

Renal vein: through the renal veins that join into the inferior vena cave, the filtered blood returns to the circulation.

Renal pelvis: it is basically a funnel, which channels the urine out of the hilus into the ureter, accepted by the renal pelvis.

Ureter: this is a narrow tube of 4 mm in diameter and 40 cm long and passing down to the bladder from the renal pelvis out of the hilus. By means of peristalsis, the urine will be carried by the ureter from the kidneys to the bladder.

Renal lobe: together with the associated overlying cortex, each pyramid forms a renal lobe.

The kidney failing: Generally, due to the nature of the diet of the prehistoric humans, as one of the kidneys has more functioning renal tissue than is needed to survive the humans can live normally with just one kidney. The chronic renal failure develops only when the amount of kidney tissue functioning is greatly diminished. When the glomerular filtration rate has fallen very low, which is a measure of renal function or when there is a severe symptom of renal dysfunction, then it indicates the renal replacement therapy, either renal transplantation or dialysis.

Medical terminology: The prefixes renal and nephro are the two involved medical terms related to the kidneys. Radical nephrectomy is the removal of the kidney, while a

surgical removal of the kidney is a nephrectomy, its surrounding tissue, potentially the adrenal gland, lymph nodes. For the removal of the cancers, a radical nephrectomy is performed. The kidneys are important excretory organs in vertebrates. Excretion is the process of eliminating waste products of metabolism and other non-useful materials. It is an essential process in all forms of life. In single-celled organisms, waste products are discharged directly through the surface of the cell. Multicellular organisms utilize more complex excretory methods. Higher plants eliminate gases through the stomata, or pores, on the surface of leaves. Animals have special excretory organs.

Human excretion: In humans, the two major excretory processes are the formation of urine in the kidneys and the formation of carbon dioxide, a human's abundant metabolic waste molecules as a result of respiration, which is then exhaled from the lungs. These waste products are eliminated by urination and exhalation respectively. In urination, hormonal control over excretion occurs in the distal tubules of the kidneys as directed by the hypothalamus.

In kidney: In humans the main organs of excretion are the kidneys and accessory urinary organs, through which urine is eliminated, and the large intestines, from which solid wastes are expelled. The skin and lungs also have excretory functions: the skin eliminates water and salts in sweat, and the lungs expel water vapor and carbon dioxide. Urea Formula CH4N2O, a colorless crystalline compound, melting point 132.7°C (270.9°F). Urea is also known as carbonyl diamide, carbamide, and also as well has numerous trade names. Although, most high purity samples have an ammonia odor, it is odorless in its purest state and highly soluble in water. The urea and the diamide of the carbonic acid have the structure as shown below. Mammals excrete urea in their urine as the end product of the metabolism containing major nitrogen content. Almost 50 g of urea is daily discharged by the adult human body. G. F. Rouelle in 1773, first isolated the urea. F. Wohler achieved a milestone and thus heralded the modern science of organic chemistry, by preparing urea from ammonium sulfate (NH4SO4) and potassium cyanate (KCNO) in 1828, which is the first synthesis of an organic molecule from the inorganic materials.

Urea is a popular fertilizer, because of its high nitrogen content. From the urea produced commercially, about three fourths of it is used for this purpose. After application to soil, urea undergoes gradually hydrolysis to carbon or carbon dioxide, and to ammonia or ammonium ion, as a solution in water. The other major use of the urea is as extremely effective adhesives which are used for plywood lamination and particle board manufacturing, as an ingredient for the production of the resins of urea formaldehyde, and the basis for the plastics as malamine

Its utilization in medicine as a diuretic is the some other use of the urea. It was used in the past as a topical antiseptic, and used as intraocular pressure and reduce intracranial. As a protein feed supplement for sheep and cattle it also find application in veterinary medicine and animal husbandry, to some extent. For the brown baked goods such as pretzels also the urea has been used. Because of its ability to accelerating the decomposition of the nitrocellulose, and to neutralizing the nitric acid, it is used as a stabilizer for nitrocellulose explosives. Even once urea was used for flameproofing fabrics. To slow the erosion by acidic pollutants and acidic rain urea is applied to limestone monuments mixing with barium hydroxide.

5. 4. Survey of literature

David et al [1] reported the alternative test platforms for the clinical analysis using optical fibers. An emerging technology, using fiber optics, has potential as an alternative in clinical diagnostics.

Jeanne et al [2] reported the usefulness and limitations of hand held refractometers in veterinary laboratory medicine. The historical and technical aspects of hand held refract meters have been reviewed with respect to their rapidity of analysis, ease of use and relatively low cost for the measurement of protein and urine solute concentrations.

Dahu et al [3] measured chemical concentrations in clinical blood serum and urine samples using liquid core optical fiber (LCOF) Raman spectroscopy to increase the collected signal strength.

Grases et al [4] described a simple procedure for routinary urinary phytate determination based on phosphorus determination through inductively coupled plasma atomic emission spectrometry.

Milton et al [5] demonstrated the refractometric analysis for the determination of several new coefficients for total solids of serum and urine. Refractometry is particularly advantageous for urine because specific gravity coefficients are considerably less accurate.

Stanly et al [6] reported the antibody production to the factor in human urine stimulating colony formation in vitro by bone marrow cells. Rabbits immunized with human urine concentrate from leukaemia patients developed antibody which neutralized the mouse bone marrow colony stimulating factor in human urine and human serum.

Koening et al [7] explained various mechanisms through which uric acid may be implicated in the atherosclerotic process and its clinical complications. Increased serum concentration of uric acid implicated in cardiovascular disease has been discussed.

Osborne et al [8] presented a comparative study of the specific gravity, refractive index and osmolality of urine for the serum biomedical profile is made with respect to their meritness in the urine profile.

Neinstein et al [9] examined the urine pregnancy tests performed at a large urban university student health centre for specific gravity, compared with a serum specimen, could alter the results of a urine pregnancy test.

Barton et al [10] reported a comparison of reagent strips and the refractometer for measurement of urine specific gravity in hospitalized children. This study was designed to provide data to determine if the reagent strip and the refractometer were interchangeable for measuring urine specific gravity in pediatric clients.

Colleen et al [11] reported the separation and quantitation of polyethylene glycols 400 and 3350 from human urine by high performance liquid chromatography. The method uses sized regenerated cellulose membranes and mixed ion exchange resin for sample preparation and high performance liquid chromatograph with refractive index determination for analysis.

March et al [12] demonstrated a capillary gas chromatography method for the analysis of inositol isomers and arabitol (extendable to theitol and adonitols to urine after derivatization. The single ion monitoring technique allows a notable improvement in sensitivity and selectivity.

Claudio et al [13] reported the isolation and characterization of a digoxin like immuno reactive substance from human urine by affinity chromatography.

Shindhara et al [14] investigated some immunochemical properties of Le^a and Le^b active substances in human urine.

Plumer et al [15] investigated some properties of lactate dehydrogenase found in human urine. The question of possible origine of urinary lactate dehydrogenase is discussed and the conclusion drawn that the kidney and not the plasma is the most likely source.

Anil et al [16] presented a comprehensive study of dielectric properties of urine collected at different intervals of time at microwave frequencies. Urine samples are collected from normal as well as persons with diabetes mellitus and the reported results provide an alternative in vitro method of diagnosing diabetes mellitus.

5. 5. Preparation and maintenance of urine samples

The urine samples were collected from the people of different age groups ranging from 22 years to 60 years with random health conditions. The samples collected from various people were taken into separate glass beakers which were well cleaned and dried. The urine samples so obtained were preserved for half an hour during which the

experimentation was conducted on them. According to literature, the physical and chemical properties of the urine sample outside the human body change even with respect to the time. Therefore, the experimentation was carried out within half an hour from the time of collection of the urine from the donors. During this time, the urine samples were preserved in a cool and dark place to avoid the samples exposing from sunlight and other environmental effects. With a view to prevent the reaction of urine samples with the containers, only glass containers were used for the purpose of preservation. Lids of all the urine containers were made as tight as possible. Proper care was taken during the course of experimentation by wrapping a black cover around the urine sample container.

5. 6. Experimental

The experimental setup consists of a U shaped thin silica glass probe, that was used and described in Chapter 4. In the present investigation, human urine samples of 25 persons were collected whose age ranges from 20 years to 60 years. A 10 ml sample of urine, collected from each person, is slowly dropped into a beaker containing silica glass u shaped probe. The two ends of the U shaped probe was in turn connected to a power meter at one end and a 633 nm laser source at the other end. Power was switched on and laser beam was sent to the glass probe surrounding the urine of single person, using a power meter. Samples of urine collected earlier were changed one after the other surrounding the glass probe and output power was noted. Using the calibration plot, refractive index was determined. Simultaneously the refractive index of urine collected from each individual was also noted using Abbe's refractometer for the verification of refractive index values. The data is presented in Table 5.1. Percentage of error is calculated using the relation.

$$\text{Error } \% = [(\mu_2 - \mu_1)/\mu_1]\ 100$$

Where μ_1 = Refractive index of urine, measured using Abbe's refractometer,

μ_2 = Refractive index of urine, measured using glass sensor technique.

5.7. Results and Discussion

As is known, any ailment in the human body is first reflected in blood picture and urine. The study and analysis of human urine is important in determining the salt contents,

sugar content (if any), proteins etc. Another important parameter, which the pathologists are interested, is the refractive index profile of human urine. The present chapter presents the results of refractive index of human urine.

Table 5.1 Data on refractive index of human urine

SL. No.	*Sample Code*	*Age (Years)*	*Power output (dBm)*	μ_2	μ_1	$[(\mu_2 - \mu_1)/\mu_1]100$
1	SN1	53	-48.0	1.325	1.324	0.151
2	HA2	60	-48.4	1.330	1.329	0.075
3	KA3	42	-48.4	1.330	1.329	0.075
4	SR4	34	-48.4	1.330	1.329	0.075
5	SA5	24	-48.4	1.330	1.329	0.075
6	KR6	22	-48.4	1.330	1.329	0.075
7	KS7	42	-49.2	1.339	1.338	0.075
8	VR8	44	-49.2	1.339	1.338	0.075
9	HS9	46	-49.2	1.339	1.338	0.075
10	AM10	40	-49.2	1.339	1.338	0.075
11	RA11	30	-49.2	1.339	1.338	0.075
12	AA12	56	-49.6	1.344	1.342	0.149
13	SK13	25	-49.6	1.344	1.342	0.149
14	PR14	22	-49.6	1.344	1.342	0.149
15	PE15	48	-50.0	1.348	1.346	0.223
16	GA16	27	-50.0	1.348	1.346	0.223
17	SU17	20	-50.0	1.348	1.346	0.223
18	PR18	20	-50.0	1.348	1.346	0.223
19	BA19	53	-50.0	1.348	1.346	0.223
20	HZ20	38	-50.0	1.348	1.346	0.223
21	AS21	48	-50.4	1.353	1.351	0.148
22	PR22	22	-50.4	1.353	1.351	0.148
23	SK23	34	-50.8	1.357	1.355	0.221
24	AV24	31	-50.8	1.357	1.355	0.221
25	GA25	50	-50.8	1.357	1.355	0.221

μ_1 : Refractive index of urine , measured using Abbe's Refractometer

μ_2 : Refractive index of urine , measured using glass sensor technique

Error %: $[(\mu_2 - \mu_1)/\mu_1]100$

Table 5.1 presents data on refractive index of urine, collected from 25 persons of age group ranging from 20 – 60 years, using optical glass sensor technique developed in the present study. Further, table reveals the data on refractive index, measured using Abbe's refractometer for the verification. The percentage of error reported in the table is I the range of 0.075% to 0.223%, which confirms the accuracy of the results obtained from the technique developed in the laboratory. The average value of refractive index of urine of healthy persons is 1.343, irrespective of age, while standard deviation is ± 0.009 ……

The significance of this study is of two fold. Firstly, to examine the usefulness, reliability and practicability of optical glass sensor technique to determine refractive index of a salt solution like human urine. Secondly, to have data on refractive index of human urine, which may be useful in medical discipline for the diagnosing a disease.

5. 8 Conclusions

1. Optical glass sensor technique is simple and elegant. It can be employed to determine refractive index of a biological salt solution like urine.
2. It is accurate as revealed by the data obtained by Abbe's refractometer.
3. The study of refractive index of urine may be helpful for diagnosing a disease and also for administration and monitoring the drug action as well as recovery of patient.
4. The parameter – refractive index can be a complementary parameter in medical discipline for the assessment of degree of disease, if this study would have been made on the urine, collected from the patients suffering from various chronic diseases.
5. This technique may serve as a potential tool to asses physiological, and ecological conditions as well as body chemistry of a person.
6. Finally, the parameter – *refractive index* can be considered as 'Index' of health status of a person.

References

[1]. David G. M. Carville, Fiber optics for the detection of clinical analytes – An emerging technology using fiber optics has potential as an alternative in platforms for clinical diagnostics, Medical device links, originally published IVD Technology, January 2002.

[2]. Jeanne W. George, The usefulness and limitations of Hand held refractometers in veterinary laboratory medicine: An historical and Technical review, Journal of veterinary clinical pathology, Vol. 30, No.4(2008), pp 201-210..

[3]. Dahu Qi and Andrew J. Berger, Chemical concentration measurement in blood serum and urine samples using liquid core optical fiber Raman spectroscopy, Appl. optics, Vol. 46, No. 10(2007), pp. 1726 – 1734.

[4]. F. Grases, J. Perello, B. Isern and R. M. Prieto, Detrmination of myo inositol hexakisphosphate (phytate) in urine by inductively coupled plasma atomic emission spectrometry, Elsevier B. V., Science Direct, available online 13, February 2004.

[5]. Br. Milton E. Rubini and A. V. Wolf, Refractrometric determination of total solids and water of serum and urine, J. Biol. Chem., Vol. 19(1956).

[6]. E. R. Stanly, T. A. Mcneill, S. H. Chan, Antibody production to the factor in human urine stimulating colony formation in vitro by bone marrow cells, Brtish Journal of Haematology, Vol. 18, No. 5(2008), pp.585 – 590..

[7]. Koening, Wolfgang, Meisinger, Christa, Uric acid, type 2 diabetes and cardiovascular diseases: Fueling the common soil hypothesis, High beam research, http://www.encyclopedia .com/doc/1P3-143350509.html, February 2008.

[8]. Osborne, Carl A, Urine specific gravity, refractive index, osmolality: Which would you choose? dvm news magazine, High beam research, http://www.encyclopedia.com/doc/1P3-36540762.html, November 1998.

[9] Neinstein, Lawrence, Harvey, Francine, Effect of low urine specific gravity on pregnancy testing, J. Amer. College Health, November 1, 1998.

[10]. Barton, Sharon, Jackson, Holmes, Sharon Sallee, A coparison of reagent strips and the refractometer for measurement of urine specific gravity in hospitalized children, The Journal of Pediatric Nursing, September 1, 1998.

[11]. Collen M. Ryan, Martin L. Yamush, Ronald G. Tompkins, Separation and quantitation of polyethelene glycols 400 and 3350 from human urine by high performance liquid chromatography, Vol. 81, No.4(2006), pp. 350-352.

[12]. G. March, R. Fosteza, and Grases, Determination of inositol isomers and arabitol in human urine by gas chromatography mass spectrometry, Chromatographer, Vol. 42, No 5-6(1996), pp. 329-331.

[13]. Claudio De Angelis, Massimiliano Riccardo Salvini, Alfonso Piccoli, Claudio Ferri and Anna Santucci, Isolation and characterizarion of a digoxin like immunoreactive substance from human urine by affinity chromatography, J.Clin. Chem., Vol. 43, pp. 1416-1420.

[14]. T. Shinohara, S. Yammoto, Iseki, Some immunochemical properties of Le^a and Le^b active substances in human urine, International journal of immunogenetics, Vol 4, No. 3(2007), pp. 159-165.

[15]. D. T. Plummer and P. D. Leathwood, Some properties of lactate dehydrogenase found in human urine, J. Biochem., Vol.103, No.1(1967), pp 172-176.

[16]. Anil Lonappan, V. Hamsakkutty, G. Bindu, Joe Jacob, Vinu Thomas, K. T. Mathew, Dielectric properties of human urine at microwave frequencies, Microwave and optical Technology Letters, Vol. 42, No.6 (2004).